SYNTHESIS, CHARACTERIZATION AND COMPUTATIONAL STUDY OF COBALT(II), COPPER(II), NICKEL(II), VANADIUM(IV) AND ZINC(II) COMPLEXES OF QUINOLINE DERIVATIVE LIGANDS FOR BIOLOGICAL APPLICATIONS

By

Tadewos Damena Kebede

A Dissertation Submitted to the Department of Applied Chemistry

School of Applied Natural Sciences

Presented in Partial Fulfillment of the Requirements for the Degree of Doctor of Philosophy in Applied Chemistry (Bioinorganic Chemistry)

Office of Postgraduate Studies
Adama Science and Technology University

November, 2022
Adama, Ethiopia

SYNTHESIS, CHARACTERIZATION AND COMPUTATIONAL STUDY OF COBALT(II), COPPER(II), NICKEL(II), VANADIUM(IV) AND ZINC(II) COMPLEXES OF QUINOLINE DERIVATIVE LIGANDS FOR BIOLOGICAL APPLICATIONS

By:

Tadewos Damena Kebede

Main Supervisor:

Dr. Tegene Desalegn (Associate Professor)

Co- Supervisor:

Dr. Taye Beyene Demissie (Senior Lecturer/Associate Professor)

A Dissertation Submitted to the Department of Applied Chemistry

School of Applied Natural Sciences

Presented in Partial Fulfillment of the Requirements for the Degree of Doctor of Philosophy in Applied Chemistry (Bioinorganic Chemistry)

Office of Postgraduate Studies

Adama Science and Technology University

November, 2022

Adama, Ethiopia

Declaration and Recommendation

Declaration

I hereby declare that this dissertation entitled "**Synthesis, Characterization and Computational Study of Cobalt(II), Copper(II), Nickel(II), Vanadium(IV) and Zinc(II) Complexes of Quinoline Derivative Ligands for Biological Applications"** is my original work. It has never been submitted for the award of any academic degree, diploma or certificate in any other university. All sources of materials used for this dissertation have been duly acknowledged through appropriate list of references.

Tadewos Damena	_____	20/09/2022
Name of student	**Signature**	**Date**

Recommendation

We, the supervisors of this dissertation, hereby certify that we have read and revised the dissertation entitled "**Synthesis, Characterization and Computational Study of Cobalt(II), Copper(II), Nickel(II), Vanadium(IV) and Zinc(II) Complexes of Quinoline Derivative Ligands for Biological Applications"** prepared under our guidance by **Tadewos Damena** and submitted in partial fulfillment of the requirements for the degree of Doctor of Philosophy in **Bioinorganic Chemistry**. Therefore, we recommend the final submission of the dissertation to the department.

Dr. Tegene Desalegn	_____	20/09/2022
Main Supervisor	Signature	Date

Dr. Taye Beyene Demissie	_____	20/09/2022
Co-supervisor	Signature	Date

Approval Page

We hereby certify that the recommendations and suggestions made by the board of examiners are appropriately incorporated into the final version of the dissertation entitled "**Synthesis, Characterization and Computational Study of Cobalt(II), Copper(II), Nickel(II), Vanadium(IV) and Zinc(II) Complexes of Quinoline Derivative Ligands for Biological Applications"** by **Tadewos Damena**.

Dr. Tegene Desalegn	_____	_____
Main Supervisor	**Signature**	**Date**
Dr. Taye Beyene Demissie		_____
Co-supervisor	**Signature**	**Date**

We, the undersigned, members of the Board of Examiners of the dissertation open defense by **Tadewos Damena** have read and evaluated the dissertation entitled "**Synthesis, Characterization and Computational Study of Cobalt(II), Copper(II), Nickel(II), Vanadium(IV) and Zinc(II) Complexes of Quinoline Derivative Ligands for Biological Applications"** and examined the candidate during open defense. This is, therefore, to certify that the dissertation is accepted for partial fulfillment of the requirement of the degree of Doctor of Philosophy in **Bioinorganic Chemistry.**

_____	_____	_____
Chairperson	**Signature**	**Date**
_____	_____	_____
Internal Examiner	**Signature**	**Date**
_____	_____	_____
External Examiner 1	**Signature**	**Date**
_____	_____	_____
External Examiner 2	**Signature**	**Date**

Finally, approval and acceptance of the dissertation is contingent upon submission of its final copy to the Office of Postgraduate Studies (OPGS) through the candidate's
Department Graduate Council (DGC) and School Graduate Committee (SGC).

_____	_____	_____
Department Head	**Signature**	**Date**
_____	_____	_____
School Dean	**Signature**	**Date**
_____	_____	_____
Office of Postgraduate Studies, Dean	**Signature**	**Date**

ACKNOWLEDGEMENTS

I would like to express my sincere thanks to my supervisors, Dr. Tegene Desalegn and Dr. Taye Beyene Demissie (University of Botswana) for their invaluable suggestions, guidance and constructive comments throughout this dissertation work.

I would like also to acknowledge Dr. Hadgu Hailekiros, Dr. Eneyew Amare and Dr. H.C.Ananda Murthy for their constructive comments. I would like to acknowledge Wachemo University for sponsorship and Adama Science and Technology University for giving me the chance to pursue the PhD program and Dr. Aschalew Tadesse head Department of Applied Chemistry. My appreciation goes to the University of Botswana for the research facilities through my co-supervisor. The computational resources were supplied by the project "e-Infrastruktura CZ" (e-INFRA CZ ID: 90140) supported by the Ministry of Education, Youth and Sports of the Czech Republic. I would like also to acknowledge ASTU staff members and my colleagues Mr. Teshome Degfie, Mr. Mamaru Bitew, Mr. Getiye Behailu, Mr. Tsegu Kiros, Mrs. Bontu Tiki, Mr. Kebede Shenkutie, Mr. Guta Amenu, Mrs. Emebet Getaneh of the Applied Chemistry Department, and Mr. Kinfe Tolera of Department of Applied Physics. I have special acknowledgement to Mr. Aklilu Guale and Dr. Digafie Zeleke for their limitless support throughout this work. Dr. Tadesse Bassie from Bangalore University, India, Dr. Raji Feyisa from Wolega University, Mr. Eshetu Wolde and Mr. Abreham Tesfaye from Wachemo University are also acknowledged for their valuable support. I want to also acknowledge external examiners Professor Abi Tadesse from Haramaya University and Professor Atakilt Abebe from Bahr Dar University for their constructive comments and valuable enquiries. Last, but not the least, my acknowledgement is extended to my lovely spouse (Birhan Ewnetu) for her support morally, financially and for her patience to play great role in taking care of our sons (Bahran and Beidemariam) and my Father Damena Kebede and My Mother Welansa Derese next to Almighty God. Thanks to all who stood by my side throughout my academic journey.

TABLE OF CONTENTS

CONTENTS **PAGES**

LIST OF TABLES

LIST OF FIGURES

LIST OF SCHEME

LIST OF APPENDIXES

ACRONYMS AND ABBREVIATIONS

A/A	Ascorbic Acid
ADMET	Absorption, Distribution, Metabolism and Excretion
ATCC	American Type Culture Collection
BBB	Blood Brain Barrier
CYP	P450 Isoenzymes
DMSO	Dimethyl Sulfoxide
DPPH	2,2-Diphenyl-1-Picrylhydrazyl
EDX	Energy-Dispersive X-Ray Spectroscopy
FMOs	Frontier Molecular Orbitals
FTIR	Fourier-Transform Infrared Spectroscopy
GIT	Gastrointestinal Tract
HBAs	Hydrogen-Bond Acceptors
HBDs	Hydrogen-Bond Donors
IC_{50}	Half-Maximal Inhibitory Concentration
IR	Infrared Spectroscopy
L	Ligand
L1	Ligand 1
L2	Ligand 2
LMCT	Ligand-To Metal Charge Transfer
MEP	Molecular Electrostatic Potential
MIC	Minimum Inhibitory Concentration
MLCT	Metal-to-Ligand Charge Transfer
MS	Mass Spectroscopy
NMR	Nuclear Magnetic Resonance
P	Partition Coefficient
PPB	Plasma Protein Binding
SEM	Scanning Electromicroscopy
SMILES	Simplified Molecular Input Line Entry System
TLC	Thin Layer Chromatography
TPSA	Topological Polar Surface Area
UV-Vis	Ultra Violet- Visible Spectrometry
PXRD	Powder X-Ray Diffraction
P-GP	Permeability Glycoprotein
MR	Molar Refractivity

ABSTRACT

The application of transition metal complexes as biochemical, medicinal, analytical, pharmaceutical, agricultural and antimicrobial agents has recently become center of interest for researchers and innovators. In this aspect, quinoline ligands containing imine are important classes of biologically active molecules that have attracted attention of bioinorganic, pharmaceutical and medicinal chemists due to their familiar coordination behavior and wide range of pharmacological properties. In this PhD dissertation work, ten(10) series of novel transition metal complexes of Zn(II), Cu(II), Co(II), Ni(II), and V(IV) were prepared from quinoline derivative ligands [(*E*)-2-(((2-((2-hydroxyethyl)amino)quinolin-3-yl)methylene)amino)ethan-1-ol, (**H_3L**) (**L1**) and 2-((2-hydroxyethyl)amino)quinoline-3-carbaldehyde (**H_2L**) (**L2**)] in 1:1 and 1:2 metal–to-ligand ratio in methanol respectively and characterized with UV-Visible spectroscopy, fluorescence spectroscopy, ^{1}HNMR spectroscopy, ^{13}CNMR spectroscopy, FTIR spectroscopy, powder X-ray Diffraction (PXRD), Scanning Electron Microscopy-Energy Dispersive X-ray Spectroscopy (SEM-EDX), Mass spectroscopy (MS), thermal analyzers, molar conductance and melting point. In addition, computational (drug likeness, DFT and molecular docking) analysis were also carried out to get further insights and to support the analyses of the results. The structural features, the crystallite size, and elemental composition of the metal complexes were deduced from molar conductance, FTIR, Mass spectroscopy, powder XRD, thermal analyzers and EDX studies. Powder XRD results indicate the average crystallite sizes of complexes **1 – 5, 7**, **8** and **10** are 28, 34, 22, 37, 8, 23, 9 and, 23 nm, respectively. The spectral data revealed that the ligands adopted a tridentate (**L1**) and bidentate (**L2**) fashion when binding to metal ions via the nitrogen atom and the oxygen atom of deprotonated hydroxyl group (O-H). *In vitro* antibacterial activity analysis of both the ligands and their synthesized complexes were studied by employing the disc diffusion and agar dilution methods, in which the complexes exhibited better activity than the precursor ligands, that all the first five (**Zn(II), Cu(II), Co(II), Ni(II) and V(IV)**) of **L1** complexes exhibited activity ranging from low to high mean inhibition zones, with 7.32 ± 0.90 mm at 150 μg/mL and 20.65 ± 0.18 mm at 300 μg/mL. All the **Zn(II), Cu(II), Co(II), Ni(II)** complexes exhibited very good activities with *Pseudomonas aeruginosa* (18.85 ± 0.34, 20.65 ± 0.18, 18.62 ± 0.19 and 15.64 ± 0.22 mm diameter at concentration of 300 μg/mL, respectively) compared to free ligand with mean inhibition zone of 6.24 ± 0.39mm diameter. Similarly, the complexes **Zn(II), Cu(II), Co(II), Ni(II)** of ligand (**L2**) exhibited activities ranging from medium to

high mean inhibition zones, with 11.79 ± 1.07 mm at 100 μg/mL and 20.90 ± 2.00 mm at 200 μg/mL. All the complexes exhibited good activities with *Pseudomonas aeruginosa* (20.75 ± 2.05, 20.90 ± 2.00, 20.75 ± 2.07 and 18.90 ± 2.06 mm diameter at concentration of 200 μg/mL, respectively) compared to free ligand with mean inhibition zone of 9.60 ± 2.00mm diameter, but among these Cu(II) complex showed higher percent activity index (*AI* = 62, 90%), than all Zn(II) (*AI* = 54, 82%), Co(*AI* = 54, 81%) and Ni(II) (*AI* = 41, 68%) with both *Escherichia coli*, and *Pseudomonas aeruginosa*, respectively. Furthermore, all the complexes (**1 – 10**) were also evaluated for their antioxidant properties using DPPH assay in which all metal complexes showed higher antioxidant activities than the free ligands. Among these: **Zn(II)**, **Cu(II)** of both ligands **L1** and **L2** and **Co(II)** of **L2** complexes exhibited better antioxidant activities with IC_{50} values of 10.46, 8.62, 8.20, 4.70 and 9.20 µg/mL, respectively, as compared to that of the positive control is 4.49 and 4.28 µg/mL. The *in silico* drug likeness analysis results indicated that all complexes of **L1** fulfil Lipinski's rule of five. Overall, the newly synthesized Zn(II), Cu(II), Co(II), and Ni(II) complexes have biological activities, with the Cu(II) complexes having much better activity than other complexes and these result were found to be in good agreement with binding mode against *E. coli* DNA gyrase B.

***Keyword*:** Aminoquinoline derivative ligand, Metallic complexes, computational studies, Antibacterial, Antioxidant activity

1. INTRODUCTION

Metal ions are known to combine with many drugs and/or organic ligands to form complexes of enhanced bioactivity compared to free ligands [1]. Metal complexes find wide use in medicinal, pharmaceutical, agricultural and chemical industries [1–3]. Recent reports indicate that due attention is being given to the chemistry of metal-organic compounds interactions and their clinical applications for the treatment of various disorders including both communicable and non-communicable diseases [1, 4–11]. Accordingly, researchers' interest has shifted towards the synthesis of metal complexes that have biological activities. The wider application of transition metal complexes as biochemical, medicinal, analytical, pharmaceutical, agricultural, antitumor and antimicrobial agents has recently become center of interest for researchers and innovations [1, 4, 12–14]. In this regard, the syntheses of complexes that are biologically active have paramount significance. Results of researches over the past decades have witnessed that metal complexes of (cadmium, chromium, cobalt, copper, iron, manganese, nickel, molybdenum, palladium, ruthenium, tungsten, vanadium and zinc) have been applied in the various biological applications, including, antimicrobial and antioxidant [15–23], anticancer [1, 4, 24, 25], antiproliferative [25], anti-inflammatory and genotoxic [26], DNA binding and cytotoxicity [15, 18, 22, 27], antitumor [12, 13, 28], antiviral [29] and antidiabetic [6] activities. These wide window of applications have initiated many researchers to study of systems containing these metal complexes [2].

In this aspect, the search for natural products with potential biologically active ligands have confirmed that quinoline derivative such as 2-chloro-8-methylquinoline-3-carbaldehyde, 2-oxo-1,2-dihydroquinoline-3-carbaldehyde, 2-oxo-quinoline, 2-chloro-quinoline and 2-chloroquinoline-3-carbaldehyde are pharmacologically active compounds that have versatile activities to cure different communicable and non-communicable diseases [30–35]. Quinoline is classified under alkaloid class of natural products [33, 36], and is present in various plants, pharmaceuticals, agrochemicals and dyes. It has been used as chelating agent due to its N-donor ligands in the synthesis of coordination compounds or complexes [35]. Quinoline derivatives that have imine are among one of the important classes of biologically active ligands. Such ligands have attracted attention of researchers due to their extensive pharmacological properties and applications, such as anticancer [37–39], antimicrobial [11, 34, 38, 40], antifungal [8, 10], antiprotozoal [8, 40], anti-inflammatory [9], antidiabetic [7, 32] and antioxidant [10, 11, 34] activities. Metal ions combined with many drugs and organic

ligands can usually enhance the bioactivity of precursor ligands, because metal ions may increase the synergetic effect of the complexes [1, 5]. The issue of metal-based therapy has witnessed increasing focus with respect to efficient strategies in the design of repository, slow-release or long-acting drugs [41]. In this regard, quinoline derivative ligands containing imine are important classes of biologically active molecules that have attracted attention of bioinorganic, pharmaceutical and medicinal chemists due to their familiar coordination behaviour and wide range of pharmacological properties [34, 41–43]. It is known that the active sites of metallo-enzymes can function with the help of transition metal ions (Zn, Cu, Fe, Mn). Therefore, the synthesis of metal complexes can be used to simulate the active centers to assist in the biological activity of organic compounds which previously used as a drug [1, 5].

In order to develop a clinically useful metallo-pharmaceutics, the study of coordination compounds focusing on their long-term toxicity including side effects, clear evidence of target compounds for the *in vivo* as well as *in vitro* pharmacological action and their pharmacokinetic property are very crucial [44–47]. In this regard, this study have synthesized cobalt(II), copper(II), nickel(II), vanadium(IV) and zinc(II) complexes with quinoline derivatives to enhance the biological activities and then evaluated for their antibacterial activities against different strains of bacterial pathogens.

Now a days, zinc based complexes have shown diverse medicinal applications such as anti-inflammatory [6], anticonvulsant, antimicrobial [2, 48], antidiabetic, antioxidant [2, 48, 49] and anti-proliferative activities [13, 50–54]. In addition, several zinc complexes are used as a major ingredient of the medicine used in the treatment of skin diseases and find significant use as a catalyst in catalytic reactions [13, 50–55]. Previous studies of a Zn(II) complex of quinoline derivative ligand indicated an *in vitro* biological screening effects tested against four bacterial strains, *E. coli* and *P. aeruginosa* (Gram-negative) as well as *S. aureus* and *B. subtilis* (Gram-positive). The results showed a moderate antibacterial activity than the free ligand due to chelation [56, 57].

Vanadium is another element, which recently caught great attention of researchers that was considered in our study. Most commonly, vanadium complexes exist in V(IV) and V(V) oxidation states. In our case, we focused with V(IV) specifically the oxovanadium form because the coordination and biochemistry of V(IV) has attracted many scholars in the recent years and have many biological activities [47, 58, 59]. In addition, oxovanadium complexes

with quinoline and pyridinone ligands showed the strongest antiproliferative activity [60] and oxovanadium(IV) complex of 8-hydroxy quinoline and 3-acetyl-6-methyl-2H-pyran-2,4(3H)-dione have shown satisfactory bacterial activity against *S .pyogenes* [61]. Even though numerous vanadium complexes have been designed and synthesized for biological activity, search for new high valent vanadium complexes that have biological activities remains to be of great interest for the development of metal based drugs to treat different diseases [47, 58, 59, 62]. There also exist reports about structures, magnetic properties, antidiabetic, anti-inflammatory and catalytic activities of oxovanadium complexes, but the study of their antimicrobial activity is relatively rare [61, 63, 64].

The third metal that we considered in this study is copper and studies have indicated that Cu(II) complexes containing heterocyclic ligand exhibited antimicrobial, anticancer and antioxidant behavior. In another study it has recently been reported that Cu(II) complexes derived from 2-oxo-1,2-dihydroquinoline-3-carbaldehyde N-substituted thiosemicarbazones showed biological properties such as protein binding, antioxidant and cytotoxic activity [16]. In addition Cu(II) complexes of quinoline derivatives also motivated researchers due to their diverse spectra of biological and pharmaceutical activities, such as antioxidant activities. [65]. Copper complexes with imines have deserved much attention, probably because of their ability to intercalate between the bases of DNA and to participate in catalytic cycles with usual reducing and oxidizing agents in biological medium [66]. Copper(II) complexes have showed promising antimicrobial, antioxidant, antiviral [21, 22, 29] and antiproliferative, [67] activities. Similarly, a copper(II) complexes of quinoline derivatives also showed moderate antibacterial activity against *E. coli,* [3] but showed higher antibacterial activities than the parent ligand [19].

The fourth metal we dealt with in this study is cobalt(II) in which its complexes exhibits interesting biological activity such as antifungal, antibacterial and anticancer activity. Various studies reported that Co(II) complexes of heterocyclic ligand were known for their wide spectrum of biological and pharmaceutical activities, such as inhibition of tumor growth, antioxidant, antimicrobial and antiviral effect [43, 68–71]. The fifth metal complex considered in this work is nickel(II) metal complex. Bioinorganic chemists were interested to study Ni(II) complexes due to its biological activity such as antitumor [72], antibacterial [73], antifungal [74], anti-inflammatory/antioxidant [72], antileishmanian [75] and their interaction with DNA as intercalating [76, 77].

However, the structural and biological properties of metal complexes with imine and N-heterocyclic ring containing ligands, [**L1** = (***E***)-2-(((2-((2-hydroxyethyl)amino)quinolin-3-yl)methylene)amino)ethanol and **L2** = 2-((2-hydroxyethyl)amino)quinoline-3-carbaldehyde], have not been reported. Hence, in this dissertation work we reported the synthesis of, Zn(II), Cu(II), Co(II), Ni(II) and V(IV) complexes from metal salts with the mentioned ligands.

Furthermore, *in silico* analysis (DFT, molecular docking and Absorption, Distribution, Metabolism, and Excretion (ADME)) had been performed to determine the 3D structure of the complexes, correlate experimental results with theoretical value and to predict drug likeness of the targeted metal complexes [78–81]. The efficiencies of metal complexes having biological activities depend on the nature of both metal ions and the ligands that the complexes made from. Accordingly, metal complexes synthesized from single ligand with different metal ions exhibited different biological properties [15, 22, 82]. These observations uplifted our interest for the synthesis of new transition metal compounds from single ligand that possess antimicrobial and antioxidant activities. In addition, we studied the binding stoichiometry, formation constants, antimicrobial activities and antioxidant activities using spectroscopy, disc diffusion and DPPH assay methods respectively. The results were supported using *in silico*, methods. Therefore, considering the medicinal and biological properties of ligands and their transition metal complexes, we reported the synthesis of novel complexes and their characterization with SEM – EDX, powder XRD, FTIR, UV-Vis spectroscopy, thermal analyzers, mass spectrometer and fluorescence spectroscopy.

1.1. STATEMENT OF THE PROBLEM

Multidrug resistant microbes are a serious health threats causing a rise in morbidity and mortality [83]. Furthermore, multidrug resistant microbes increase so quickly in spite of having large number of antibiotics to cure the infection. Hence, there is a substantial need for the development of potential antimicrobial agents [84]. Therefore, chemists and pharmacist are engaged in extensive pharmaceutical research to design and develop the promising and effective drugs with wide range antimicrobial activity having a novel therapeutic approach [85, 86].

Quinolines and their derivatives are biologically and pharmacologically active compounds that have versatile activities to cure different communicable and non-communicable diseases. Recently, wide varieties of synthetic quinoline derivative drugs are being used for antibacterial, antifungal, antimalarial, anti-tuberculosis, antipyretic, anti-inflammatory and antiviral properties. This is due to the presence of imine linkage [87–89]. Accordingly, organic compounds with heterocyclic moiety are prominent ligands in coordination chemistry due to the presence of various binding sites and wide role in medicinal chemistry and pharmacological activities [90, 91]. Even though different quinoline derivative ligands were reported for biological activities, there were very few previous works reported with regards to their metal complexes, hence, we were motivated to synthesize the ligands and their metals complexes and simultaneously evaluate their biological properties.

Transitional metals and their complexes have been of significant interest in medicinal chemistry. Coordination compounds are commonly used in medicinal chemistry since the discovery of cisplatin, a widely known and used anticancer drug [92]. Several coordination compounds with various metal ions have been applied in treatment of diseases including, cancers, malaria, syphilis and neurodegentative diseases [93–96]. However, metal based compounds in the treatment of microbial diseases were given less attention. Therefore, the development of coordination compounds as antimicrobial drugs are very important to control the resistance developed by microbes, hence metal complexes change their kinetics and thermodynamic behavior towards biological receptors due to their variation in geometry and oxidation potentials [97]. Therefore, keeping in mind the biological applications of heterocyclic ligands and their complexes, herein we report the successful synthesis of ten novel complexes from essential and non-essential metal with quinoline derivatives ligands and then evaluation of their biological activities.

1.2. OBJECTIVES OF THE STUDY

1.2.1. General Objective

- The overall objective of this work was to synthesize, characterize and computational study of transition metals (Zn(II), Cu(II), Co(II), Ni(II) and V(IV)) complexes with ligands of quinoline derivatives to evaluate their antibacterial and antioxidants activities.

1.2.2. Specific Objectives

- To synthesize quinoline derivative ligands ((*E*)-2-(((2-((2-hydroxyethyl) amino) quinolin-3-yl) methylene) amino) ethan-1-ol,)) and 2-((2-hydroxyethyl)amino)quinoline-3-carbaldehyde
- To characterize the synthesized ligands with ^{1}HNMR spectroscopy,^{13}CNMR spectroscopy, elemental analyzer, mass spectroscopy and FTIR spectroscopy
- To synthesize Zn(II), Cu(II), Co(II), Ni(II) and V(IV) complexes with ((*E*)-2-(((2-((2-hydroxyethyl) amino) quinolin-3-yl) methylene) amino) ethan-1-ol,)) as ligand using standard protocol
- To synthesize Zn(II), Cu(II), Co(II), Ni(II) and V(IV) complexes with 2-((2-hydroxyethyl)amino)quinoline-3-carbaldehyde as ligand using standard protocol
- To characterize the transition metal complexes using UV-Vis, FTIR, XRD, SEM, EDX, fluorescence, mass spectrometer and thermal analyzers
- To investigate *in vitro* antioxidants activities of complexes using DPPH free radical scavenging method and compare with that of free ligands and positive control
- To evaluate *in vitro* antibacterial activities of complexes against Gram positive and Gram negative bacterial strains and compare the result with that of free ligands and positive control
- To carry out *in silico* (DFT, ADME and Molecular docking) study of the synthesized ligands and their transition metal complexes

1.3. SIGNIFICANCE AND BENEFICIARIES

The dramatically increasing trend of microbial drug resistance has motivated scholars to search for different mechanism to overcome the problem. Studies on antioxidant and antimicrobial activities of metal-based medication are still scarce, and there is a need for further investigations along this line to strengthen the pharmacological study profile, evaluate the effectiveness of metal complexes against disease causing agents and their ultimate utilization in drug development. Some complexes' may be safe and effective for the treatment of microbial infection. Metal complexes being mostly cationic with metal centers as scaffolds are the ideal starting point for designing the new antimicrobial drugs, and thus allowing them to induce less resistance in bacteria [85, 86, 98, 99]. The researchers benefited from this study as different manuscripts were published on American chemical Society Journal which is most trusted, cited and read due to its high impact factor. In addition researchers, research institutions, academia, pharmaceutical industries and local communities who are interested to work on a related project could be the main beneficiaries of the current study.

1.4. EXPECTED OUTPUT

The prevalence of microbial infection and its drug resistance has been drastically increasing all over the World and no fully effective treatments that can tackle the infection have been discovered till present. In this research work we have designed to develop and accordingly successfully synthesized, characterized novel series transitional metal complexes with quinoline derivative ligands and evaluated their performance for biological application with focus on expected antimicrobial and antioxidant activities. The outcome shows that the targeted metal complexes of quinoline derivatives were effective against selected gram negative and gram positive bacterial strains and also exhibited promising radical scavenging activity phenomenon. The outcomes were also supported with computational (DFT, ADME and molecular docking) studies because this work represents an excellent approach to study biological and medicinal activity of molecular systems where the experimental results supported by chemical computations. In addition to the publication of two articles as per the requirement of ASTU postgraduate guideline, a valuable research experience was obtained.

2. LITERATURE REVIEW

2.1. Quinoline and Quinoline Derivatives

2.1.1. Quinoline or 1-aza-naphthalene

Quinoline or 1-aza-naphthalene or benzo[*b*]pyridine is a planner hetero-aromatic compound in which 10π electrons move throughout the structure and having a molecular formula of C_9H_7N (Scheme 1). Quinoline is a hetero-bicyclic system consists of six member benzene ring fused with pyridine, which is an important building block in medicinal chemistry [100]. Both quinoline and its derivatives have natural as well as synthetic origin, in which, they are classified based on structural modification as well as biological activity [11, 34, 101, 102].

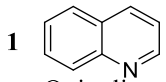

Quinoline

Scheme 1. Structure of quinoline

The quinoline ring system occurs in various natural products, especially in alkaloids and is present in various plants [33, 36]. Quinolines are also classified on the basis of substitutions present, these are: **A.** Aminoquinolines (2-aminoquinolines, 3-aminoquinolines, 4-aminoquinolines, 5-aminoquinolines, 8-aminohydroquinolines, 2,8-diaminoquinolines and 4-amidoquinolines), **B.** Hydroxyquinolines (4-hydroxyquinolines and 8-hydroxyquinolines). **C.** Fused quinolines [101, 103] (Scheme 2).

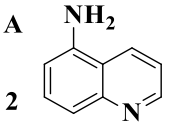

Quinolin-5-amine

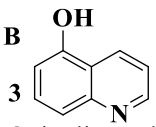

Quinolin-5-ol

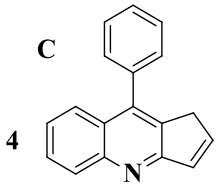

9-phenyl-1*H*-cyclopenta[*b*]quinoline

Scheme 2. Types of quinolines derivatives

2.1.2. Quinoline Derivatives

Quinoline derivatives represent the major class of heterocycles, and a number of preparations have been known since the late 1800s. The synthesis of quinoline and its derivatives have attracted considerable attention of organic, pharmacist and medicinal chemists for many years [104]. The structural core of quinoline and its derivatives are frequently associated with medicinal applications in which intensive efforts needed to find effective therapeutic agents

with antimicrobial activities that have directed many researchers to synthesize a series of quinoline derivatives or their analogues [11, 34, 102, 105].

Quinoline motif plays an important role in drug development and always remains as a lead in the field of pharmaceutical prospective [106]. The antimalarial drugs bearing quinoline rings are quinine, quinidine, chloroquine, as quinoline derivatives [106–108] and antibacterial drugs like ciprofloxacin, [106] and styrylquinoline derivatives [109] showed potent biological properties (Scheme 3). Quinoline derivatives exhibit human serum albumin binding properties and also entail in the synthesis of novel dispiro heterocyclic derivatives [101, 109]. There are different synthesis methods of quinoline derivatives and among this Vilsmeier reagent method is one of known method.

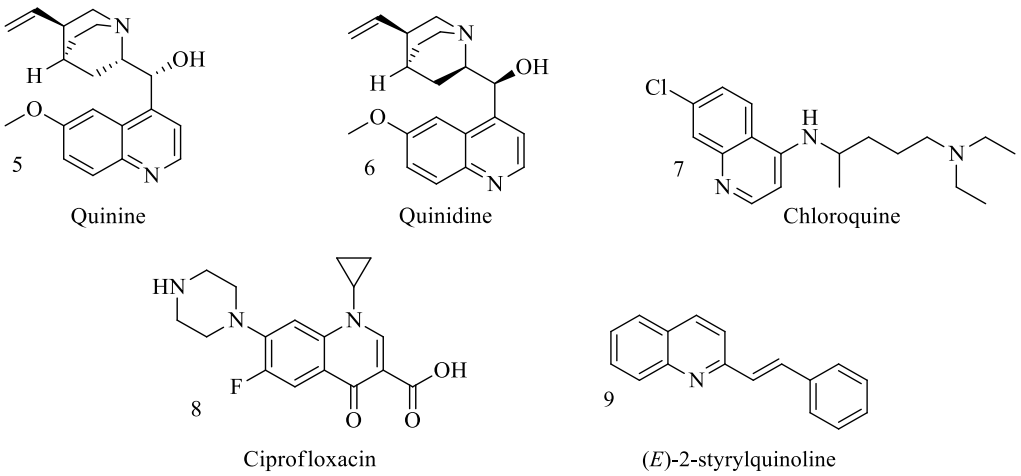

Scheme 3. Quinoline derivative drugs

Vilsmeier reagent (VR) is a versatile new synthesis of 2-chloroquinoline-3-carbaldehydes and also called (Chloromethylene)dimethyliminium chloride which is well known as a flexible synthetic tool for the formylation of electron-rich aromatics, chlorination of alcohols, conversion of carboxylic acid into the corresponding acid chloride [110, 111]. Typical preparation methods of VR are by the treatment of N,N-dimethylformamide (DMF) with chlorinating agents such as phosphoryl trichloride, thionyl chloride, phosgene, or phosphorus oxychloride [11, 34, 101, 102, 112]. Those chlorinating agents are not suitable though for large scale synthesis due to the expensive or hazardous nature of the reagents [113].

Vilsmeier reagents also find application in the synthesis of a number of heterocyclic compounds. Among these applications, the treatment of acetanilide and its activated analogs with dimethylformamide (2.5 mol equiv) in phosphors oxychloride (7 mol equiv) under

reflux in a drying tube fitted flask afforded quonoline-3-carbaldehyde in good yield (Scheme 4) [11, 34, 101, 102, 114]. Quinoline-3-carbaldehyde analogs demonstrated considerable biological and pharmacological activities as antimicrobial,[115] anti-inflammatory,[116] antimalarial [117] and antivirus activities[118].

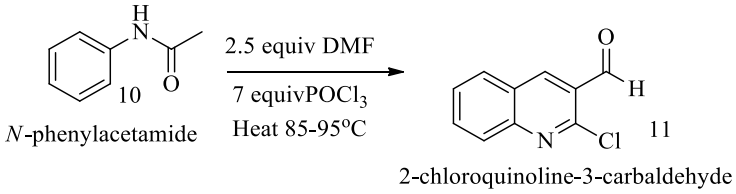

Scheme 4. Synthesis of 2-chloroquinoline-3-carbaldehyde [11, 34, 102, 119]

The main purpose of this work has updated knowledge for the scientists, chemists or researchers regarding the design and recent development of metal complex with quinoline derivative drugs like molecules hence the market has a lot of quinoline ring containing drugs [17, 101]. The frequency of infectious disease in humans has increased dramatically because of rising multidrug resistance. The rising clinical importance of drug-resistant bacterial pathogens has impelled additional exigency to investigate agents that are more effective. Therefore, searching for new antimicrobial agents with specific activity, possibly acting through mechanism, which are different from those of familiar classes is of main interest. The modification in the molecular structure of potential lead compounds is still an organized and ruler approach to widen the vicinity of antimicrobial medicine investigation. Among the ligand systems, quinoline derivatives are highly important because, these ligands developed due to their diverse chelating ability, structural flexibility and pharmacological activities.

Different review of literature indicates that quinoline-based derivatives scaffolds are known to exhibit excellent properties towards communicable and non-communicable disease. This broad spectrum of biological and biochemical activities has been further aided by the synthetic flexibility of quinoline derivatives which allows the generation of a large number of structurally diverse derivatives and their metal complexes [11, 34, 105, 120]. Ongoing search for natural products with potential biologically active ligands have confirmed that quinoline and its derivative (2-chloro-quinoline, 8-hydroxyquinoline and 2-chloroquinoline-3-carbaldehyde) (Scheme 5) ligands containing imine lie among one of an important class of biologically active ligands that attracted attention of chemists due to their extensive range of pharmacological properties and applications [34, 41, 43], such as anticancer [37–39, 101, 106, 121], antibacterial [11, 34, 38, 40, 102, 105], antifungal [8, 10], antiprotozoal [40], anti-

inflammatory [9, 11], antiviral [122], anti-diabetic [32], antituberculosis [123] and antioxidants [10, 11, 34].

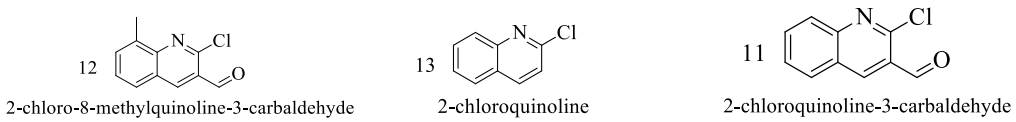

Scheme 5. Types of 2-chloroquinoline derivative

Among these, derivatives of 2-chloroquinoline-3-carbaldehyde having imine, have attracted attention of researchers due to their anticancer, antimicrobial, antifungal, antiprotozoal, antidiabetic and antioxidant activities [11, 34, 35, 102].

2. 2. Quinoline Based Transition Metal Complexes

The study of coordination compounds with biologically active metals and bioactive ligands (*N*-, *S*- and *O*- donor ligands) is at the forefront of the field of coordination chemistry [124]. One of the quinoline derivatives, 8-quinolinol (8-hydroxyquinoline, 8-HQ) and its derivatives like halogen derivatives, exhibit significant biological activities [125] and, it has been found that the activities of bioactive molecules (ligands) can be enhanced upon their coordination to different biologically active metals [126, 127].

Metal-based compounds are relatively uncommon drugs compared with organic compounds, having made their clinical entrance in 1978 with the endorsement of cisplatin, while some metal complexes are currently used in clinical applications such as anticancer therapies [128, 129]. In the last few decades, a renewed interest in metal-based therapy has been raised in fact, on coordination, not only bioactive ligands might improve their bioactivity profiles, but also inactive ligands may acquire pharmacological properties hence organic chemistry alone is not adequate to supply the world with new effective antimicrobial agents [130] to overcome antimicrobial resistance. In particular, recently, it is reported that quinoline derivatives and their metal complexes showed significant activity against the *Mycobacterium tuberculosis* strain, at low micro-molar levels [120].

Different researches' reports have witnessed in biological applications of metal coordination of biologically active ligands [3, 50, 72, 74, 120, 131, 132], in which, transition metal ions have the ability to switch between several oxidation states, due to the redox activity of metals and, therefore, a possible disturbance of the sensitive cellular redox homeostasis, a tight regulation of the metal and redox balance is crucial for health. In addition naturally occurring

coordination compounds with metal atoms in their centers have vital importance in biological systems, such as hemoglobin, chlorophyll and vitamin B-12 [133]. These natural complexes have shed light on the preparation of synthetic derivatives, thus new syntheses and their applications in various fields have gained importance. These coordination compounds are used in many areas such as biochemistry, pharmaceutical chemistry and dyes, in which their importance is increasing day by day. In addition coordination compounds are used in a large part of industrial areas due to their important roles in many enzyme reactions [134].

Since quinoline derivatives are a group of ligands which play an important role in the syntheses of biologically active coordination compounds, many chemists have been working on the syntheses of quinoline derivatives Schiff bases chelate complexes, since they could form complex structures with different metals in different oxidation states [135, 136]. The chelate complexes have been able to prepare by the presence of two or more vicinal coordinating groups in the Schiff base ligands. The ligands and metal ions used in the syntheses of the complex compounds play an important role in gaining different properties of these complexes [137–139]. Studies on transition metal complexes of Schiff bases have shown that the complexes can be used as catalysts like enzymes in many fields such as enzymatic and industrial applications. For this reason, these types of complexes and their applications have attracted much attention in recent years [140, 141]. In recent years, there are studies in the literature showing that some transition metal complexes carry oxidase, peroxidase and catalase-like activities [142, 143]. Examples include peroxidase-like activity of oxovanadium(IV) Schiff base complex, [144] and catechol oxidase mimetic properties of mononuclear copper complexes [145].

Researchers have prepared and characterized different metal complexes such as Co(III), Ni(II), Cu(I/II), Zn(II), Mn(II), Fe(II) and Ru(II) for the biological application [13, 146], accordingly, numerous complexes have been probed in quest of new developed inorganic drugs [3, 50, 72, 74, 120, 131, 132, 136]. Similarly, different current reviews provide insight into the interaction between the reactive oxygen species and the transition metals complexes [10, 45, 153, 154, 69, 101, 147–152]. These all studies were focused on a novel approach to design synthetic antioxidant metal-based compounds and to study their activities in the oxidation processes with heterocyclic organic ligands.

Coordination of halogen derivatives of 5-chloro-7-iodo-8-quinolinol (HCQ)), to copper(II) exhibit increased antimicrobial activity against gram-positive and gram-negative microorganisms [155] and increased antiproliferative effects [125].

Metal compounds have been used in medicine since ancient times. Nevertheless, organic drugs have traditionally dominated modern medicinal chemistry and pharmacology. Inorganic medicinal chemistry is a growing research area whose current development has been triggered by the unexpected discovery of the antitumor activity of cisplatin. This discipline exploits the singular properties of metal ions for designing metal compounds with therapeutic and diagnostic applications. Either coordination or organometallic chemistry offer wide possibilities to develop novel metal-based drugs bearing quite different mechanisms of action aiming at different targets. Most significant investigations on inorganic medicinal chemistry have been directed to the development of antitumor compounds of different metals (Pt, Ru, Sn, Ga, Au, Ti, Sn, among others) that could show improved therapeutic indexes and wider activity spectra [4, 17, 129, 156]. Different previous work, focused on the synthesis of 3*d* and 4*d* metals with 8-HQ derivatives simulating the structure of cisplatin or other platinum anticancer drugs and has shown that many of the prepared Pd(II) ionic compounds interact with DNA and exhibit more pronounced antitumor activity than cisplatin [157–159].

Many N, O-donor ligands form stable complexes with metal ions and a wide variety of such complexes have been investigated as cancer treatments. One of the most prominent examples is the Ga complex with its 8-hydroxyquinoline (8-HQ) ligands, which has been investigated in clinical studies and the use of privileged structures, or pharmacophores, is a well-known and effective approach in drug design and development [160]. 8-Hydroxyquinoline is one of the most common and versatile derivatives of the heterocyclic pharmacophore quinoline, which has been extensively studied and used as a privileged structure due to its broad range of bioactive properties, often due to the ability to coordinate naturally abundant metal ions such as copper, zinc and iron [126, 160].

Researcher also designed a novel series of organoplatinum(II) complexes with quinoline-coumarin derivatives and evaluated for the cytotoxic property. All the synthesized compounds evaluated against human lung adenocarcinoma cells and cervical carcinoma cells, by MTT assay *in vitro* and showed a potent antitumor effect *in vivo* [161]. Moreover, the presence of 3-(20-quinolyl)-6,8- dichloro-hydroxy-coumarin (H-QC5) ligand showed a

significant enhancement in the antineoplastic properties of the coumarin-modified organo-platinum(II) complexes [101].

Other researcher reported the synthesis of metal complexes with dianion of 8-hydroxy quinoline-5-sulphonic acid and the cytotoxicity activity was measured against a panel of cancer cell lines and investigated for antibacterial activity against 9-strains of pathogenic bacteria [162]. The result showed that the complex exhibited significant antifungal activity than reference drug fluconazole. In other way, researcher designed and synthesized the organometallic compounds (Ru, Os, Rh, Ir) bearing the quinolines motif. They had a promising antiproliferative activity with a lack of aqueous solubility. All the synthesized compounds investigated against many cancer cell lines by the sulforhodamine B cytotoxicity assay using cisplatin as the reference [163]. Other researcher also synthesized new quinoline derivatives with their Cu(II), Ni(II) and Co(II)] complexes. These were screened using the disc diffusion method against different strains of bacteria (*Bacillus subtilis* and *Escherichia coli*) and pathogenic strain of fungi (*Aspergillus fumigates)*. The drugs ampicillin and fluconazole were used as standard and methanol used as a negative control [3]. The synthesized compounds indicated that *in vitro* and *in silico* had a prospective view to be used as a drug and could be toxic. The series of quinoline-derivative coordination with Zn(II), Cu(II), Ru(II) were synthesized and evaluated for their antimicrobial activity [164, 165]. Therefore, antimicrobial studies had been performed by using *Escherichia coli, Pseudomonas aeruginosa* compared with the standard drug vancomycin and piperacillin of known concentration. The synthesis of quinoline-3-carbaldehyde with copper(II) complex derivatives and evaluated the cytotoxic effect against human cancer cell lines by using MTT assay and the complexes exhibited *in vitro* antitumor activity better than metal, free ligands using cisplatin as standard. All the synthesized compounds were tested by UV spectroscopy absorption and ethidium bromide competitive studies indicated the compounds interact with calf thymus DNA through intercalation and induced cell death by copper(II) complex [166].

The synthesis of Pd(II) complexes with 7-bromo-quinolin-8-ol derivatives and evaluated their biological properties as antimicrobial and antitumor activities. The *in vitro* studies performed against 9 strains of bacteria and 5 strains of fungi for antimicrobial activity [158]. The synthesis of copper(II) complexes with hydroxyquinoline-thiosemicarbazone derivatives was reported for the treatment of cancer and Alzheimer's diseases. In particular, the most active

Cu(II) complexes showed the inhibition, cell proliferation with lower IC_{50} values [101, 164, 167].

Development of a new chemotherapeutic Schiff bases and their metal complexes is now attracting the attention of medicinal chemists. This review compiles examples of the most promising applied Schiff bases and their complexes in different areas. Still there is need to explore the biological properties of these already synthesized transition metal complexes and to synthesize new complexes with more properties.

2.2. 1. Zinc(II) complexes

Zinc, as the second most abundant metal ion the human body, is an important bio essential trace element which has been recognized as a crucial element in a large number of proteins and enzymes after iron and has a major regulatory role in the metabolism of cells [54, 120, 168]. Zinc deficiency has been known to contribute much in multiple diseases, such as growth retardation, sexual impairment, malabsorption syndrome, sickle cell disease, chronic liver disease and diabetes [44–46]. Zinc being the most abundant metal ion in the human body, it is an important bio-essential trace element and also known to be a crucial element in a large number of proteins and enzymes. Zinc plays great roles in biological processes like gene expression, metabolism of cells, apoptosis, and it is responsible for some neurological disorders like Parkinson and Alzheimer diseases. Zinc is extensively used to treat children suffering from deadly diarrhea resulting in significant reduction of child mortality in many countries [169]. The role of zinc in nucleic acid chemistry is noteworthy since zinc(II) ions are the only metal ions able to facilitate the rewinding of molten DNA [123]. Zinc is an important trace element in human beings, and is participating in several biological processes in the form of complexes with proteins and nucleic acids. Moreover, Zn(II) ions are important for the expression of genetic information and structural maintenance of chromatin with numerous examples of Zn(II) complexes have been investigated for their significant antibacterial activity. Recently it is reported that quinoline derivative and their Zn(II) complexes showed significant activity against the *Mycobacterium tuberculosis* strain, at low micromolar levels [120, 123, 170].

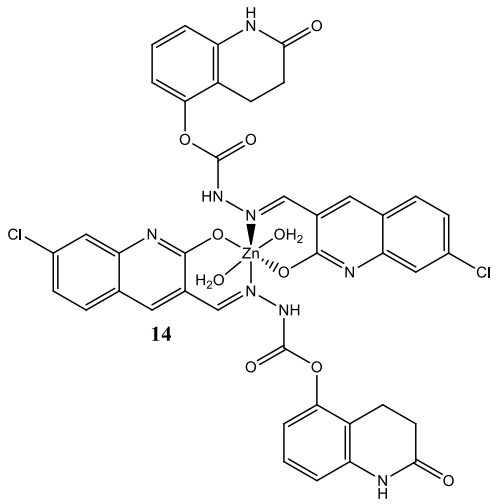

14

diaquabis((*E*)-2-oxo-1,2,3,4-tetrahydroquinolin-5-yl 2-((7-chloro-2-hydroxyquinolin-3-yl)methylene)hydrazinecarboxylate)Zn(II)

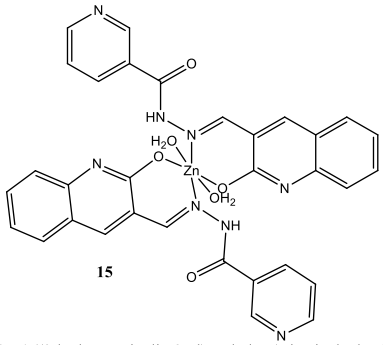

15

diaquabis((*E*)-*N*'-((2-hydroxyquinolin-3-yl)methylene)nicotinohydrazide)Zn(II)

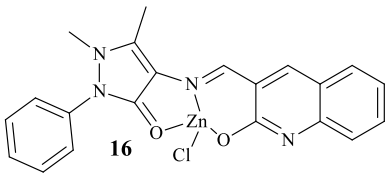

16

Chloro(*E*)-4-(((2-hydroxyquinolin-3-yl)methylene)amino)-1,5-dimethyl-2-phenyl-1*H*-pyrazol-3(2*H*)-oneZn(II)

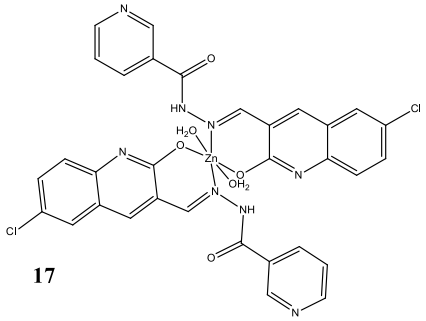

17

diaquabis((*E*)-*N*'-((6-chloro-2-hydroxyquinolin-3-yl)methylene)nicotinohydrazide)Zn(II)

Scheme 6. Zinc complexes of quinoline derivatives [19, 120, 123, 171]

Fluorescence properties of zinc(II) complexes, especially in the function of light-emitting materials (LEDs), have been intensively explored and the results indicate that the fluorescence intensity and properties of Zn(II) complexes are sensitive to the structure and donor acceptor potentials of the employed organic ligands as catalyst, and have been used in phenol oxidation [172], CO_2 fixation [173], and ring opening polymerization [54, 174]. In addition, there are various reports in literature that zinc complexes possess potential luminescent properties, optoelectronic light devices, enzyme inhibition, bio-imaging and antibacterial agents [123, 175].

The study accomplished on complex of Zn(II) and *in vitro* antimicrobial and antioxidant activities of quinoline derivative based ligands, reveals the synergistic effect of the ligands a promising one in the development of antimicrobial and antioxidant agents [176]. In addition Zinc(II) dichloride complexed with two quinoline-N-oxide molecules has luminescent properties, resulting in a stronger emission and significant quantum yield in comparison to more polar media [123, 177], this is due to having no empty d – orbitals [178]. Zinc(II)

complexes with one of quinoline derivatives called quinolin-8-ol have *in vitro* antimicrobial activity have better activity than the positive control and ligand and the antibacterial activity of all the tested complexes was better than their precursor ligand; hence, all complexes had better activity than positive control (fluconazole) [57].

Zinc complexes of quinoline derivatives bearing 3,4-dihydroquinolin-2(1H)-one demonstrated very good antituberculosis activity which is comparable to ‘‘first and second line’’ drugs used to treat tuberculosis (Scheme 6 (**14**)) [123]. The observed results of the test compounds indicate the future potential for the development of metal coordination complexes to solve the limitations due to currently existing anti-tuberculosis agents to treat multiple drug resistant Tuberculosis [120, 123, 124, 171]. In the literature zinc compounds have exhibited a potential biological activity with drugs being tested for the treatment of Alzheimer disease [179] and zinc(II) complexed with tolfenamato have antioxidant activities [123]. Similarly, complexes of zinc(II) with quinoline derivative have higher activity towards *Mycobacterium tuberculosis* than which is comparable to ‘‘first and second line” drugs used to treat tuberculosis [171].

Literature reports indicate that zinc based complexes have shown diverse medicinal applications such as antioxidant [49], antimicrobial [2, 48], anti-inflammatory, and anti-diabetic [6] activities. In addition, several zinc complexes are used as a major ingredient of the medicine used in the treatment of skin diseases and find significant use as a catalyst in various catalytic reactions [54]. The zinc complexes derived from Schiff bases are extensively studied due to their wide applications in material and biological science [180–182]. In addition, zinc(II) complex with slight distorted tetrahedral geometry derived from a bidentate Schiff base ligand could be a good candidate in treatment of inflammatory disorders [55, 183, 184]. Similarly, study indicated that zinc(II) complex, coordinating with macrocyclic ligands has more antibacterial activity than the standard antibiotics of neomycin and nitrofurantoin [180].

The antibacterial property of zinc ion is significantly enhanced upon complexation with ligand, particularly with nitrogen containing ligands [55, 175, 182, 184–186]. *In vitro* and *in silico* biological activity of five zinc(II) complexes with 3,5–dichloro–salicylaldehyde showed radical scavenging and bacterial activities than its free ligand. Similarly, these complexes are interacted with CT DNA via intercalation and bind tightly and reversibly to bovine and human serum albumin [187].

2.2. 2. Copper(II) complexes

Copper is an essential trace metal or as a constituent of various compounds in humans. It is bound to ligands of various types (ceruloplasmin, albumin, and other proteins) forming complexes that interact with biomolecules [188, 189]. Among the transition metal ions, Cu(II) is a biologically essential ion whose positive redox potential allows biological electron transfer reactions and several copper species showed a broad spectrum of activity with a low toxicity overcoming inherited and/or acquired resistance to platinum drugs [190]. These features are consistent with the hypothesis that copper complexes possess mechanisms of action different from platinum drugs that covalently bind to DNA and this study indicate that copper complexes exhibit ability to interact with DNA [190].

Copper(II) complexes containing heterocyclic hydrazones exhibited wide range of biological and pharmaceutical activities that includes DNA binding and cleavage, antimicrobial, anticancer and antioxidant behavior [41, 189]. According to the study copper complexes with imines have deserved much attention, probably because of their ability to intercalate between the bases of DNA and to participate in catalytic cycles with usual reducing and oxidizing agents in biological medium and Cu(II) is also involved in the causation and cure of cancer [41, 188, 189]. In addition, copper complexes derived from 4-aminoantipyrine derivatives act as more bactericidal and fungicidal agents as compared to the uncomplexed Schiff base ligand and the copper acetate from which they are derived. In addition, the synthesized complexes exhibit significant supper oxide dismutase (SOD) mimetic and reducing power activities [66].

Copper(II) complexes are known for their antimicrobial, anti-inflammatory/ antioxidant, DNA binding, and antiviral and anticancer activities [21, 22, 29, 43, 191]. Due to the fact that many cytotoxic drugs have undesirable side effects, the subject of study of many scientists is to find a substance that does not have such effects [192]. *In vitro* biological activity study of copper(II) complexes with NSAIDs and nicotinamide indicated that the complexes exhibit cytotoxic effects on lung carcinoma cells, DNA binding activities and may suggest the non-electrolytic nature (Λ_M = 7 – 9 S cm^2 mol^{-1}) of the complexes because the Λ_M value should be higher than 70 S cm^2 mol^{-1}) to be an electrolyte material [189, 193].

Copper ion, as the central atom of active site of various metalloprotein, plays an essential role in a number of widely differing biological processes like electron transfer, oxidation and dioxygen transport [194].

A number of Cu(II) chelate complexes that exhibit cytotoxic activity through cell apoptosis or enzyme inhibition have been reviewed [2]. Similarly Cu(II) chelates are potent antiproliferative agents, exhibiting strong cytotoxic effects comparable to that of adriamycin, standard by inducing cell cycle arrest and apoptosis. Their action may involve the inhibition of the enzyme topoisomerase II activity, by preventing dimer formation of the enzyme and its interaction with DNA [14, 21, 66, 176, 195]. The diverse biological activity of these complexes compared to one of the widely used platinum anticancer drugs cisplatin, indicates different mechanism(s) of action, which have not been yet resolved. It is likely that copper complexes interact with enzymes and inhibit vital cell functions, rather than interact with DNA and induce crosslinks [196].

Copper(II) complexes with a variety of aromatic molecules coordinated through N, and O donor atoms have been synthesized and tested for biological activity. The Cu(II) Schiff base complexes has been shown to exhibit polyphenol oxidase and peroxidase like activities [196]. It binds to bovine serum albumin causing site specific cleavage of the protein when the system is incubated in atmospheric conditions which takes place through binding and activation of molecular oxygen by the metal [197]. In such complexes, the metal is coordinated either to neutral heteroatomic molecules such as phenanthroline or to anionic organic ligands such as 8-hydroxyquinolinate, pyrrolidine dithiocarbamate, or (pyridine-2-ylmethylamino)methyl phenolate. It is noticeable that the free ligands themselves are not efficient inhibitors, and complex formation is necessary for the transportation of copper ions through the cell membrane, in order to achieve proteasome inhibition which seems to be the result of the increasing lipophilicity of the metal upon ligand coordination [14, 21, 66, 176, 195]. Distorted tetrahedral bis-(N,S) bidentate Schiff base complexes of Cu(II) interact strongly with CT-DNA by an intercalative mode and BSA confirmed that the complexes have a greater binding affinity via the static mode [197]. Copper(II) complexes of 2-oxo-1,2-dihydroquinoline-3-carbaldehyde (benzoyl) hydrazone exhibited effective cytotoxic activity against a panel of human cancer cell lines and antioxidant activities(scheme 7 (**19**)) [198].

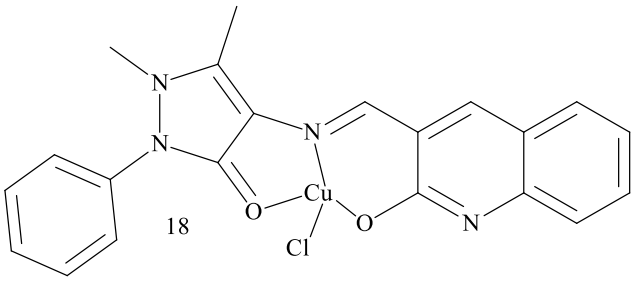

18

Chloro (*E*)-4-(((2-hydroxyquinolin-3-yl)methylene)amino)-1,5-dimethyl-2-phenyl-1*H*-pyrazol-3(2*H*)-oneCu(II)

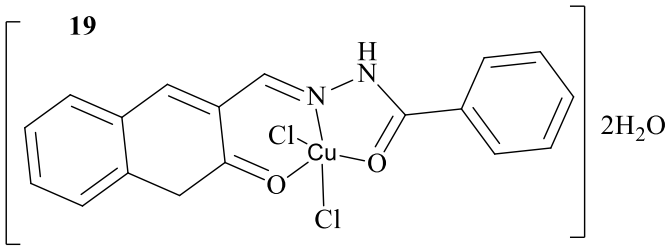

19

$2H_2O$

dichloro(*E*)-*N*'-((3-oxo-3,4-dihydronaphthalen-2-yl)methylene)benzohydrazideCu(II) hydrated

Scheme 7. Copper complexes of quinoline derivatives [3, 19]

2.2. 3. Nickel(II) complexes

Nickel metal concentrations in living things are low when compared with others (Zn, Cu and Fe). Nickel (Ni) is an essential trace element for bacteria, plants, animals and humans. Studies to investigate the biological functions of nickel have expanded dramatically following the discovery of nickel as an active site metal in the jack bean urease in 1975 and since then, the list of nickel-dependent enzymes has been significantly increased. A number of enzymes depend on nickel, including urease, NiFe hydrogenase, CO dehydrogenase, acetyl-CoA (acetyl coenzyme A) synthase, methyl-Coenzyme M reductase, glyoxalase I, and nickel containing superoxide dismutase and the role of nickel in bioinorganic chemistry has been rapidly expanded since the discovery [73, 199, 200]. In addition, a large number of nickel complexes of biological interest has been reported with the most structurally characterized acting as vitamins or showing anticancer, anticonvulsant, antiepileptic [76, 199, 201], antibacterial and fungicidal activity [73, 74]. The antimicrobial activity of the complexes has been tested against three microorganisms (*E. coli, P. aeruginosa* and *S. aureus*) and similarly, nickel(II) complexes with the antibacterial drug sparfloxacin exhibit good binding propensity to human and bovine serum albumin proteins having relatively high binding constant values [73].

Furthermore, different studies reported a number of nickel complexes bearing biological activity including antitumor [72], antibacterial [73], antifungal [74], anti-inflammatory/antioxidant [72], antileishmanian [75] and their interaction with DNA as intercalating [76, 77, 202]. More bioinorganic chemists were interested to the nickel compounds and reported the biological activity of Ni(II) complexes bearing the above mentioned biological importance [20, 29, 76, 202–204]. Recent research "evaluation of DNA binding and DNA cleavage of nickel(II) complexes with tridentate α-N-heterocyclic thiosemicarbazones ligands" showed that nickel(II) complexes are able to interact with DNA via intercalative mode with a moderate binding affinity [205].

Nickel-diflunisal complexes were tested for their activity to scavenge in vitro the DPPH, and hydroxyl radicals and were more active than free diflunisal ligand. Specially, the complexes are very active scavengers of hydroxyl and superoxide radicals. The interaction of the complexes with BSA and HSA was studied by fluorescence emission spectroscopy revealed the significant affinity of the complexes to the albumins [202].

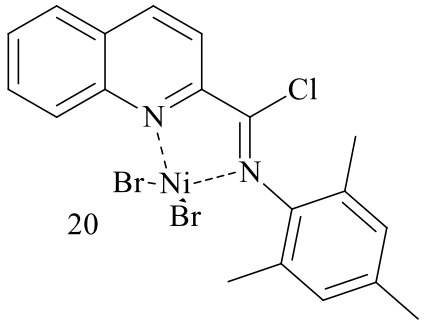

20

dibromo(*E*)-2,4,6-trimethyl-*N*-(1-(quinolin-2-yl)ethylidene)aniline)Ni(II)

Scheme 8. Nickel complexes of quinoline derivatives [206]

2.2. 4. Cobalt(II) complexes

The biological interest of cobalt is mainly focused on its presence in vitamin B12 and other proteins as well as in compounds showing biological activity [42, 133]. Being in the active center of vitamin B12, cobalt is indirectly involved in the DNA-synthesis. Furthermore, cobalt is used as a supplement of vitamin B12 and is related to at least different cobalt dependent proteins [203]. The first studies concerning the biological activity of cobalt compounds were reported in 1952 [207], since then, many structurally characterized cobalt compounds have been involved in the hydrolytic cleavage and binding of DNA [203] and have antimicrobial, antifungal, antiviral, antioxidant and antiproliferative agents [43, 68–71].

From the pharmacology point of view, cobalt complexes are noted for their significant biological properties, namely cobalt(II) complexes are known for their promising biological activity such as antimicrobial, anticancer, and antiviral activity [22, 28, 43, 68, 69, 72, 208]. The study performed on investigation of antioxidant activity of cobalt–quercetin complex shows that the complex has higher antioxidant activity as compared to the pure quercetin which suggests that the Co(II) ions significantly change the chemical properties of the quercetin [42]. The cobalt complexes have high tight binding affinity to BSA and HSA as revealed by the relatively high binding constants, which indicate their binding to SA and transfer towards their biological targets. The complexes were more active than the corresponding free ligand in regard to the ability to scavenge in vitro DPPH, and especially, hydroxyl and superoxide radicals [209].

Cobalt complexes of a Schiff base ligand containing mixed donors have attracted much attention because they have shown diverse coordination sphere and promising anticancer activity [210]. In particular, cobalt complexes bearing typical Schiff bases, incorporating with N'-((2Z, 3E)-3-(hydroxyimino)butan-2-ylidene)-2- phenyl acetohydrazide ligand was synthesized and showed impressive antimicrobial activity [69]. Similarly, cobalt-hydrazone complexes exhibit antimicrobial activities, in which the complexes act as more potent bactericidal agents than the hydrazone ligands and metal salt [211]. The anticancer properties of these compounds are also tested against colon carcinoma cells and breast carcinoma cells. The Co(II) complexes display more significant cytotoxic activities against these cells than those of the free ligands [211]. Two Co(II) complexes constructed from the aroylhydrazone ligand can effectively interact with BSA and change the secondary structure of BSA, and Superoxide dismutase (SOD) mimic activity of the complexes was investigated and the results showed that complex showed a stronger radical scavenging potency with an IC_{50} value of 16.10 μM [69]. Other recently reported cobalt(II) complexes that derived from 2-acetonaphthone benzoyl hydrazone and 2-acetonaphthone salicylylhydrazone Schiff bases showed DNA binding, protein binding, antioxidative and cytotoxic activities [69, 212]. Similarly, cobalt(II) complex constructed from the aroylhydrazone ligand indicated that the complexes can effectively interact with BSA and have Superoxide dismutase (SOD) mimic activity of the complexes in which complex showed a stronger radical scavenging potency against O_2^- radical [69].

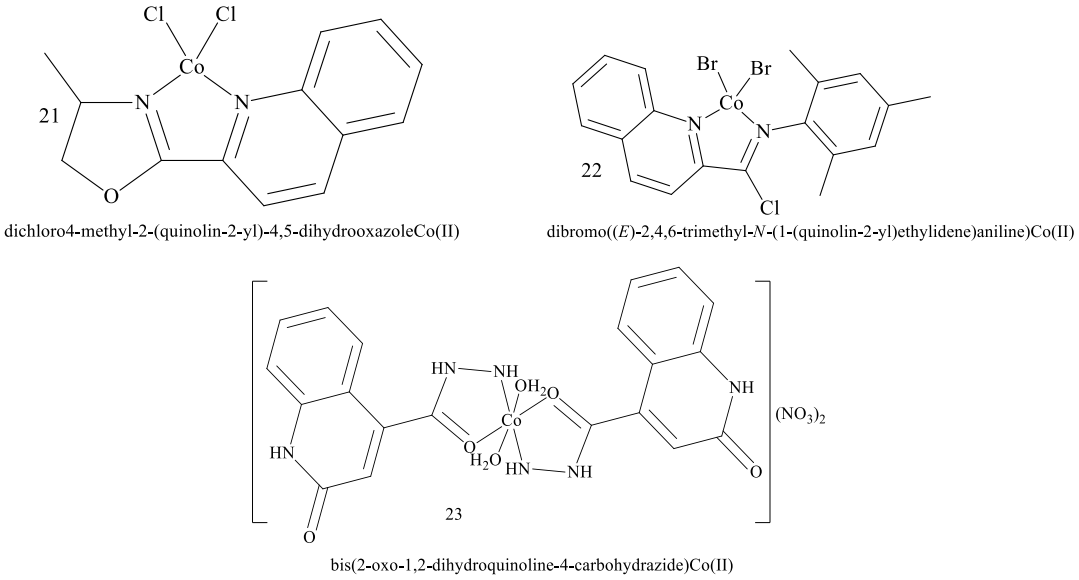

Scheme 9. Cobalt complexes of quinoline derivatives [70, 206]

2.2. 5. Vanadium(IV) complexes

Vanadium is a transition metal existing in oxidation states ranging from -3 to +5, showing interaction with biomolecules in its various forms [213]. Vanadium occurs in different oxidation states with the ability to participate in reactions involving the formation of free radicals. The most essential oxidation states of the vanadium complexes are V(III), V(IV), and V(V). The two most biologically and physiologically stable states are vanadium(IV) and vanadium(V) [214]. The importance of coordination chemistry of vanadium has attracted much attention in recent years and has witnessed the discovery of enzymatic and physiological activities of vanadium complexes. Vanadium complexes paid attention to the exploitation of diversity of the oxidation states and flexibility of change in the coordination sphere around the metal center [215]. Vanadium has a regulatory role in the biotic system: influences several important enzymes, and stimulates the studies on vanadium in many enzyme systems involving tyrosine kinase, phosphoribosyl phosphates, adenylate cyclase, and ribonuclease due to oxidation state in oxocomplexes so determined by the number of oxo groups that bind to centeral atom [216]. The current focus is to create pharmaceuticals that will take advantage of its insulin-mimetic anti-diabetic properties and treatment of tumors [217].

Vanadium is present in trace amounts as physiologically essential element with wonderful biological properties. There are suggestions that vanadium plays important roles in cells such

as regulation of phosphoryl transfer enzymes and cell's redox potential [218]. Pharmacologically, vanadium compounds with oxidation states +4 (IV) and +5 (V) have demonstrated anti-diabetic and anticarcinogenic effects in humans [219, 220]. Considering the biological properties of vanadium and the antimicrobial activities of thiourea derivatives, it can be concluded that the combination of them can lead to the generation of novel improved antimicrobial agents.

Generally, high oxidation states of vanadium complexes(V(V) and V(IV)), with organic ligands as prodrugs have shown insulin mimetic activity [219]. In spite of extensive investigations on insulin-enhancing properties and anti-diabetic effects of vanadium compounds, a few researchers have studied antimicrobial activity of vanadium complexes, particularly, with different ligands [217, 221–224]. Considering the antibacterial activities of these compounds [214], recently many researchers have been concentrating on the coordination chemistry of vanadium complexes [153] with well-established different chemical and biological functions. Vanadium plays a central role in a variety of biochemical processes, such as phosphorylation [217, 225] glycogen metabolism [217], insulin mimicking [217] and in anti-parasitic agents [217, 226]. In other case, study accomplished on an antioxidant activity of V(IV), Mo(VI)/(IV) and Ru(II) complexes indicate that the scavenging activity of the complexes towards DPPH is high for the oxovanadium(IV) complexes with lower IC_{50} values which are comparable to ascorbic acid as a standard antioxidant [227]. In addition, vanadium compounds have been shown to exhibit several biological effects, may act as phosphatase inhibitors [148, 217, 225] displaying insulin-like effects. Oxovanadium complexes with quinoline and pyridinone ligands showed the strongest antiproliferative activity, which is comparable potent with cisplatin [60]. On the other hand, the study performed on oxovanadium(IV) complex of 8-hydroxy quinoline and 3-acetyl-6-methyl-2H-pyran-2,4(3H)-dione have shown satisfactory bacterial activity against *S .pyogenes* [61], and other vanadium(IV) complexes showed that good antioxidant, antibacterial, antifungal activities and strong interaction binding with DNA [228].

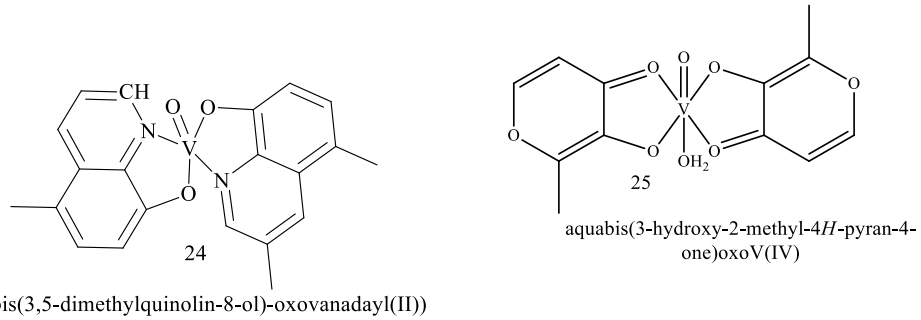

Scheme 10. Vanadium complexes of quinoline derivatives [60, 217]

In view of this, the researcher focused on the synthesis, characterization antibacterial and antioxidant activity of two novel quinoline derivatives and their oxidovanadium(IV) complexes. The antibacterial properties of all compounds were screened in vitro against two standard Gram-positive (*Staphylococcus aureus and Enterococcus faecalis*) and two standard Gram-negative (*Escherichia coli* and *Pseudomonas aeruginosa*) bacterial strains. Theoretical calculations show that the antibacterial activities of thiourea ligands and their oxidovanadium(IV) complexes have some relation with the LUMO energy and the difference between LUMO and HOMO energies. The results of antibacterial experiments show that both the synthesized compounds have good ability to inhibit growth of the bacteria.

2.3. Biological application of Transition Metal Complexes

2.3.1. Antimicrobial activity of Transition Metal Complexes

Microbial infections are one of the leading diseases which are responsible for millions of deaths every year because of lack of effective antimicrobial therapy and this situation becomes more complicated because of microbial resistance towards conventional antibiotics [229]. Occurrence of the antibiotic resistance pathogen has become a severe health issue and thus, numerous studies have been stated to improve the current antimicrobial therapies. It is known that over 70% of bacterial infections are resistant to one or more of the antibiotics that are generally used to eradicate the infection [230]. As mentioned above quinoline and its derivatives are an important class of heterocyclic compounds found in many synthetic and natural products with a wide range of pharmacological activities such as anticancer [39, 231, 232], antimicrobial [11, 17, 34, 102], antifungal and antiprotozoal [8], anti-inflammatory [9], antidiabetic [7] and antioxidant [10, 11, 17, 34, 102] activities. The use of antibiotics has significantly improved public health worldwide. However, due to the improper use of antibiotics in daily life, bacteria develop drug resistance quickly to most of the antibiotics.

This may imply that the battle against bacterial infections is endless [233, 234]. These days, the issue of antimicrobial resistance is critical and becomes a worldwide problem. The bacteria, methicillin-resistant *Staphylococcus aureus* (MRSA) and vancomycin resistant *Enterococcus faecium* (VREF), are resistant to the clinically used antibiotics such as methicillin and vancomycin [234]. Considering the fast emergence of drug-resistant bacteria and limited clinically used antibiotic treatment options, developing another strategy to fight against bacterial infections is therefore urgently needed. Therefore, quinoline derivatives have been the target of synthetic investigations. Accordingly, several thousand quinoline derivatives are known and many of these have important pharmacological activity but still, there is a demand for general strategies that can efficiently provide variously substituted and functionalized quinoline [11, 232]. Furthermore, some quinoline and its derivatives such as serotonin and melatonin influence many important biochemical processes. They act as antioxidants and play an important role in the human immune system [10, 11]. Therefore searching novel and effective antimicrobial agent is important to overcome this problem, accordingly, metal complexes of Schiff base derived organic ligand (HL) and Fe(III), Co(II), Cu(II), Zn(II) and UO_2(II) showed a good antibacterial activity against *Escherichia coli*, *Pseudomonas aeruginosa* and *Staphylococcus pyogenes* [1, 14, 20–23]. Similarly, *in vitro* antimicrobial and antioxidant activities of Co(II), Ni(II), Cu(II) and Zn(II) complexes of bisphenolic mannich base and 8-hydroxyquinoline based mixed ligands were screened by disc diffusion method and showed antibacterial activity order as: Cu(II) > Co(II) > Ni(II) > Zn(II) > Ligand [14].

Similarly, a series of new two different iron(II) Schiff base amino acid complexes derived from condensation of 5-bromosalicylaldehyde (bs) and a-amino acids (L-alanine (ala), L-phenylalanine (phala), L-aspartic acid (aspa), L-histidine (his) and L-arginine (arg)) have been synthesized and the structure of the investigated iron(II) complexes was elucidated using elemental analyses, infrared, ultraviolet visible, thermogravimetric analysis, mass spectroscopy as well as conductivity and magnetic susceptibility measurements. Moreover, the prepared compounds are screened for their *in vitro* antibacterial activity against two Gram-negative (*Escherichia coli, Pseudomonas aeruginosa*) and one Gram-positive (*Bacillus cereus*) bacterial strains and antifungal activities against three fungal cultures (*Penicillium purpurogenium, Aspergillus flavus, Trichotheium rosium*) using disk diffusion method [235] and the results indicated that the complexes shows enhanced microbial activities compared with parent ligand.

In addition, Schiff bases and their Cu(II) complexes were tested *in vitro* for their antibacterial activity against two Gram-Positive bacteria (*Micrococcus luteus* and *B. cereus*) and one Gram negative bacteria (*P. aeruginosa*). All the complexes showed activity against the organisms more than the free ligands and the activity increases with the increase in concentration of test solution containing the new complexes [14, 21, 176]. The activity data show that the metal complexes have a promising biological activity comparable with the parent Schiff base ligand against bacterial species [22, 236].

Therefore, it has been found interesting to study the structural property and biological activity of metal complexes containing the quinoline moiety. On the other hand, the ligand derived from 2-chloroquinoline-3-carbaldehyde form stable complexes with metal ions due to the presence of a phenolic hydroxyl group, which coordinates to the metal ion *via* deprotonation.

For the evaluation of the antibacterial potential of a given compounds, it is preferred to test them against several targets, because each of them has cell structures and a particular metabolism. The sensitivity of the strains to the different compounds was classified according to the diameter of the zone of inhibition as mentioned in the previous study [237]. Diameter less than 8 mm: not sensitive; Diameter from 9 − 14 mm: sensitive; Diameter from 15 − 19 mm: very sensitive; Diameter more than 20 mm: extremely sensitive [237]. The results reveal variable responses depending on the strain and the concentration of the compound tested. According to the results of study on nickel(II), copper(II) and zinc(II) complexes containing ONNO donor atoms Schiff base ligands showed that, all complexes have highest zone of inhibition against all the tested strains [21]. It was observed that the antibacterial activity of these compounds has high effect on the Gram-negative bacterium *S. aureus* and *B. cereus*, that was extremely sensitive 50 μg/mL (above 20 mm), Gram-positive bacteria *E. coli* and *P. aeruginosa are* less sensitive to these compounds [21, 237].

The results of previously reported studies indicated that all metal complexes have higher antimicrobial activities than the parent ligand. This higher activity of the metal complexes may be owing to the effect of metal ions on the normal cell membrane. Metal chelates bear polar and nonpolar properties together; this makes them suitable for permeation to the cells and tissues. In addition, chelation may enhance or suppress the biochemical potential of bioactive organic species [14, 21, 66, 176, 195]. The character of the metal ion coordinated to ligand may have its own role to such difference, in addition to, the chelation which considerably increases the lipophilic character of the central metal ion, because of the partial

sharing of its positive charge with the donor groups and possible π-electron delocalization over the chelate ring. This favours the permeation through the lipid layer of cell membrane. The increased liposolubility of the ligand up on metal chelation may contribute to its facile transport into the bacterial cell which blocks the metal binding sites in enzyme of microorganisms [56, 120, 123, 124, 171, 176]. In general the studies indicated that for metal complexes showing antimicrobial activity, the following five principal factors should be considered: (i) the chelate effect; (ii) the nature of the ligands; (iii) the total charge of the complex; and (iv) the nature of the ion neutralizing the ionic complex [56, 120, 123, 124, 171, 235].

2.3.2. Antioxidant activity of Transition Metal Complexes

2.3.2.1. DPPH (1, 1-Diphenyl-2-Picrylhydrazyl) radical scavenging activity

Free radicals are inevitably produced in biological systems and also encountered exogenously, and are known to cause various degenerative disorders, like mutagenesis, carcinogenesis, cardiovascular disturbances and ageing [24, 25, 232, 238]. Antioxidants are the compounds, which combat the free radicals by intervening at any one of the three major steps of the free radical mediated oxidative process, initiation, propagation and termination and these antioxidants are also produced by biological system and occur naturally in many foods and the balance between oxidants and antioxidants decides the health and vigor [239]. In biological systems such as cells, tissues and bio-molecules, antioxidants prevent oxidative damage by acting as scavengers to reactive oxygen species (ROS) [240]. Vitamin C and vitamin E are well known non-enzymatic antioxidants within normal cells that interact directly with radicals such as hydroxyl and peroxyl intermediates and help to minimize the consequences of lipid peroxidation in membranes. Natural antioxidants are more suitable compared to synthetic antioxidants. However, natural antioxidants have their own merits and demerits such as a lack of water solubility and average antioxidant activity. Most antioxidants are lipid-soluble with a lower absorption capacity, such as vitamin E, carotenoids, and lipoic acid. Many synthetic antioxidants that have been developed recently exhibit good antioxidant properties [241] hence synthetic antioxidants are widely used because they are effective and cheaper than natural antioxidants.

The search for metal-derived antioxidants has received much attention and effort in order to identify the compounds having high capacity in scavenging free radicals related to various disorders and diseases associated with oxidative damage, caused by reactive oxygen species

(ROS). Currently a number of Schiff-base metal complexes have been investigated as effective scavengers of ROS, acting as antioxidants. Methods for antioxidant activity determination, thus it is important to know the antioxidant content and their efficacy in foods, for preservation or protection against oxidative damage, to avoid deleterious changes and loss of commercial and nutritional value [239]. This necessitates the development of a rapid method for determining the potential antioxidant capacity in various foods.

1, 1-Diphenyl-2-Picrylhydrazyl (DPPH; $C_{18}H_{12}N_5O_6$, M=394.33) assay method was developed by Blois (1958) with the viewpoint to determine the antioxidant activity. The assay is based on the measurement of the scavenging capacity of antioxidants towards it. The odd electron of nitrogen atom in DPPH is reduced by receiving a hydrogen atom from antioxidants to the corresponding hydrazine. DPPH is characterized as a stable free radical by virtue of the delocalization of the spare electron over the molecule as a whole (Scheme 11(**26**)), so that the molecules do not dimerize, like most other free radicals. The delocalization also gives rise to the deep violet color, with an absorption in ethanol solution at around 517 nm. On mixing DPPH solution with a substance that can donate a hydrogen atom, it gives rise to the reduced form with the loss of violet color [11, 22, 82, 241, 242]. While DPPH can accept an electron or hydrogen radical to become a stable, diamagnetic molecule, it can be oxidized only with difficulty, and then irreversibly. DPPH shows a strong absorption band at 517 nm due to its odd electron and solution appears a deep violet color, the absorption vanishes as the electron pairs off and the resulting de-colorization is stoichiometric with respect to the number of electrons taken up and it can also be used to quantify antioxidants in complex biological systems, for solid or liquid samples [14, 241].

The method is unique in carrying out the reaction of the sample with DPPH in methanol/water, which facilitates the extraction of antioxidant compounds from the sample. Determination of antioxidant activity of various types of foods using DPPH is comparable to other methods. Antioxidant analysis by other methods may be limited to those compounds soluble in the selected solvents. The advantage of this method is that DPPH is allowed to react with the whole sample and sufficient time given in the method allows DPPH to react slowly even with weak antioxidants [243].

DPPH assay is considered a valid accurate, easy and economic method to evaluate radical scavenging activity of antioxidants, since the radical compound is stable and need not be generated [11, 22, 82, 241, 242]. It considers not only the antioxidant concentration but also

the reaction time of scavenging reaction to reach the plateau. The antioxidant efficiency is measured at ambient temperature so that the risk of thermal degradation of the molecules tested is eliminated [11, 22, 82, 241, 242].

DPPH can only be soluble in organic solvent and the interference of absorbance from the sample compounds could be a problem for the quantitative analysis. It is a stable radical where the unpaired electron is located on nitrogen atom. One of the main applications of DPPH is its uses in the *in vitro* antioxidant assays and the compounds that can scavenge DPPH radicals are mainly related with anticancer, antiaging and anti-inflammatory activity involved in the protection from rheumatoid arthritis and inflammation [244]. DPPH radical scavenging activity assay is based on the measurement of the scavenging ability of antioxidants towards the stable radical (DPPH). The free radical DPPH˙(**26**) is reduced to the corresponding hydrazine (**28**) when it reacts with hydrogen donors (**27**) [245, 246]. Antioxidants react with free radicals by different mechanisms: hydrogen atom transfer (HAT) or single electron transfer mechanism (SET); or the combination of both HAT and SET mechanisms. The HAT reaction is a concerted movement of a proton and an electron in a single kinetic step, as shown in Scheme 11 [247].

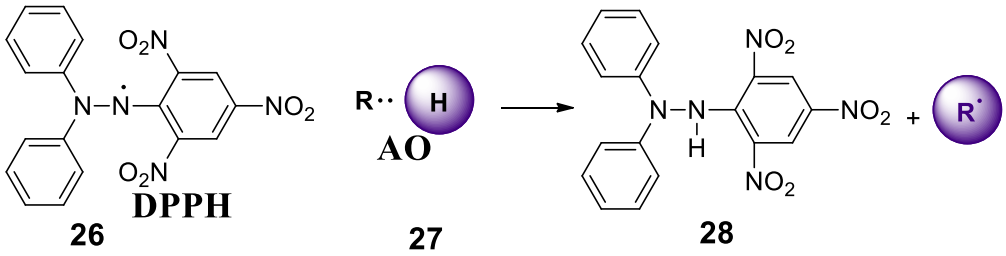

Scheme 11. Reaction mechanism of DPPH with antioxidant.

Scavenging the DPPH radical by antioxidant substances will result in a decrease in its absorption readings which is being proportional to the concentration of radicals that are being scavenged [17, 247]. The measurements are made using a UV-Visible spectrophotometer at room temperature and the scavenging capacity is reported as the percentage of DPPH radical inhibition (eq. 1).

$$\%\ \boldsymbol{DPPH}_{\boldsymbol{radical\ scavenging\ activity}} = \frac{\boldsymbol{A_C - A_S}}{\boldsymbol{A_C}}\ \boldsymbol{X\ 100} - - - - - - - - (\mathbf{1})$$

where A_C the absorbance of the control, and A_S is is the absorbance of the sample. Then % of inhibition was plotted against concentration. The half-maximal inhibitory concentration

(IC_{50}) could be calculated from this plot [17, 247, 248]**.** Generally, DPPH is a stable free radical that accepting hydrogen or electron from a corresponding donor, which causes it to lose the characteristic deep purple color [241, 242, 249].

2.3.2.2. ABTS (2,2-azinobiz-3-ethylbenthiazoline-6-sulfonic acid) radical cation scavenging activity

The basis of the ABTS assay is the interaction between an antioxidant and the pre-generated $ABTS^{\bullet+}$ radical cation. $ABTS^{\bullet+}$ scavenging can be easily quantitatively detected due to the bleaching of absorption spectrum characteristic maxima at 414, 417, 645, 734, and 815 nm (Scheme 12) [250]. The usually applied characteristic maxima to monitor are 414 – 417 nm and 730 – 734 nm; however, the latter is the recommended range due to the possible interference of many samples, which can be expected at lower wavelengths, resulting in the underestimated antioxidant capacity [250]. It is important to consider that $ABTS^{\bullet+}$ absorbance maximum bands shift a little in different solvents due to the solvatochromic effect: methanol (744 – 745 nm), ethanol (753 nm), and propanol (757 nm) [250]. The pH impacts the λ_{max} either, for example, in 0.1 M acetate buffer pH 5 a hypsochromic shift is observed with a maximum at 728 nm [40]. The commonly used end-points for $ABTS^{\bullet+}$ loss detection are 4 or 6 min. Usually, $ABTS^{\bullet+}$ is pre-generated a day before, by mixing the potassium persulfate (PP) and ABTS to stand overnight (for 12 – 16 h) (Scheme 12) [251]. PP stoichiometrically oxidizes ABTS (ABTS/PP ratio 2:1) to form $ABTS^{\bullet+}$, which can be easily observed by a color change from almost colorless to deep bluish-green (eq.2). The ABTS to $ABTS^{\bullet+}$ conversion degree under these conditions is approximately 60% [250, 252]. Generally, the characteristic color of ABTS radical cation is discolored from dark green to light green when the radical is bleached by antioxidants [250, 252].

$$ABTS + S_2O_8^{2-} \rightarrow ABTS^{\bullet+} + SO_4^{\bullet-} + SO_4^{2-}$$

$$ABTS + SO_4^{\bullet-} \rightarrow ABTS^{\bullet+} + SO_4^{2-}$$

The percentage of inhibition of ABTS oxidation was calculated using the following formula:

$$\boldsymbol{ABTS^{\cdot+}\ scavenging\ effect\%} = \left(\frac{A_{control} - A_{sample}}{A_{control}}\right) \boldsymbol{X\ 100} \quad (2)$$

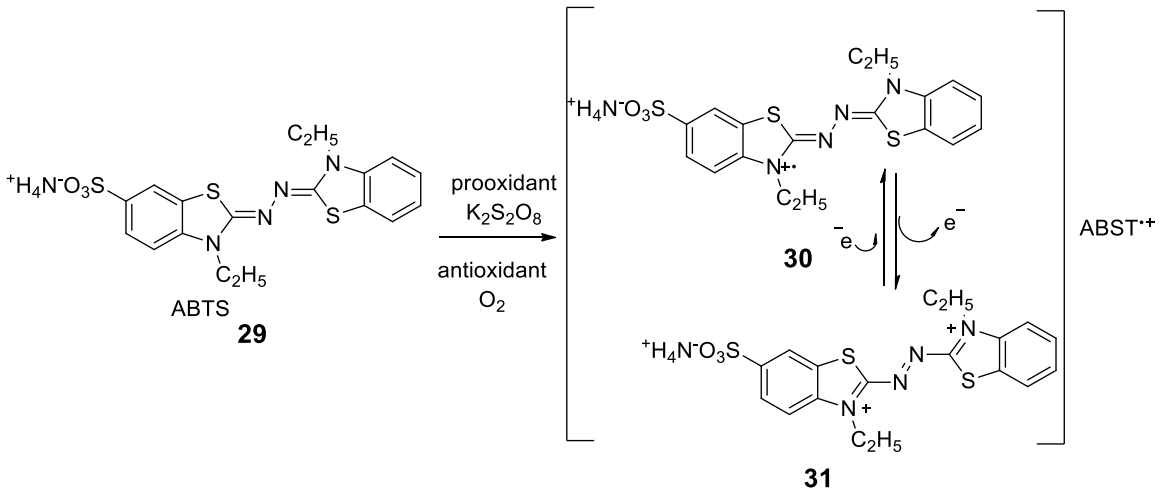

Scheme 12. Hypothetical structures and mechanisms involved in ABTS activation under pro-oxidant conditions and antioxidant scavenging action of oxygen

2.3.2.3. FRAP (Ferric Reducing Antioxidant Power) Assay

The FRAP assay is a relatively simple, quick, and inexpensive direct method of measuring the combined (total) antioxidant activity of reductive (electron donating) antioxidants in a test sample [253]. The assay uses the reduction of ferric ions (Fe^{3+}) to ferrous ions (Fe^{2+}) as the signal, or indicator reaction and this is tied to a color change [254, 255]. Ferric to ferrous ion reduction at low pH causes a colored ferrous-tripyridyltriazine complex [255]. FRAP values are obtained by comparing the absorbance change at 593 nm in test reaction mixtures with those containing ferrous ions in known concentration. Absorbance changes are linear over a wide concentration range with antioxidant mixtures, including plasm and with solutions containing one antioxidant in purified form [255]. Reagents are stable and of low toxicity, the sensitivity and precision of the method are high, stoichiometric factors of reacting antioxidants are constant over a wide range of concentrations, and the test is strong, in that small differences in reaction conditions do not markedly affect results [254]. The Fe^{3+} in the reaction mixture is in large excess, and is in the form of an aqueous ferric tripyridyltriazine (Fe^{3+}-TPTZ) salt solution. Therefore, the limiting factor in the reaction is the total, or combined, electron donating ability of reductive antioxidants in the sample added to the reaction mixture [254]. The ferric salt solution is a pale yellow color but when reduced to the ferrous form, this changes to blue, and absorbance at 593 nm increases. Reaction conditions (temperature, pH, reagent and sample volumes, reaction duration) are fixed, and the timed change in absorbance at 593 nm is transformed into total antioxidant activity by comparing the change in absorbance induced, under the same reaction conditions, by a known

concentration of Fe^{2+} added (as a measured aliquot of ferrous sulfate solution) to the reagents in place of sample. Results are expressed as the FRAP value expressed in µmol/L, calculated as follows (eq.3):[254, 256].

$$\frac{\textbf{Absorbance at 593nm of test sample reaction mixture}}{\textbf{absorbance at 593 of } Fe^{2+} \textbf{ standard reaction mixture}} \; \boldsymbol{X} \; Fe^{2+} \textbf{ concentration } \left(\frac{\mu g}{mL}\right) - (3)$$

2.3.2.4. Hydrogen peroxide (H_2O_2) radical scavenging activity.

The ability of a sample to scavenge hydrogen peroxide was determined according to the method developed by literature report [257]. A solution of hydrogen peroxide was prepared in phosphate buffer (pH 7.4). Samples (100 µg/mL) in distilled water were added to a hydrogen peroxide solution. Absorbance of hydrogen peroxide at 230 nm was determined 10 minutes later against a blank solution containing the phosphate buffer without hydrogen peroxide. The percentage of hydrogen peroxide scavenging of sample and standard compounds were calculated (eq.4) [258].

$$\%\, \textbf{Scavenged}\, [H_2O_2] = [\frac{A_C - A_S}{A_S}]\, \boldsymbol{X}\, \mathbf{100} - (4)$$

where A_C is the absorbance of the control and A_S is the absorbance in the presence of the sample or standards.

2.4. *In-silico* drug-likeness predictions

According to statistics, the success rate of candidate compounds found in preclinical detection is about 40%, while the rate of candidate compounds entering the market is only 10% due to their poor biopharmaceutical properties (poor chemical stability, poor solubility, poor permeability and poor metabolic) [259]. Thus, generating worthy computational methods for prediction of drug-likeness of bioactive molecule is very important to increase the success of drug discovery and development. According to previous study, [260] drug-like compounds are molecule which contain functional groups and/or have physical properties consistent with the majority of known drugs, and hence can be inferred as compounds which might be active biologically or might show therapeutic potential. Lipinski (2000) defines those compounds as ‘drug-like’, which have sufficiently acceptable ADMET (absorption, distribution, metabolism, excretion, and toxicity) properties to survive through the Phase I clinical trial [261]. The concept of drug-likeness, generated based the structural, physicochemical, biochemical, pharmacokinetic (PK), and toxicity characteristics of a

compound; thus, a drug-like compound possesses sufficiently acceptable ADME properties, as well as sufficiently acceptable toxicity properties [261, 262]. Currently there are various available online resources for drug-likeness prediction, including integrated databases, drug-likeness evaluating servers, and resources for drug-likeness based on natural products and special drugs.

Thus, understanding these properties has become an integral part of drug discovery and has enabled the accurate selections of hits that are suitable starting points for the identification of new clinical candidates [263]. Lipinski's Rule of 5 was developed to set 'drug ability' guidelines for New Molecular Entities (NMEs) [264]. The Lipinski "Rule of Five" states that compounds are likely to have good absorption and permeation in biological systems and are more likely to be successful drug candidates if they meet the following criteria:[265]: five or fewer hydrogen-bond donors (HBD), ten or fewer hydrogen-bond acceptors (HBA), molecular weight (MWt.) less than or equal to 500, and calculated logP (cLogP) less than or equal to 5 and topological polar surface area (TPSA) less or equal to 140 $Å^2$ to survive through the Phase I clinical trials which were considered drug-like [266]. As a guideline, the Lipinski's rule of five is conceptually simple and straightforward to implement, hence its widespread adoption. However, it does not apply to natural products or substrates of biological transporters [263]. Further research has added two more conditions. It has been reported that compounds with topological polar surface area (TPSA) of 140 $Å^2$ and above would be poorly absorbed (< 10% fractional absorption) and those with a TPSA 60 $Å^2$ would be well absorbed (> 90%) [79, 267] and <10 rotatable bonds (Rot B) which are correlated with drug permeability and flexibility, respectively [262].

2.5. Molecular docking

Molecular docking is one of the most frequently used methods in structure-based drug design, due to its ability to predict the binding-conformation of compounds to the appropriate target binding site [268]. Molecular docking assists in the process of computer-aided drug designing by considering every possible conformation of the protein and targeted molecules [268]**.** Molecular docking techniques aim to predict the best matching binding mode of a ligand to a macromolecular partner [269]. Ligand binding to macromolecules plays a key role in biology and medicine as guiding mechanism in biological processes. The binding of drugs to proteins and DNA has led to vast structural studies using both experimental and theoretical methods. Because of the major role of DNA in replication and transcription, DNA has been a major

target for antibiotic, anticancer and antiviral drugs [270]. Nucleic acid binding drugs are known for various diseases such as cancer, malaria, AIDS and other viral, bacterial and fungal infections [270]. The different modes of drug binding to DNA include intercalation between adjacent base pairs, intrusion into the minor groove and into the major groove. Intercalation and minor-groove binding are the predominant DNA-binding modes of small molecules [270].

Molecular docking or computer-simulated ligand binding is a powerful technique for investigating intermolecular interactions. It is an attractive scaffold to understand drug biomolecular interactions for the rational drug design and discovery, as well as in the mechanistic study by introducing a molecule (ligand) into the preferred binding site of the target specific region of the DNA/protein (receptor) mainly in a non-covalent fashion to form a stable complex of potential efficacy and more specificity. The information obtained from the docking technique can be used to suggest the binding energy, free energy and stability of complexes. At present, docking technique is utilized to predict the tentative binding parameters of ligand-receptor complex beforehand [271, 272].

3. MATERIALS AND METHODS

3.1. Chemicals and Reagents

The chemicals and reagents used for this study were acetic anhydride 99.8%, acetic acid glacial 99.5%, aniline 99%, zinc dust 95%, N, N- dimethyl formamide 99%, phosphorus oxychloride 98%, potassium dichromate 99.5%, acetone 99%, sulfuric acid 98%, methanol 99.5%, n-Hexane 99%, dichloromethane 98%, Ethyl acetate 99.5%, Chloroform 99%, Triethylamine 99%, cobalt chloride hexahydrate 98%, copper nitrate trihydrate 98%, nickel nitrate hexahydrate 98%, zinc chloride 98%, vanadyl sulphate 96%, silver nitrate 99.9%, L-Ascorbic acid 99%, Dimethyl sulphoxide 99% and 2, 2-diphenyl-1-picrylhydrazyl (DPPH). All these chemical and reagents were purchased from Loba chemie PVT. LtD (Mumbai, India) and all chemical reagents, including salts and solvents, were of analytical grade and used without further purification.

3.2. Instruments and Apparatus

The NMR spectra were obtained using NMR Bruker Avance 400 spectrometer operating at 400 MHz using DMSO-d6 and $CDCl_3$ as a solvent and chemical shifts (δ) were reported in ppm and the coupling constants (J) are reported in Hertz at department of chemistry, Addis Ababa University. Elemental compositions were analyzed using FESEM-EDX (CARL ZE 155, OXFORD instrument's EDX, USA) at Mangalore University India. Fluorescence spectra measurements were performed on Agilent: MY-18490002/PC spectrofluorophotometer at department of physics, Adama Science and Technology University. Mass spectra was recorded with SHIMADZU, LC-MS 8030 (model LCMS-8030, mass range *m/z* 10 to 2000, sensitivity ESI positive: 1 pg reserpine, S/N>3,000:1 (RMS), resolution R < 0.7 FWHM) at Mangalore University India. The UV-Visible spectral data were recorded on a (SM-1600 Spectrophotometer) at department of biology, Adama Science and Technology University, Powder XRD were recorded on X-ray diffractometer SHIMADZU ((model: XRD-7000 X-RAY DIFFRACTOMETER) at department of material science, Adama Science and Technology University, FTIR was recorded with Perkin-Elmer BX Spectrometer at department of Chemistry, Addis Ababa University. Thermogravimetric analyses (TGA) data were recorded using DTG-60H SHIMADZU thermal analyzer at department of Chemistry, Bahr Dar University. Molar conductances of the complexes were recorded at room temperature in methanolic solution of the samples, and melting point analysis was done using conductometre (AD8000: Resolution 0.1 mV (± 699.9 mV)/1 mV

(±2000 mV), 0.01, 0.1, 1 µS/cm; ppm, 0.01, 0.1 mS/cm; ppt 0.1°C, Accuracy: at 25 °C ± 0.2 mV up to ± 699.9 mV, ± 1 mV up to ± 2000 mV, ± 0.5 °C) and digital melting point (Hanchen digital auto melting point apparatus: model 934), respectively. Thin Layer Chromatography (TLC) was run on a 0.2 mm of silica gel GF254 (Merck) on aluminum plate and Spots were detected and visualized with 254 nm and 366 nm wavelength using UV light and at department of Chemistry, Adama Science and Technology University.

3.3. Synthesis of ligands

3.3.1. Synthesis of (*E*)-2-(((2-((2-hydroxyethyl)amino)quinolin-3-yl)methylene) amino)ethan-1-ol (**L1**)

The ligand (**L1**) [L1 = (*E*)-2-(((2-((2-hydroxyethyl)amino)quinolin-3-yl)methylene) amino)ethan-1-ol] was prepared based on the previous reported procedure [11], accordingly, 2-chloroquinoline-3-carbaldehyde (2.5 g, 0.013 mol) was added to 10 mL 2- aminoethan-1-ol in a 250 mL round-bottom flask and heated to 90 – 95 °C for 2 h in oil bath. The completion of the reaction was monitored by Thin Layer Chromatography (TLC). The resulting mixture was cooled to room temperature and added to 200 mL cold ice water. The precipitate was separated by suction filtration and washed with 400 mL ice cold water to remove the excess amount of ethanolamine which served both as solvent and reagent and then dried at room temperature [11, 34].

3.3.2. Synthesis of 2-((2-hydroxyethyl)amino)quinoline-3-carbaldehyde (L2)

The target ligand **(L2),** [L2 = 2-((2-hydroxyethyl)amino)quinoline-3-carbaldehyde] was synthesized based on the previous reported procedure [102] in which (*E*)-2-(((2-((2-hydroxyethyl)amino)quinolin-3-yl)methylene) amino)ethan-1-ol (2.5 g, 0.013 mol) was refluxed in 20% H_2SO_4 (10 mL) for 2 h. The accomplishment of the reaction was monitored by TLC and once the reaction was completed, the resulting product was cooled to room temperature and then put into 200 mL cold ice water and then the precipitate was separated using suction filtration and washed with 100 mL ice cold water [11, 34, 102].

3.4. Synthesis of transition metal complexes

All metal complexes were synthesised in methanolic solution in which complexes **1 – 5** and **6 – 10** were synthesised from **L1** and **L2** in 1:1 and 1:2 metal: ligand ratios respectively.

3.4.1. Synthesis of Zinc(II) complex (1)

Under constant stirring, a drop of triethylamine was added to 10 mL methanolic solution of **L1** (0.5 g, 1.93 mmol) in 250 mL two neck round bottom flask. After 30 min of stirring, methanollic solution (10 mL) of $ZnCl_2$ (0.13 g, 0.96 mmol) was added drop wise to stirred ligand solution, and then refluxed for 3 h at 80 ^oC under continuous stirring in water bath [43, 273]. The reaction was monitored by TLC [274]. Once the TLC results indicated the completion of the reaction, the mixture was cooled to room temperature and filtered, washed repeatedly using ice cold methanol to remove unreacted metal and ligand. The light yellow powder like product was obtained and the product was kept for five more days to dry before it was sent for analysis.

3.4.2. Synthesis of Copper(II) complex (2)

A methanollic solution (10 mL) of **L1** (0.25 g, 0.96 mmol) was mixed with a drop of triethylamine under constant string at room temperature. Then methanollic solution (10 mL) of $Cu(NO_3)_2 \cdot 3H_2O$ (0.232 g, 0.96 mmol) was added drop wise to the solution of the ligand under constant stirring and the resulting greenish solution was heated under reflux for 3.5 h at 80 ^oC. The reaction process is monitored using TLC and after completion of the reaction, the mixture was allowed to cool to room temperature. The resulting precipitate was filtered, washed with ice cold methanol to remove unreacted metal ion and ligand and deep green powder product was obtained [275]. Then the product was dried at room temperature for five days and kept for analysis.

3.4.3. Synthesis of Cobalt(II) complex (3)

Methanollic solution of the **L1** (0.5 g, 1.93 mmol) (10 mL) was mixed with a drop of triethylamine under constant string at room temperature then after 30 min the 10 mL of warm methanollic solution of cobalt chloride, $CoCl_2.6H_2O$ (0.228 g, 0.9 mmol) was added dropwise to the stirred solution of the ligand under constant stirring and refluxed for 3.5 h at 80 ^oC. The reaction process was monitored using TLC. After TLC results indicated, the completion of the reaction, the mixture was allowed to cool to room temperature. The resulting precipitate was filtered, washed with ice cold methanol to remove unreacted metal ion and ligand and a brownish purple powder product was observed and kept the filtrate under slow evaporation for about a week [69].

3.4.4. Synthesis of Nickel(II) complex (4)

Under constant stirring, a drop of triethylamine was added to the methanollic solution (10 mL) of **L1** (0.25 g, 0.96 mmol) in 250 mL two neck round bottom flask at room temperature. After 30 min of stirring, warm 20 mL methanollic solution of nickel nitrate hexahydrate $Ni(NO_3)_2.6H_2O$ (0.279 g, 0.96 mmol) was added dropwise to the solution of the ligand under constant stirring and the resulting green colour solution was refluxed for 3.5 h at 80 ^oC [276]. The reaction process was monitored using TLC [274]. After TLC results indicated the completion of the reaction, it was allowed to cool to room temperature and filtered off, washed with ice cold methanol, and dried at room temperature. Brownish red powder product was obtained on slow evaporation.

3.4.5. Synthesis of Vanadium(IV) complex (5)

Under constant stirring, a drop of triethylamine was added to the methanollic solution (10 mL) of **L1** (0.5 g, 1.93 mmol) in 250 mL two neck round bottom flask. After 30 min of stirring, warm methanollic solution (10 mL) of vanadyl sulfate (0.16 g, 0.96 mmol was added drop wise to it, under continuous stirring and then refluxed for 3.5 h at 80 ^oC under water bath [277, 278]. The reaction was monitored by TLC. After the completion, the reaction was allowed to cool to room temperature and filtered off, washed with ice cold methanol, and dried at room temperature and deep green powder product was obtained on slow evaporation [279].

3.4.6. Synthesis of Zinc(II) (6) and Copper(II) (7) Complexes

Under constant stirring, a drop of triethylamine was added to hot methanolic solution of **L2** (0.5 g, 2.3 mmol) (20 mL) in different two, 250 mL two neck round bottom flasks separately. After 30 min of stirring, methanollic solution of: $ZnCl_2$, (0.157g, 1.15 mmol, 20 mL) and $Cu(NO_3)_2 \cdot 3H_2O$ (0.278 g, 1.15 mmol, 20 mL), were added drop wise to the two flasks separately, under continuous stirring and then both the mixtures were refluxed for 4 h at 80 ^oC under water bath. Progress of the reaction was monitored by TLC and after the completion, the reaction mixtures were cooled to room temperature and then washed repeatedly using ice cold methanol to remove unreacted metal ion and ligand and then dried at room temperature [43, 273–275, 277–279].

3.4.7. Synthesis of Cobalt(II) (8), Nickel(II)(9) and Vanadium(IV)(10) complexes

Metal complexes were synthesised based on the previous report. Accordingly, at room temperature, a drop of triethylamine was added to methanolic solution of **L2** (1.00 g, 4.6 mmol, 25 mL) in different three, 250 mL two neck round bottom flasks. After 30 min of stirring, a warm methanollic solution of: $CoCl_2.6H_2O$ (0.55g, 25 mL, 2.3 mmol), $Ni(NO_3)_2.6H_2O$ (0.67 g, 25 mL, 2.3 mmol) and $VOSO_4$ (0.38 g, 25 mL, 2.3 mmol) were added drop wise to the flasks containing the solution of ligand separately, under continuous stirring, then all the three mixture were refluxed for 4 h at 80 ^oC under water bath. The progresses of reaction was monitored with TLC and after completion of the reaction, the mixtures were cooled to room temperature and filtered then washed repeatedly using cold absolute methanol to remove unreacted metal and ligand. The dried products were collected and kept for analysis [43, 274, 277–279].

3.5. Stability Constant and Thermodynamic parameters

The stoichiometric and formation constants or stabilities were recorded using Job's method, which is also known as continuous variation method. In this method, from transition metal salts of Zn(II), Cu(II), Co(II), Ni(II) and V(IV), the standard solution (1×10^{-5} M) were prepared and put into ten 50 mL volumetric flasks (0, 1, 2 . . . 10 mL) and similarly a solution of the ligands (10, 9, 8 . . . 0 mL) were prepared and added, respectively, in order to retain constant mole ratio and the absorbance were measured at λ_{max} (380, 406, 427, 401and 409 nm) and λ_{max} (393, 351, 407, 397 and 408 nm) at temperatures of 25, 30, 37 and 40 ^oC for Zn(II), Cu(II), Co(II), Ni(II) and V(IV) complexes, of both **L1** and **L2** respectively [280, 281]. The pH of the solution was adjusted with triethylamine. The stoichiometric calculations were made by varying the mole fraction of the metal ion and the ligand between 0 and 1 at constant total concentration and then the absorbance of the solutions of different composition were measured [280, 281]. The absorbance was then plotted against the mole fraction of the ligands and then “n”, the average bound ligands have been calculated from the abscissa of the maximum of the curve (X_{max}) using equation 5:

$$n = \frac{X_{max}}{1 - X_{max}} \quad \text{---------- (5)}$$

In addition, formation constants of the complexes were determined spectroscopically using, equation 6 [15].

$$K' = \frac{\left[{A_2}/{A_1}\right]}{\left[1 - {A_2}/{A_1}\right]\left[1 - {A_2}/{A_1}\right]} ----------------------- (6)$$

where, A_2 = absorbance at extrapolated point, A_1 = actual absorbance

Similarly, the thermodynamic parameters (ΔG, ΔH and ΔS) were evaluated, [280, 281] in which the changes in enthalpy and entropy (ΔH and ΔS) were determined from the slope and intercept of the lnK vs 1/T (van't Hoff) plot, respectively [42, 282]. The Gibbs free energies (ΔG) of the reactions were determined using equations 7 and 8 simultaneously.

$$\Delta G = \Delta H - T\Delta S \text{-- (7)}$$

$$\Delta G = -RT\ ln\ K \text{-- (8)}$$

3.6. *In silico* study of the ligands and their transition metal complexes

3.6.1. Drug likeness and ADME prediction

The drug likeness of ligand (**L1**) and its complexes (**1 – 5**) were recorded using SwissADME web tool. The Swiss Institute Bioinformatics (SIB) web tool (SwissADME) was used to convert the two dimensional structure into its simplified molecular input line entry system (SMILES) and then used to predict the *in silico* pharmacokinetic properties [283].

3.6.2. DFT calculations

Geometry optimizations of the ligands and their metal complexes (**1** – **10**) were performed using the Gaussian 16 program package [284] and the results were visualized using GaussView 06 and Chemcraft. The density functional theory (DFT) and time dependent density functional theory (TD-DFT) calculations were performed using the B3LYP hybrid functional [285–287] together with 6-311++G(d,p) basis set [288] for the light atoms and LanL2DZ basis sets for the metal atoms to account for relativistic effects. Grimme's dispersion correction [289] was employed to treat non-bonding interactions during the calculations. In order to mimic the experimental conditions, the polarizable continuum model in its integral equation formalism (IEF-PCM) [290] together with methanol solvent was employed to correct the solvent effects. The optimized geometries were confirmed to be real minima without any imaginary vibrational frequency by performing vibrational frequency calculations at the same level of theory. The Eigen values of highest occupied molecular orbital (HOMO) and lowest unoccupied molecular orbital (LUMO) were calculated and

visualized. Quantum chemical descriptors such as band gap energy ($E_g = E_{LUMO} - E_{HOMO}$), electronegativity ($\chi = -½ (E_{HOMO} + E_{LUMO})$), electronic chemical potential ($\mu = ½ (E_{HOMO} + E_{LUMO}) = -\chi$), global chemical hardness ($\eta = ½ (_{E}LUMO - E_{HOMO})$), global softness ($\sigma = 1/2\eta$), global electrophilicity index ($\omega = \mu^2/2\eta$), nucleophilicity index ($Nu = 1/\omega$), and dipole moment were calculated and analysed at the same level of theory [81].

3.6.3. Molecular Docking study of the Synthesized Compounds

The interaction and the binding affinity of the free ligands and their metal complexes **1** – **10** were performed using AutoDock 4.2 (MGL tools 1.5.7) with standard protocol [291], against the active sites of the proteins of *E. coli* DNA gyrase B (PDB ID: 6F86) and *P. aeruginosa* LasR (PDB ID: 2UV0). To study the interactions and binding affinity between the bacterial proteins and the targeted compounds in a 3D fashion, the compounds were docked within the binding site of the protein [11, 292, 293]. The chemical structures were prepared using Chem Draw 16.0 which was followed by the energy minimization by ChemBio3D. The energy minimized molecules were used as input file for AutoDock, to carry out the molecular docking simulation [291]. The crystal structure of the receptor molecules and crystal structure of DNA gyrase B (PDB ID: 6F86) and LasR Binding Domain (PDB: 2UV0) was downloaded from protein data bank [294]. The protein preparation was done using the reported standard protocol by removing the co-crystallized ligand, deleting water molecules, adding polar hydrogens and cofactors, then the target protein file was prepared by leaving the associated residue with protein by using Auto preparation of target protein file Auto Dock 4.2 (MGL tools1.5.7) [11, 291]. The grid box was constructed using 58, 58, and 40, pointing in x, y, and z directions, respectively, with a grid point spacing of 0.375 Å with the center grid box was 14.527, 56.689 and −5.122 Å. for both *E. coli* DNA gyrase B (PDB ID: 6F86) *P. aeruginosa* LasR (PDB ID: 2UV0). The best docked conformation between the compounds and the protein was explored with the docking algorithm provided with Auto Dock. During the docking process, a maximum of nine conformers were considered for each compounds. The conformations with the most favorable free binding energy were selected for analyzing the interactions between the target receptor and compounds by discovery studio visualizer. The ligands and their compounds are represented in different color, H-bonds (distance range 2 – 3.5 Å) and the interacting residues are represented in ball and stick model representation. The conformations with the lowest free binding energy were selected for analyzing the interactions between the target receptor and the compounds using PyMOL [11, 291, 295].

3.7. Biological Activity

3.7.1. Antibacterial activity of the ligands and their metal complexes

Antibacterial activity of the free ligands and their complexes were examined using paper disc diffusion technique in which two Gram-positive bacteria (*Staphylococcus aureus,* ATCC25923, and *Streptococcus pyogenes,* ATCC19615 and two Gram-negative bacteria (*Escherichia coli,* ATCC 25922, and *Pseudomonas aeruginosa,* ATCC 27853) were used to examine their activity. The medium was prepared from molten nutrient and Mueller–Hinton agar. Ciprofloxacin and dimethyl sulfoxide were used as positive and negative controls, respectively. The different concentrations were prepared for both first and second five metal complexes based biological activities of ligands, accordingly, the bacterial strains were tested with 150 and 300 μg/mL concentrations for **1 – 5** and 100 and 200 μg/mL for **6 – 10** concentration using paper disc-diffusion technique. In the process, each of the compounds were dissolved in DMSO and 6 mm diameter Whatman filter paper discs were soaked in 1mL solution of the above four concentrations. Then these saturated paper discs were inoculated at the centre of Petri dish having bacterial lawn in triplicate. The plates were incubated at 37 °C for 48 h, and then inhibition zone was determined by measuring the diameter of the inhibition zone [11, 34]. The bacterial activities of the synthesized complexes were also confirmed by calculating percent activity index (AI), [22] equation 9.

$$\%\ Activity\ index\ (AI) = \frac{Mean\ inhibition\ zone\ \ of\ compounds}{Mean\ \ inhibition\ zone\ of\ standard} \times 100 - - - (9)$$

Besides the disc diffusion method, the minimum inhibitory concentration (MIC) values for the investigated complexes were determined by agar dilution assay method against all of bacterial strains as reported [15, 18]. Bacterial suspension was prepared by inoculated nutrient broth with a loopful of the bacterial culture from the slant and incubated at 37 ± 1°C for 24 h. A few mL of the above bacterial suspensions (24-h broth cultures) of each strain was added to 20 mL fresh broth until the final inoculum concentration is closely approximates to 5×10^5 CFU/mL(colony-forming unit per milliliter) and a two-fold serial dilution method was followed [19, 296–298]. The complexes were dissolved in water separately to a concentration of 2.5 mg/mL solution. A 0.2 mL solution of the complex was added to 1.8 mL of the seeded broth to form the first dilution in each case (250 μg/mL concentration). Then, ten various dilutions were prepared for each complex by diluting 1 mL of this dilution with further 1 mL of the seeded broth to produce the second dilution. The

process was repeated until the tenth dilution generating a concentration of 250.00, 125.00, 62.50, 31.25, 15.63, 7.81, 3.91, 1.95, and 0.98, 0.49 µg/mL respectively. A positive control was prepared using ciprofloxacin in the same concentration as the complexes against all of the four bacterial strains. A set of tubes containing only seeded broth and suitable solvent were kept for negative control. After incubation for 24 h at 37 ± 1°C, the last tube with no visible growth of the microorganism was taken to represent the minimum inhibitory concentration (MIC) of the complexes in each strain. All experiments were performed in triplicate and the mean of the triplicates were reported [19, 296, 297].

3.7.2. Antioxidant activity of the ligands and their metal complexes

The antioxidant studies of the free ligands and their transition metal complexes were performed using a 2,2-diphenyl-1-picrylhydrazyl (DPPH) assay as this free radical scavenging assay is a quick and effective method to examine the antioxidant activity of potential antioxidants [241, 249]. Different concentration of the sample compounds (5, 10, 25, 40, 55, 70, 85, 100 and 115 µg/mL) for complexes **1** – **5**, (1.56, 3.13, 6.25, 12.50, 25.00, 50.00, 100.00 and 200.00 µg/mL) for complexes **6** – **10** were prepared. The concentration (4 × 10^{-3}%) of the DPPH solution was prepared. In the experimental process, 2 mL of this solution was added into each 2 mL samples of the synthesized compounds in methanol and the control was prepared by adding 2 mL of the DPPH solution to 2 mL of methanol, while 4 mL methanol was used as a blank. The results were shaken vigorously and allowed to stand at 37 °C in dark incubator (Labfreez: TSI-200) for 30 min and absorbance was recorded at 517 nm using double beam UV-Vis spectrophotometer, then the quenching of the absorbance at 517 nm of the DPPH radical was examined at constant time of 30 min and ascorbic acid was used as a positive control [11, 34, 241, 249, 299]. All the activities were performed in triplicate and the average absorbance was taken for calculating the percentage of inhibition using equation 1 (see section 2.3.2.1).

3.8. Statistical Analysis

The antibacterial data analyses generated by triplicate measurements were reported as mean plus standard deviation. GraphPad Prism version 5.00 for Windows was used to perform the Analysis (GraphPad Software, San Diego California USA) [300]. Groups were analyzed for significant differences using a linear model of variance analysis (ANOVA) test for comparisons with significance accepted for $p < 0.05$ (Appendix 1 and 2).

4. RESULTS AND DISCUSSION

4.1. Synthesis of ligands and their transition metal complexes

The preparation of ligands and their all metal complexes were performed following established procedure presented in Section 3.3 and 3.4.1–3.4.7 respectively. The first ligand (**L1**), (*E*)-2-(((2-((2-hydroxyethyl)amino)quinolin-3-yl)methylene)amino)ethan-1-ol was prepared from 2-chloroquinoline-3-carbaldehyde in good yield (See Table 1). The complexes (**1 – 5**) were then synthesized in 1:1 metal: Ligand [**M:L1**] ratio. The second ligand (**L2**) (2-hydroxyethyl)amino)quinoline-3-carbaldehyde was prepared from the first ligand (**L1**) and five (**6** – **10**) novel complexes were synthesised in 1:2 metal : Ligand [**M:L2**] ratio with metal salts of zinc chloride, copper nitrate trihydrate, cobalt chloride hexahydrate, nickel nitrate hexahydrate and vanadyl sulphate. The physicochemical properties of the aforementioned ligands and their metal complexes are summarized in Table 1.

Table 1. Physicochemical properties of ligands and their transition metal complexes

Compounds	**Colour**	**Yield (%)**	**Melting point (^{o}C)**	**Conductivity (Ω^{-1}mol^{-1} cm^{2}.25 ^{o}C)**
$C_{14}H_{17}N_3O_2$ **(L1)**	Yellow	(2.91 g) 86	80 – 85	-
[Zn(H_2L)Cl] **(1)**	Light yellow	(0.25 g) 63	225 – 230	7.21 ± 0.15
[Cu(H_2L)(H_2O)(NO_3)] **(2)**	Deep green	(0.24 g) 62	195 – 200	18.57 ± 0.35
[Co(H_2L)Cl)($H_2O)_2$] **(3)**	Brownish purple	(0.25 g) 63	215 – 220	8.47 ± 0.25
[Ni(H_2L)(NO_3)]. 2H_2O **(4)**	Reddish brown	(0.26 g) 66	115 –120	15.07 ± 0.43
[V(O)(H_2L)(H_2O)(SO_4)] **(5)**	Deep green	(0.19 g) 59	205 – 210	13.20 ± 0.29
$C_{12}H_{12}N_2O_2$ (**L2**)	Yellow	(3.50 g) 88	-	-
[Zn($HL)_2$] (**6**)	Yellowish white	(0.41 g) 72	290 – 295	19.82 ± 0.48
[Cu($HL)_2$($H_2O)_2$] (**7**)	Deep green	(0.39 g) 64	260 – 265	21.47 ± 0.50
[Co($HL)_2$)($H_2O)_2$] **(8)**	Brownish red	(0.46 g) 76	285 – 290	18.60 ± 0.61
[Ni($HL)_2$($H_2O)_2$] **(9)**	Brick red	(0.39 g) 65	270 – 275	18.49 ± 0.40
[V($HL)_2$(O)(H_2O)] **(10)**	Deep green	(0.32 g) 56	265 – 270	15.07 ± 0.41

Note: [$C_{14}H_{17}N_3O_2$ (Ligand**1** = **L1**) = **H_3L**], [**H_2L**=deprotonated ligand**1**]

[$C_{12}H_{12}N_2O_2$ (Ligand**2** = **L2**) = **H_2L**], [**HL** = deprotonated ligand**2**]

4.1.1. Ligand 1 (L1)

The schematic representation for the synthesis and proposed mechanisms of **L1** is presented in scheme 13 below.

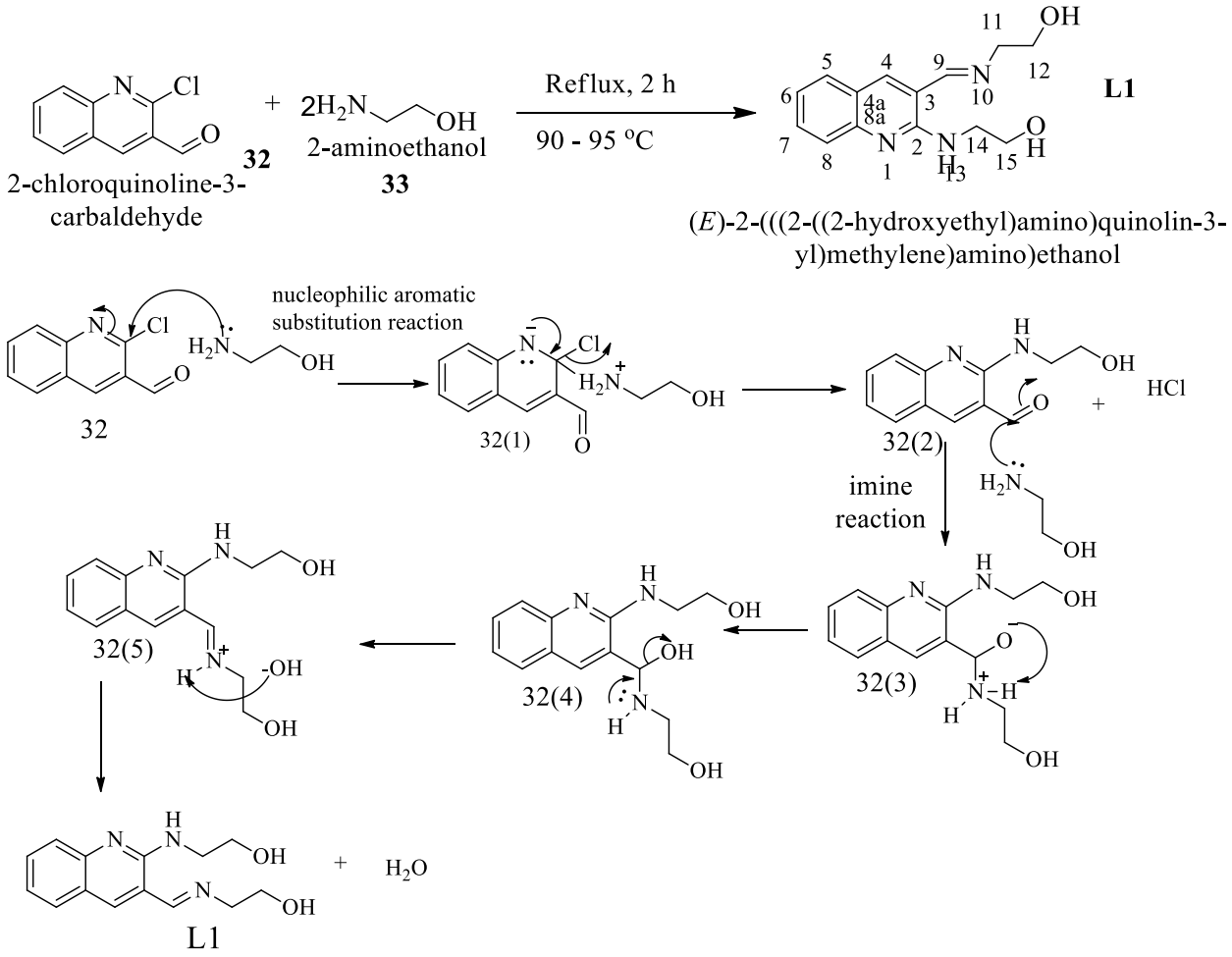

Scheme 13. Proposed synthesis and reaction mechanisms of **L1**

The **L1**: $C_{14}H_{17}N_3O_2$ [**H_3L**]; yield 86%; yellow powder; melting point. 80 – 85 ℃; Rf = 0.25 (*n*-hexane: Methanol = 7:3); UV-Vis λ_{max} (MeOH) = 383 nm; FTIR (υ cm^{-1}, KBr (pellet)): 3368 ν(O-H), 3275 ν(N-H), 1639 ν(imine C=N), 1620 ν(quinoline C= N). ^{1}H NMR (400 MHz, DMSO-d6): δ_H 3.65 (8H, *d*, H-11, H-12, H-14, and H-15), 4.72((1H, *s*, OH), 4.92 (1H, *s*, OH), 7.19 (1H, *t*, *J* = 7.25Hz, H-6), 7.55(2H, *m*, H-5, H-8), 7.72 (1H, *d*, *J* = 8.36 Hz, H-7), 8.21 (1H, *s*, H-4), 8.5(1H, *s*, H-9), and 9.55 (1H, *s*, NH); ^{13}C NMR (100 MHz, DMSO-d6): δ_C 43.4(C-14), 60.5 (C-12), 61.2(C-15), 63.7(C-11), 117.2 (C-3), 121.9 (C-8), 122.4(C-4a), 125.7 (C-5), 128.9(C-6), 131.5 (C-7), 143.0 (C-4), 148.3(C-8a), 155.4 (C-2), and 163.8 (C-9) ; DEPT-135 δC 43.4(C-14 negative), 60.5 (C-12 negative), 61.2(C-15 negative), 63.7 negative (C-11), 121.9 (C-8), 125.7 (C-5), 128.9(C-6), 131.5 (C-7), 143.0 (C-4), and 163.8

(C-9) (Appendix 5). Composition: Calc. for $C_{14}H_{17}N_3O_2$; C, 64.85; H, 6.61; N, 16.20; O, 12.34%. Found C, 64.71; H, 6.65; N, 16.08 and O, 12.56%.

4.1.2. Ligand 2 (L2)

The schematic representation for the synthesis and proposed mechanisms of the **L2** is presented in scheme 14 below.

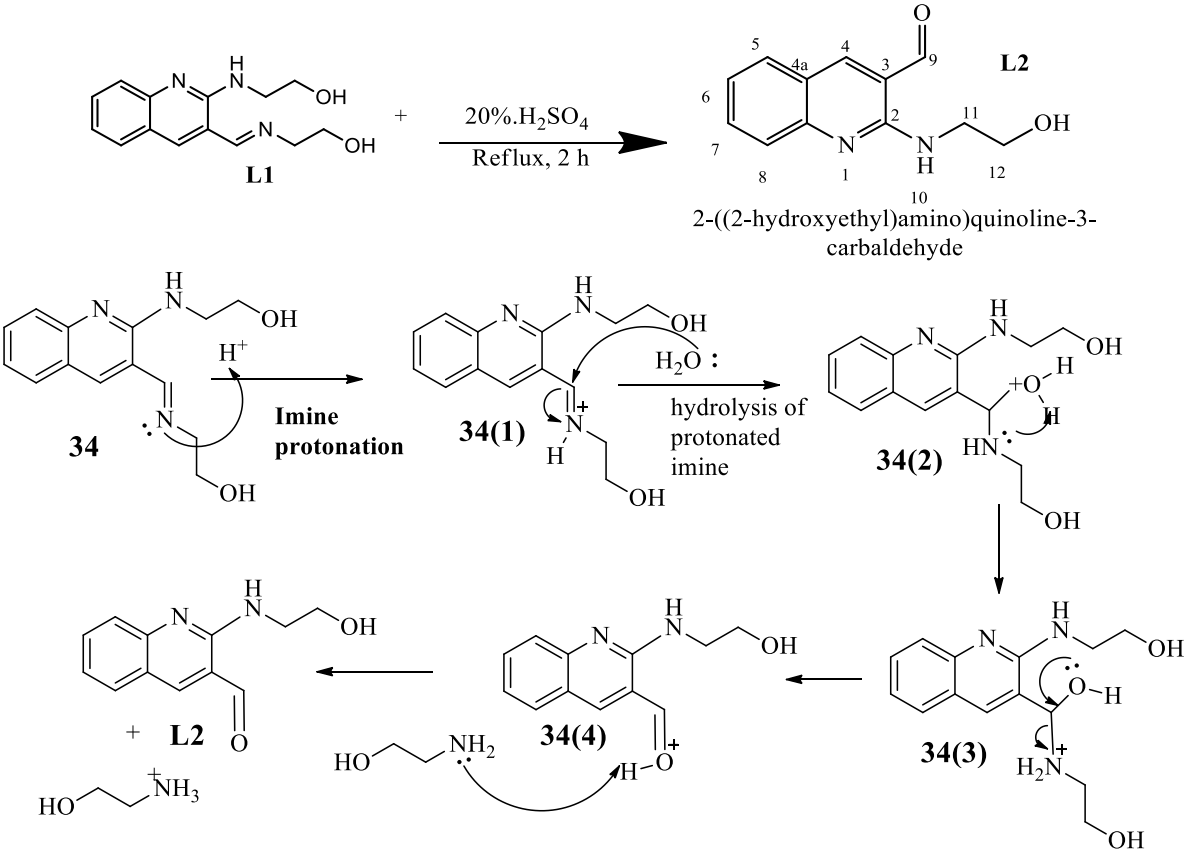

Scheme 14. Proposed synthesis and reaction mechanisms of **L2**

The **L2** has formula $C_{12}H_{12}N_2O_2$ [**H_2L**]; yield 2.42 g, 88%; yellow powder; decompose before melting at 130 – 132 ^oC; UV-Vis λ_{max} (MeOH) = 408 nm; FT-IR (υ cm^{-1}, KBr (pellet)): 3361 ν(O-H), 3245 ν(N-H), 1679 ν(carbonyl C=O), 1618 ν(quinoline C= N) ^1H NMR (400 MHz, $CDCl_3$): δ_H , 3.65 (4H, H-11, H-12), 4.96 (1H, *s*, O-H), 7.26 (1H, *s*, H-8),7.55-7.84 (3H, *m*, H-6, H-7, H-5), 8.24 (1H, *s*, H-4), 8.68(1H, *s*, H-9), and 10.02 (1H, *s*, N-H); ^{13}C NMR (100 MHz, DMSO-d_6): δ_C 43.1 (C-11), 60.1 (C-12), 117.7 (C-3), 122.1(C-4a), 122.8(C-8), 126.2 (C-6), 130.2 (C-7), 134.0 (C-5), 149.7 (C-4), 151.6(C-8), 154.7 (C-2), and 194.8(C-9) (Appendix 7 and 8). Composition: Calc. for $C_{12}H_{12}N_2O_2$; C, 66.65; H, 5.59; N, 12.96 and O, 14.80. Found C, 67.05; H, 5.56; N, 12.74 and O, 14.65%.

4.1.3. Complex 1

The schematic representation for the synthesis of the complex **1** is presented in scheme 15 below.

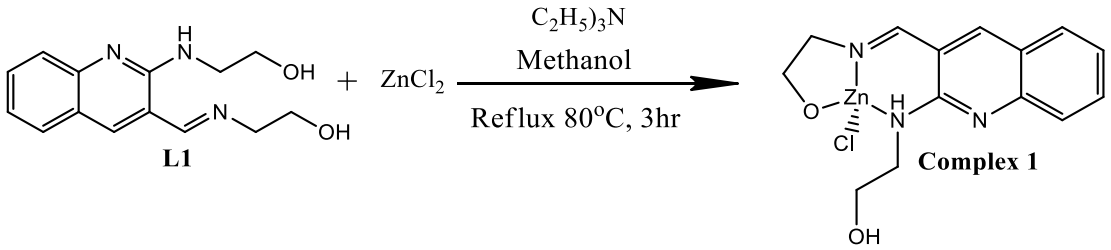

Scheme 15. Proposed chemical reaction of complex **1**

Complex **1** has molecular formula [Zn(H_2L)Cl]; found to be light yellow powder and, yield: 63%; melting point: 225 – 230 ^{o}C and is soluble in methanol, ethanol, DMSO, DMF, acetonitrile and water. Molar conductance (MeOH): 5.21 ± 0.35 $\Omega^{-1}mol^{-1}cm^{2}$ at 25 ^{o}C. Composition: Calc. for $C_{14}H_{16}ClN_3O_2Zn$; C, 46.82; H, 4.49; N, 11.70; O, 8.91; Cl, 9.87 and Zn, 18.21%. Found C, 46.85; H, 4.36; N, 11.80; O, 8.55; Cl, 10.25 and Zn, 18.19%. FTIR (υ cm^{-1}, KBr (pellet)): 1657 ν(Imin C=N), 1034 ν(C-O), 524 ν(Zn-O), 460 ν(Zn-N). UV-Vis (MeOH, nm): 231, 258 (π→π*) and 300, 380 (n→π*).

4.1.4. Complex 2

The schematic representation for synthesis of the complex **2** is presented in scheme 16 below.

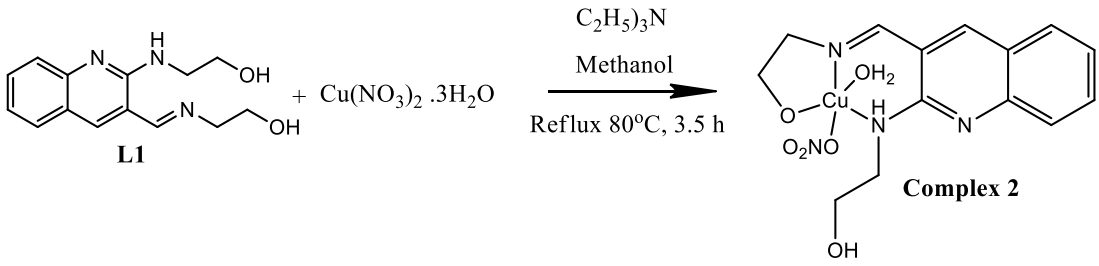

Scheme 16. Proposed chemical reaction of complex **2**

Complex **2** has molecular formula [Cu(H_2L)(H_2O)(ONO_2)]; found to be deep green powder and, yield: 62%, has melting point 195 – 200 ^{o}C and are soluble in methanol, ethanol, DMSO, DMF, acetonitrile and water. Molar conductance: 18.57 ± 0.35 $\Omega^{-1}mol^{-1}cm^{2}$ at 25 ^{o}C. Composition: Calc. for $C_{14}H_{18}CuN_4O_6$; C, 41.84; H, 4.51; N, 13.94; O, 23.89 and Cu, 15.81%. Found C, 41.62; H, 4.90; N, 13.80; O, 24.15; and Cu, 15.53%. FT-IR (υ cm^{-1}, KBr (pellet)): 1652 ν(Imin C=N), 1059 ν(C-O), 626 ν(Cu-O), 474 ν(Cu-N). UV-Vis (MeOH, nm): 235 (π→π*), 267, 317 (n→π*) and 406 (LMCT).

4.1.5. Complex 3

The schematic representation for the synthesis of the complex **3** is presented in scheme 17 below.

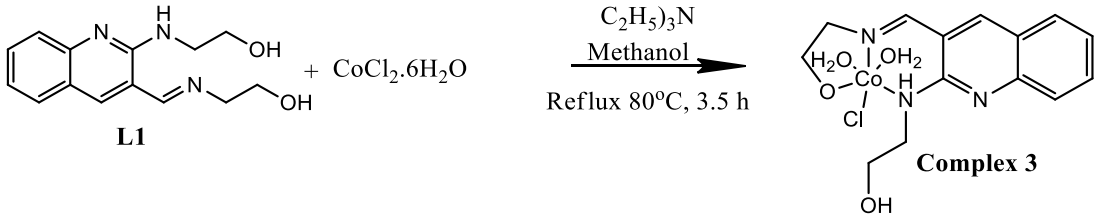

Scheme 17. Proposed chemical reaction of complex **3**

Complex **3** has molecular formula $[Co(H_2L)(H_2O)_2Cl]$ brownish purple powder, yield: 63%; has melting point 215 – 220 ^oC and is soluble in methanol, ethanol, and water. Molar conductance: 8.47 ± 0.25 $\Omega^{-1}mol^{-1}cm^2$ at 25 ^oC. Anal. Calc. for $C_{14}H_{20}ClCoN_3O_4$; C, 43.26; H, 5.19; N, 10.81; O, 16.46, Cl, 9.12 and Co, 15.16%. Found C, 43.50; H, 5.95; N, 10.82; O, 16.18; Cl, 8.65 and Co, 14.90%. FT-IR (υ cm^{-1}, KBr (pellet)):1647 ν(Imin C=N), 1059 ν(C-O), 546 ν(Co-O), 466 ν(Co-N). UV-Vis (MeOH, nm): 234, 258 (π→π*), 293 (n→π*) and 427 (LMCT).

4.1.6. Complex 4

The schematic representation for the synthesis of the complex **4** is presented in scheme 18 below.

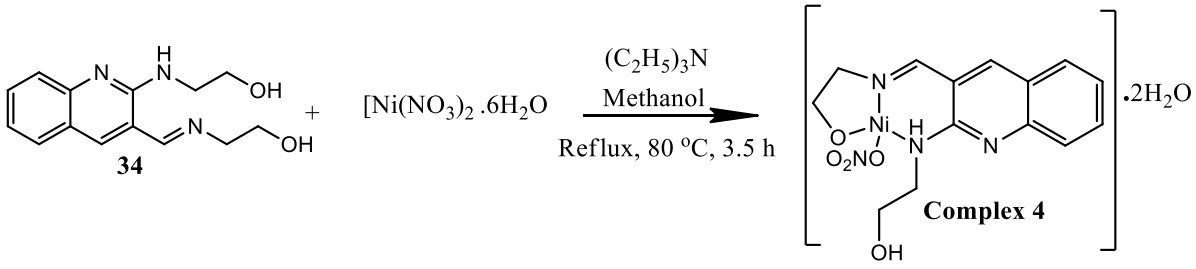

Scheme 18. Proposed chemical reaction of complex **4**

Complex **4** has molecular formula $[Ni(H_2L)(NO_3)].2(H_2O)$; reddish brown, like powder, Yield: 66%; melting point 115 – 120 ^oC and are soluble in methanol, ethanol, DMSO, DMF , acetonitrile and water. Molar conductance (MeOH): 15.07 ± 0.83 $\Omega^{-1}mol^{-1}cm^2$ at 25 ^oC. Composition: Calc. for $C_{14}H_{20}N_4NiO_7$; C, 40.52; H, 4.86; N, 13.50; O, 26.99 and Ni, 14.14%. Found C, 40.86; H, 4.95; N, 13.35; O, 26.90 and Ni, 13.94%. FT-IR (υ cm^{-1}, KBr (pellet)): 1650 ν(Imin C=N), 1037 ν(C-O), 534 ν(Ni-O), 462 ν(Ni-N). UV-Vis (MeOH, nm): 229, 259 (π→π*), 302 (n→π*) and 401 (LMCT).

4.1.7. Complex 5

The schematic representation for the synthesis of the complex **5** is presented in scheme 19 below.

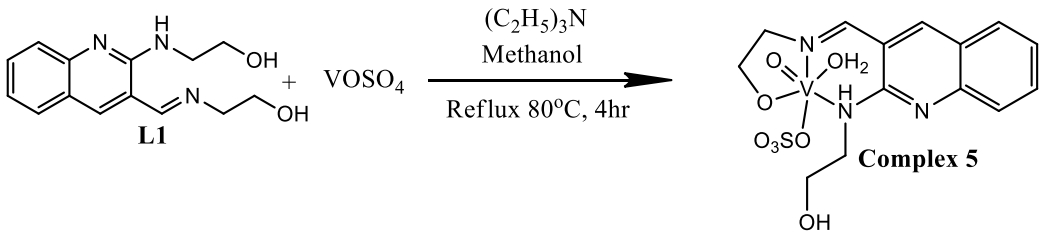

Scheme 19. Proposed chemical reaction of complex **5**

Complex **5** has molecular formula $[V(H_2L)(O)(H_2O)(SO_4)]$; deep green like powder and yield: 59%, melting point 205 – 210 ^{o}C and is soluble in methanol, ethanol, DMSO, DMF and water. Molar conductance (MeOH): 13.20 ± 0.59 $\Omega^{-1}mol^{-1}cm^{2}$ at 25 ^{o}C. Composition: Calc. for $C_{14}H_{19}N_3O_8SV$; C, 38.19; H, 4.35; N, 9.54; O, 29.07; S, 7.28 and V, 11.57%. Found C, 37.96; H, 4.68; N, 9.66; O, 28.91; S, 6.71 and V, 12.08%. FT-IR (υ cm^{-1}, KBr (pellet)): 1688 ν(Imin C=N), 1070 ν(C-O), 977 ν(V=O), 604 δ(V-O), 459 δ(V-N) (Figure S4C). UV-Vis (MeOH, nm): 231, 260 (π→π*), 304 (n→π*) and 409 (LMCT).

4.1.8. Complex 6

The schematic representation for the synthesis of the complex **6** is presented in scheme 20 below.

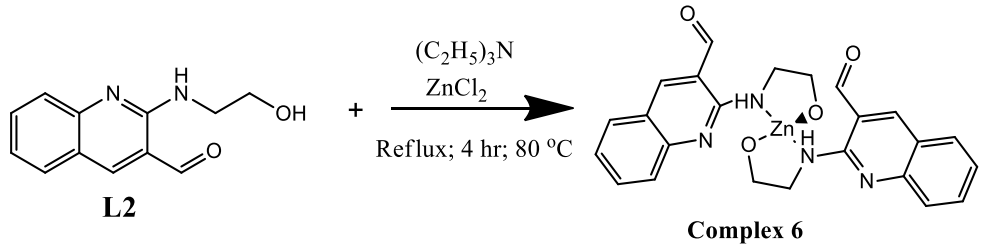

Scheme 20. Proposed chemical reaction of complex **6.**

Complex **6** has molecular formula $[Zn(HL)_2]$; yellowish white in colour and powder like, yield: 72% (0.41 g); melting point: 290 – 295 ^{o}C and are soluble in polar solvent. Molar conductance (MeOH): 19.82 ± 0.48 $\Omega^{-1}mol^{-1}cm^{2}$ at 25 ^{o}C. Composition: Calc. for $C_{24}H_{22}N_4O_4Zn$; C, 58.14; H, 4.46; N, 11.30; O, 12.91, and Zn, 13.19%. Found C, 58.27; H, 4.41; N, 11.08; O, 12.84; and Zn, 13.40%. FT-IR (υ cm^{-1}, KBr (pellet)): 1642 ν(Imin C=O),1622 ν(quin C=N), 953 ν(C-O Str), 758 ν(Zn-O), 529 ν(Zn-N). UV-Vis (MeOH, nm): 231, 259 (π→π*) and 303, 393 (n→π*).

4.1.9. Complex 7

The schematic representation for the synthesis of the complex **7** is presented in scheme 21 below.

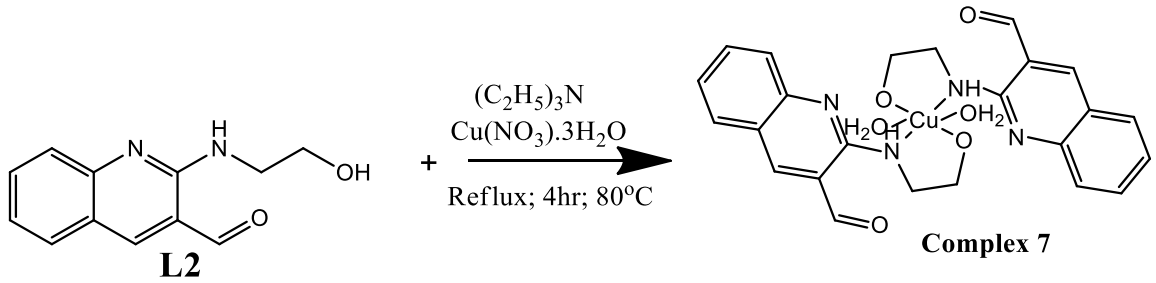

Scheme 21. Proposed chemical reaction of complex **7**

Complex **7** has molecular formula $[Cu(HL)_2(H_2O)_2]$; yellowish white in colour powder like, yield: 64% (0.39 g), has melting point 260 – 265 ^oC and are soluble in polar solvent. Molar conductance: 21.47 ± 0.50 $\Omega^{-1}mol^{-1}cm^2$. Composition: Calc. for $C_{24}H_{26}CuN_4O_6$; C, 54.38; H, 4.94; N, 10.57; O, 18.11and Cu, 11.99%. Found C, 54.55; H, 4.95; N, 10.35; O, 18.09; and Cu, 12.06%. FT-IR (υ cm^{-1}, KBr (pellet)): 1646 ν(C=O), 1562 ν(quinol C=N), 1057 ν(C-O), 607 ν(Cu-O), 544 ν(Cu-N). UV-Vis (MeOH, nm): 255, (n→π*) and 351(LMCT).

4.1.10. Complex 8

The schematic representation for the synthesis of the complex **8** is presented in scheme 22 below.

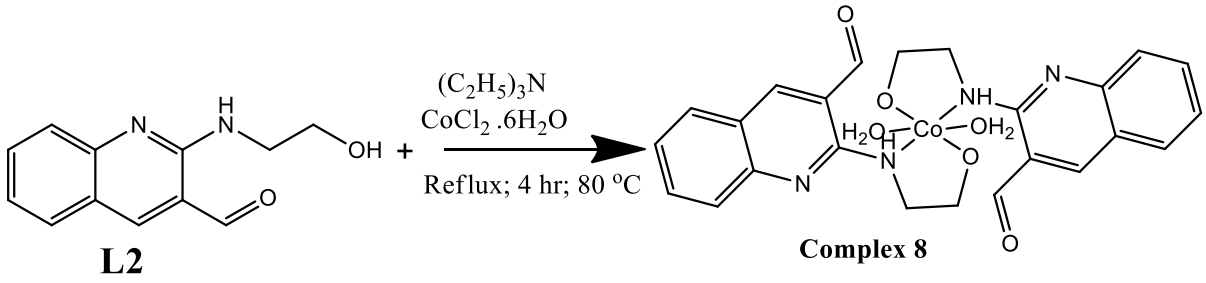

Scheme 22. Proposed chemical reaction of complex **8**

Complex **8** has molecular formula $[Co(HL)_2(H_2O)_2)]$, brownish red powder, yield: 76%; has melting point 285 – 290 ^oC and is soluble in methanol, ethanol and water. Molar conductance: 18.60 ± 0.61$\Omega^{-1}mol^{-1}cm^2$ at 25^oC. Anal. Calc. for $C_{24}H_{24}CoN_4O_6$; C, 55.07; H, 4.62; N, 10.70; O, 18.34 and Co, 11.26%. Found C, 55.40; H, 4.93; N, 10.28; O, 18.33 and Co, 11.06%. FT-IR (υ cm^{-1}, KBr (pellet)): 1622 ν (C=O), 1569 (quinol C=N), 1035 ν (C-O),

807 ν(Co-O), 517 ν(Co-N). UV-Vis (MeOH, nm): 231, 260 (π→π*), 304 (n→π*) and 407 (LMCT).

4.1.11. Complex 9

The schematic representation for synthesis of the complex **9** is presented in scheme 23 below.

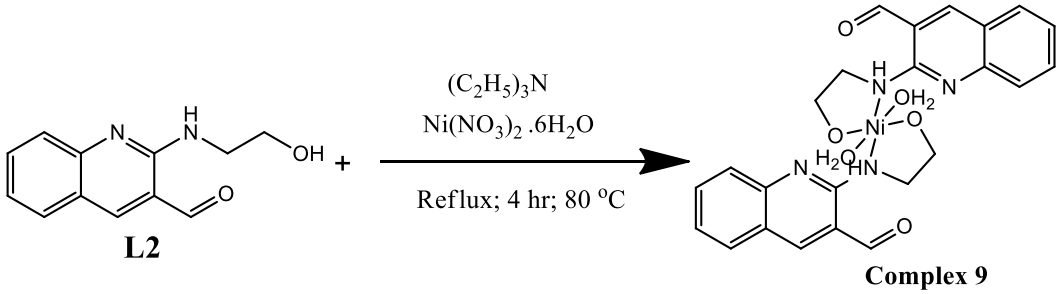

Scheme 23. Proposed chemical reaction of complex **9**

Complex **9** has molecular formula $[Ni(HL)_2(H_2O)_2]$; brick red powder, yield: 65%; melting point 270 – 275 ^oC and are soluble in methanol, ethanol, DMSO, DMF , acetonitrile and water. Molar conductance (MeOH): 18.49 ± 0.40 $\Omega^{-1}mol^{-1}cm^2$ 25 ^oC. Composition: Calc. for $C_{14}H_{19}N_5NiO_{10}$; C, 44.54; H, 3.74; N, 12.99; O, 29.67; and Ni, 9.07%. Found C, 45.26; H, 2.95; N, 13.05; O, 29.80 and Ni, 8.94%. FT-IR (υ cm^{-1}, KBr (pellet)): 1621 ν(C=O), 1573 ν(Quinol C=N) , 527 ν(Ni-O), 474 ν(Ni-N). UV-Vis (MeOH, nm): 229, 259 (π→π*), 302 (n→π*) and 397(LMCT).

4.1.12. Complex 10

The schematic representation for the synthesis of the complex **10** is presented in scheme 24 below.

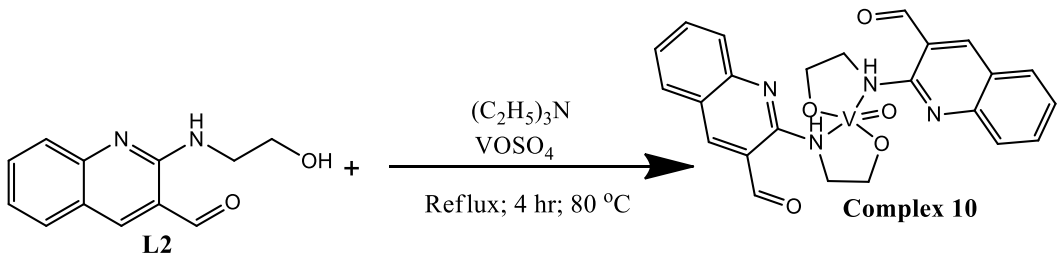

Scheme 24. Proposed chemical reaction of complex **10**

Complex **10** has molecular formula $[VO(HL)_2]$; deep green like powder and yield: 56%, melting point 265 – 270 ^oC and are soluble in methanol, ethanol, DMSO, DMF and water. Molar conductance (MeOH): 15.07 ± 0.41 $\Omega^{-1}mol^{-1}cm^2$ at 25 ^oC. Composition: Calc. for $C_{24}H_{20}N_4O_5V$; C, 58.19; H, 4.07; N, 11.31; O, 16.15; and V, 10.28%. Found: C, 57.83; H, 4.16; N, 11.28; O, 16.65; and V, 10.08%. FT-IR (υ cm^{-1}, KBr (pellet)): 1688 ν(Imin C=N),

1070 ν (C-O), 977 ν(V=O), 604 ν(V-O), 459 ν(V-N). UV-Vis (MeOH, nm): 231, 260 (π→π*), 304 (n→π*) and 409 (LMCT).

4.2. Characterization of compounds

4.2.1. UV- Visible Spectroscopy

The electronic spectra of both the ligands and their metal complexes were recorded at wavelength range (200 – 800 nm) using 1×10^{-5} M methanolic solution of the sample at room temperature and the results are shown in (Figure 1 – 4 and Appendix 9). The UV-Vis absorption spectra are produced possibly due to the electronic transitions from the highest occupied molecular orbital (HOMO) to the lowest unoccupied molecular orbital (LUMO) [3]. The obtained spectra show ligand bands due to (π→π*), (n→π*) transitions, which undergo red and blue shifts under metal complexation. The bathochromic and hypsochromic shifts showed the formation of the targeted metal complexes [3].

The free **L1** absorption bands were recorded at (231, 258, 300, 383) nm (Figure 1 and Appendix 9) representing π→π* (C=N) and n→π* (C-O) transition respectively. However, in the case of metal complexes other than complex 1, these bands exhibit bathochromic (red) shifted at different absorbance due to the dominance of inter ligand electron transfer since zinc has a d^{10} electron configuration [301].

The Cu(II), Co(II), V(IV) and Ni(II) complexes' characteristic spectra were observed in the ranges of 231–293 nm and 302–304 nm that would be assigned to the π→π* and n→π* transitions, respectively [302]. Additionally, the broad band observed at 406, 427, 408 and 401 nm, for Cu(II), Co(II), V(IV), and Ni(II) respectively, were observed. These red shifts from free ligand are mainly due to the ligand to metal charge transfer (LMCT) which is in line with the previous reported studies [81, 195, 302–309], hence the ligand might be participated in metal complex and this is because the ligand (**L1**) has lone pair electrons and the complexes have vacant d-orbitals [302, 310]. Moreover, as it can be seen from the insets of the absorption plots presented in Figure 2, there is a very weak d→d transition around 480 nm in the case of the Ni(II) complex. In addition, to shed more light on the absorption spectra of the ligand and its complexes, we used TD-B3LYP to calculate the absorption spectra. Comparison of the experimental electronic spectra with TD – DFT calculations has been carried out and it was found that the experimental results are in very good agreement with the

calculated results as presented in Figure 2. This further confirms the successful syntheses of the intended complexes.

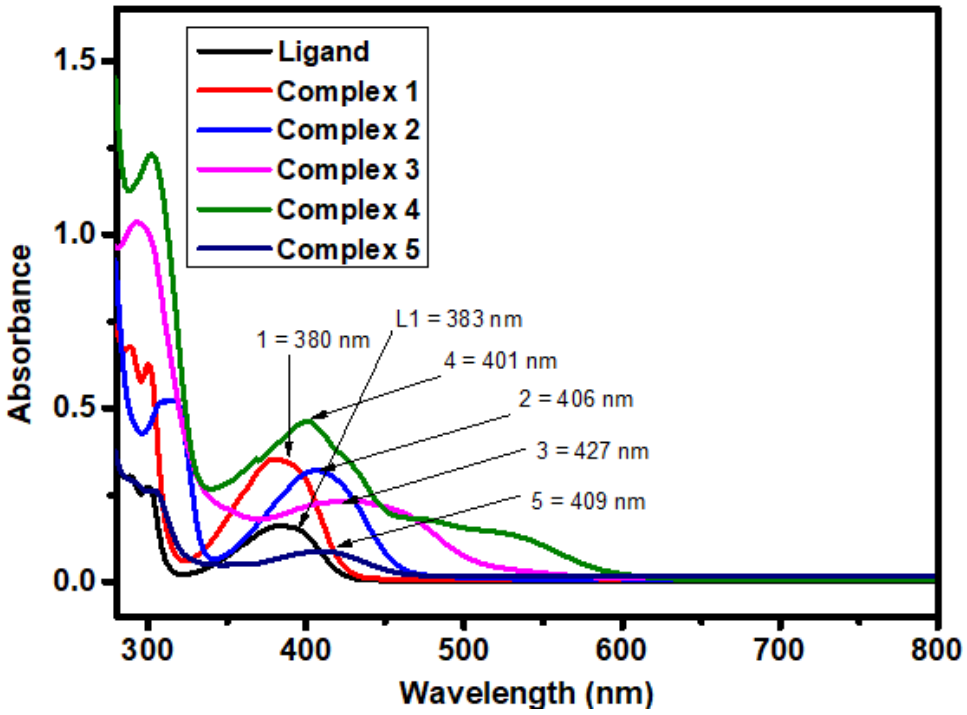

Figure 1. UV-Vis spectra of **L1** and its metal complexes

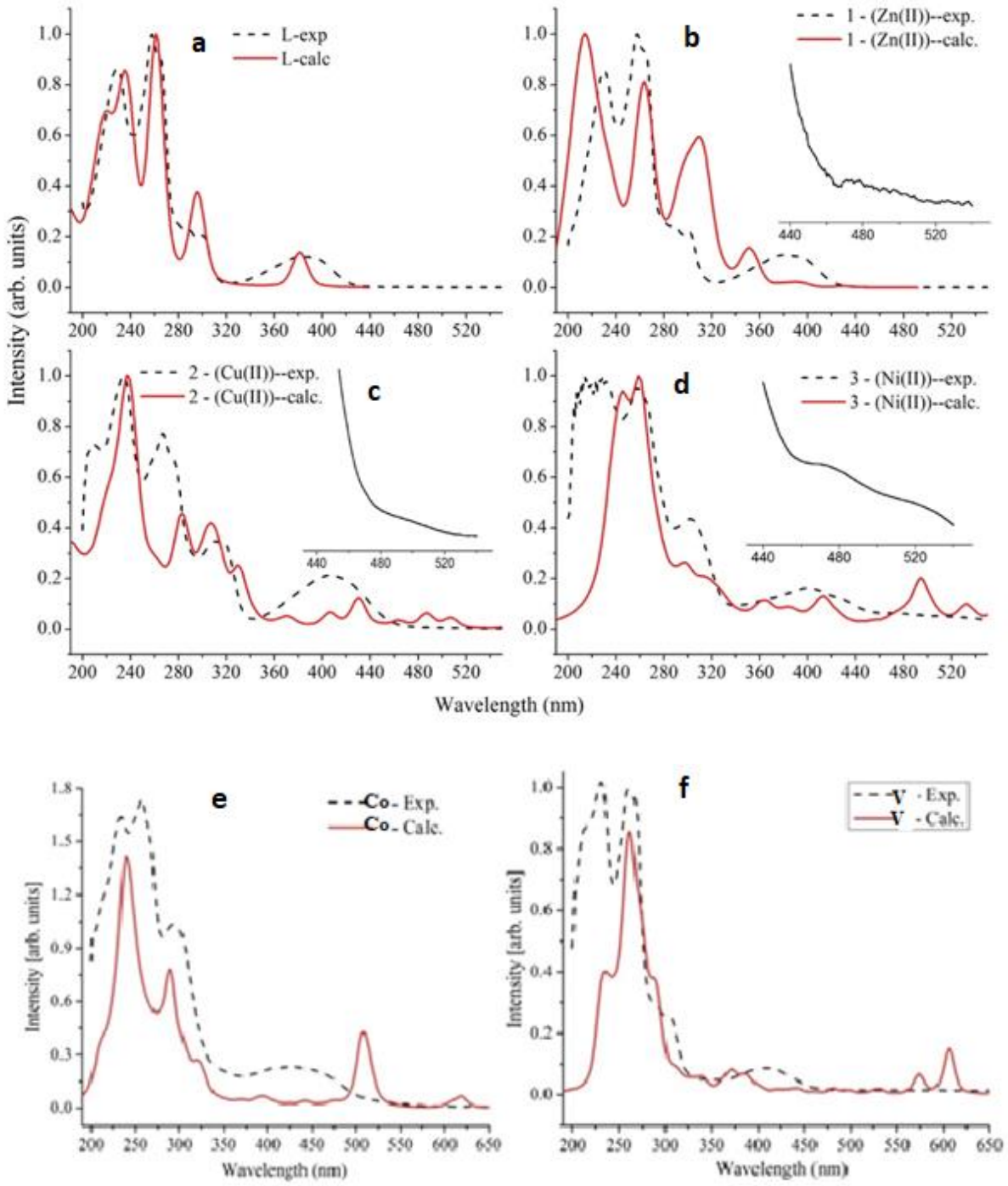

Figure 2. Comparison of the experimental absorption wavelengths with calculated results of the **L1** and (**1 – 5**). Insets are experimental plots for the range between 440 and 540 nm.

Similarly the electronic spectra of the ligand (**L2**) and its complexes **6 – 10** were recorded and showed in (Figure 3 and Appendix 9). The obtained spectra show ligand bands due to ($\pi\rightarrow\pi^*$), ($n\rightarrow\pi^*$) transitions, which undergo blue shifts under metal complexation. The hypsochromic effect shows the formation of the metal complexes [3]. Accordingly, the free ligand exhibited absorption bands at 231 and 261 nm ($\pi\rightarrow\pi^*$) (C=N) imine group, 305 and

408 nm (n→π*) (C-O) hydroxyl group (Appendix 9). But these bands show blue shift at different absorbance in case of metal complexes as a result of the complexation through oxygen and amine groups [183, 301].

The observed characteristic bands in spectra of all the complex between 255 and 305 nm would be attributed to the n→π* transition [3]. Moreover, the broad band observed at 351 – 407 nm, for the complexes may be assigned to Ligand to Metal charge transfer (LMCT), indicating the coordination of the ligand to the metal ions which is in line with the previous reported studies [3, 197, 238]. Similarly, it is also in agreement with DFT calculations (Figure 4) which showed the presence of electron transitions from the HOMO of the ligand to the LUMO of the metal center [49, 197, 304, 311]. The expected d→d transition bands of the Cu(II), Co(II), Ni(II) and V(IV) complexes may be masked due to the dominant ligand-to-metal charge transfer which is in agreement with previously reported studies [303–305, 312]. This is due to the presence of vacant d-orbital of the complexes and ON donor groups with lone-pair of electrons within the ligand [302, 310].

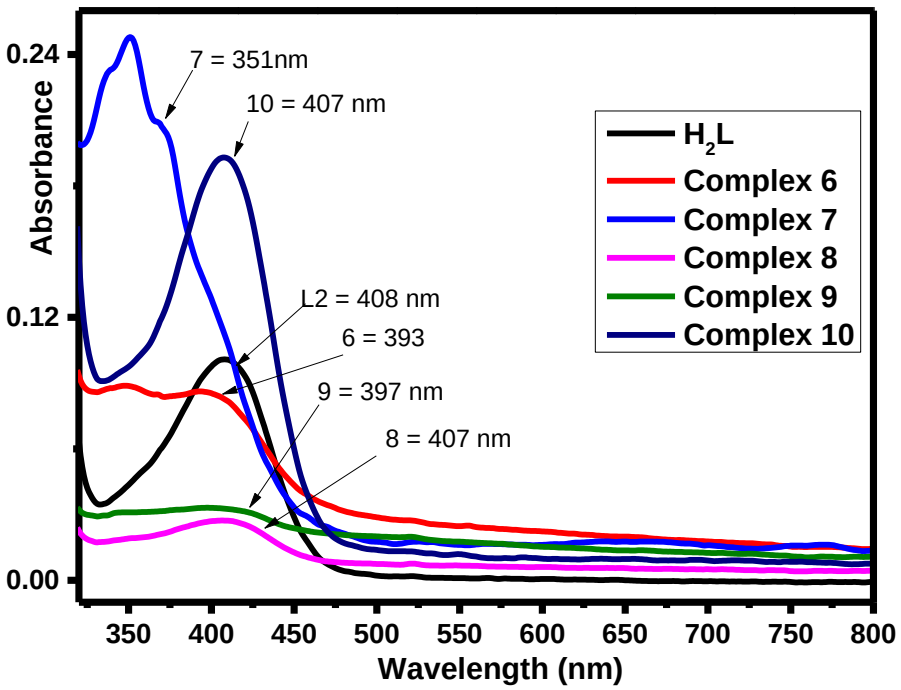

Figure 3. UV-Vis spectra of the **L2** and its metal complexes (**6** – **10**)

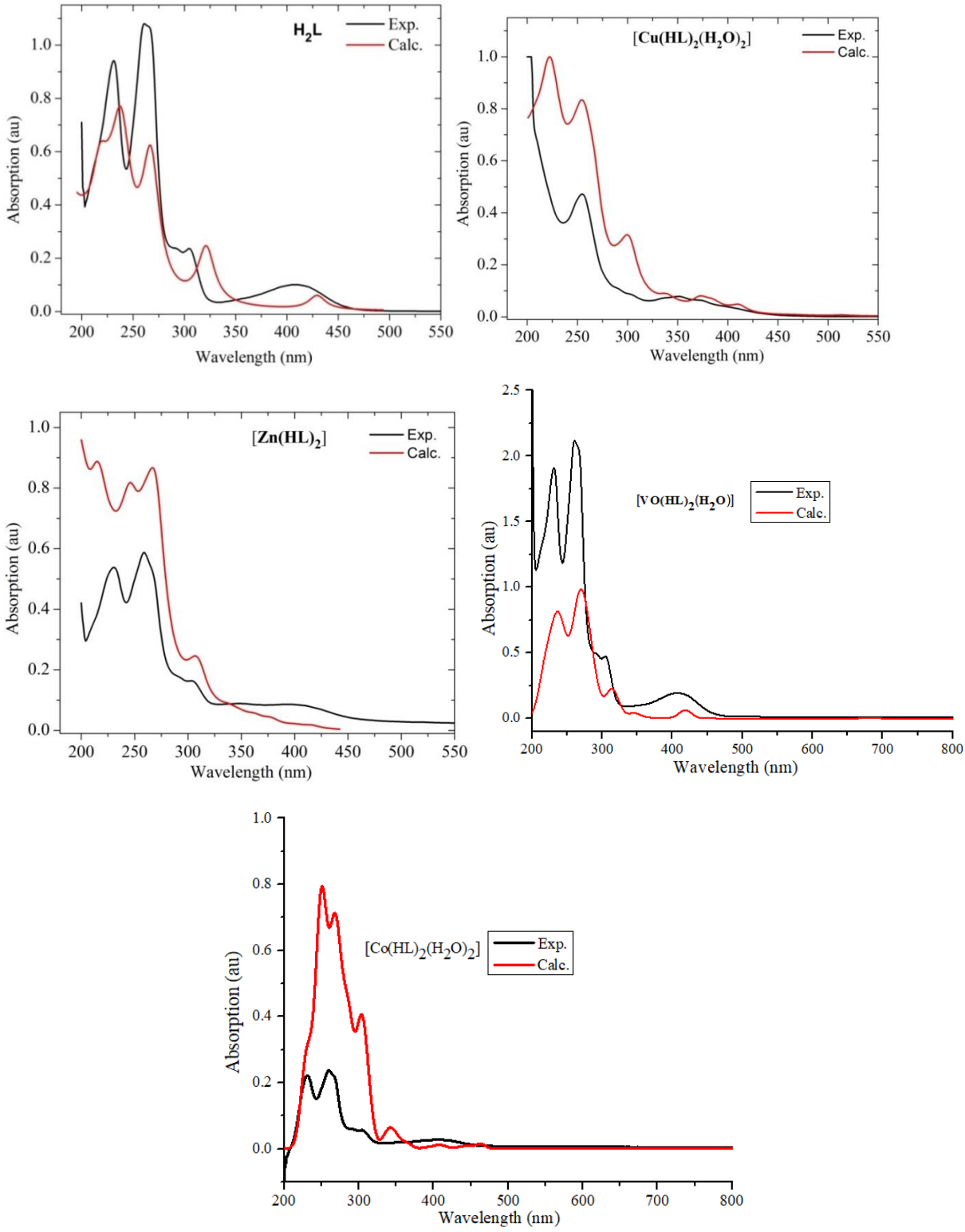

Figure 4. Comparison of the experimental absorption wavelengths with calculated results of the **L2** and its complexes.

4.2.2. Fluorescence spectroscopy

Fluorescence spectral of the ligands and their metal complexes were recorded in methanol solvent within the wavelength range of 350 – 700 nm at room temperature using 10^{-5} M concentration of both free ligands and their metal complexes [313, 314].

The emission spectra of the ligand (**L1**) and its complexes (**1 – 5**) showed emission bands at 526, 608, 511, 521, 420 and 471 nm, respectively. Similarly, the emission spectra of the ligand (**L2**) and its complexes (**6** – **10**) showed emission bands at 486 and 460, 471, 463, 457 and 469 nm, respectively which appeared in Figure 5, 6 and Appendix 10. Fluorescent intensity changes were observed after complexation which is in agreement with literature reports [123]. This corroborates with the fact that coordinating with metal ions might make the ligand more rigid as coordination complexes transfer energy from the excited state of the ligand to the metal ions. This resulted in fluorescence intensity shifts of the complexes, demonstrating that the material may be suitable for photochemical applications. [123, 183, 315].

The photoluminescence properties of zinc complexes are typically caused by intraligand emissions because of the d^{10} electron configuration; as a result, the complexes' luminescence is primarily caused by the coordination of the ligand to the Zn(II), which can be explained by intraligand emissions, and is consistent with a recently published studies [54, 183, 316]. In the case of Cu(II), Co(II), Ni(II) and V(IV) exhibit altered emission intensities relative to free ligands due to charge transfer, which is consistent with earlier research [3, 65, 197, 198, 317]. Generally, emission intensities showed hyperchromic / hypochromic and bathochromic / hypsochromic shifts upon complexation and this indicate the ligands fully participated in coordinate covalent bond formation in agreement with reported studies in which the emission peaks of the complexes have been blue-shifted [65, 183, 198, 316, 317].

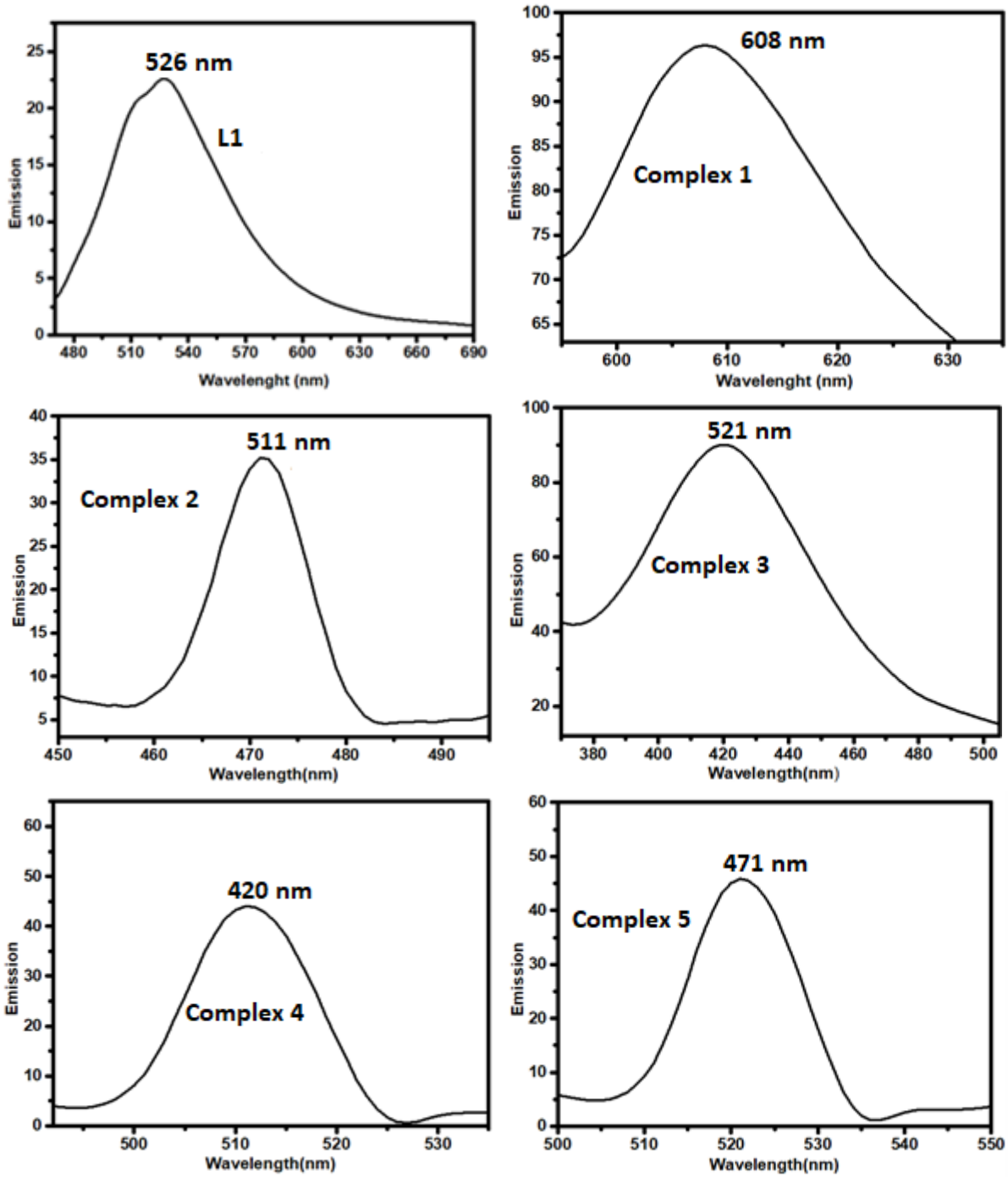

Figure 5. Fluorescence spectra of ligand (**L1**) and its complexes (**1** – **5)**

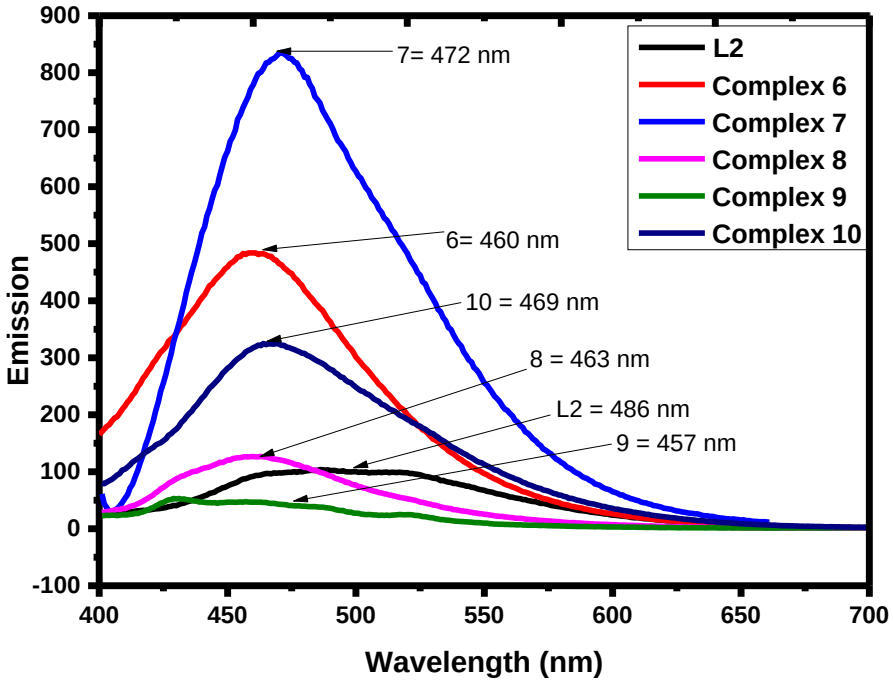

Figure 6. Fluorescence spectra of ligand (**L2**) and its complexes (**6** – **10)**

4.2.3. FTIR spectroscopy

FTIR spectra of free ligands and their metal complexes were recorded using 10 mg sample with KBr pellets at the wavenumber range of 4000 – 400 cm^{-1}. FTIR spectra of the complexes were compared with that of ligands to determine the coordination of compounds and then coordination sites that may be involved in complexation process in which the detail explanation was shown in Table 2, 3 and Appendixes 11 – 22. The IR spectrum of **L1** shows a stretching band at 1639 cm^{-1} for ν(C=N) imine group, but this band shifted towards different frequency in the spectral of all metal complexes (**1** – **5**) to the range (1647 – 1688 cm^{-1}) indicating the participation of nitrogen atom of imine group ν(C=N), in coordinate covalent bonds (Table 2 and Appendixes 11 – 16), in line with the reported studies [11, 34, 318, 319]. In other case FTIR stretching frequency of ligand (**L1**) at 3368cm^{-1} ν(O-H) is decreased in case of all Cu(II), Co(II), Ni(II) Zn(II) and V(IV), this also shows the deprotonation of hydroxyl group and participation of oxygen in dative bond formation of complexation. In addition FTIR stretching frequency of ligand at 3275 cm^{-1} ν(N-H) is diminished in case of all the synthesised metal complexes, which indicate that participation of nitrogen of amine group to complex formation [320, 321].

Weak and broad band stretching frequency which ranged from (3687 – 3000) cm^{-1}, is clearly emerged which could be assigned as stretching vibration of water molecules as water of coordination for Cu(II), Co(II), V(IV) and as lattice water for Ni(II) respectively. In addition new stretching vibration band of the spectral are displayed at 524 cm^{-1} ν(Zn-O), 460 cm^{-1} ν(Zn-N) bonds, 626 cm^{-1} ν(Cu-O), 474 cm^{-1} ν(Cu-N) bonds, 546 cm^{-1} ν(Co-O), 466 cm^{-1} ν(Co-N) bonds, 534 cm^{-1} ν(Ni-O), 462 cm^{-1} ν(Ni-N), bonds and the bending bond at 604 cm^{-1} δ(V-O), 459 cm^{-1} δ(V-N), for, Zn(II), Cu(II), Co(II), Ni(II) and V(IV) complexes respectively (Table 2 and Appendixes 11 – 16). These shows that all metal ions are participated in coordinate covalent bond formation process [320–322].

The stretching band at 977 cm^{-1} is special for ν(V=O), for the V(IV) complex which is in line with reported studies [277, 309, 320, 323, 324]. In addition, the presence of nitrate in both Cu(II) and Ni(II) complexes were signaled by the strong and broad band IR peaks at 1380 cm^{-1} and 1351 cm^{-1}, [3] respectively, which gave good indication for the participation of nitrate in complexation reaction [3, 146], and weak bending vibration of δ(O-H) was clearly observed in the range of 1200–1450 cm^{-1} in case of all metal complexes confirming the appearance of free bending hydroxyl (O-H) group in good agreement with the reported studies [3, 43, 278, 309, 320, 322, 324].

Similarly, the IR spectra of free ligand (**L2**) shows strong stretching band at 1679 for ν(C=O) aldehyde carbonyl group and 1618 cm^{-1} for ν(C=N) quinoline group, but this band shifted towards lower frequency in the spectral of both metal complexes to the range (1621 – 1646 cm^{-1}) for ν(C=O) and to higher frequency ranged from (1562 – 1673 cm^{-1}) for ν(C=N) which indicating the involvement of ligand in dative bond formation in case of all metal complexes (Table 3 and Appendixes 17 – 22). In other case FTIR medium stretching frequency of ligand at 3361 cm^{-1} ν(O-H) disappeared in case of all complexes (**6 – 10**) due to deprotonation and medium FTIR stretching frequency of the ligand at 1079 cm^{-1} for ν(C-O) was diminished to lower frequency regions of 1056, 1057, 1035, 1029 and 1051cm^{-1} for Zn(II), Cu(II), Co(II), Ni(II) and V(IV) complexes respectively. This is an indication for the participation of deprotonated oxygen atom of hydroxyl group in complex formation. However, there exists coordinated water molecule in complexes (**7 – 9**) that contributes to the O-H group in which broad bands ranges from (3695 – 3394) cm^{-1} were observed. Both the experimental and calculated results indicated the participation of oxygen atom of the ligand through deprotonated hydroxyl group in complex formation but complex **10** did not contains both

lattice and coordinated water; this results are in very good agreement with thermal analysis study (see section 4.2.8). Similarly, medium IR stretching frequency of ligand at 3245cm^{-1} ν(N-H) is enhanced to higher frequency ranged from (3290 – 3398) cm^{-1} in all metal complexes, which showed that participation of amine nitrogen atom in complex formation [320, 321], this is because the NH group is preferred for coordination hence N from the quinoline ring (imine group) is sterically hindered when compared with the aliphatic nitrogen atom of the amine group. In addition, low solubility which might arise from generation of polynuclear structure due to nitrogen atom of the quinoline ring participating in coordination is not observed; and hence the complexes were found to be soluble in polar solvents, which is in line with previously reported studies [316, 319, 321, 325, 326].

In addition the IR spectral data have shown that, new vibrational bands were observed: accordingly, very weak band at 598 cm^{-1} and medium band 529 cm^{-1} for ν(Zn-O and Zn-N) bonds for zinc complex, 607 cm^{-1} and 544 cm^{-1} for ν(Cu-O and Cu-N) bonds for copper complex, very weak band at 665 cm^{-1} and medium bands 517 cm^{-1} for ν(Co-O and Co-N) bonds for cobalt complex, 527 cm^{-1} ν(Ni-O), 474 cm^{-1} ν(Ni-N), for nickel complex and the bending bond at 603 cm^{-1} ν(V-O), 540 cm^{-1} ν(V-N), for V(IV) complex respectively. The stretching band at 929 cm^{-1} is special for ν(V=O), for the V(IV) complex (Table 3 and Appendixes 17 – 22). These confirmed that all metal ions have participated in coordinate covalent bond formation process in the complexes, which is in line with the previous reported studies [3, 66, 324, 80, 146, 277, 309, 320–323]. The DFT calculated IR frequencies and TD-DFT calculated absorption spectra were also in good agreement with the corresponding experimental results (Table 2 and 3), which further confirmed the successful synthesis of the targeted complexes.

Table 2. Selected FTIR vibrations and band assignments for the ligand and its complexes (**1** – **5)**. Experimental results are without parenthesis whereas the B3LYP-GD3/6-311++G**/LanL2DZ calculated results are presented in parenthesis.

	ν(O-H)	ν(N-H)	Im. ν(C=N)	Ql. ν(C=N)	δ(O-H)	ν(NO_3)[c]	ν(C-O)	ν(V=O)	ν(M-O)	ν(M-N)
L1	3368[m] (3564)	3275 [m] (3359)	1639[s] (1579)	1620[s] (1532)	1411 [m] (1323)	-	1055[m] (987)	-	-	-
1	3349 [w] (3575)	3294 [w] (3374) [w]	1657[s] (1680)	1633[s] (1608)	1446 [m] (1362)	-	1034 [m] (1054)	-	524 [m] (490)	460[m] (464)
2	3664-3334 (3734, 3713[b])	3168 [w] (3374)	1652[s] (1661)	1627[s] (1586)	1460 [m] (1426),	1380[s] (1381)	1059 [m] (1044)		626 [m] (703, 466)	474[m] (467)
3	3687[b,w] (3652)	3346 [w]	1647[s] (1642)	1630[s] (1538)	1437[m] (1508)		1059[s] (1102)		546[w] (486)	466[w] (382)
4	3673-3373 [b] (3736, 3574 [b])	3197[w] (3088)	1650[s] (1669)	1634[s] (1593)	1439 [m] (1421)	1351[s] (1457)	1037 [m] (1038)		534 [m] (750, 563)	462 (503, 470)
5	3668[b,w] (3675)	3282[w]	1688[s] (1610)	1652[s] (1540)	1449[m] (1395)		1070[w] (1011)	977[s] (1070)	604[b.m] (619)	459[w] (502)

S= strong m = mediam, b = broad, w= weak, Need dicusion based on metal d- electron

Table 3. Selected FTIR vibrations and band assignments for the ligand and its complexes (**6** – **10**). Experimental results are without parenthesis whereas the B3LYP-GD3/6-311++G**/LanL2DZ calculated results are presented in parenthesis.

	ν (O-H)	ν(N-H)	Aldehy ν(C=O)	Ql. ν(C=N)	ν(C-O)	ν (V=O)	ν(M-O)	ν(M-N)
L2	$3361^{s,w}$ (3709)	$3245^{b,w}$ (3535)	1679^{s} (1678)	1618^{s} (1584)	1079^{m} (1047)	-	-	-
6	-	3398^{w} (3428)	1642^{s} (1679)	1622^{s} (1588)	1056^{m} (1085)	-	598^{w} (560)	529^{w} (482)
7	$3689 – 3394^{b,s}$ (3740 – 3265)	3290^{w} (3400)	1646^{s} (1679)	1562^{s} (1586)	1057^{s} (1076)	-	607^{m} (576)	544^{m} (490)
8	$3695 – 3445^{b,w}$ (3671 – 3559)	3386^{w} (3283)	1622^{s} (1617)	1569^{s} (1531)	1035^{m} (1014)		665^{w} (556)	517^{w} (506)
9	$3690 – 3423^{b,w}$ (3657 – 3381)	3379^{w} (3214)	1621^{s} (1627)	1573^{s} (1537)	1029^{m} (1002)		527^{m} (567)	474^{w} (468)
10	-	3341^{w} (3149)	1672^{s} (1622)	1621^{s} (1531)	1051^{m} (992)	929m (945)	$603^{b.m}$ (596)	540^{w} (527)

s = strong, m= medium, b= broad, w= weak; Ql= quinoline

4.2.4. X-ray Diffraction Analysis of complexes (1-10)

The powder X-ray diffraction (PXRD) patterns of the synthesised all metal complexes (**1 – 10**) were recorded using 80 mg of dried powdered samples. The patterns of the synthesized metal complexes were performed using measurement conditions of X-ray tube target: Cu (λ = 1.5406 Å), voltage: 40.0 kV, current: 30.0 mA, divergence slit: 1.0^{o}, scatter slit: 1.0^{o}, receiving slit: 0.3 mm, scanning drive axis: 2θ, scan range: 5.0 – 80.0^{o}, scan mode: continuous scan, Scan speed: 3.0^{o}/min, sampling pitch: 0.02^{o}.

The results of powder X-ray diffraction (PXRD) analysis of all complexes were showed in Appendixes 24 – 25 The patterns of the complexes (**1 – 5, 7, 8** and **10)** have showed polycrystalline like characteristic peaks because the complexes showed many diffraction peaks which are in line with previously reported studies [2, 274, 275, 327]. It is important to note that the average crystallite size (D) can be calculated from the XRD pattern according to Debye–Scherrer equation [14, 319, 327].

$$D = \frac{K\lambda}{\beta \cos\theta} \quad (11)$$

The equation uses the reference peak width at angle θ, where λ is the wavelength of X-ray radiation (1.5406 Å), *K* is Scherrer constant (0.9) and β is the width at half maximum of the reference diffraction peak measured in radians. Accordingly, the average crystallite sizes of complexes **1 – 5, 7**, **8** and **10** are 28, 34, 22, 37, 8, 23, 9 and, 23 nm, respectively, which is in line with previously reported studies [14, 238, 275, 327]. On the other hand the PXRD pattern for synthesised metal complexes of **6** and **9** indicates broad peaks at the range of at 2θ = 5 – 80^{o} (Appendix 25) and this might be due to the amorphous nature of the complexes which in agreement with previous reported studies [26, 274, 277, 312, 319, 327, 328].

4.2.5. SEM – EDX analysis

In EDX spectrum complex **1** shows five characteristic signals which correspond to C (carbon), O (oxygen), N (nitrogen), Cl (Chlorine) and Zn (zinc) atoms and confirms the formation of CHZnNOCl compound (Figure 7A). Similarly, in EDX complex **2** spectrum shows four characteristic signals which correspond to C (carbon), O (oxygen), N (nitrogen), and Cu (Copper) atoms and it clearly confirms the formation of CHCuNO complex (Figure 7B). The EDX spectrum of complex **3** shows five characteristic signals which correspond to C (carbon), O (oxygen), N (nitrogen), Cl (Chlorine) and Co (cobalt) atoms and are signalled

the formation of CHCoNOCl compound (Figure 8A), in EDX spectrum the complex **4** shows four characteristic signals which correspond to C (carbon), O (oxygen), N (nitrogen), and Ni (nickel) atoms. The characteristic peak confirms the formation of CHNiNO compound (Figure 8B) and the EDX spectrum of complex **5** shows five characteristic signals which correspond to C (carbon), O (oxygen), N (nitrogen), S(sulphur) and V(vanadium) atoms and indicated the formation of CHVSNO compound (Figure 9A) which is in line with the previous reported studies [14, 329].

Similarly, in EDX spectrum of complexes **6** – **10** showed different characteristics peaks, accordingly, the complex **6** shows four characteristic signals which correspond to C (carbon), O (oxygen), N (nitrogen) and Zn (zinc) atoms and confirms the formation of CHZnNO compound (Figure 9B). The EDX spectrum of the complex **7** shows four characteristic signals which is related to C (carbon), O (oxygen), N (nitrogen), and Cu (Copper) atoms and it shows the formation of CHCuNO complex (Figure 10A). The EDX spectrum of complex **8** shows the characteristic signals, which correspond to C (carbon), O (oxygen), N (nitrogen), and Co (cobalt) atoms. The spectra indicate the metal complex present as CHCoNO compound (Figure 10B), and complex **9** shows characteristic signals which corresponds to C (carbon), O (oxygen), N (nitrogen), and Ni (nickel) atoms, which indicate the formation of CHNiNO complex (Figure 11A), similarly, the EDX spectrum of complex **10** shows characteristic signals which corresponds to C (carbon), O (oxygen), N (nitrogen) and V(vanadium) and clearly confirmed the formation of CHVNO compound (Figure 11B). Finally, in EDX spectrum the free ligands shows three characteristic signals which correspond to C (carbon), O (oxygen), and N (nitrogen) atoms, which clearly confirms the formation of CHNO compound (Figure 12A and 12B). Generally, the EDX spectra showed both the ligands and all their metal complexes are presented without impurity in which the analysis indicated that the experimental percentage composition of atom is in agreement with the expected (theoretical) values.

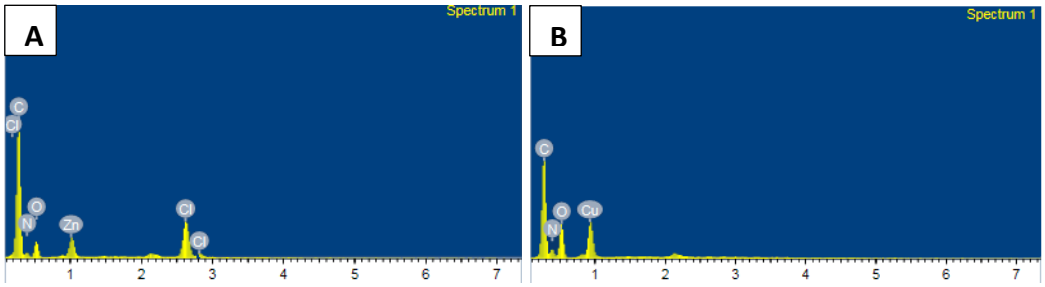

Figure 7. EDX spectra of: A) complex **1** and B) complex **2**

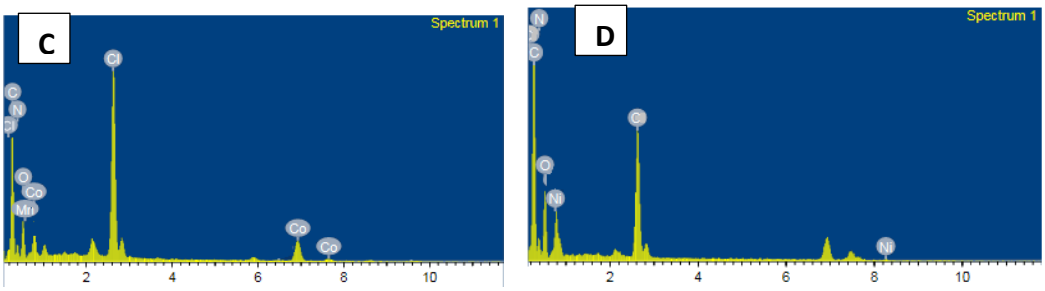

Figure 8. EDX spectra of: C) complex **3** and D) complex **4**

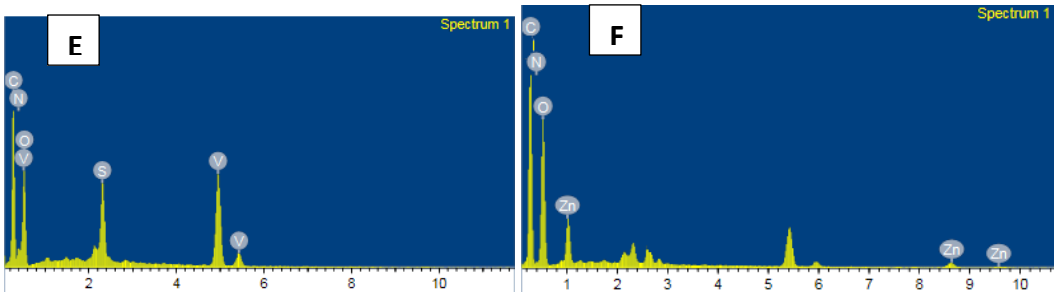

Figure 9. EDX spectra of: E) complex **5** and F) complex **6**

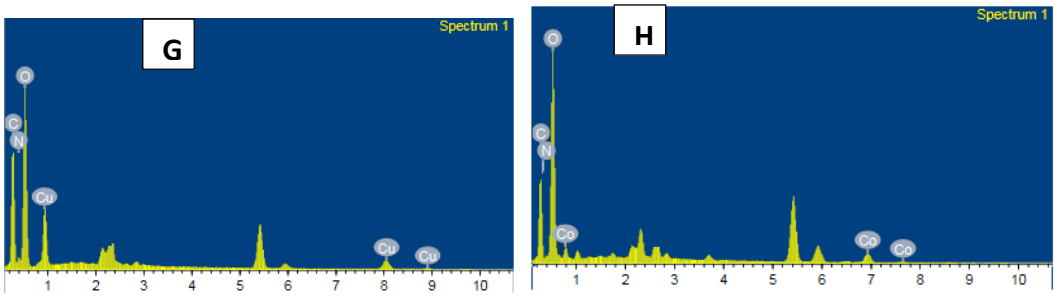

Figure 10. EDX spectra of: G) complex **7** and H) complex **8**

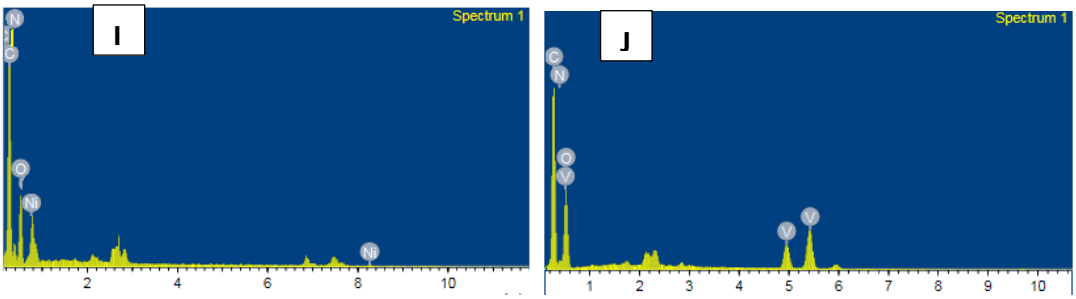

Figure 11. EDX spectra of: I) complex **9** and J) complex **10**

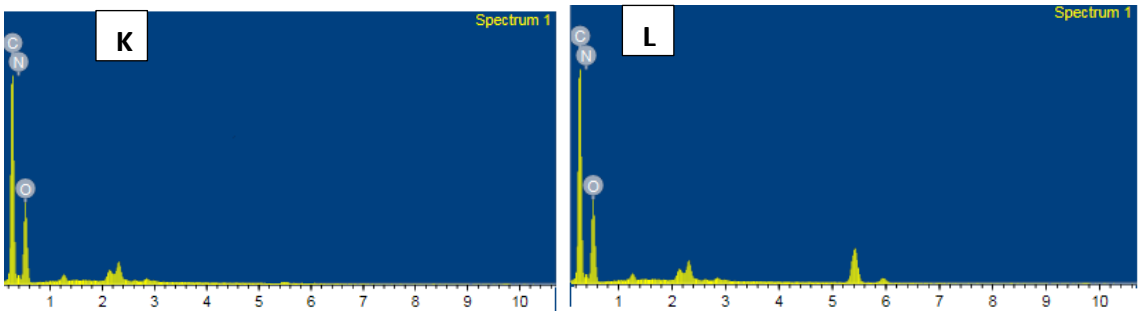

Figure 12. EDX spectra of: K) **L1** and L) **L2**

4.2.6. Mass spectra of transition metal complexes

The fragmentation of organic compounds have been studied intensively and systematically for many decades but the studies of fragmentation of the metal-containing compounds are much less and not well established, but there are some basic ground rules that apply in both situations. For coordination compounds $\mathbf{ML_n}$ where **M** is a metal and **L** are atoms or groups of atoms bonded to M, nearly all the ions in the mass spectrum may contain **M** [176, 330].

The mass spectra of the transition metal complexes (**1** – **10**) are characterized using LC-MS. Accordingly, the mass spectrum of complex **1** exhibits a parent molecular ion peak at *m/z* = 392.90 (Found = 392.98) which corresponds to the formula of $[C_{14}H_{15}Cl_2N_3O_2Zn]$ (M.Wt.= 393.57 g/mol). The mass spectra of this complex displayed another peaks at *m*/*z* 357.05 (7.70%) (Found = 356.01), 322.07 (8.75 %) (Found = 321.05), 259.63 (54.75 %) (Found = 260.14) assigned to the $[C_{14}H_{15}ClN_3O_2Zn]^+$, $[C_{14}H_{15}N_3O_2Zn]^+$ and $[C_{14}H_{18}N_3O_2]^+$ fragments respectively (Appendix 26). The complex **2** exhibits a parent molecular ion peak at *m/z* = 400.08 (Found = 400.04) which corresponds to the formula of $[C_{14}H_{17}CuN_4O_6]$ (M.Wt= 400.85 g/mol). It also displayed another peaks at *m*/*z* 322 95(6.70 %) (Found = 322.06), 260.01 (54.75 %) (Found = 260.14) and 226.13 (14.75 %) (Found = 226.13) leading to $[C_{14}H_{17}CuN_3O_2]^+$, $[C_{14}H_{18}N_3O_2]^+$ and $[C_{14}H_{16}N_3]^+$ fragments respectively (Appendix 27) and the mass spectrum of complex **3** exhibits a parent molecular ion peak at *m/z* = 404.05 (Found= 404.00) which is similar to the formula of $[C_{14}H_{17}Cl_2CoN_3O_3]$ (M.Wt= 405.14 g/mol). In addition, this complex showed other peaks at *m*/*z* = 316 06(34.70 %) (Found = 316.05) and 260.14.00 (34.75 %) (Found = 260.14) assigned to $[C_{14}H_{15}CoN_3O_2]^+$ and $[C_{14}H_{18}N_3O_2]^+$ fragments respectively (Appendix 28). Complex **4** exhibits a parent molecular ion peak at *m/z* = 413.09 (Found = 413.06) which is similar to the formula of $[C_{14}H_{19}N_4NiO_7]$ (M.Wt= 414.02 g/ mol). In other way the additional peaks for complex **4** are observed at *m*/*z* = 351.09 (10.9 %) (Found = 351.07), 315.9 (30.70 %) (Found = 315.05) and 260.33 (29.9 %) (Found = 260.14) assigned to $[C_{14}H_{19}N_3NiO_4]^+$, $[C_{14}H_{15}N_3NiO_2]^+$ and $[C_{14}H_{18}N_3O_2]^+$ fragments respectively (Appendix 29). Complex **5** exhibits a parent molecular ion peak at *m/z* = 438.11 (Found = 438.02) which related to the formula of $[C_{14}H_{17}N_3O_8SV]$ (M.Wt = 438.31 g/mol). The spectra of this complex also showed another peaks at *m*/*z* = 309. 05 (9.70 %) (Found = 308.06) and 259.33 (12.75 %) (Found = 259.13) leading to $[C_{14}H_{15}N_3O_2V]^+$ and $[C_{14}H_{17}N_3O_2]^+$ fragments respectively (Appendix 30). This analysis is in agreement with the reported studies [43, 146, 176, 318, 327, 330].

Similarly, the ligand (**L2**) showed molecular ion peak at *m/z* = 215.75 (calcd = 216.09) which correspond to $[C_{12}H_{12}N_2O_2]$ (M. Wt = 216.24 g/mol) (Appendix 31), which is the same as to its molecular weight. In the case of metal complexes, complex **6** showed molecular ion peak, at *m/z* = 493.95 (calcd = 494.09) corresponding to $[C_{24}H_{22}N_4O_4Zn]$ (M. Wt = 495.84 g/mol). The spectrum of this complex also displayed another peaks at *m/z* = 435.95 (62.30%) (calcd. = 436.09) and 386.35 (30.80%) (calcd. = 386.07) which correspond to $[C_{22}H_{20}N_4O_2Zn]^+$ and $[C_{18}H_{18}N_4O_2Zn]^+$ respectively, (Appendix 32). Complex **7** showed parent molecular ion peak at *m/z* = 529.45 (calcd = 529.11) which related to the formula of $[C_{24}H_{26}CuN_4O6]$ (M. Wt = 530.03 g/mol). On the other hand, this complex showed other peak at *m/z* = 392.75 (60.80%) (calcd = 393.04), leading to $[C_{19}H_{14}CuN_4O_2]^+$ fragment (Appendix 33). Complex **8** exhibits a parent molecular ion peak at *m/z* = 524.85 (calcd = 525.12) which correspond to the formula of $[C_{24}H_{26}CoN_4O_6]$ (M.Wt = 525.42 g/mol). The observed peaks for complex **8** at *m*/*z* = 467 85 (18.50%) (calcd = 467.11) and 392.85 (60%) (calcd = 393.08 can be assigned to $[C_{22}H_{24}CoN_4O_4]^+$ and $[C_{19}H_{18}CoN_4O_2]^+$ (Appendix 34), similarly, complex **9** exhibits a parent molecular ion peak at *m/z* = 524.40 (calcd = 524.12) which is similar to the formula of $[C_{24}H_{26}N_4NiO_6]$ (M. Wt= 525.18 g/mol). In other way the additional peaks for complex **9** are observed at *m*/*z* = 466.40 (10.9 %) (calcd = 466.12) and 393.40 (65%) (calcd = 393.09) assigned to $[C_{22}H_{24}N_4NiO_4]^+$ and $[C_{19}H_{19}N_4NiO_2]^+$ (Appendix 35) and finally the mass spectrum of complex **10** exhibits a parent molecular ion peak at *m/z* = 497.25 (calcd = 497.10) which is similar to the formula of $[C_{24}H_{22}N_4O_5V]$ (M.Wt = 497.40 g/mol) and showed other peaks at *m*/*z* = 391.25 (65%) (calcd = 391.10) and 273.25 (35%) (calcd = 273.03) which assigned to $[C_{18}H_{20}N_4O_3V]^+$ and $[C_{10}H_{12}N_3O_3V]^+$ (Appendix 36) fragments respectively for all (**6 – 10**) and these analysis are in line with previous reported studies [43, 146, 176, 318, 327, 330].

4.2.7. Molar Conductance

The molar conductance of the synthesised ligands and their metal complexes was recorded in triplicate using concentration of 1mM in methanol at room temperature. The molar conductance of metal complex (**1** – **5**) was ranged from 5 to 19 ($\Omega^{-1}mol^{-1}cm^2$ 25 ^oC). Similarly, the molar conductance of the complexes (**6** – **10**) was 10 to 21 $\Omega^{-1}mol^{-1}cm^2$ 25 ^oC (Table 1). These indicate that the conductivity of the synthesized metal complexes is relatively low; hence the non-electrolytic nature of the complexes and which are very low to account for their electrolytic behavior. Generally, molar conductance of complexes (**1** – **10**) are very low, this is because there is no primary valance in the complexes, in other word the

complexes consists lower electrolytes which results in non-electrolytic nature of the complexes [81, 331]. This is mainly due to the fact that the metal cations received electrons from the ligand to make the net charge balance of the complexes to be zero in line with the previous reported studies [80, 123, 146, 301, 318, 323, 332].

The molar conductance also used in the investigation of the geometrical structures of the complexes [146]. According to the non-electrolytic nature of the metal complexes specifically metal complexes **1** and **3,** the chloride ion is coordinated to metal ion to satisfy the valence of the coordination sphere hence, the presences of chloride ions inside the coordination sphere of the specified complexes were confirmed by reaction with silver nitrate ($AgNO_3$) solution whereas, there is no precipitate formation during the experiment. Therefore, the formed Zn(II) and Co(II) complex would be formulated as $[Zn(H_2L)Cl]$ and $[Co(H_2L)(H_2O)_2Cl]$ in line with the reported studies [81, 332].

4.2.8. Thermogravimetric Analysis

Thermogravimetric analyses (TGA) of metal complexes were recorded under N_2-atmosphere (20 ml/min) using 8 mg dried sample. In this analysis, heating rate was controlled at 10 ^oC min^{-1} under nitrogen atmosphere and the weight loss is measured at temperature ranges from 25 to 800 ^oC. Accordingly, thermogravimetric analysis (TGA) of the synthesised Zn(II), Cu(II), Co(II), Ni(II) and V(IV) complexes (**1** – **10**) were carried out to get information about their thermal stability and to suggest a general scheme for their thermal decomposition as well as to assure the presence and absence of water molecules.

The TG and Differential thermal analysis (DTA) curves are presented in Figures 13 – 17 for the first five complexes (**1** – **5**) and Figures 18 – 22 for the second five complexes (**6** – **10**), whereas the temperature range values for decomposition along with the corresponding weight loss values for each step of the decomposition reaction for complexes **(1** – **5)** are presented in Table 4 and in Table 5 for complexes **(6** – **10)**.

Accordingly, thermogravimetric analysis (TGA) diagram of complex **1** $[C_{14}H_{16}ClN_3O_2Zn]$ showed three decomposition steps (Figure 13). The first step of degradation observed in temperature range of 255 – 350 ^oC (DTA_{max} = 325 °C), which indicate mass loss of 17.8% (calcd. = 17.96%) that attribute to the loss of chloroethane (C_2H_5Cl) like moiety. The complex is stable up to 200 ^oC which indicate the absence of both lattice and coordination water in the specified complex, which in agreement with reported studies [184, 227, 333,

334]. The second step observed with a weight loss of, 21% (calcd. = 21.19%) attributed to the loss of C_6H_4 quinoline ring moiety at 360 – 520 ^oC (DTA_{max} = 515 °C), which in line with previous studies [2, 227]. The third step of degradation has been arising from mass loss of 29.99% (calcd. = 30.38%), attributed to the loss of $C_5H_5N_2O$ moieties at temperature range of 535 – 765 ^oC (DTA_{max} = 655 °C) and the actual weight loss occurred from all these steps is 68.79%, which is in very good agreement with the calculated value (69.53%) [334], hence gradual degradation was observed up to 765 ^oC and the residue corresponds to zinc oxide (ZnO) about 22.52% (calcd = 22.66%) and imine (CHN) moiety about 7.40% (calcd. = 7.53%) in agreement with reported studies [184, 316, 333–336].

The TGA diagram of complex **2**, $[C_{14}H_{18}CuN_4O_6]$, indicates three decomposition steps (Figure 14). The first step of degradation observed due to mass loss of 41.69% (calcd. = 41.69%) related to the elimination of one water molecule, $C_3H_6N_2O$ moieties and nitrate ion species at temperature ranges of 100 – 266 ^oC (DTA_{max} = 213 °C) [3]; the second step is arising due to weight loss of 7.26% (calcd. = 7.00%) at temperature ranges 240 – 498 ^oC (DTA_{max} = 245 °C), corresponding to the elimination of C_2H_4 ethane like moiety. The final step occurs at temperature ranges of 520 – 640 ^oC (DTA_{max} = 530 °C), due to the loss of 32.14% (calcd. = 31.89 %) related to C_9H_6N moiety, and other leaving residue copper(II) oxide (CuO), representing 18.91 % (calcd. = 19.80 %) of the complex and the actual weight loss is 81.09 % ;very close to the calculated one 80.33 %, in line with reported studies [184, 333, 334].

The thermal decomposition of complex **3**, $[C_{14}H_{20}ClCoN_3O_4]$ exhibits three degradation steps (Figure 15). The first step of decomposition occurs within temperature range of 100 to 130 ^oC (DTA_{max} = 125 °C), which shows mass loss of 9.26% (calcd. = 9.26%) that corresponds to the loss of two water molecules. The second step of decomposition occurs within a temperature range of 150 to 510 ^oC (DTA_{max} = 360 °C), which is accompanied by a weight loss of, 19.89% (calcd. = 20.71%) corresponding to the loss of C_2H_4ClOH molecules [2, 227]. The third step of degradation occurs in the temperature range of 535 – 778 ^oC (DTA_{max} = 669 °C) and is accompanied by a weight loss of 51.43% (calcd. = 51.0%) corresponding to the loss of $C_{12}H_{12}N_3$ species of the quinoline ring. The actual mass loss from these steps is 80.58 % which is close to the calculated value of 80.97% [334]. Thereafter, the compound showed a gradual decomposition up to 778 ^oC with a weight loss of organic moiety. The

weight of the residue corresponds to the respective metal oxide (CoO) about 19.42% (calcd = 19.03%).

The thermal decomposition of complex **4,** [$C_{14}H_{20}N_4NiO_7$] exhibits four degradation steps (Figure 16). The first step of decomposition occurs in temperature ranges of 100 – 155 ^oC (DTA_{max} = 125 °C), which is accompanied by weight loss of 8.65% (calcd. = 8.67%) corresponding to the elimination of two lattice water molecule [333]. The second step of decomposition occurs in temperature ranges of 220 – 255 ^oC (DTA_{max} = 229 °C), which is accompanied by a weight loss of 10.23% (calcd. = 10.13%) corresponding to the loss of imine (C_2H_4N) moiety. The third step of decomposition occurs in temperature ranges of 260 – 361 ^oC (DTA_{max} = 278 °C), which is accompanied by a weight loss of 22.44% (calcd. = 22.41%) corresponding to the loss of (CH_3O + NO_3^-) methanol and nitrate ion moieties, corresponding to the previous reported study [3]. The fourth and final step decomposition occurs between temperature ranges of 382 – 610 ^oC (DTA_{max} = 508 °C), which is due to the loss of C_8H_9N the quinoline ring, moiety which is 28.74% (calcd. = 28.96%), and other leaving residue of organic compound moieties and nickel oxide (NiO) representing 29.24% (calcd. = 27.22%) of the total complex. From the data, the actual mass loss from these steps is 70.06 % which is very close to the calculated value of 69.91% in line with the previous studies [184, 333, 334].

Similarly, the thermal decomposition of complex **5**, [$C_{14}H_{18}N_3O_8SV$] exhibits three degradation steps (Figure 17). The first step of decomposition occurs in temperature ranges of 100 – 182 ^oC, (DTA_{max} = 113 °C) which is accompanied by mass loss of 14.23% (calcd. = 14.34%) corresponding to the loss of one water molecule and C_2H_4OH ethanol molecule. The second step of decomposition occurs in temperature ranges of 185 – 450 ^oC (DTA_{max} = 215 °C), which is accompanied by a mass loss of 31.35% (calcd. = 31.44%) corresponding to the loss of ethyl amine unit and sulphate moiety. The third and final step decomposition occurs between temperature ranges of 455 – 680 ^oC (DTA_{max} = 471 °C), which is due to the loss of C_7H_5N the quinoline ring moiety, which is 22.86% (calcd. = 23.45%), other leaving residue of carbon, nitrogen and VO_2 representing 31.56% (calcd. = 32.52%) of the total complex. From the data, the actual mass loss from these steps is 68.44 % which is close to the calculated value of 69.23% in agreement with reported studies [184, 227, 333, 334].

Table 4. Temperature range and weight loss values for (**1** – **5**)

	Decom. Temp (^oC)	DTA_{max} (°C)	Mass loss (%)		Interpretation
			Obsd.	Calcd.	
1	255 – 350	325	17.8	17.96	loss due to chloroethane (C_2H_5Cl) like moiety
	360 – 520	515	21.00	21.19	loss due to C_6H_4 species of quinoline ring
	535 – 765	655	29.99	30.38	loss due to $C_5H_5N_2O$ species of the quinoline ring moiety
2	100 – 225	213	41.69	41.44	loss of one water molecule, quinoline ring moiety $C_3H_6N_2O$ and nitrate ion
	240 – 498	245	7.26	7.00	loss of C_2H_5 ethane like moiety
	520 – 640	530	32.14	31.89	loss due to C_9H_6N of the imine with quinoline moiety
3	100 – 130	125	9.26	9.26	loss due to two water molecules
	150 – 510	360	19.89	20.71	loss due to one coordinated chlorine atoms and ethanol moiety
	535 – 778	669	51.43	51.00	loss due to $C_{12}H_{12}N_3$ species of quinoline ring
4	100 – 155	125	8.65	8.67	loss of two lattice water molecule
	220–255	229	10.23	10.13	loss of C_2H_4N fragment of imine
	260 – 361	278	22.44	22.41	loss of CH_3O + NO_3 fragments of methanol moiety and
	382 – 610	508	28.74	28.96	loss due to C_8H_9N, fragment of the quinoline ring
5	100 – 182	113	14.23	14.34	loss of one water and C_2H_4OH molecules
	185 – 450	215	31.35	31.44	loss of ethyl amine unit moiety and sulphate ion
	455 – 680	471	22.86	23.45	mass loss of C_7H_5N of quinoline ring moiety

Decom. Temp = decomposition temperature, Obsd = observed, Calcd = calculated, Exo = exothermic

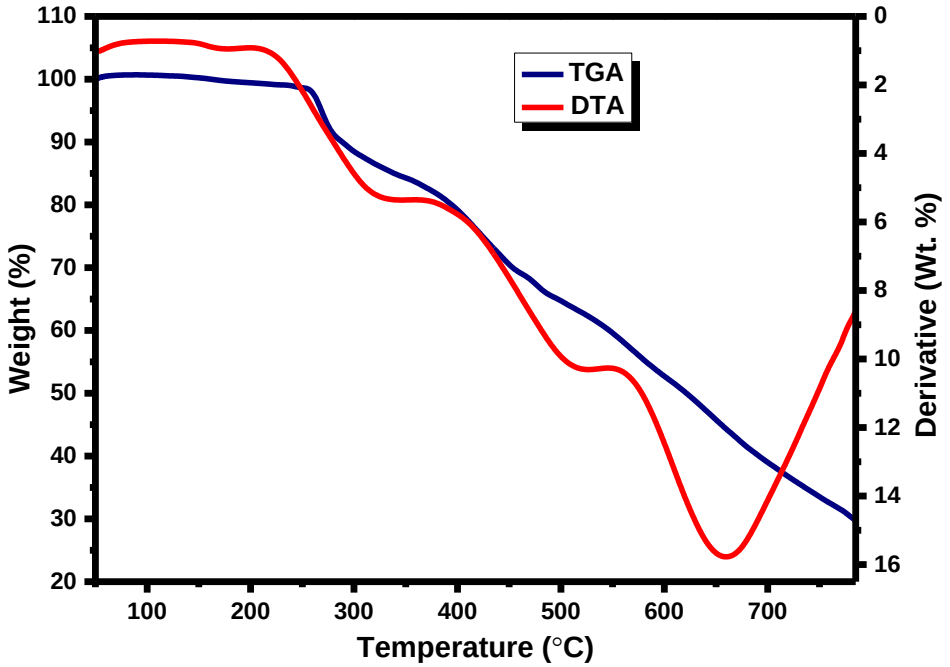

Figure 13. TGA and DTA curve of complex **1**

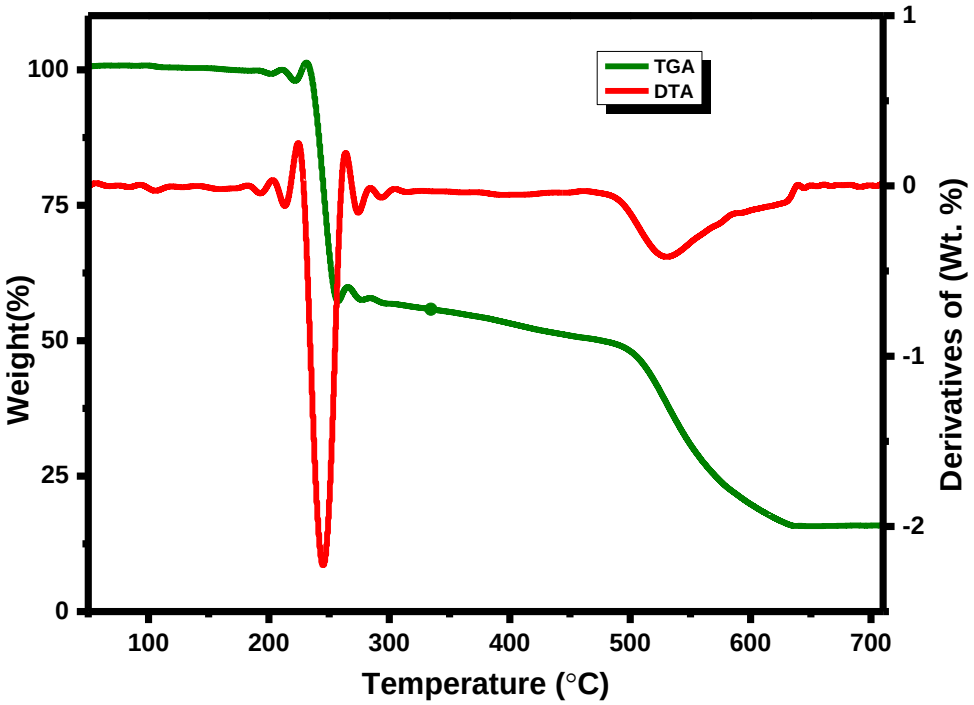

Figure 14. TGA and DTA curve of complex **2**

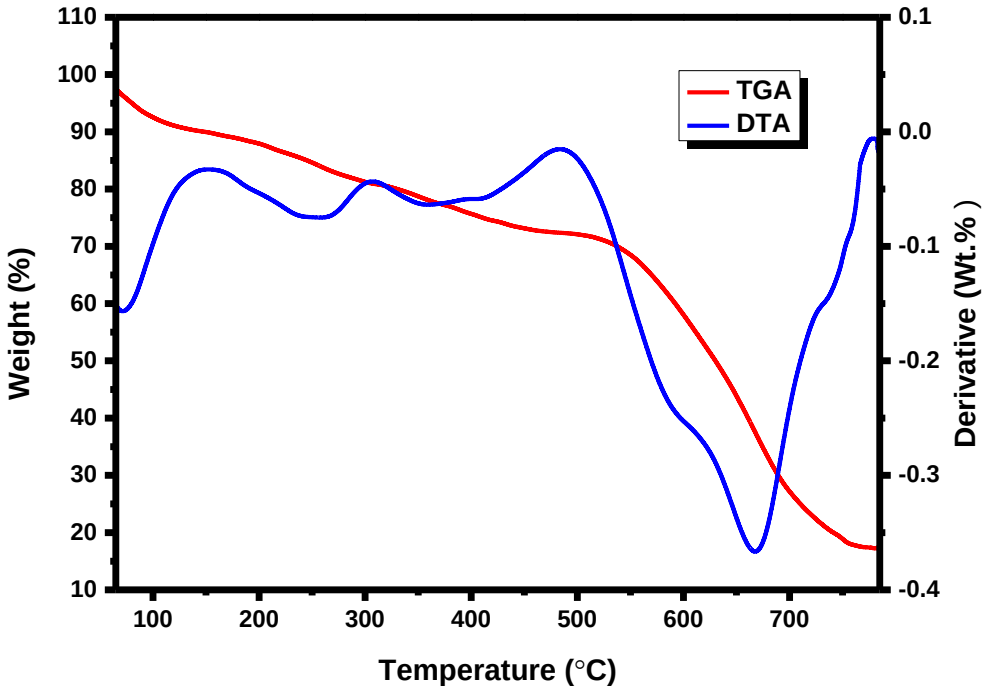

Figure 15. TGA and DTA curve of complex **3**

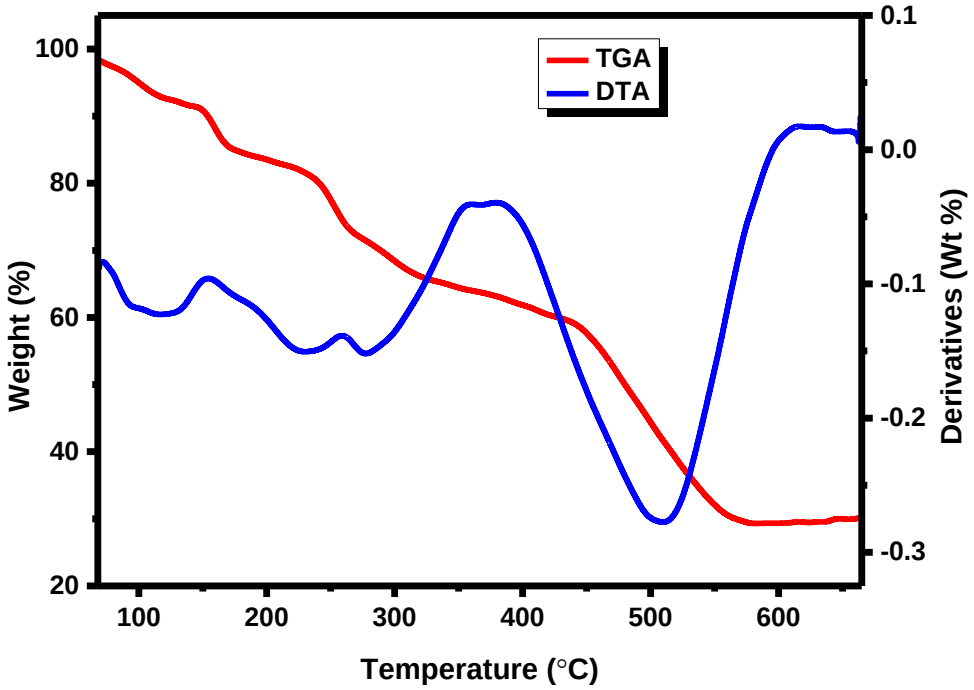

Figure 16. TGA and DTA curve of complex **4**

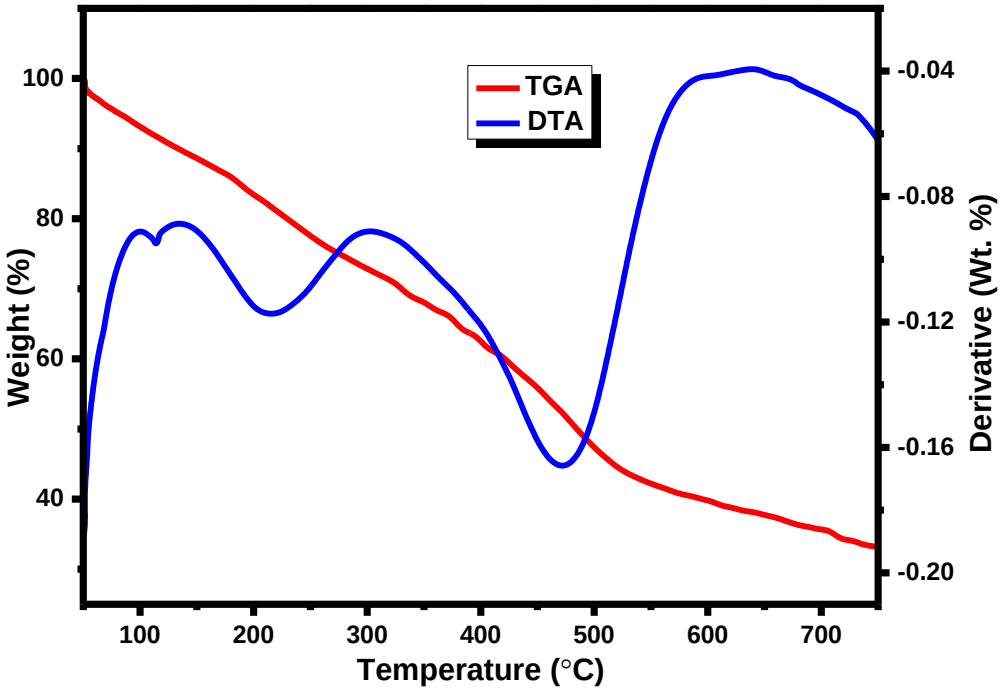

Figure 17. TGA and DTA curve of complex **5**

Similarly, to confirm the proposed formulae for all complexes (**6** – **10**) thermogravimetric (TG) and differential thermogravimetric analysis (DTG) were shown in (Figure 18 – 22). The TGA curve of complex **6** [$C_{24}H_{22}N_4O_4Zn$] exhibits approximately five stages of decomposition (Figure 18). The first stage occurs at temperature range 100 – 250 ^oC (DTA_{max} = 215 °C) corresponds to the C_6H_4N quinoline ring moiety with mass loss of 18.06% (calc. 18.16%) [333]. The second step of decomposition occurs within a temperature range of 280 – 385 ^oC ^oC (DTA_{max} = 346 °C), which is accompanied by a weight loss of, 10.78% (calcd. = 10.89%) corresponding to loss due to C_3H_2O carbonyl moiety [2, 227]. The third step of degradation occurs in the temperature range of 395 – 505 ^oC (DTA_{max} = 453 °C) and is accompanied by a weight loss of 19.82% (calcd. = 20.58%) corresponding to C_7H_4N of the quinoline ring with amine substituent. The fourth step of degradation occurs in the temperature range of 510 – 610 ^oC (DTA_{max} = 528 °C) and is accompanied by a weight loss of 5.21% (calcd. = 5.44%) corresponding to CHN of amine moiety. The fifth and final step of degradation occurs in the temperature range of 620 – 665 ^oC (DTA_{max} = 627 °C) and is accompanied by a weight loss of 6.16% (calcd. = 6.26%) corresponding loss due to CH_3O carbonyl moiety. The actual mass loss from these steps is 60.03%, which is close to the

calculated value of 61.33 [334]. Thereafter, the compound showed a gradual decomposition up to 665 ^{o}C with a weight loss of many organic moieties. The weight of the residue corresponds to the respective zinc oxide (ZnO) and some organic moiety ($C_4H_7NO + C_2H_4$) about 39.97% (calcd = 38.83%) which indicated with straight line in agreement with previous reported studies [316, 333].

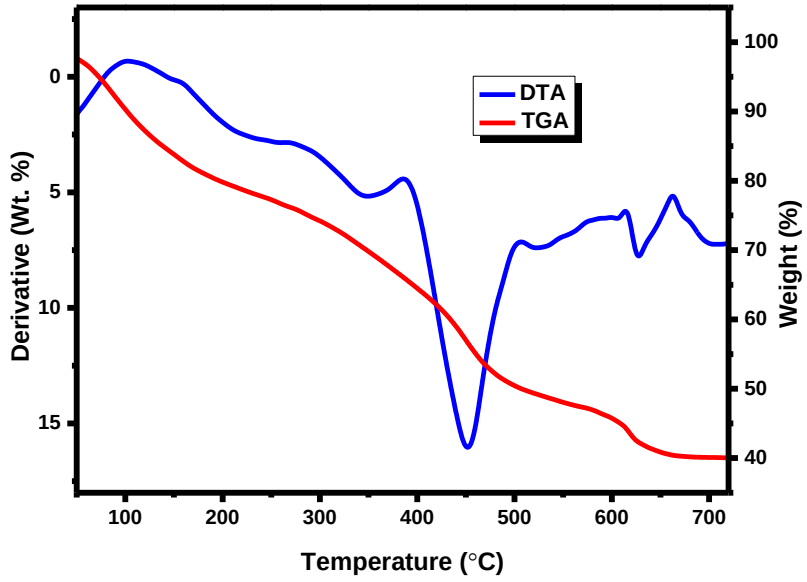

Figure 18. TGA and DTA curve of complexes **6**

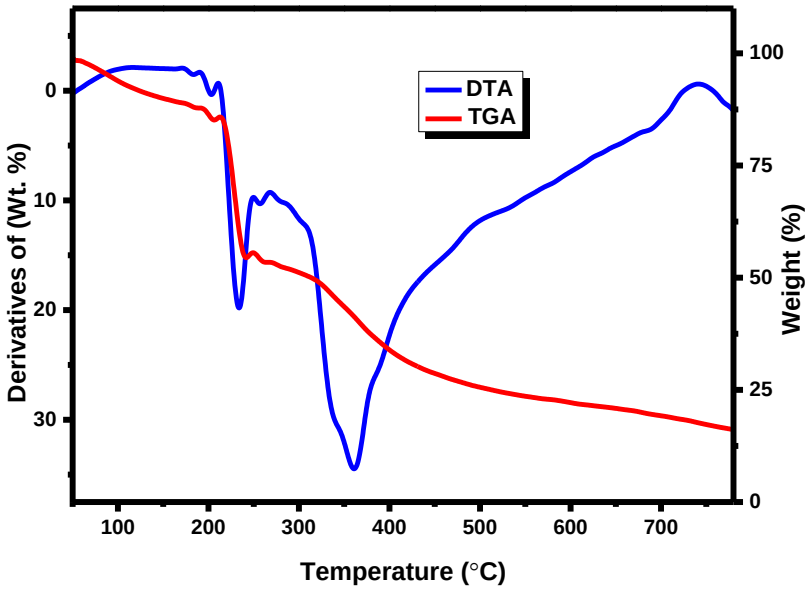

Figure 19. TGA and DTA curve of complex **7**

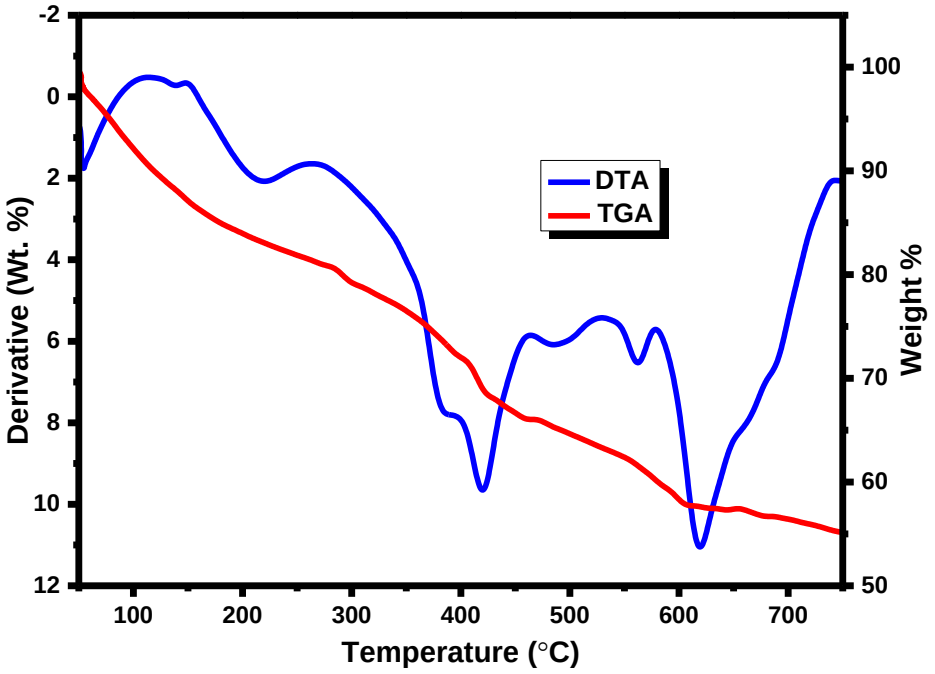

Figure 20. TGA and DTA curve of complex **8**

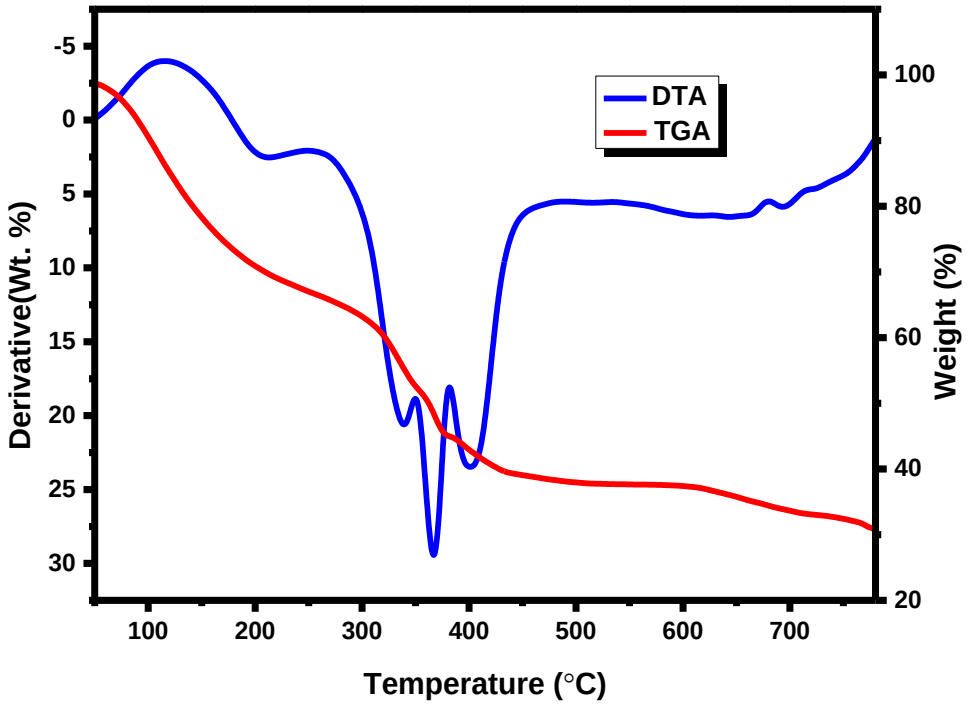

Figure 21. TGA and DTA curve of complex **9**

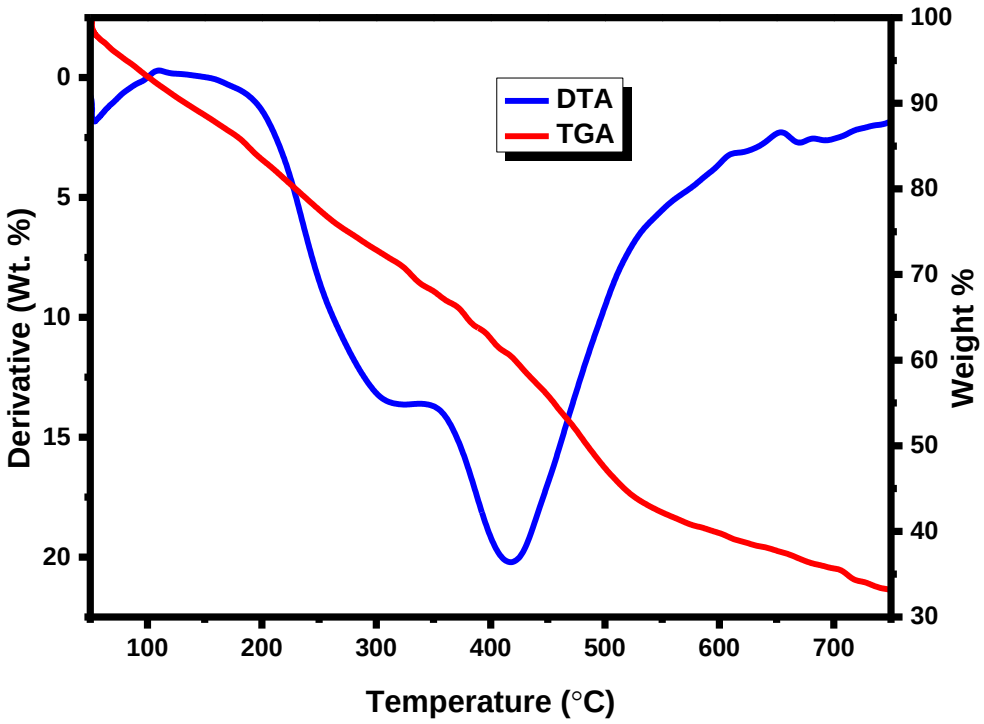

Figure 22. TGA and DTA curve of complex **10**

The thermal decomposition of complex **7** [$C_{24}H_{26}CuN_4O_6$] proceeds with three main degradation steps (Figure 19) and the first stage of decomposition occur at temperature range of 100 – 210 ^{o}C (DTA_{max} = 200 °C). The found weight loss associated with this step is 9.86% and may be attributed to the loss of two water molecule, and carbonyl oxygen moiety, which is in good agreement with the calculated values of 9.81%. In addition, the second stage of decomposition occurs at temperature range of 215 – 312 ^{o}C (DTA_{max} = 233 °C). The found weight loss associated with this step is 39.87% and may be attributed to loss of $C_{13}H_{12}N_2O$ quinoline ring moiety with amine substituent, which is in good agreement with the calculated value of 40.01%. The third and final stage of decomposition occurs at temperature range of 320 – 720 ^{o}C (DTA_{max} = 364 °C) and the weight loss found at this stage equals to 33.9% corresponds to loss due to $C_{11}H_5N_2O$ the amine with quinoline ring moieties, which is in good agreement with the calculated value of 34.16%. This complex was decomposed with total mass loss 83.64% (calcd.= 83.98%) and 16.36% mass loss leaving copper oxide (CuO) as residue (Table 5), which is in good agreement with the calculated value of 15.01% in line with the previous studies [227, 334].

The TGA curve of complex **8** [$C_{24}H_{26}CoN_4O_6$] exhibits approximately five stages of decomposition (Figure 20). The first stage occurs at temperature range 150 – 260 ^oC (DTA_{max} = 214 °C) corresponds to loss due to two water molecule with mass loss of 6.85% (calc. 6.85%) [333]. The second step of decomposition occurs within a temperature range of 390 – 460 ^oC (DTA_{max} = 420 °C), which is accompanied by a weight loss of, 14.47% (calcd. = 14.47%) corresponding loss due to C_6H_4 quinoline ring moiety [2, 227]. The third step of degradation occurs in the temperature range of 470 – 530 ^oC (DTA_{max} = 489 °C) and is accompanied by a weight loss of 7.35% (calcd. = 7.43%) corresponding loss due to C_3H_3 the quinoline ring moiety. The fourth step of degradation occurs in the temperature range of 542 – 575 ^oC (DTA_{max} = 562 °C) and is accompanied by a weight loss of 13.67% (calcd. = 13.85%) corresponding loss due to C_4NO carbonyl oxygen with imine of quinoline moiety. The fifth step of degradation occurs in the temperature range of 560 – 655 ^oC (DTA_{max} = 619 °C) and is accompanied by a weight loss of 3.07% (calcd. = 3.05%) corresponding loss due to oxygen of carbonyl moiety. The actual mass loss from these steps is 45.41 %, which is close to the calculated value of 45.65%. [334]. Thereafter, the compound showed a gradual decomposition up to 655 ^oC with a weight loss of many organic moieties. The weight of the residue corresponds to the respective cobalt(II) oxide (CoO) and some organic moiety ($C_2H_5N + C_9H_{11}N_2O$) which is in line with previous reported studies [316, 333].

The thermal decomposition of complex **9**, [$C_{24}H_{26}N_4NiO_6$] proceeds with four main degradation steps (Figure 21). The first stage of decomposition occurs at temperature range of 120 – 250 ^oC (DTA_{max} = 210 °C). The found weight loss associated with the step is 6.85% and may be attributed to the loss of two water molecule, which is in good agreement with the calculated values of 6.86%. In addition, the second stage of decomposition occurs at temperature range of 280 – 350 ^oC (DTA_{max} = 338 °C). The found weight loss associated with step is 32.59 and may be attributed to loss of $C_{10}H_8N_2O$ quinoline ring with amine substituent moieties, which is in good agreement with the calculated value of 32.8%. The third stage of decomposition occurs at temperature range of 355 – 380 ^oC (DTA_{max} = 365 °C) and the weight loss found at this stage equals to 18.79% corresponds to loss due to C_7H_2N the amine with quinoline ring moieties, which is in good agreement with the calculated value of 19.04%. The fourth stage of decomposition occurs at temperature range of 382 – 455 ^oC (DTA_{max} = 400 °C) and the weight loss found at this stage equals to 9.16% corresponds to loss due to C_2H_6O ethanol moiety, which is in good agreement with the calculated value of 8.77%. This complex was decomposed with total mass loss 67.39% (calcd.= 67.47%) and

14.08% mass loss leaving nickel(II) oxide (NiO) as residue (Table 5), which is in good agreement with the calculated value of 14.1% [227, 334].

Finally, the thermal decomposition of complex **10**, $[C_{24}H_{22}N_4O_5V]$ proceeds with three main degradation steps (Figure 22). The first stage of decomposition occurs at temperature range of 200 – 325 ^oC (DTA_{max} = 316 °C). The found weight loss associated with step is 28.97% and may be attributed to loss of C_9H_7NO quinoline ring with carbonyl oxygen moieties, which is in good agreement with the calculated values of 29.20%. In addition, the second stage of decomposition occurs at temperature range of 330 – 450 ^oC (DTA_{max} = 416 °C). The found weight loss associated with step is 10.18% and may be attributed to loss of C_4H_4 quinoline ring moiety, which is in good agreement with the calculated value of 10.48%. The third stage of decomposition occurs at temperature range of 470 – 740 ^oC (DTA_{max} = 669 °C) and the weight loss found at this stage equals to 27.67% corresponds to loss due to $C_7H_{10}N_2O$ quinoline ring moiety with amine substituent, which is in good agreement with the calculated value of 27.80%. This complex was decomposed with total mass loss 66.82% (calcd. = 67.48%) and 16.69% mass loss leaving vanadium (IV) oxide (VO_2) as residue.

The general degradation pattern of the complexes (**1**, **2**, **3**, **5**, **7** and **10**) arisen in three stages, while that of complexes (**4**, and **9**) occurred in four and that of (**6**, **8)** in five stages. The thermogram above 765, 640,778, 610, 680, 665, 720, 655, 455 and 740 °C temperature for complex (**1** – **10**) respectively, gave a straight line, indicating the formation of metal oxides [184, 333]. The obtained percentage content of elements in all these complexes from both the elemental and TGA analyses are in a very good agreement and in line with the formulae proposed from the analytical data (Section 3.5), and all the thermogram of the complexes showed that the complexes are stable up to 100 ^oC hence no weight loss occurs before this temperature. This is also confirmed from DTA_{max} (°C), in agreement with the spectroscopically determined stability constant of complexes, which did not show any change up to 40 ^oC (Table 7, see section 4.4) and this inferring that, the metal complexes can be used for different biological application.

Table 5. Temperature range and weight loss values for (**6** – **10**)

	Decom. Temp. (^oC)	DTA_{max} (°C)	Mass loss (%)		Interpretation
			Obsd.	Calcd.	
6	100 – 250	215	18.06	18.16	loss due to C_6H_4N quinoline ring moiety.
	280 – 385	346	10.78	10.89	loss due to C_3H_2O carbonyl moiety
	395 – 505	453	19.82	20.58	loss due to C_7H_4N the quinoline ring with amine substituent
	510 – 610	528	5.21	5.44	loss due to CHN amine moiety
	620 – 665	627	6.16	6.26	loss due to CH_3O carbonyl moiety
7	100 – 210	200	9.86	9.81	loss of two water molecule, and carbonyl oxygen moiety
	215 – 312	233	39.87	40.01	loss of $C_{13}H_{12}N_2O$ quinoline ring with amine substituent
	320 – 720	364	33.9	34.16	loss due to $C_{11}H_5N_2O$ the amine with quinoline ring moiety
8	150 – 260	214	6.85	6.85	loss due to two water molecule
	390 – 460	420	14.47	14.47	loss due to C_6H_4 quinoline ring moiety
	470 – 530	489	7.35	7.43	loss due to C_3H_3 the quinoline ring moiety
	542 – 575	562	13.67	13.85	loss due to C_4NO carbonyl oxygen with imine of quinoline ring moiety
	560 – 655	619	3.07	3.05	loss due to oxygen of carbonyl moiety
9	120 – 250	210	6.85	6.86	loss of two water molecule
	280 – 350	338	32.59	32.8	loss of $C_{10}H_8N_2O$ quinoline ring with amine substituent moiety
	355 – 380	365	18.79	19.04	loss due to C_7H_2N the amine with quinoline ring moiety
	382 – 455	400	9.16	8.77	loss due to C_2H_6O ethanol moiety
10	200 – 325	316	28.97	29.20	loss of C_9H_7NO quinoline ring with carbonyl oxygen moiety
	330 – 450	416	10.18	10.48	loss of C_4H_4 quinoline ring moiety
	470 – 740	669	27.67	27.80	loss due to $C_7H_{10}N_2O$ quinoline ring with amine substituent moiety

Decom. Temp = decomposition temperature, Obsd = observed, Calcd = calculated, Exo = exothermic

4.3. Biological application

4.3. 1. Antibacterial Activity of Ligands and their metal complexes

In vitro antimicrobial activity of the compounds was tested against four human pathogenic bacteria two Gram negative *(Escherichia coli* (*E. coli*) and *Pseudomonas aeruginosa)* and two Gram positive bacteria (*Staphylococcus aureus* and *Streptococcus pyogenes).* The zone of inhibition values of the studied compounds shown their potential antimicrobial activity when compared to the ligand and the obtained results are shown in, Figure 23, Figure 24, Appendix 37 and Appendix 38.

All the synthesized complexes were proven to have a range of activity against two or more bacterial strains, with the mean zones of inhibition for complexes 1 through 5 ranging from the lowest (7.32 0.90 mm at 150 g/mL) to the highest (20.65 0.18 mm at 300 g/mL). When compared to the positive control drug ciprofloxacin, which has a mean inhibition zone of 22.98 0.08 mm, the first four of these complexes, with mean inhibition zones of 18.85 0.34, 20.65 0.18, 18.62 0.19, and 15.64 0.22 mm diameters at 300 g/mL, respectively, showed good activities against *Pseudomonas aeruginosa*. Complexes **1** – **3** have medium to high bacterial activities with the mean inhibition zones ranged from 10.62 ± 0.36 to 20.65 ± 0.18 mm at both concentration 150 and 300 μg/ for all bacterial strain (*E.coli, P. aeruginosa, S. pyogenes* and *S. aureus*). Among these complex **2** has comparable antibacterial activities with positive standard that has maximum mean inhibition zones of 20.65 ± 0.18 and 22.98 ± 0.08 mm for ciprofloxacin at the same concentration (300 μg/mL) respectively. Complex **4** has low to medium mean inhibition zones range from 8 ± 0.13 to 15.64 ± 0.22 mm diameter at both 150 and 300 μg/mL for gram negative (*E.coli, P. aeruginosa)* and gram positive *(S. aureus),* but has no antibacterial activity for gram positive bacteria specifically *Streptococcus pyogenes*. Complex **5** has low antibacterial activities with mean inhibition zone of 7 ± 0.31 to 8 ± 0.52 for gram positive bacteria *(S. aureus*) and 7.32 ± 0.90 to 9.52 ± 0.49 for gram negative bacteria (*E.coli*) at both 150 and 300μg/mL concentration, while has no effect on both bacteria called *P. aeruginosa, S. pyogenes.* The free ligand has very low mean inhibition zone of 6.22 ± 0.14 to 7 ± 0.11 range for *E.coli, P. aeruginosa* and *S. pyogenes* while has no antibacterial activity effect for gram positive bacteria *S. aureus,* this indicate that free ligand has lower antibacterial activity than its metal complexes (Figure 23).

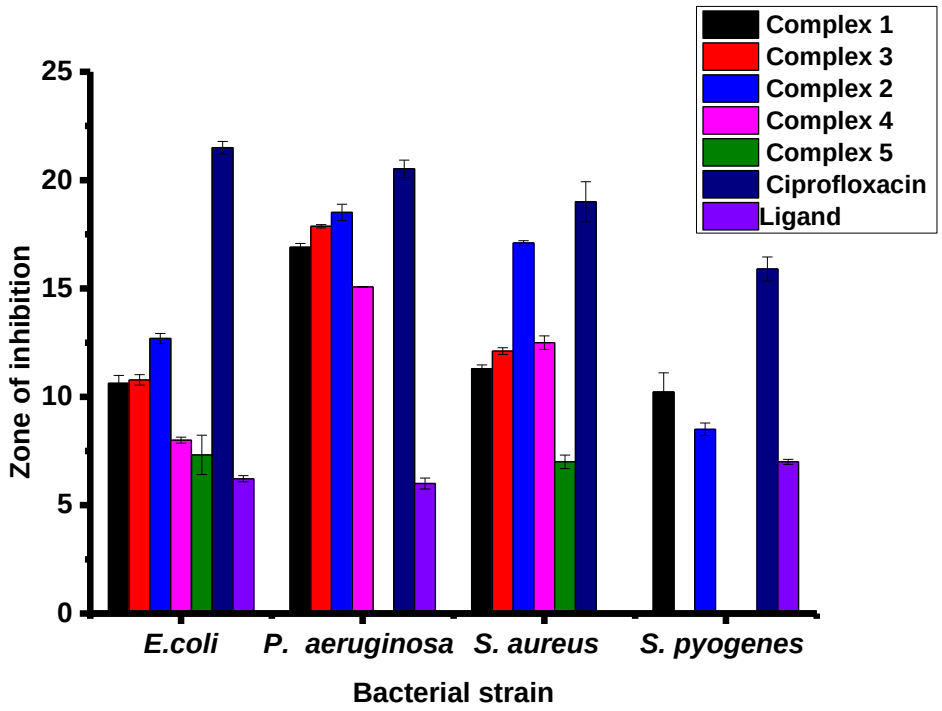

Figure 23. Mean inhibition zone of antibacterial activity of complexes **(1** – **5)**

n = 3. Error bars indicate standard deviation

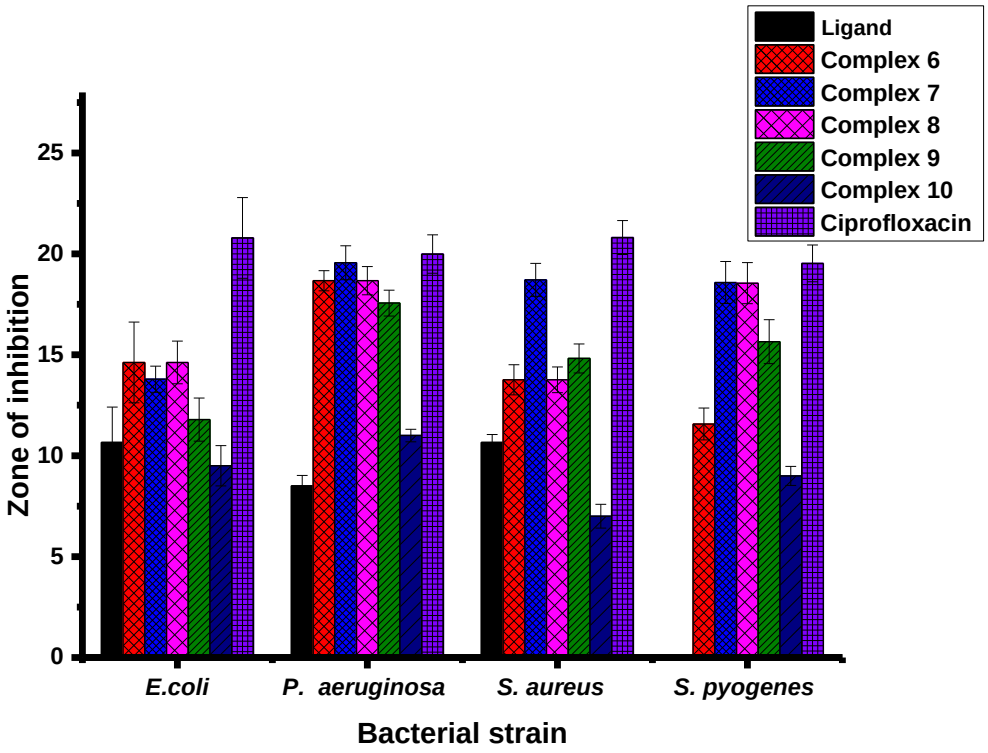

Figure 24. Mean inhibition zone of bacterial activity of complexes (**6** – **10)**

n = 3. Error bars indicate standard deviation

Antibacterial activity of **L2** and its transition metal complexes (**6 – 10**) also evaluated, and the obtained results are shown in Figure 24 and Appendix 46. The data was shown that complexes (**6** – **9**) revealed from medium to high activity against targeted bacterial strains with mean inhibition zones ranged from medium (11.57 ± 0.79 mm at 100 μg/mL) to the highest (20.90 ± 2.00 mm at 200 μg/mL). These four complexes showed good activities against *Pseudomonas aeruginosa*, with mean inhibition zones of 20.75 ± 2.05, 20.9 ± 2.00, 20.75 ± 2.07 and 18.90 ± 2.06 mm diameter at 200 μg/mL, respectively when compared with positive control ciprofloxacin with mean inhibition zones of (20.94 ± 2.01mm). Relatively complex **7** showed better antibacterial activities with the range of mean inhibition zones rages from 18.58 ± 1.04 to 20.9 ± 2.00 mm at both concentration 100 and 200 μg/mL for all tested bacteria. The precursor ligand has lower antibacterial activity than its metal complexes (Figure 24), which is in line with the previous reported studies [56, 102].

Furthermore, results shown in Table 6 indicated better antibacterial activity for complex **7** against *P. aeruginosa, S. aureus* and *S. pyogenes* with MIC values of 0.98, 3.91, and 62.5 (µg/ml) respectively. The complex showed significant antibacterial activity against *P. aeruginosa* in comparison to other bacterial strains and have smaller MIC values against this bacteria in which complex **7** is stronger than other complex**es** in all the four bacterial strains. However, in all cases, the minimum inhibitory concentrations are somewhat larger than that of ciprofloxacin.

Table 6. Minimum inhibitory concentration (MIC in µg/mL) of the complexes

Complexes	Bacterial strains			
	E. coli	*P. aeruginosa*	*S. aureus*	*S. pyogenes*
6	125.0	1.95	15.63	>250
7	125.0	0.98	3.91	62.5
8	125.0	1.95	15.63	62.5
9	125.0	1.95	15.63	62.5
Ciprofloxacin	<0.49	<0.49	0.98	31.25

From the complexes obtained from the two ligands, Cu(II) complexes showed the highest percent activity index against all the examined bacterial strains. This is may be due to borderline Lewis acid nature of Cu(II) ion. It helps Cu(II) to easily bind with similar biomolecules such as protein and enzyme by “hard soft acid-base (HSAB)” Principle hence copper complexes showed good binding activity with both G. negative and G. positive

(*Pseudomonas aeruginosa and S. aureus)* bacterial due to H- bonding interaction with amino acid like arginine having both acid and base end (Table 11 and 12 see section 4.5.3). In addition to this, copper(II) coordination compounds can be highly effective in treating microbial infections due to the redox activity of copper ions which interacted with the bacterial chromosome, which led to a decrease in bacterial reproduction [337].

Moreover, all the complexes showed higher antibacterial activity than the precursor ligand which might be due to chelation of the metal with the ligand that promoted the ability of the complexes to penetrate the cell membrane of the bacterial strains [14, 176, 195]. On chelation, the ligand orbital overlaps with the metal ions, in which the charge of the metal is partially, shared with the donor (ONN) groups, and it enhances the delocalization of π–electrons that increase the lipophilicity of the complexes. Due to increase in lipophilicity, the permeation of the specified complexes could be enhanced, which leads to inhibition of the binding sites in the enzymes of microorganisms [14, 21, 56, 66, 80, 176, 195, 277, 333]. This may result in the disturbance of the respiration system of the cell and prevents the synthesis of the proteins, which ultimately leads to disappearance of the binding sites in the enzymes of the microorganisms. Generally, the activity increases suggested that the complexes having antimicrobial activity may act either by killing the microbe or by inhibiting multiplication of the microbe by blocking their active sites. Comprehensively, the antimicrobial evaluation of any metal complexes is affected by the following items: (i) the chelate effect of the ligands, (ii) the nature of the donation, (iii) the whole charge of the metal complexes and in case of the present study only the chelates (binding) effect on the inhabitation behavior of complexes against bacteria proteins which is in agreement with previous reported studies [14, 21, 56, 66, 80, 176, 195, 277, 333].

4.3.2. Antioxidant Activity of the ligands and their metal complexes

The antioxidant activities of the free ligands and their metal complexes were conducted in terms of their proton donating ability with UV- Visible absorbance using DPPH assay. It is widely used to assess the ability of compounds as scavengers of free radicals and evaluate the antioxidant activity of target free ligands and their metal complexes. Accordingly, compounds that have antioxidant activity may reduce the absorbance of DPPH at 517 nm, which is resulted in changes in color of DPPH in the reaction process [14]. Accordingly, the absorbance of DPPH at 517 nm is decreased in this study which was shown in Figure 25.

In this research work, the radical scavenging activity of the synthesised ligands and their **1** – **10** metal complexes were evaluated and the findings are shown in Figure 26 – 29 and Appendix 39 and 40. The radical scavenging activity of the free ligands and their metal complexes were compared with positive standard, and from these finding we observed that complexes have higher antioxidant activities than the precursor ligands because metal ions could significantly change the chemical properties of the ligands and the synthesised complexes, have good radical scavenging activity, when compared with ascorbic acid [338].

The data shows that the entire synthesised complex (**1** – **5**) showed antioxidant activities, while complex **1** and **2 (**Figure 26) shown better antioxidant activity (with percent scavenging activities 94.19 and 93.96 at 115 µg/mL) respectively and the complexes showed higher antioxidant activities than the corresponding ligands. This is anticipated due to synergetic effects, hence the complexes have a strong potential to be useful as radical scavengers [14, 22]. This activity was also confirmed with half maximal inhibitory concentration (IC_{50}) values of 10.46, 8.62, 16.01, 27.56, 34.79 and 35.36 µg/mL for complexes **1**– **5** and the **L1**, respectively. From IC_{50} values, complexes **1** and **2** have comparable activities; with positive control (IC_{50} = 4.49 µg/mL), (Figure 27). This has direct correlation with the good antioxidant properties [79, 241, 317, 333, 339].

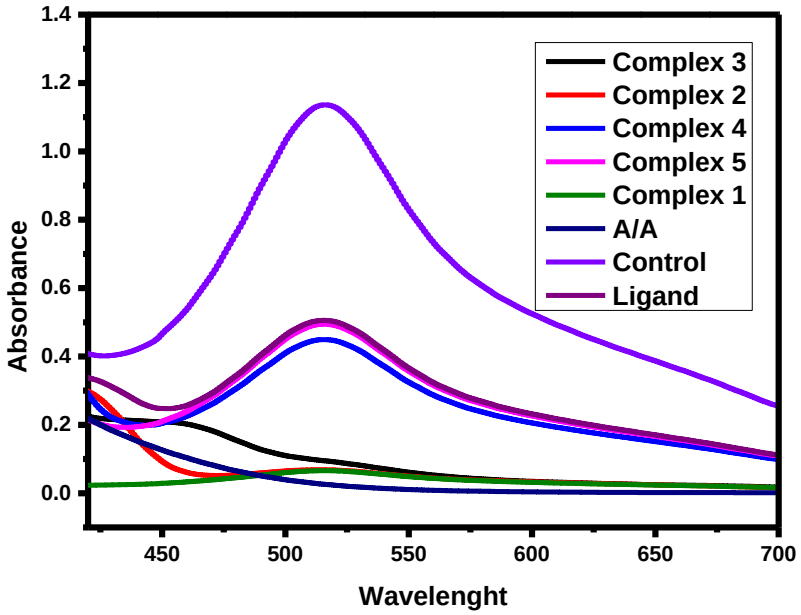

Figure 25. Absorbance spectra of DPPH and with 115 µg/ml of complexes (**1** – **5)**

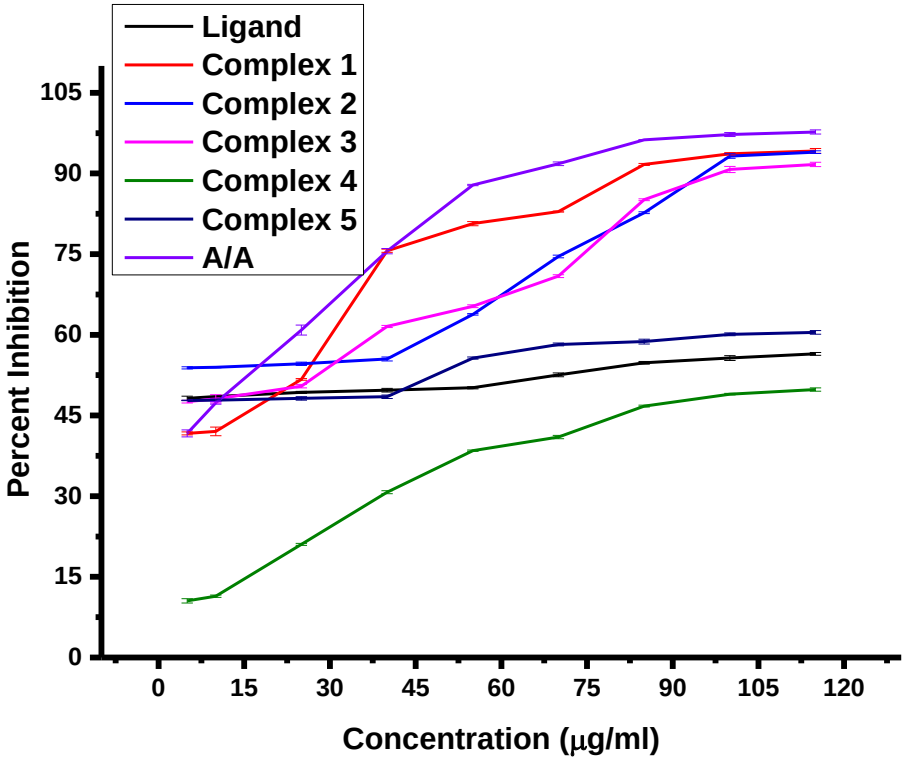

Figure 26. Percent free radical scavenging activities of complexes (**1** – **5)**

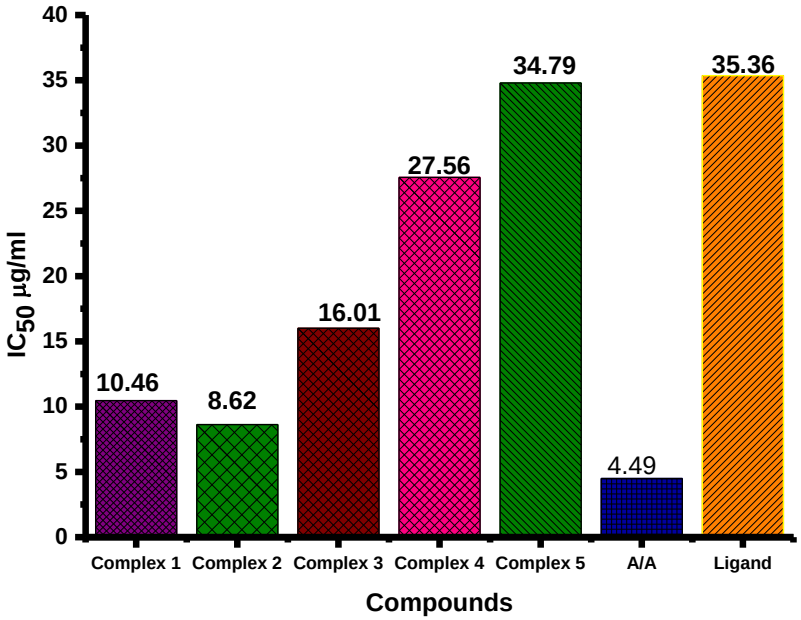

Figure 27. Half maximal inhibitory concentration of ligand (**L1**) and its complexes (**1** – **5)**

Similarly, the antioxidant activities of the free ligand (**L2**) and its complexes (**6** – **10**) were also conducted and findings shown in Figure 28 and Appendix 40 and all the complexes showed more antioxidant activity than the parent ligand. This was also confirmed with IC_{50}

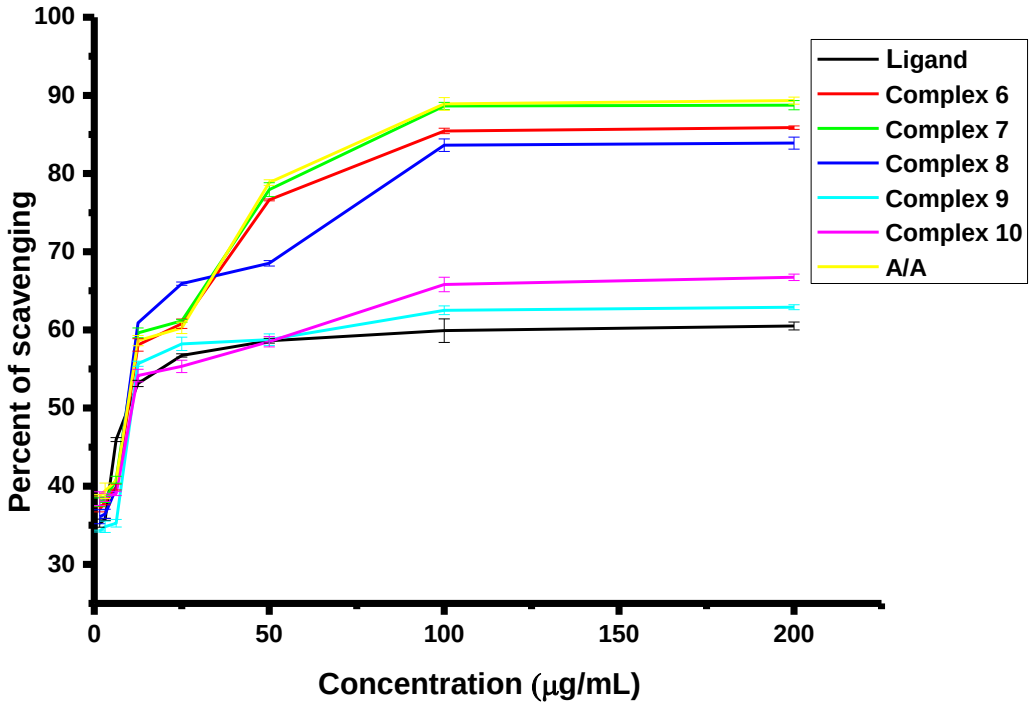

Figure 28. Percent free radical scavenging activities of complexes (**6** – **10)**

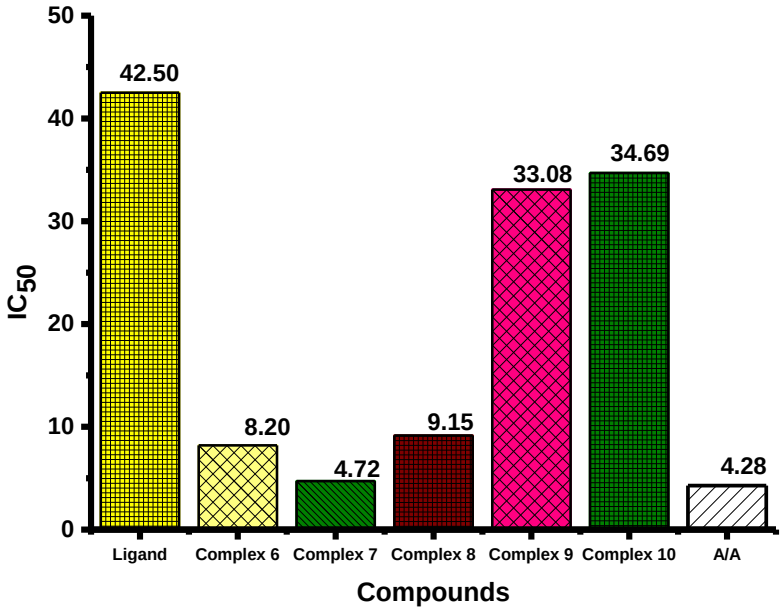

Figure 29. IC_{50} of ligand (**L2**) and its complexes (**6** – **10**)

values of 8.2, 4.72, 9.15, 33.08, 34.69 and 42.5 µg/mL for complexes **6** – **10** and **L2**, respectively. From IC_{50} values, complexes **6** – **8** have comparable activities; with positive control with 4.28 µg/mL (Figure 29), this might be due to high redox activity. It is also well known that copper complex is important for the formation and functioning of several enzymes and proteins, such as cytochrome C oxidase and Cu/Zn superoxide dismutase, which are involved in the processes of respiration, energy metabolism, and DNA synthesis [337], hence copper is involved in catalysis (electron transfer), while zinc plays a structural role in these proteins. In addition to, this high activity was probably due to the presence of the OH group in addition to oxidation potential of the metal ions and the decrease of the antioxidant activity of the ligands is indicated that the terminal N-substitution in the ligands does not have any appreciable influence much on the antioxidant properties in agreement with previous studies [13, 79, 276, 308]. This has direct correlation with the good antioxidant properties and it is obvious that the compounds that can scavenge DPPH radicals might exhibit anticancer, antiaging and anti-inflammatory activities, involved in the protection from rheumatoid arthritis and inflammation [244].

4.4. Stoichiometry and Thermodynamic parameter

In this study, the stoichiometry of transition metal complexes (**1 – 5**) were determined as 1:1 ratio (Metal: Ligand) from linear plot of mole fraction versus absorbance at different temperature using equation 5 (Section 3.6) in which similar results are obtained at all temperature (Table 7). This is determined from the maximum point existed at a mole fraction (X) = 0.5, and this indicates the formation of transition metal complexes having 1:1 metal to ligand ratio and there is no change in Job's curves during temperature elevations up to 40 ^{o}C (Appendix 41 and 42) which is in line with reported studies [15, 42, 280, 281, 338, 340].

By using Job's method, which is also called continuous variation method, the stability constant of the transition metal complexes have been also determined (Equation 6 see section 3.6) [340] from the elongated line (A_2 and $A_{1)}$ at the point of cross section of the graph which is related to the total absorbance of the metal complexes and experimental values of absorbance at a given temperature respectively (Appendix 41 and 42), then after the values of lnK vs 1/T (Vant Hof) were plotted (Appendix 43 and 44) for each temperature as reported in different literature [15, 42, 282]. From this, the thermodynamic parameters such as change in enthalpy (ΔH) and entropy (ΔS) were calculated, respectively, from the slope and intercept of the Vant Hof plots and then Gibbs free energy (ΔG) were also calculated and was tabulated in

Table 8 using equation (**7** and 8, see section 3.6) simultaneously. From these equation the slope and intercept of the graph is equal to -ΔH/R and ΔS/R respectively.

Gibbs free energy and heat enthalpy values were found to be negative, indicating that the metal complexes (**1** – **5**) are thermally stable at specified temperature and in other way the change in enthalpy (ΔH) calculated for transition metal complexes are low and negative indicating that small change in total internal energy during complex formation (Table 8). Similarly, the negative and large value of Gibbs free energy (*ΔG*) shows the spontaneous formation of all the synthesised transition metal complexes and negative value of change in enthalpy (*ΔH*) indicates the exothermic nature of transition metals–ligand interaction and finally, the positive value of change in entropy (*ΔS*) inferring that formations of the complexes are entropically favoured in agreement with reported studies [42, 280–282, 338].

Table 7. Formation constants and stoichiometric calculated for complexes (**1 – 10**)

		Stability constant (K) at different Temperature (^{o}C)							
Complexes	Metal : Ligand ratio	25 ^{o}C		30 ^{o}C		37 ^{o}C		40 ^{o}C	
		K	LogK	K	LogK	K	LogK	K	LogK
1	1:1	2.38×10^{6}	6.3761	2.37×10^{6}	6.3742	2.34×10^{6}	6.3697	2.34×10^{6}	6.3697
2	1:1	2.97×10^{6}	6.4723	2.93×10^{6}	6.4682	2.94×10^{6}	6.4683	2.94×10^{6}	6.4683
3	1:1	1.10×10^{8}	8.0437	1.09×10^{8}	8.0382	1.09×10^{8}	8.0378	1.08×10^{8}	8.0356
4	1:1	3.81×10^{5}	5.5812	3.79×10^{5}	5.5787	3.80×10^{5}	5.5803	3.80×10^{5}	5.5803
5	1:1	8.06×10^{5}	5.9064	7.58×10^{5}	5.8799	7.49×10^{5}	5.8749	7.49×10^{5}	5.8749
6	1:2	2.48×10^{8}	8.3945	2.47×10^{8}	8.3942	2.47×10^{8}	8.3940	2.47×10^{8}	8.3940
7	1:2	4.30×10^{8}	8.6335	4.30×10^{8}	8.6335	4.29×10^{8}	8.6334	4.29×10^{8}	8.6334
8	1:2	2.05×10^{6}	6.3114	2.05×10^{6}	6.3109	2.04×10^{6}	6.3104	2.04×10^{6}	6.3100
9	1:2	2.36×10^{7}	7.3740	2.26×10^{7}	7.3541	2.16×10^{7}	7.3347	2.06×10^{7}	7.3136
10	1:2	6.29×10^{5}	5.7985	6.29×10^{5}	5.7985	6.29×10^{5}	5.7984	6.29×10^{5}	5.7983

Table 8. Thermodynamic parameters of transition metal complexes (**1** – **5**).

Complexes	**1**				**2**				**3**				**4**				**5**			
Temp.(ºC)	25	30	37	40	25	30	37	40	25	30	37	40	25	30	37	40	25	30	37	40
lnk	14.7	14.7	14.7	14.7	14.9	14. 9	14.9	14.9	18.5	18.5	18.5	18.5	12.9	12.9	12.9	12.9	13.6	13.5	13.5	13.5
-ΔG (kJmol $^{-1}$)	36.4	37.0	37.8	38.2	36.9	37.5	38.4	38.8	45.89	46.6	47.7	48.2	31.8	32.4	33.1	33.4	33.69	34.11	34.9	35.2
-ΔH (kJmol $^{-1}$)	0.4				0.8				0.9				0.1				3.6			
ΔS (Jmol $^{-1}$)	122.5				119.3				151.1				106.7				101.1			

Table 9. Thermodynamic parameters of transition metal complexes (**6** – **10**).

Complexes	**6**				**7**				**8**				**9**				**10**			
Temp.(ºC)	25	30	37	40	25	30	37	40	25	30	37	40	25	30	37	40	25	30	37	40
lnk	19.3	19.3	19.3	19.3	19.9	19.9	19.9	19.9	14.5	14.5	14.5	14.5	16.9	16.9	16.9	16.9	13.4	13.4	13.4	13.4
-ΔG (kJmol $^{-1}$)	47.8	48.6	49.7	50.2	49.2	50.0	51.2	51.7	35.7	36.3	37.1	37.5	28.6	29.2	30.0	30.4	33.0	33.6	34.4	34.7
-ΔH (kJmol $^{-1}$)	0.05				0.02				0.16				6.73				0.22			
ΔS (Jmol $^{-1}$)	160.5				165.2				120.3				118.6				110.9			

In similar ways, the binding stoichiometry of the complexes **6** – **10** were determined as 1:2 metal to ligand [**M:L2**] stoichiometric ratio from the point of intersection that found at 0.65 Job's plot (Figure 30 – 34). In addition to this the formation constant (K) was evaluated spectroscopically at different temperatures from the extrapolated Job's plot, accordingly, the complexes showed formation constant (K) values of 2.47×10^8, 4.29×10^8 , 2.05×10^6 , 2.36×10^7 and, 6.29×10^5 respectively, (Table 7). which is in line with previous reported studies [17, 341–343].

The thermodynamic parameters (ΔG, ΔH and ΔS) were determined from the plot of lnK vs 1/T (Figure 35 – 39), hence the negative values of change in Gibbs free energy and enthalpy showed the spontaneity of the metal-ligand interactions and exothermic nature of the reactions. Moreover, the positive values of the change in entropy (ΔS) showed that complex formations are entropically favored, which is in line with reported studies [280, 281].

Generally, all complexes (**1** – **10**) are stable up to 40 ^{o}C (Table 7). This is in good agreement with the thermal analysis study which indicated that all complexes are stable up to 100 °C, and hence weight loss was not observed up to this temperature range (Table 4 and 5 see section 4.2.8).

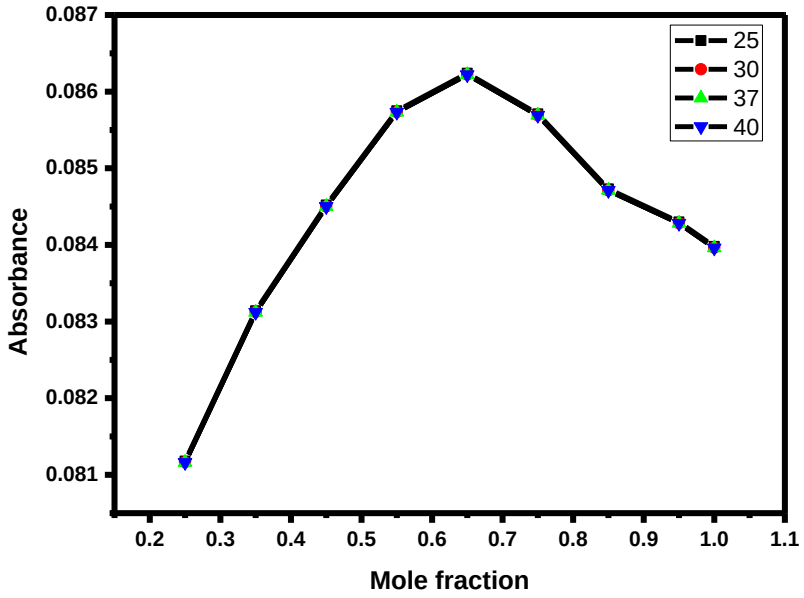

Figure 30. Job's curves at 25, 30, 37 and 40 ^{o}C for complex **6**

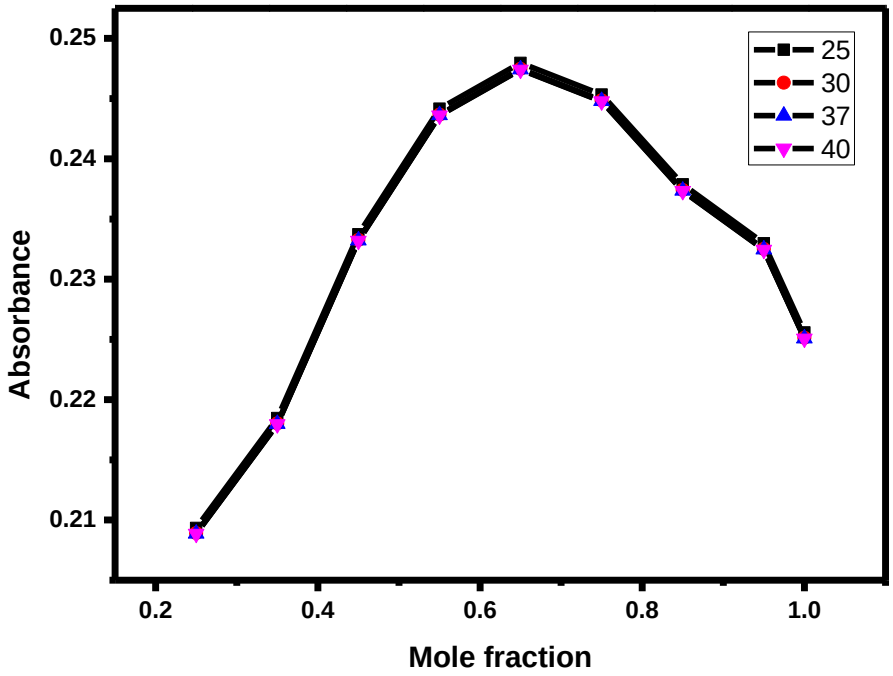

Figure 31. Job's curves at 25, 30, 37 and 40 ^{o}C for complex **7**

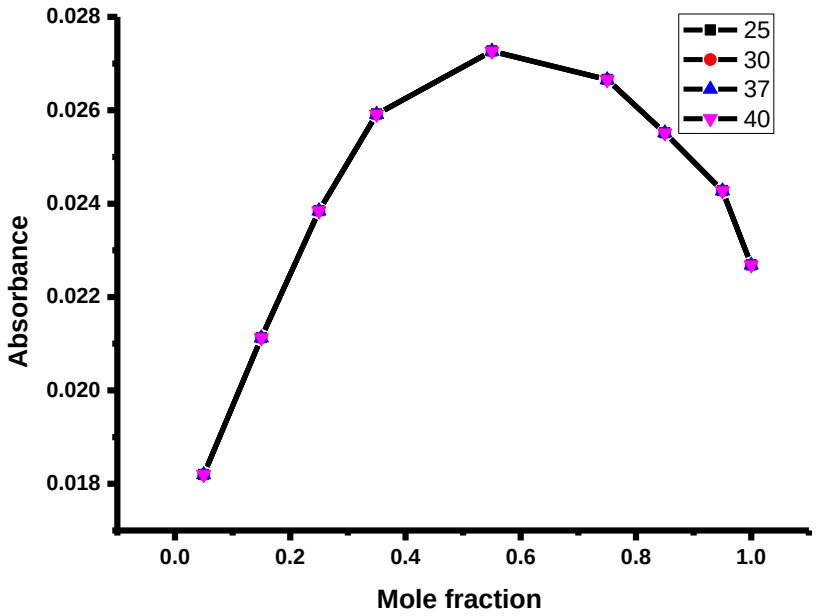

Figure 32. Job's curves at 25, 30, 37 and 40 ^{o}C for complex **8**

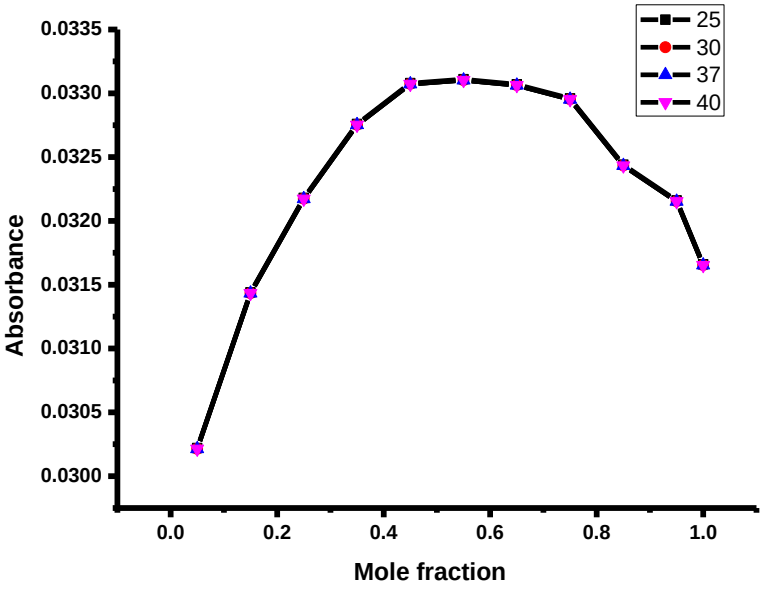

Figure 33. Job's curves at 25, 30, 37 and 40 ^{o}C for complex **9**

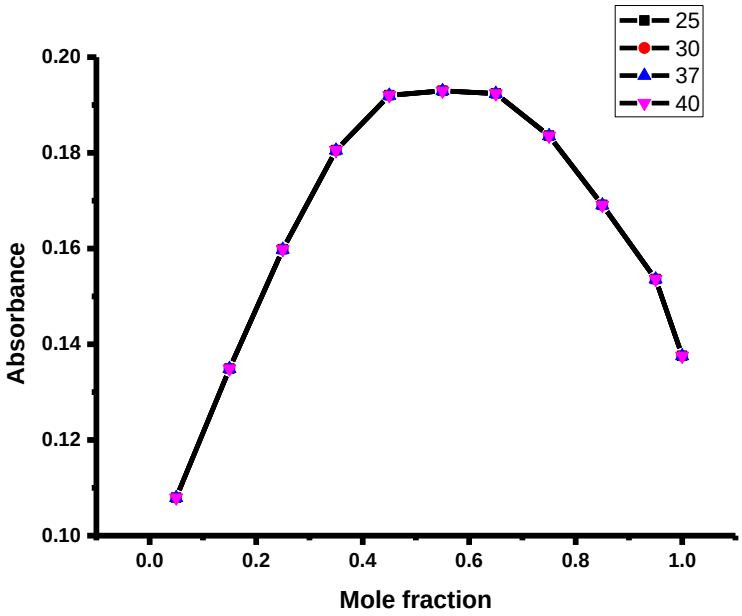

Figure 34. Job's curves at 25, 30, 37 and 40 ^{o}C for complex **10**

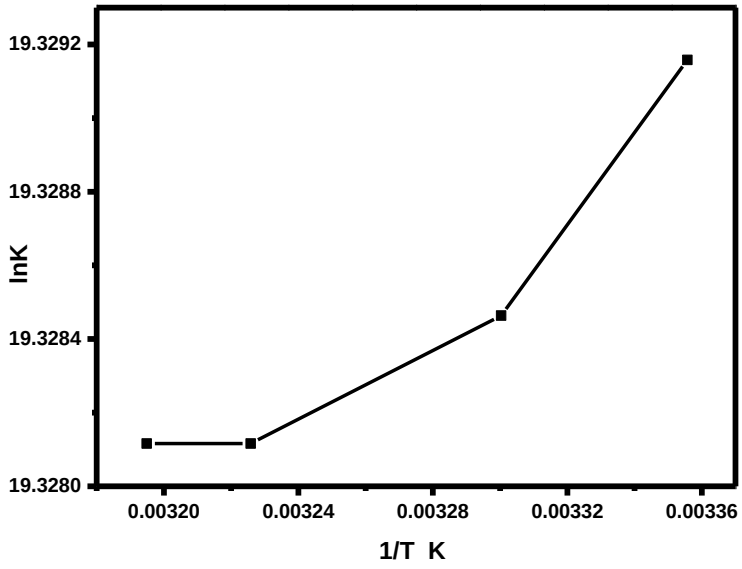

Figure 35. Plot of lnK versus 1/T for complex **6**

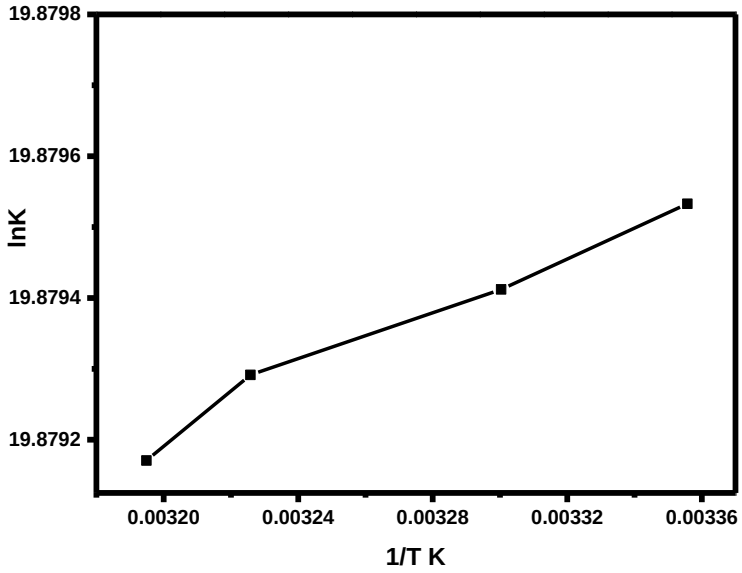

Figure 36. Plot of lnK versus 1/T for complex **7**

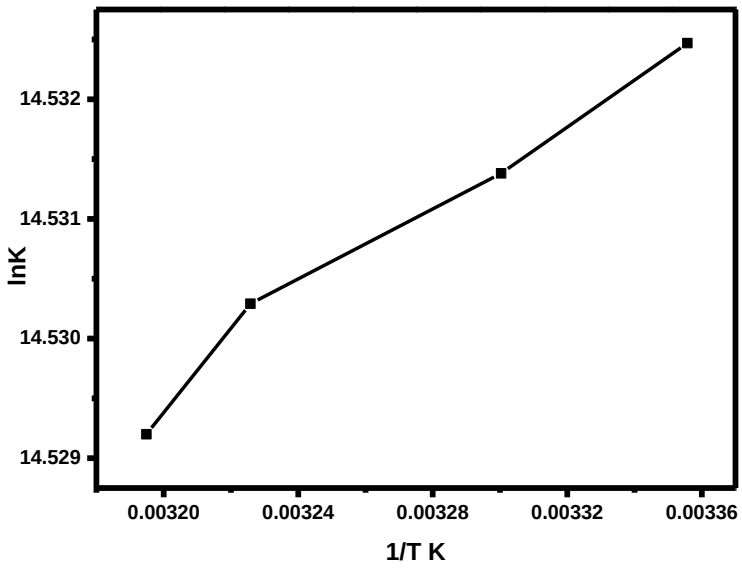

Figure 37. Plot of lnK versus 1/T complex **8**

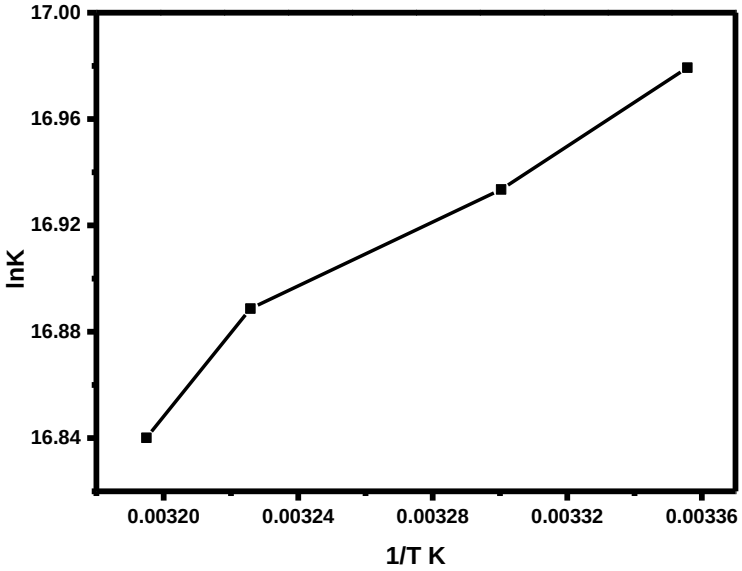

Figure 38. Plot of lnK versus 1/T for complex **9**

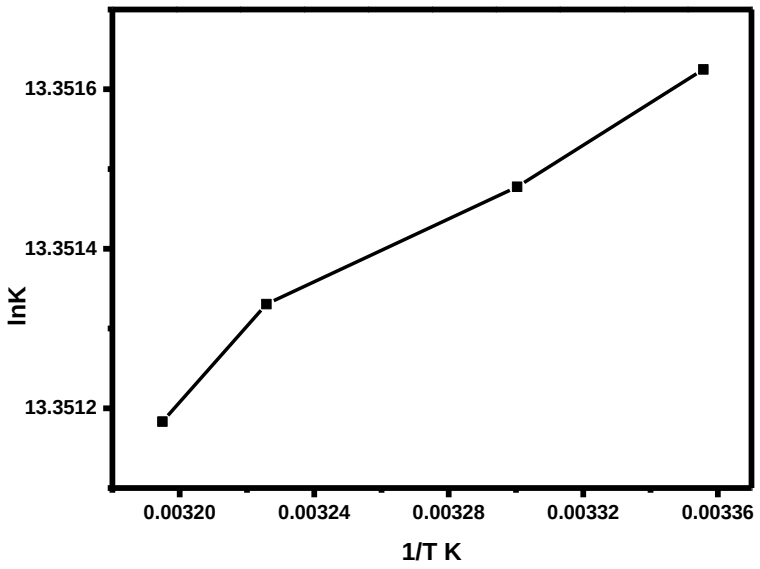

Figure 39. Plot of lnK versus 1/T for complex **10**

4.5. *In silico* analysis of ligand and its metal complexes

4.5.1. Drug-likeness and ADME predictions

SwissADME web tool provides information on physicochemical properties, pharmacokinetic parameters, drug likeness of a compound, and providing *in silico* aided drug design and development [283]. The physicochemical, ADME properties and drug likeness of the ligand (**L1**) and its metal complexes (**1** – **5**) are presented in Appendix 45. The compounds have molecular weights ranging from 259.30 to 440.32 g/mol. The iLogP value of the ligand was found to be 2.22 and that of all the metal complexes showed similar iLogP value of zero compared to ciprofloxacin (2.24). The low value of iLogP for the metal complexes indicates good water solubility of the metal complexes relative to the ligand and the control [344]. This is in agreement with the experimental solubility values.

The number of hydrogen bond donors of all the compounds range from 2 to 3 (≤ 5), whereas, the number of hydrogen bond acceptors range from 4 to 8 (≤ 10). The predicted physicochemical properties for drug likeness screening showed that the synthesized compounds (**L1** and complexes **1** – **5**) fulfil drug-like molecular nature in agreement with previous reported studies [17, 267]. Moreover, the topological polar surface area (TPSA) ranges from 66.74 to 142 $Å^2$ for the synthesized compounds. It has been reported that

compounds with TPSA of 140 $Å^2$ and above would be poorly absorbed (< 10% fractional absorption) and those with a TPSA 60 $Å^2$ would be well absorbed (> 90%) [78, 79, 267]. Therefore, from the TPSA data of the synthesized compounds, it is possible to deduce that the ligand and its complexes (**1** – **5**) have very good intestinal absorption [267, 283]. Skin permeability (logKp) value of the free ligand and its metal complexes were found within the range of -7.1 to -8.29 cms^{-1} (Appendix 45), deducing that all compounds have low skin permeability in agreement with reported studies [78, 267, 283]. Similarly, the synthesized compounds were predicted as a substrate of P-glycoprotein (P-gp) which is a transporter and biological barrier and responsible for the ADME of drugs [283]. This inferred that the compounds have no tendency to interact to other drugs fingered by the transporter and hence no drug-drug interactions. The inhibition of CYPs leads to toxicity end points [345]. The high gastrointestinal absorption (GI) together with their fewer tendencies to inhibit cytochrome P450 family enzymes of the liver (CYPs) gives the compounds theoretically safe from toxicity point of view.

4.5.2. Quantum Chemical Analysis

Transitional metals and their complexes have been investigated by computational chemistry. However, the main problem associated in studying the calculations with these systems is the electron degeneracy, which is partially configured in d– orbitals. Over the years, several studies have been reported to confirm the efficacy of various DFT approaches for investigating the chemical properties of transition metal complexes. Among various properties, mixed basis set have been very promising in computational studies and cover a wide range of ligands and their metal complexes [346].

The band gap energy (E_g) is correlated with various biological aspects like antibacterial, antioxidant and DNA binding activities [3, 17, 81]. It has been reported that the band gap energy between the E_{HOMO} and E_{LUMO} is an important stability descriptor [344]. A large band gap energy is associated with stable systems, whereas small band gap energy is associated with little stable systems making more reactive compound [344]. A decrease in the band gap energy upon coordination may be associated with the presence of LMCT [81]. The quantum chemical parameters of the ligand and its metal complexes are tabulated in Table 10. The highest occupied molecular orbital (HOMO) and lowest unoccupied molecular orbital (LUMO) analysis was performed to predict the reactivity of the ligand and the complexes. The energy gap ($E_g = E_{LUMO} - E_{HOMO}$) for possible electron transition were calculated to be

3.834, 4.002, 3.272, 3.684, 3.669 and 3.991 eV for the **L1** and its complexes **1 – 5** respectively. These results predict good reactivity of the synthesized compounds [81].

The wave function analysis of the ligand revealed that the electron density of the molecule is circulating between the secondary amine substituent nitrogen and the quinoline ring amine from HOMO to LUMO and throughout the molecule due to π-bond delocalization. The HOMO and LUMO of the **L1** reside on the quinoline ring, confirming the presence of π→π* electron transition. It is also observed that the electron densities of the HOMO reside on the amine part of the molecule and the LUMO reside on its imine part. This is due to the fact that the amine and imine part of the ligand are in the same plane making it suitable for metal coordination [347].

The selected quantum chemical parameters had been derived from E_{HOMO}, E_{LUMO}, and used to evaluate the chemical reactivity of the complexes. The chemical reactivity of the complexes increases with decrease in the energy gap (ΔE) values. In other ways, the complexation between the metal ions and the ligand has reduced the HOMO–LUMO energy gap, which can be considered as an indication for better biological activities [3, 81]. Accordingly, from the band gap analyses, the metal complexes were predicted to have better biological activities than the free ligand, in good agreement with the experimental biological activities.

Table 10. The HOMO, LUMO, energy gap (*Eg*), chemical potential (*μ),* hardness (η), softness (*σ*), electrophilicity (ω), nucleophilicity index (Nu) of the ligands and complexes.

Cpds.	HOMO	LUMO	Eg(eV)	μ	η	σ	ω	Nu
L1	-5.960	-2.126	3.834	4.043	1.917	0.261	4.264	0.235
1	-6.364	-2.362	4.002	4.363	2.001	0.250	4.756	0.210
2	-6.571	-3.299	3.272	4.935	1.636	0.306	7.445	0.134
3	-6.219	-2.536	3.684	4.378	1.842	0.921	5.202	0.192
4	-6.303	-2.634	3.669	4.468	1.834	0.273	5.441	0.184
5	-7.158	-3.167	3.991	5.163	1.996	0.998	6.678	0.150
L2	-6.117	-2.584	3.533	4.350	1.766	0.283	5.357	0.187
6	-6.352	-2.772	3.580	4.562	1.790	0.279	5.814	0.172
7	-6.120	-3.147	2.973	4.633	1.487	0.336	7.220	0.138
8	-3.809	-3.491	0.360	3.629	0.180	2.778	36.561	0.0274
9	-4.695	-3.506	1.189	4.100	0.594	0.841	14.147	0.070
10	-4.448	-3.529	0.918	3.988	0.459	1.089	17.326	0.058

The biological activity of the complexes toward appropriate molecules can be discussed with the hard–soft–acid–base (HSAB) principle, which states that soft acids prefer to bind with soft bases and hard acids prefer to bind with hard bases [81, 348]. Hence, the biological activity of a compound increases with increasing softness and decreasing hardness [81, 348]. Accordingly, the biological structures of enzymes, which are commonly soft, prefer to bind with soft complexes. The order of chemical hardness (η) it is possible to suggesting that complex **1** is more stable. This is in agreement with the TGA analysis (Table 8 see section 4.2.8). In other way, chemical potential (μ) measures the tendency of an electron to escape from equilibrium, and it has been reported that the chemical reactivity of a compound increases with decreasing chemical potential [79]. Chemical potential (μ) is also directly proportional with the Gibbs free energy and related to spontaneity (Table 15 and 16 see section 4.4).

Other important parameters predicted are the electrophilicity and nucleophilicity indexes. The electrophilicity index implies the ability of the complexes to accept electrons, while nucleophilicity index displays the ability to donate electrons [81]. In this aspect, complex **2** has stronger electron accepting potential than the remaining complexes while the free ligand is more electron donor, based on their electrophilicity index and nucleophilicity index value, respectively (Table 10). This activity is in line with antioxidant properties of complex 2.

Similarly, the energy gap ($E_g = E_{LUMO} - E_{HOMO}$) for possible electron transition were calculated to be 3.533, 3.580, 2.973, 0.360, 1.118 and 0.918 eV for the **L2**, and its complexes **6 – 10** complexes (Table 10 and Figure 42 and 43), respectively. The chemical reactivity of the complexes increases with decrease in the energy gap (E_g) values [3, 81]. From the band gap results, the metal complexes showed better biological activities than the free ligand, also in line with the experimental biological activities. The Eigen values for the HOMO of the ligand and its metal complexes (Table 10) showed the improvement of the softness of the metal complexes than the ligand, inferring the potential of the synthesized metal complexes to interact with soft molecules, and it is observed that the highest global softness of the complexes is in a good agreement with the results obtained for antibacterial activities (See section 4.3.1).

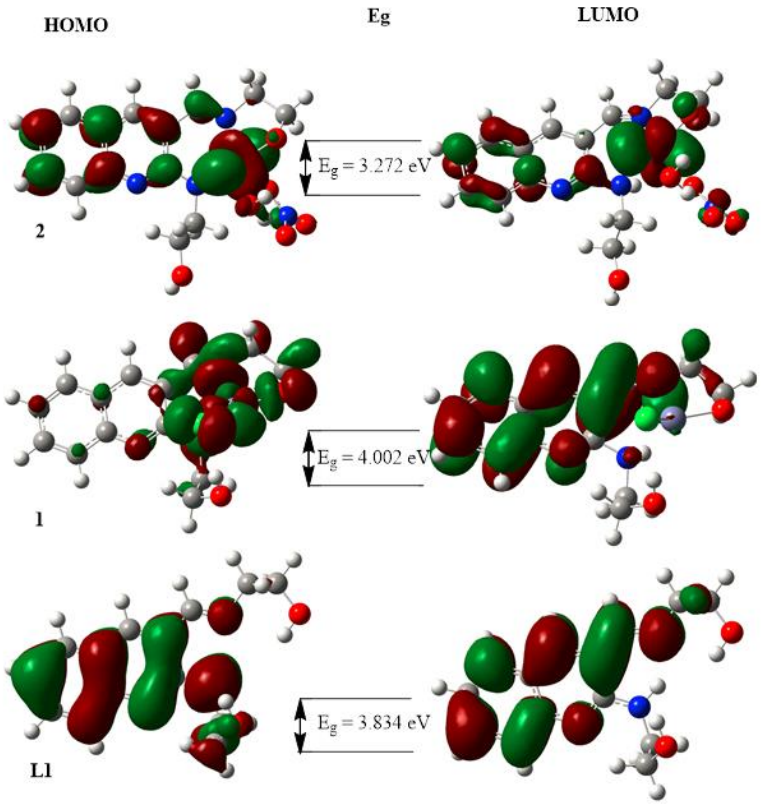

Figure 40. The HOMO and LUMO of **L1, 1** and **2** (DFT/ B3LYP/6-311++Gdp).

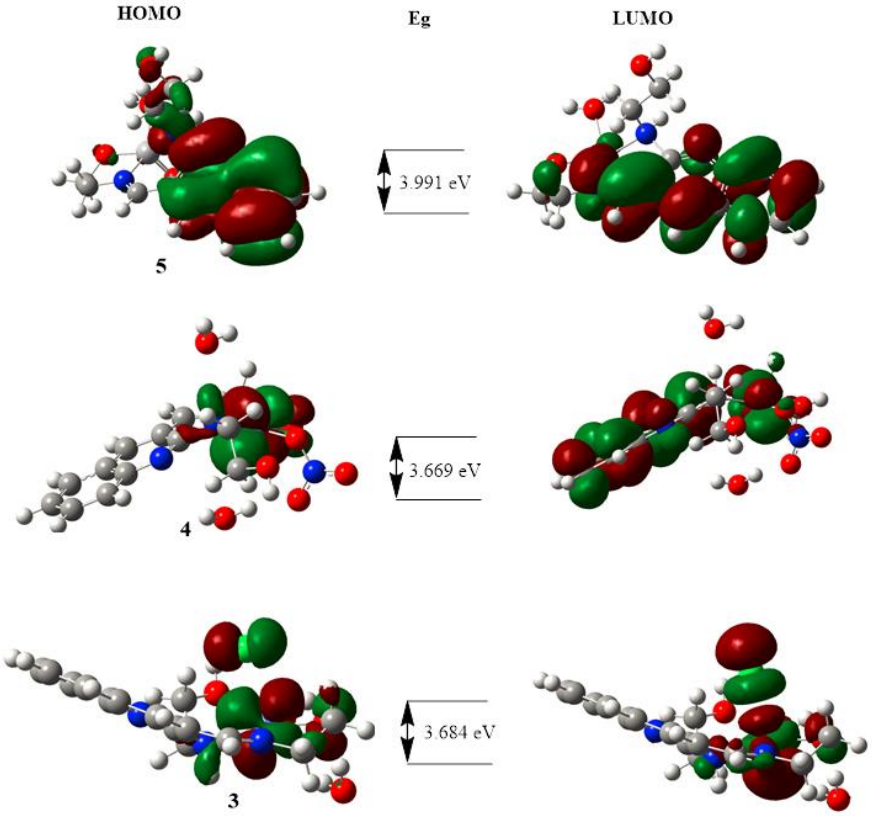

Figure 41. The HOMO and LUMO of **3, 4** and **5** (DFT/ B3LYP/6-311++Gdp).

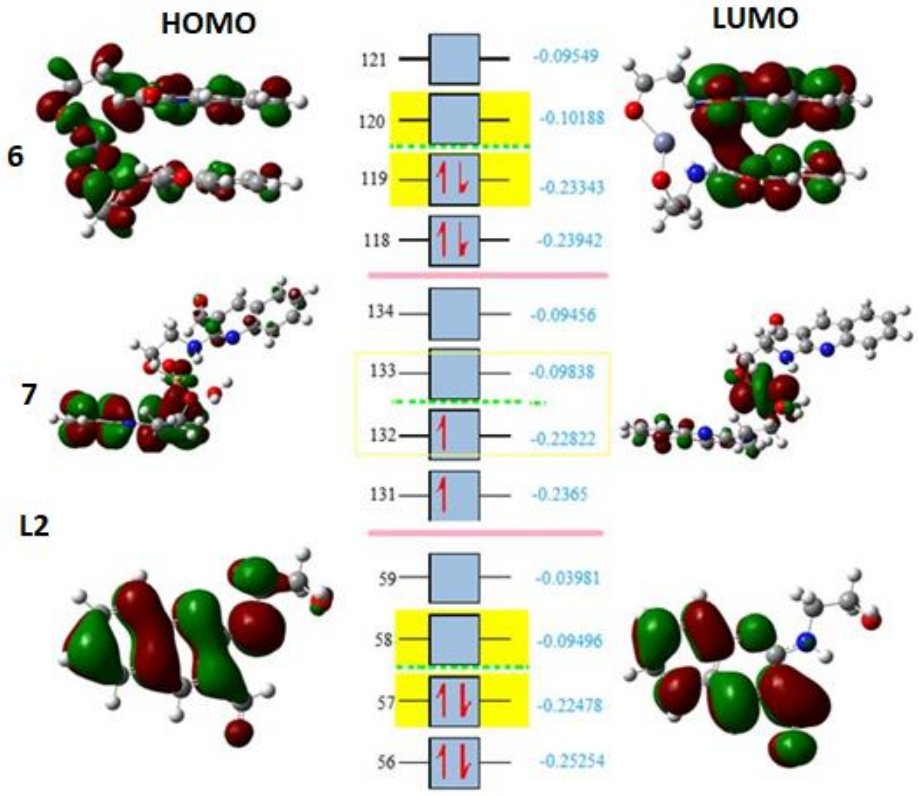

Figure 42. The HOMO and LUMO of the **L2, 6** and **7** (DFT/B3LYP/6-311++Gdp).

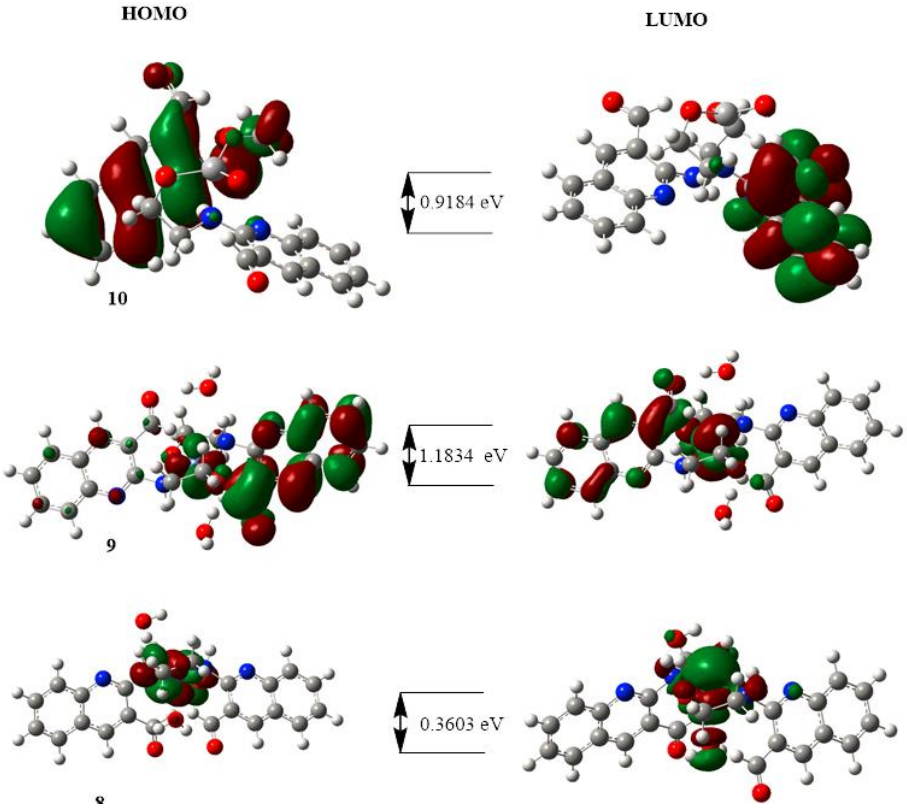

Figure 43. The HOMO and LUMO of **8, 9** and **10** (DFT/ B3LYP/6-311++Gdp).

From both experimental (EDX, MS and TGA) and DFT analysis, the ligand (**L1**) acts as an ONN donor tridentate chelating agent while **L2** act as bidentate ligand. The analyses also indicated that the complex **1** has a distorted tetrahedral geometrical structure, in line with previously reported studies [50, 183, 184]. On the other hand, the complex **2** showed distorted square pyramidal geometry [43, 349, 350], complex **3** showed octahedral, while that of complex **4** has square planar geometry, complex **5,** showed octahedral structure, complex **6** showed tetrahedral and complex **7, 8** and **9** showed octahedral structure while complex **10** showed bipyramidal structure, in agreement with previous reported studies [20, 29, 132, 351]. These have been further confirmed from the visualization of the DFT optimized geometries.

4.5.3. Molecular Docking analysis

Bioactive molecules inhibit either the reproduction of pathogenic bacteria or kill them by acting on some essential components of bacterial strains. DNA gyrase is one of the essential enzymes which induce negative supercoils into bacterial DNA. In this aspect, the fluoroquinolones are among DNA gyrase-targeted drugs [352]. Some bacteria also secrete a variety of toxic substances, including exotoxin A (ETA), phospholipases, and several proteases. *Pseudomonas aeruginosa* is opportunistic pathogenic bacteria which activate the expression of LasR gene required for transcription of the genes for elastase (LasA and LasB) protease, associated with virlence [353, 354]. Therefore, the molecular docking of the complexes were docked against DNA gyrase of *E. coli* and LasR of *P. aeruginosa* to investigate their mode of action and the results were compared with the *in vitro* antibacterial assays. We studied the molecular interaction between the synthesized ligands and their complexes against the *E.coli* DNA gyrase (PDB ID 6F86) to understand the mechanism of action. Autodock 4.2 was used to explore the protein-ligand interactions between complexes and *E.coli* DNA gyrase (PDB ID 6F86) (Figure 44 – 46). The compounds interacted with the key amino acids by forming hydrogen bond with Asp-73, Gly-77, Thr-165, and hydrophobic interaction with Ile-78, Ile-94, Glu-50, and Pro-79 within the active site. The results clearly show that the free hydroxyl chain in the complexes was interacted with the amino acids within the active sites of the protein. All the complexes shown similar docking score within the range of -6.3 to -6.8 kcal/mol compared with the ligand (-7.1 kcal/mol) (Table 11). Among them copper and cobalt complexes shown better docking score compared to other complexes reported. The *in vitro* antimicrobial analysis results are matching with the molecular docking analysis docking score. Overall, *in silico* analysis results reveals that the ranking of complexes as antimicrobial agent as follows Cu > Co > Zn > V > Ni complexes

Table 11 which is in very good agreement with *in vitro* antibacterial (specifically against *E.coli* strain) activities.

To get more insight, we also studied the ligand-protein interactions of the *P. aeruginosa* LasR·DNA protein against the synthesized metal complexes. The 2D and 3D representation of the interactions for the compounds and ciprofloxacin are presented in Figure 47 – 51, whereas the binding scores and the residual protein-ligand interactions are summarized in Table 12. The metal complexes have shown significant interactions within the active site of the LasR. DNA protein with the key amino acids, Tyr-47, Trp-60, Asp-73, Tyr-64, Leu-36, Trp-88, Arg-61, Thr-75, Cys-79, and Ala-127 [355]. All the investigated compounds showed moderate to equivalent binding scores compared to the clinical drug ciprofloxacin (Table 12). The overall *in silico* docking analysis indicated that the Cu(II) complex interacted with the LasR.DNA residues of Tyr-47 (H-bond), Trp-60, Asp-73, Tyr-64, Leu-36, Arg-61, Thr-75, and Ala-127 with binding energies of -8.2 kcal/mol. This result is comparable with the binding energy of ciprofloxacin (-8.00 kcal/mol). Similar docking activity trends were observed for both *E. coli* DNA gyrase B and *P. aeruginosa* LasR, in very good agreement with the *in vitro* bacterial activities (Appendix 45).

Table 11. Molecular docking results of ligands and their complexes against *E. Coli* DNA Gyrase (PDB ID 6f86).

	Binding Affinity (kcal/m	**H-bond**	**Residual interactions**	
			Hydrophobic/Pi-Cation	**Van der Waals**
L1	-7.1	Asp-73, Gly-77, Thr-165	Val-43, Ile-94, Ile-78	Ala-47, Asn-46, Glu-50, Pro-79
1	-6.5	Asp-73, Thr-165	Ala-47, Val-43	Gly-77, Arg-76, Glu-50, Asn-46, Ile-78, Gly-164
2	-6.8	Asp-73, Asn-46, Gly-77	Arg-76, Pro-79,	Glu-50
3	-6.8	Thr-165	Gly-77, Arg-76	Asp-73, Glu-50, Ile-78, Pro-79
4	-6.3	Thr-165	Ile-78	Asp-73, Ala-47, Asn-46, Glu-50, Gly-77, Pro-79
5	-6.5	Arg-76	Glu-50, Gly-77, Ile-78, Pro-79	Asp-73
L2	-6.5	Asp-73, Thr-165, Gly-77	Asn-46, Ile-94, Ile-78, Val-43	Val-71, Ala-47, Arg-76
6	-7.4	Asn-46, Arg-76	Thr-165, Ala-47, Ile-78, Val-167, Gly-77, Glu-50	Ile-94, Pro-79, Asp-73, Val-43
7	-7.0	Thr-165	Glu-50, Arg-76, Pro-79	Gly-77, Ile-78, Asp-49, Asn-46, Ile-94
8	-7.1	Thr-165, Gly-77, Asn-46, Arg-76	Ile-78, Val-167, Ala-47	Ile-94, Pro-79
9	-6.7	--	Ile-94, Arg-76, Pro-79	Gly-77, Glu-50, Ile-78, Asp-49, Asn-46
10	-6.6	Gly-77	Glu-50, Arg-76, Pro-79, Ile-94	Thr-165, Ile-78, Asn-46, Val-120, Gly-119
Cipro	–7.2	Asp-73, Asn-46, Arg-76	Glu-50, Gly-77, Pro-79, Ile-78, Ile-94, Ile-78	Ala-47

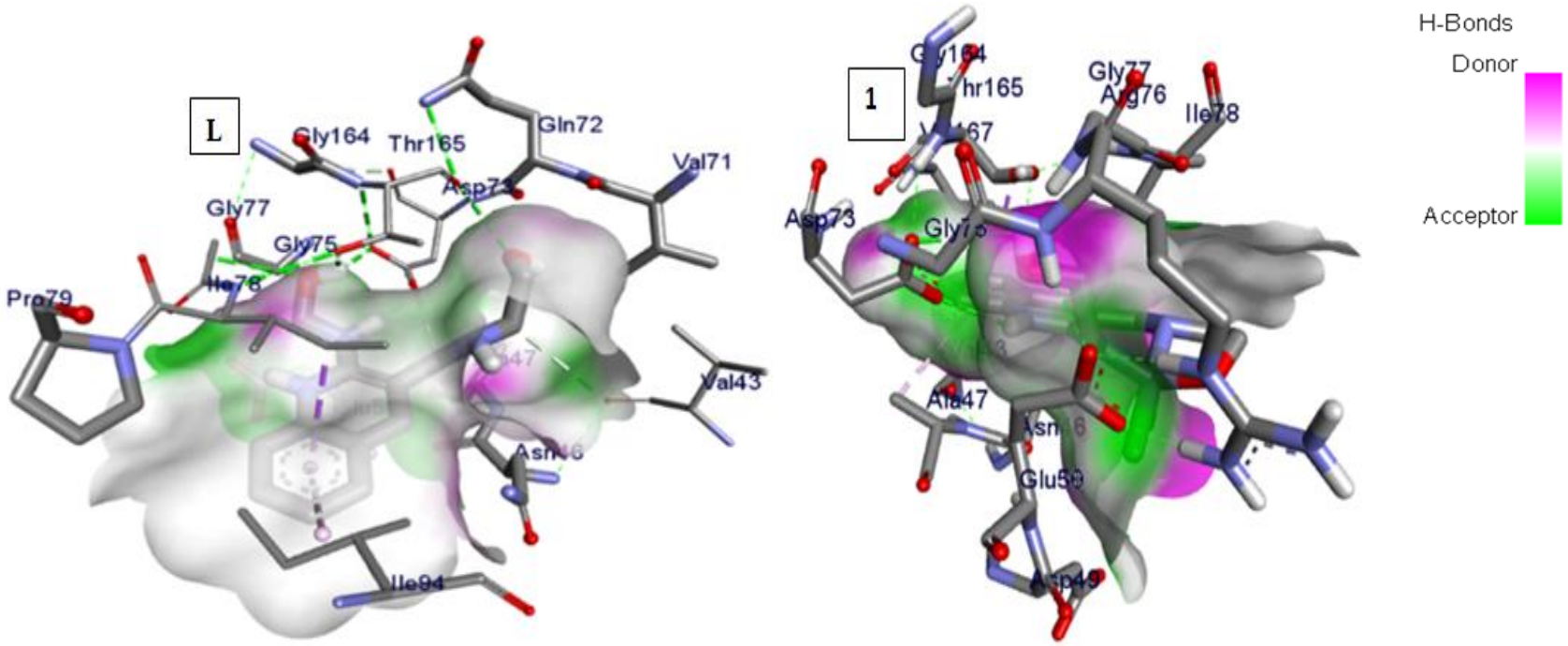

Figure 44. The interactions of **L1** and **1** against *E.Coli* DNA gyrase (PDB ID: 6F86)

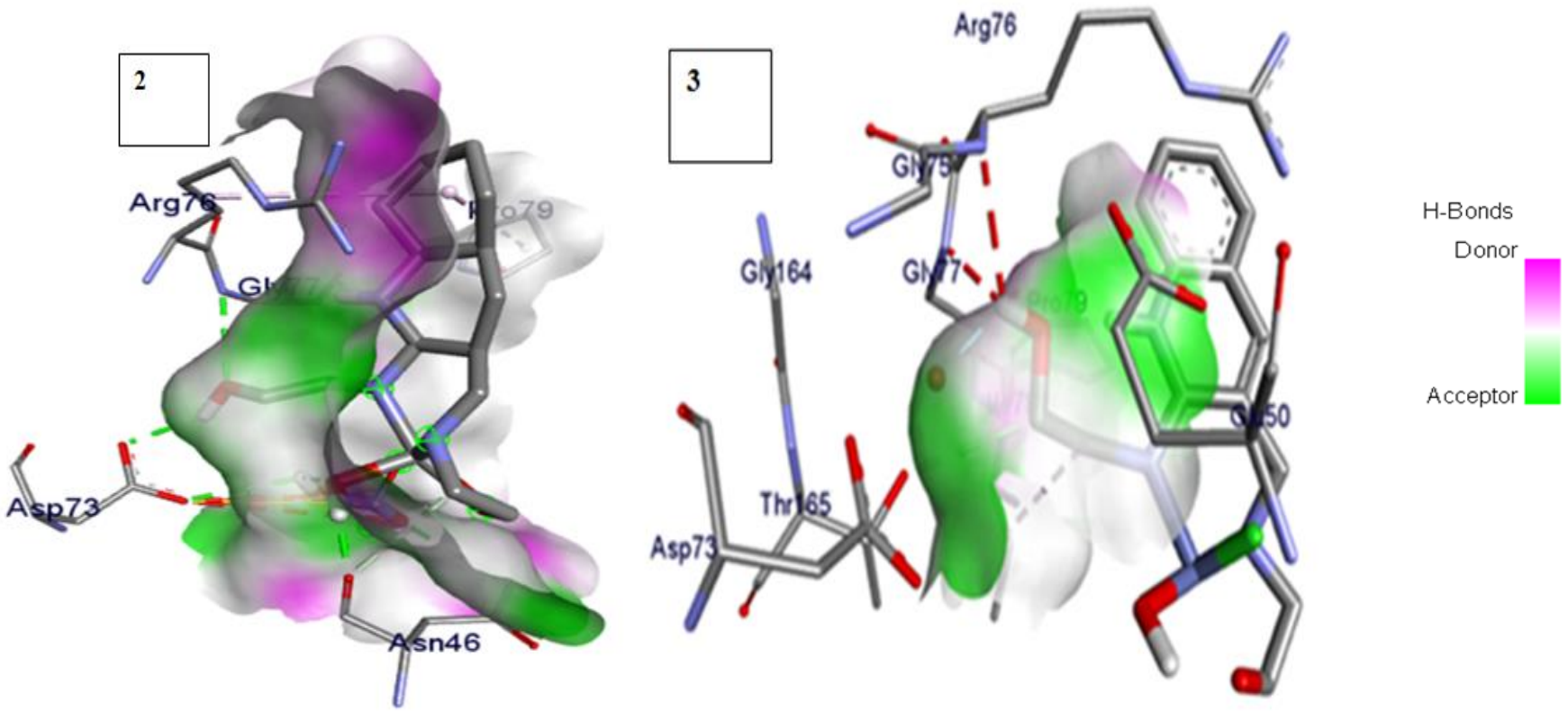

Figure 45. The interactions of **2** and **3** against *E.Coli* DNA gyrase (PDB ID: 6F86)

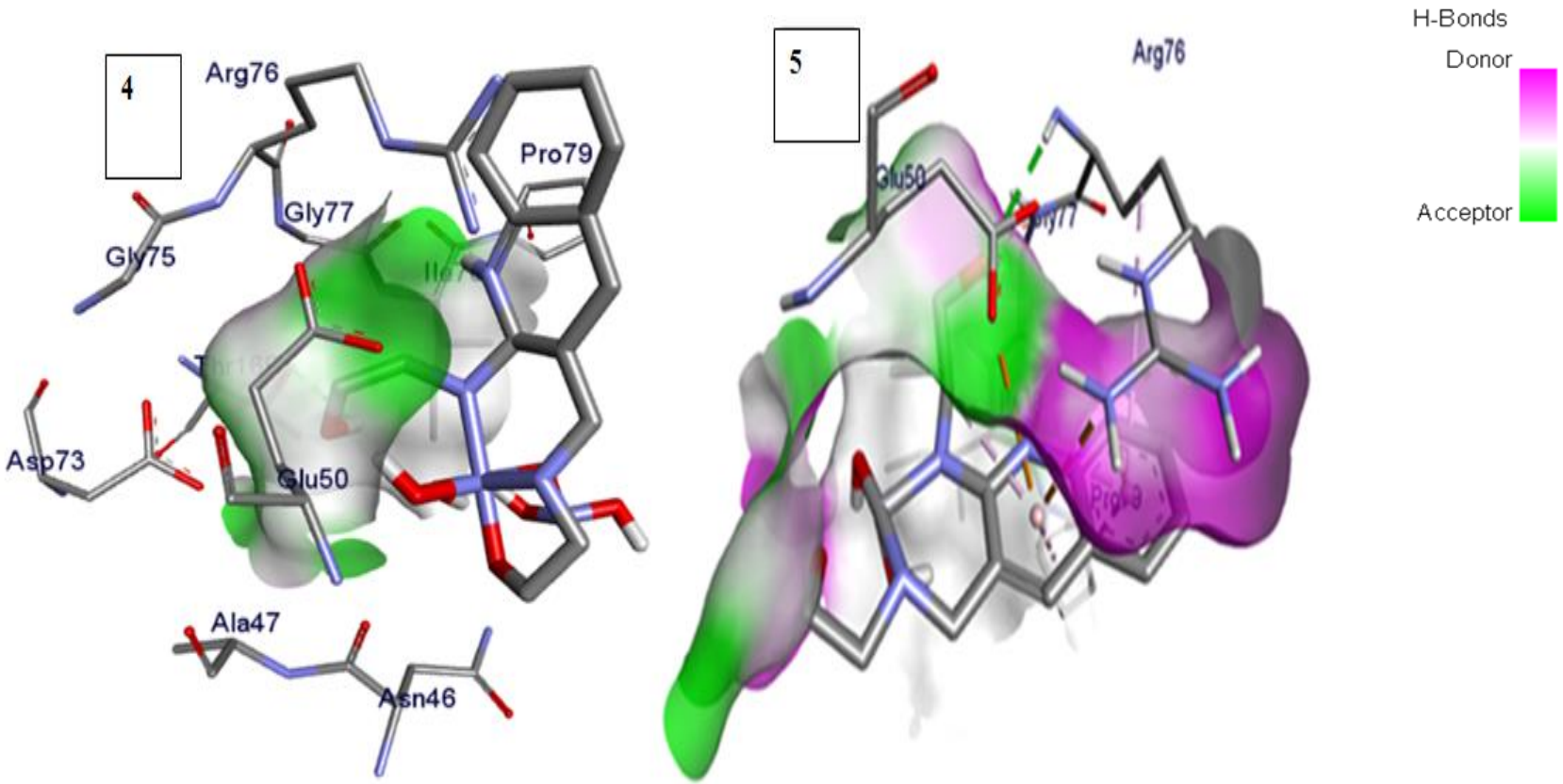

Figure 46. The interactions of **4** and **5** against *E.Coli* DNA gyrase (PDB ID: 6F86)

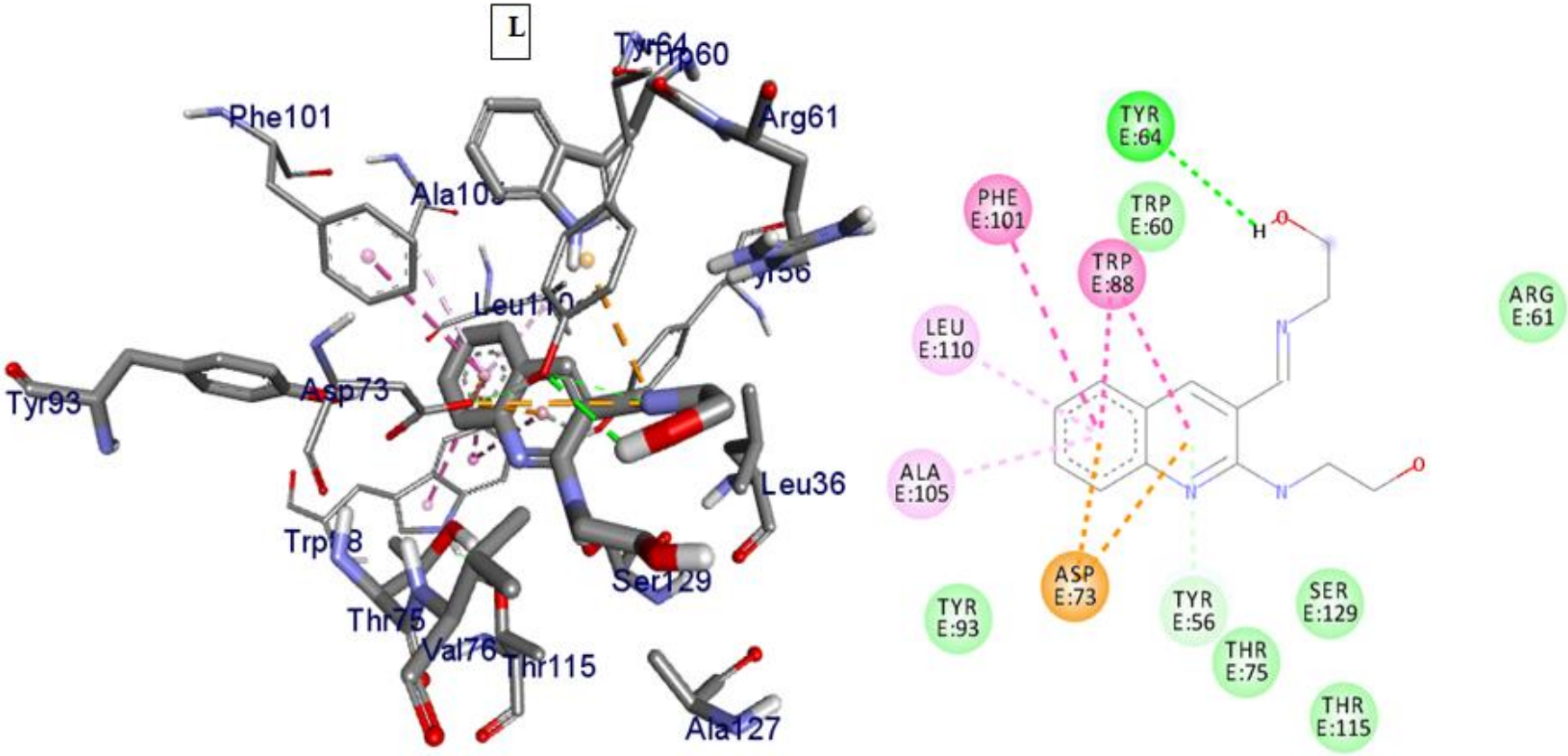

Figure 47. The interactions of **L1** against *P. aeruginosa* LasR.DNA (PDB: 2UV0).

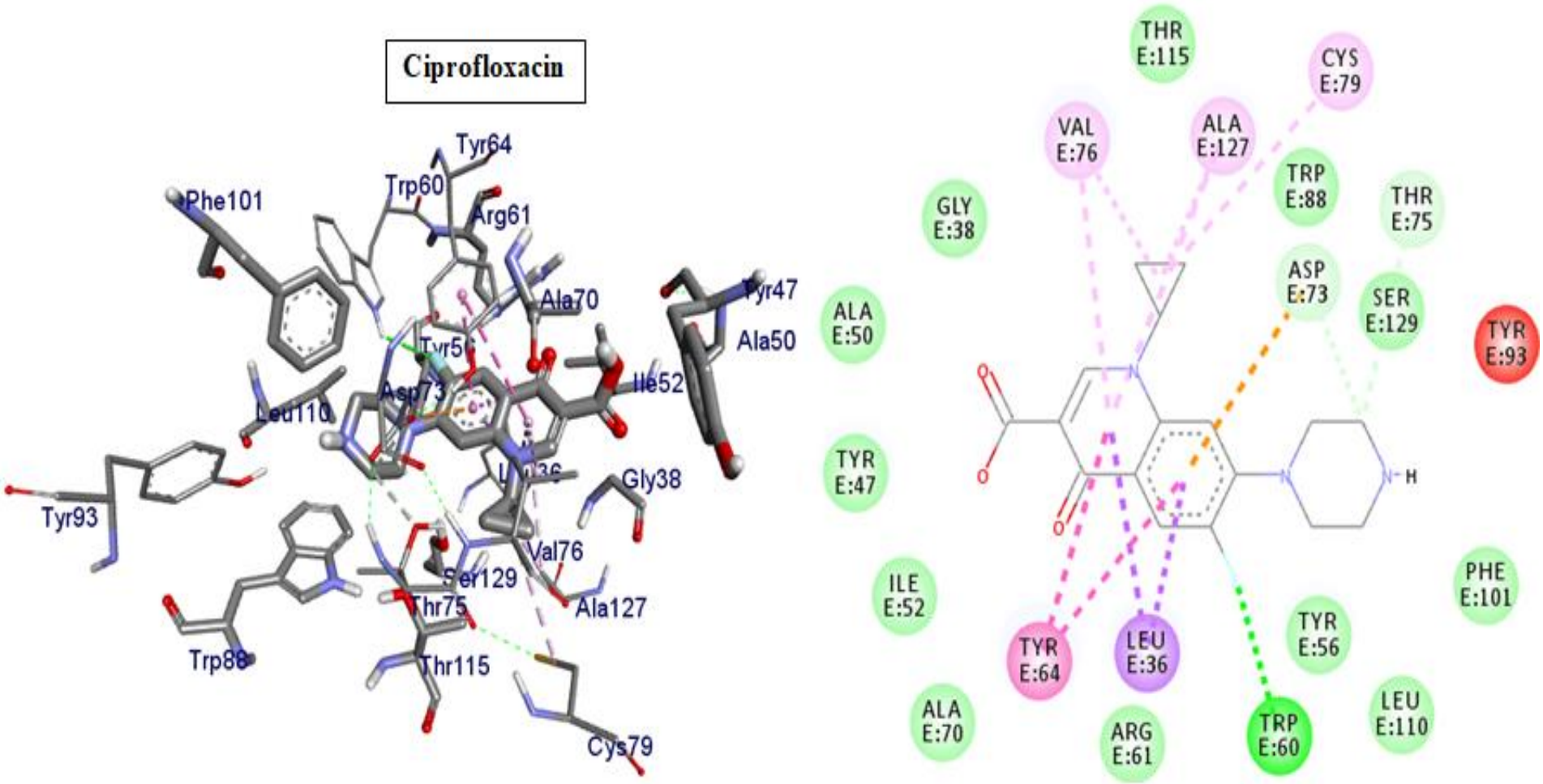

Figure 48. The interactions of Cipro. with *P. aeruginosa* LasR.DNA (PDB: 2UV0).

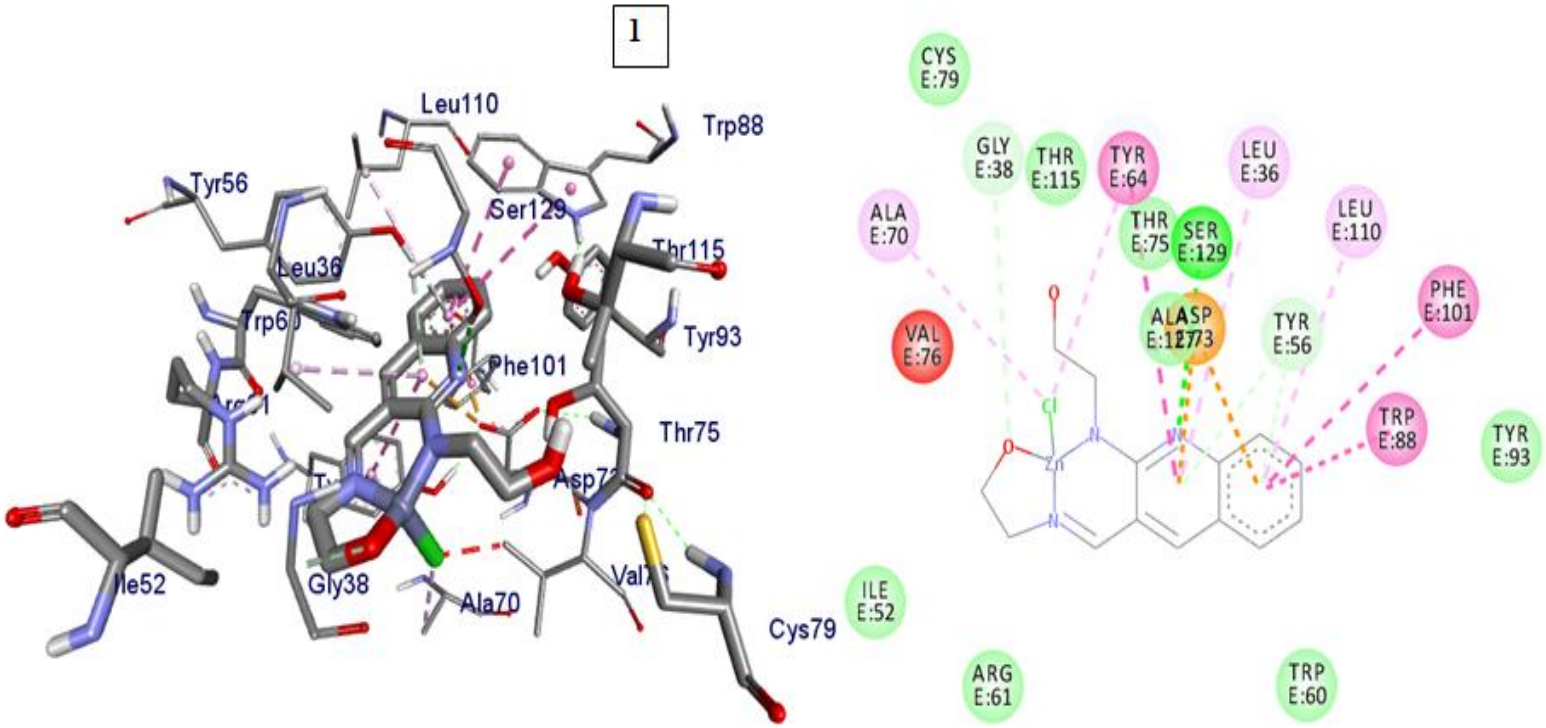

Figure 49. The interactions of **1** against *P. aeruginosa* LasR.DNA (PDB: 2UV0).

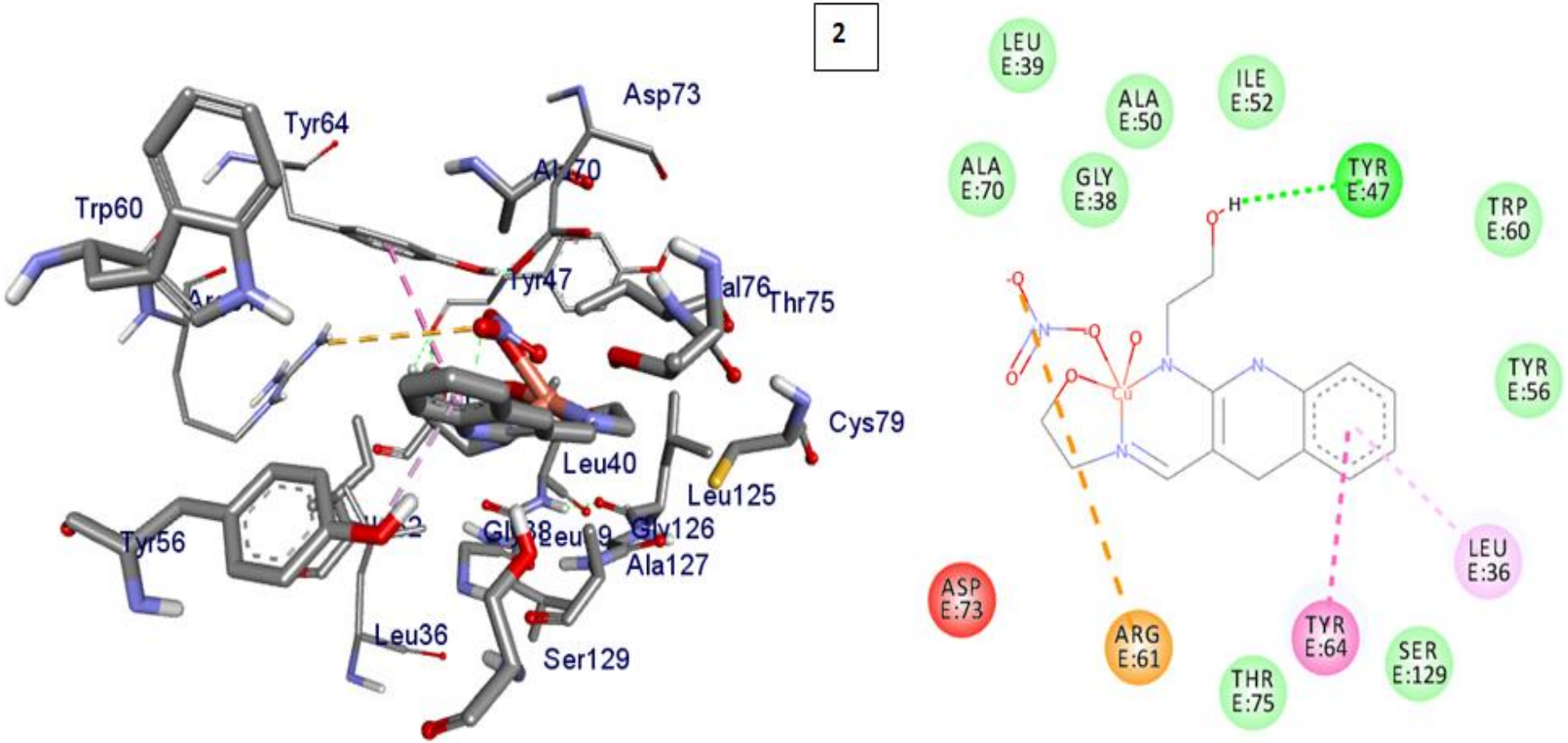

Figure 50. The interactions of **2** against *P. aeruginosa* LasR.DNA (PDB: 2UV0).

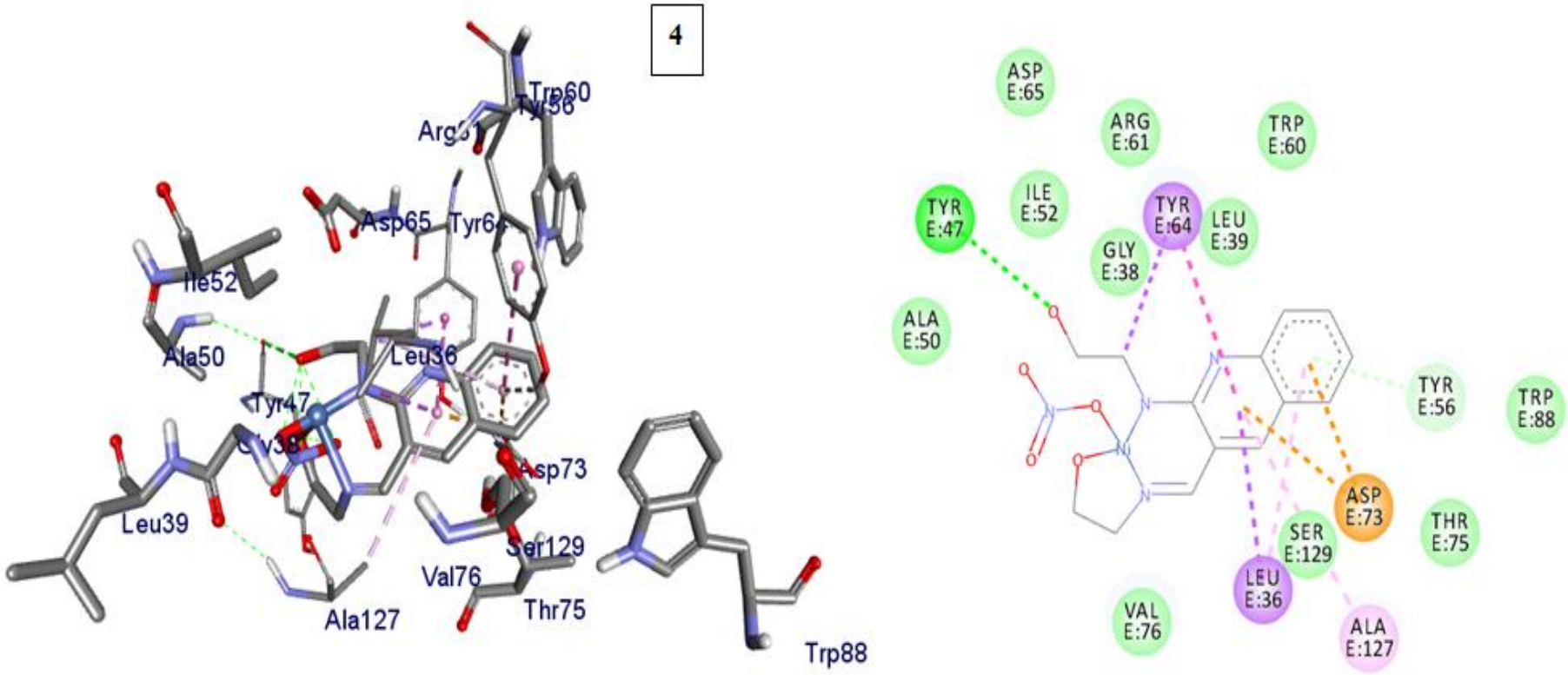

Figure 51. The interactions of **4** against *P. aeruginosa* LasR.DNA (PDB: 2UV0).

The molecular docking interaction was also performed between the ligand (**L2**) and it's complexes against the proteins of *E. coli* DNA gyrase B (PDB ID 6F86) (Figure 52 – 57) and *P. aeruginosa* LasR (PDB ID: 2UV0) (Figure 58 – 63). Accordingly, the targeted compounds interacted with the key amino acids of *E. coli* DNA gyrase B by forming hydrogen bond and hydrophobic interaction.

The molecular docking results of the ligand (**L2**) and its complexes (**6 – 10)** against *E. coli* DNA gyrase B (PDB ID 6F86), found to be -6.5, -7.4, -7.0, -7.1, -6.7 and -6.6 kcal/mol respectively whereas the affinity energy of ciprofloxacin in this case was found to be –7.2 kcal/mol (Table 11). Complex **6** has a stronger binding energy than ciprofloxacin since it interacts through more van der Waals forces within the active sites of the enzyme via Ile-94, Pro-79, Asp-73, and Val-43 amino acid residues, while the van der Waals interaction of the ciprofloxacin was only via Ala-47. On the other hand, the *in vitro* activities of the complexes against *E. coli* showed a higher mean inhibition zone (MIZ) for the Zn(II) complex; indicating that the docking results are in good agreement with the *in vitro* activities.

The molecular docking results of the ligand (**L2**) and its complexes (**6 – 10)** against *P. aeruginosa* LasR binding domain were -7.6, -8.6, -5.3, -5.3, -5.4and -6.4 kcal/mol respectively, whereas the affinity energy of ciprofloxacin in this case was found to be -8.3 kcal/mol (Table 12). The *in vitro* mean inhibition zones of complexes have slight differences with the docking results compared to those of *E. Coli* DNA gyrase B (Appendix 46). Thus, the complexes may hinder the bacterial growth through inhibition of their DNA gyrase rather than LasR protein. Indeed, this is in good agreement with literature report that quinolones (fluoroquinolones) target the DNA gyrase of bacteria [352]. Since the complexes in the current work were also developed on a quinoline scaffold, their mode of action could be through hindering the DNA gyrase of bacteria, hence the overall *in silico* docking analysis for *E. coli* DNA gyrase B was found to be in good agreement with the *in vitro* bacterial activities.

Table 12. Molecular docking results of ligands and their complexes against *P. aeruginosa* LasR.DNA (PDB: 2UV0).

Cpds.	Affinity (kcal/mol)	H-bond	Residual Hydrophobic/Pi-Cation/Pi-Anion/ Pi-Alkyl interactions
L1	– 7.8	Tyr-64	Asp-73, Trp-88, Phe-101, Ala-105, Leu-110, Trp-60, Tyr-93, Tyr-56, Thr-75, Ser-129, Thr-115, Arg-61
1	– 7.3	Ser-129	Asp-73, Tyr-64, Leu-36, Trp-88, Phe-101, Leu-110, Ala-70, Gly-38, Cys-79, Ile-52, Thr-115, Ala-127, Thr-75, Tyr-56, Tyr-93
2	– 8.2	Tyr-47	Asp-73, Tyr-64, Leu-36, Arg-61, Thr-75, Ser-129, Tyr-56, Trp-60, Ile-52, Ala-50, Gly-38, Ala-70, Leu-39
4	– 8.2	Tyr-47	Asp-73, Tyr-64, Leu-36, Tyr-56, Ala-127, Gly-38, Ala-50, Ile-52, Asp-65, Arg-61, Leu-39, Trp-60, Trp-88, Thr-75, Ser-129
L2	-7.6	Thr-75, Arg-61	Val-76, Ala-50, Ala- 127, Leu-40, Tyr-47, Cys-79, Leu-125
6	- 8.6	Arg-61	Tyr-47, Ala-70, Ala-50, Ala-127, Cys-79, Leu-125, Val-76, Asp-73, Tyr-56, Trp-88, Ala-105, Leu-110, Phe- 101, Tyr-64
7	-5.3	Arg-61, Tyr-64, Ser-129	Leu-36, Trp-88, Ala-50, Leu-40, Gly-38, Ala-127, Gly-126, Cys-79, Val-76, Thr-115, Thr-75
8	-5.3	Trp-60, Thr-75	Leu-125, Leu-40, Val-76, Ala-50, Ala-105, Leu-110, Trp-88, Phe-101, Tyr-56, Tyr-64, Thr-115
9	-5.4	Asp-73, Tyr-64,	Tyr-56, Ala-50, Leu-40, Gly-126, Ala-127, Val-76, Leu-36, Leu-110, Trp-88
10	-6.4	Leu-39, Arg61,	Ala-105, Trp-88, Leu-110, Phe-101, Ile-52, Leu-36, Gly-38, Ala-50, Tyr-47, Cys-79, Leu-125, Ala-127,
Cipro	– 8.0	Asp-73, Trp-60, Tyr-47,	Tyr-64, Leu-36, Val-76, Ala-127, Cys-79, Ala-50, Gly-38, Thr-115, Trp-88, Thr-75, Tyr-56, Leu-110, Phe-101, Arg-61, Ala-70

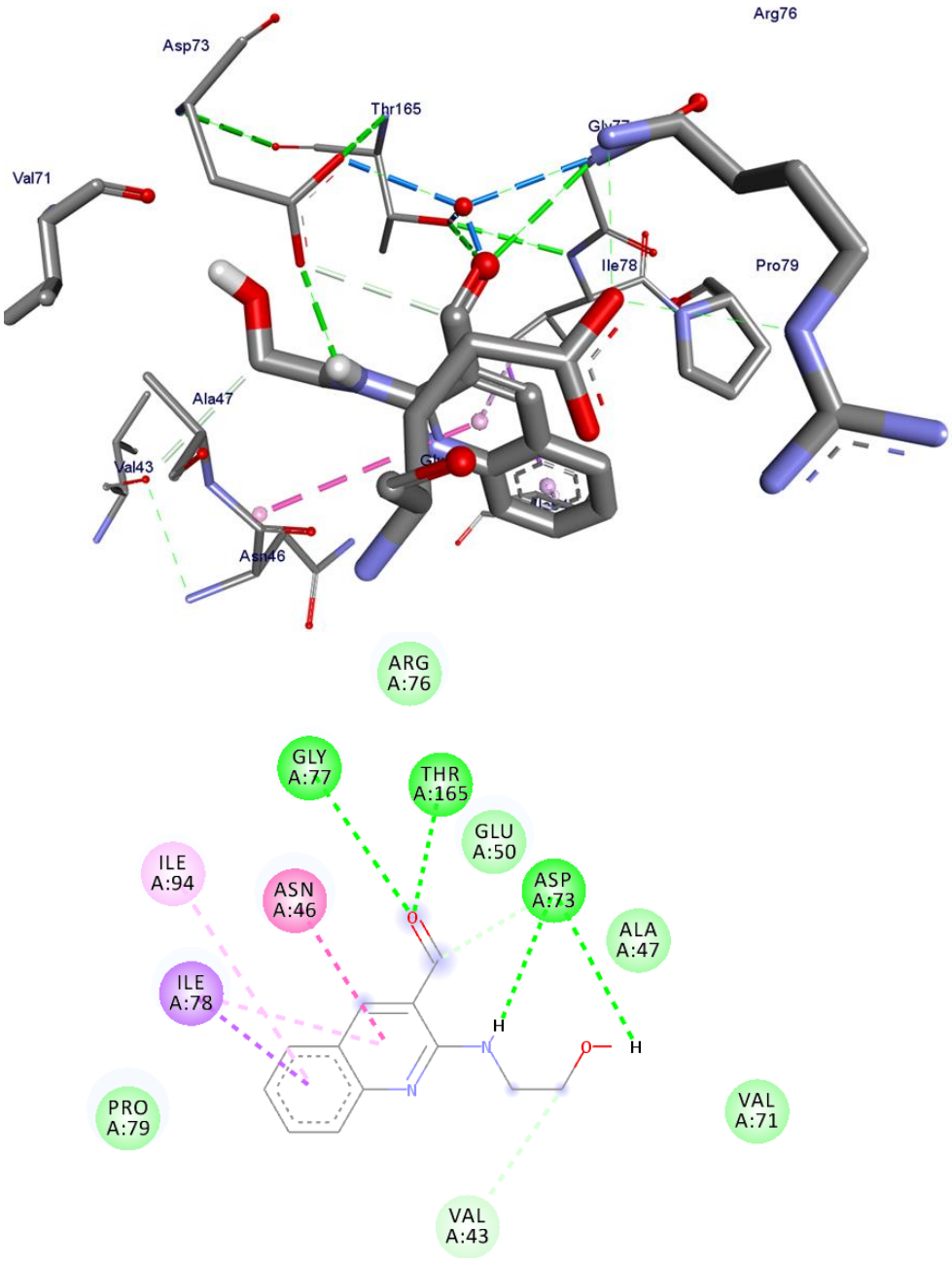

Figure 52. The interactions of the **L2** against *E. Coli* DNA gyrase B (PDB ID: 6F86)

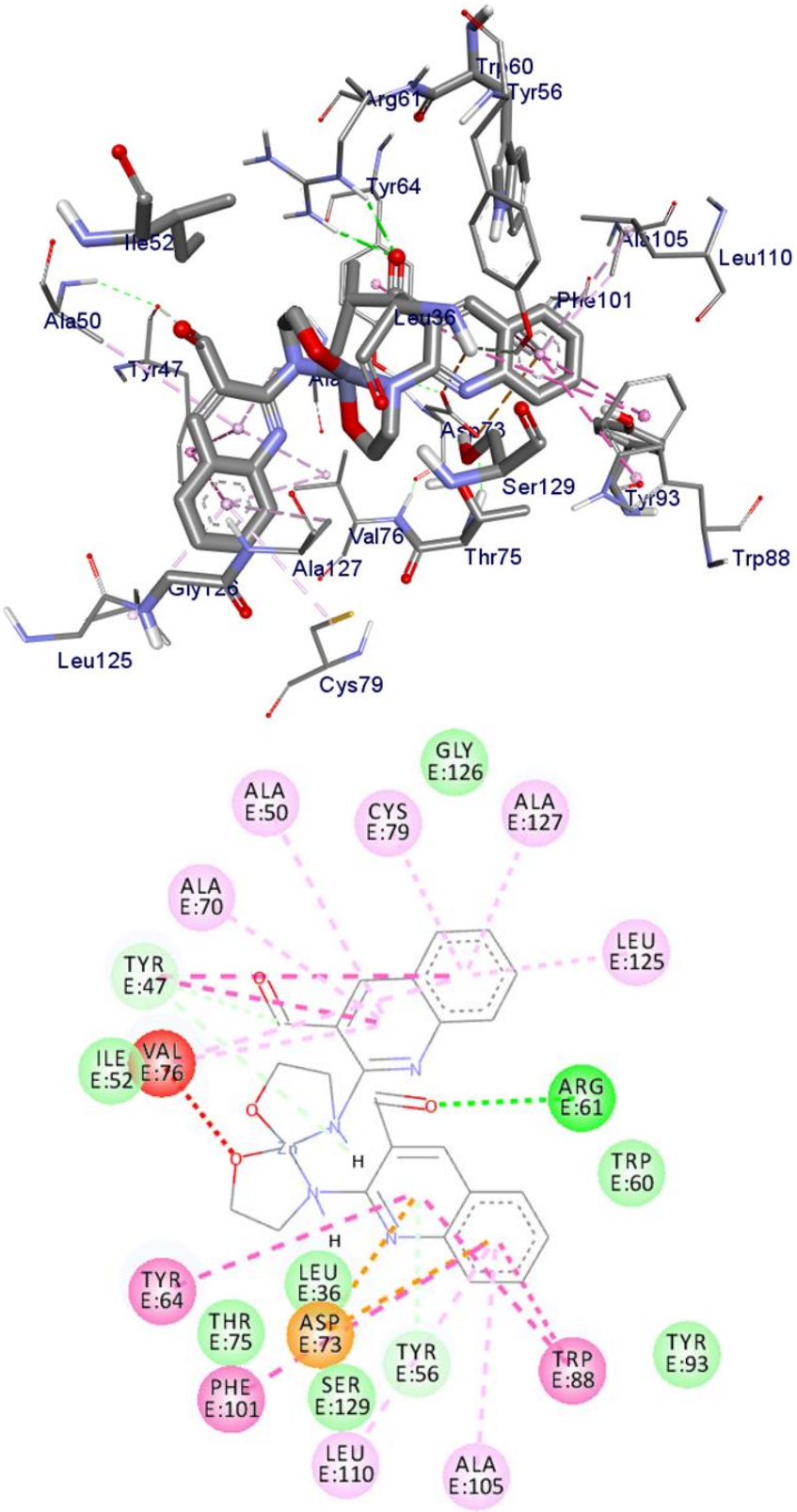

Figure 53. The interactions of the **6** against *E. Coli* DNA gyrase B (PDB ID: 6F86).

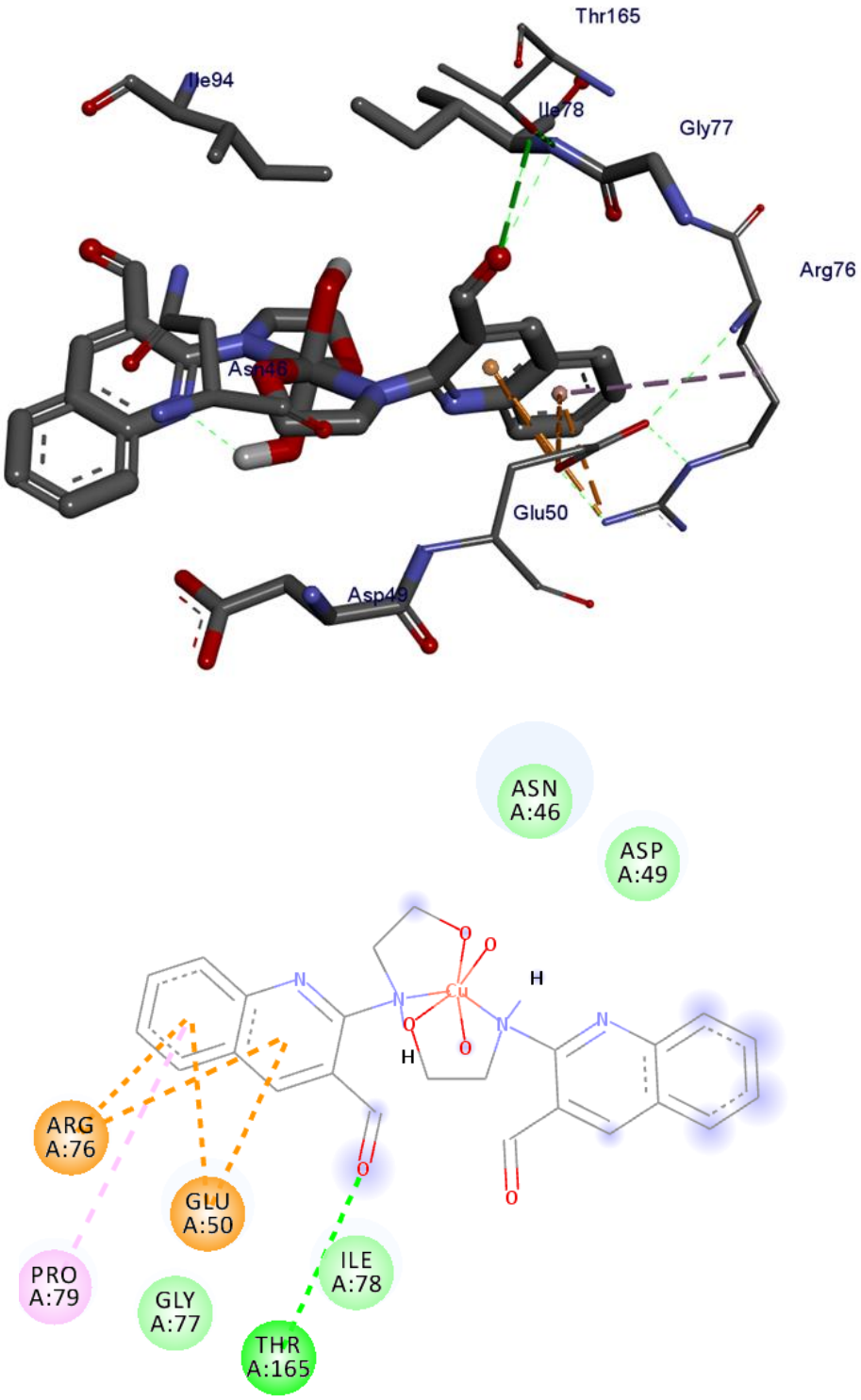

Figure 54. The interactions of the **7** against *E. Coli* DNA gyrase B (PDB ID: 6F86).

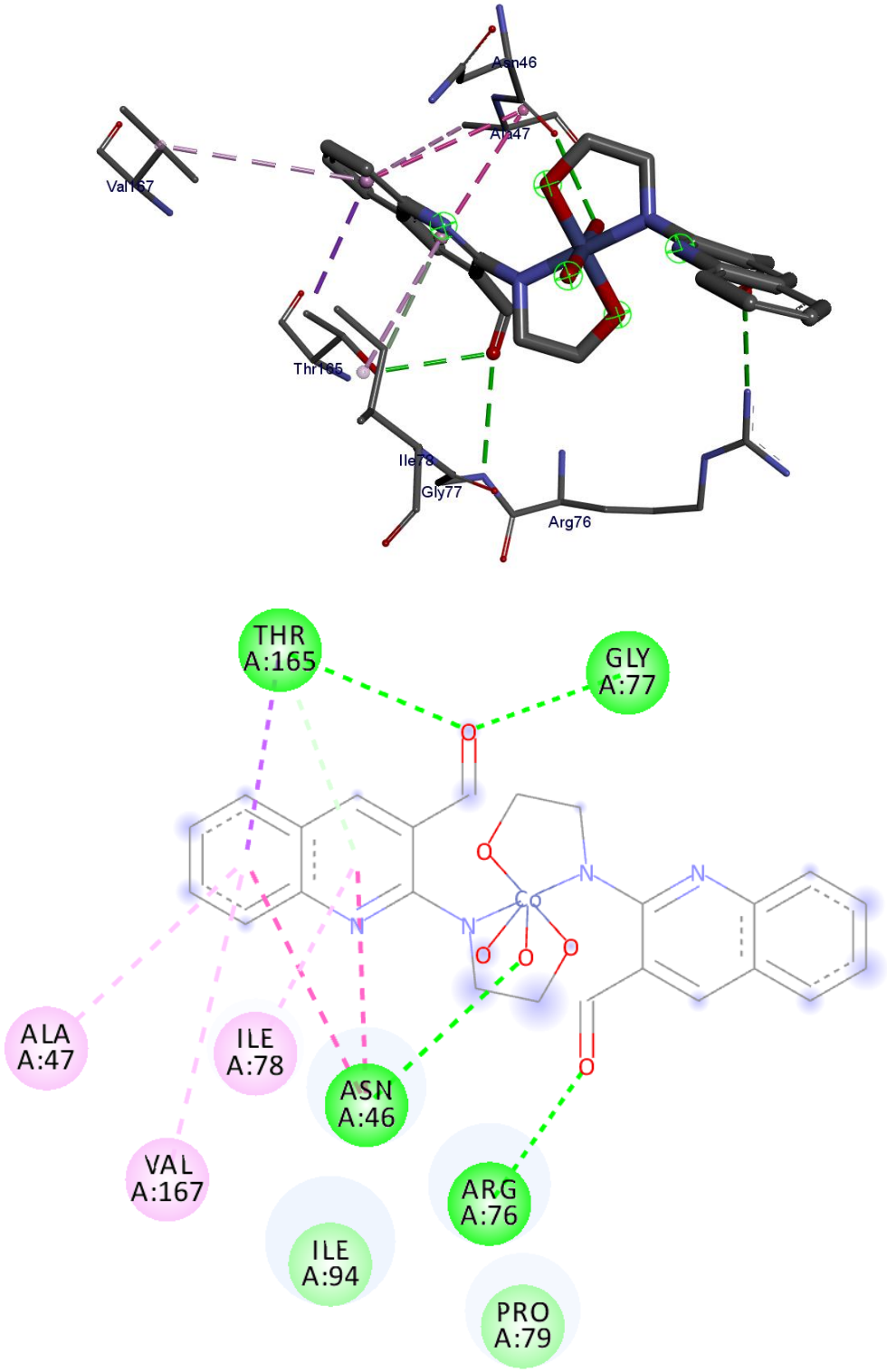

Figure 55. The interactions of the **8** against *E. Coli* DNA gyrase B (PDB ID: 6F86).

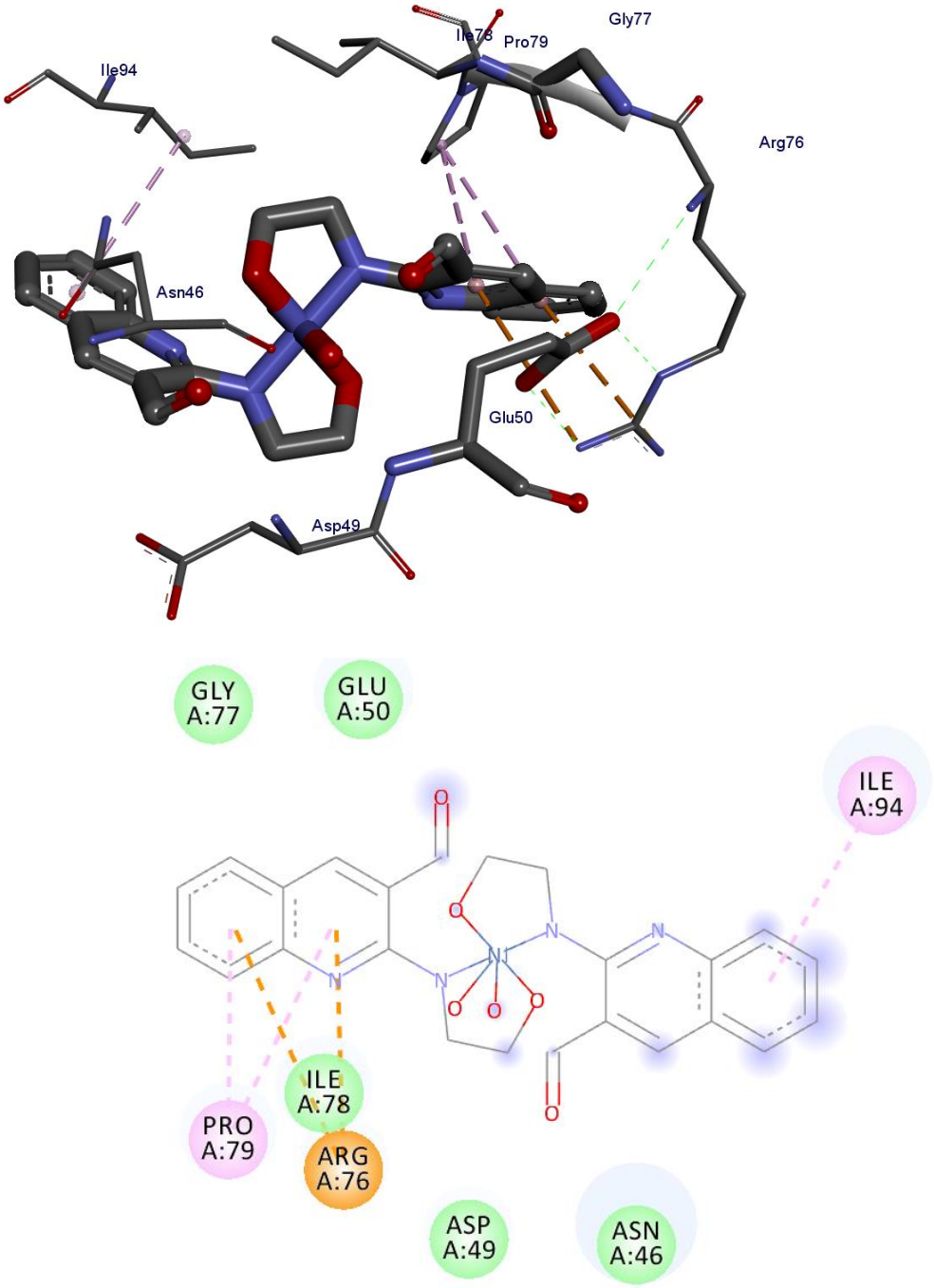

Figure 56. The interactions of the **9** against *E. Coli* DNA gyrase B (PDB ID: 6F86).

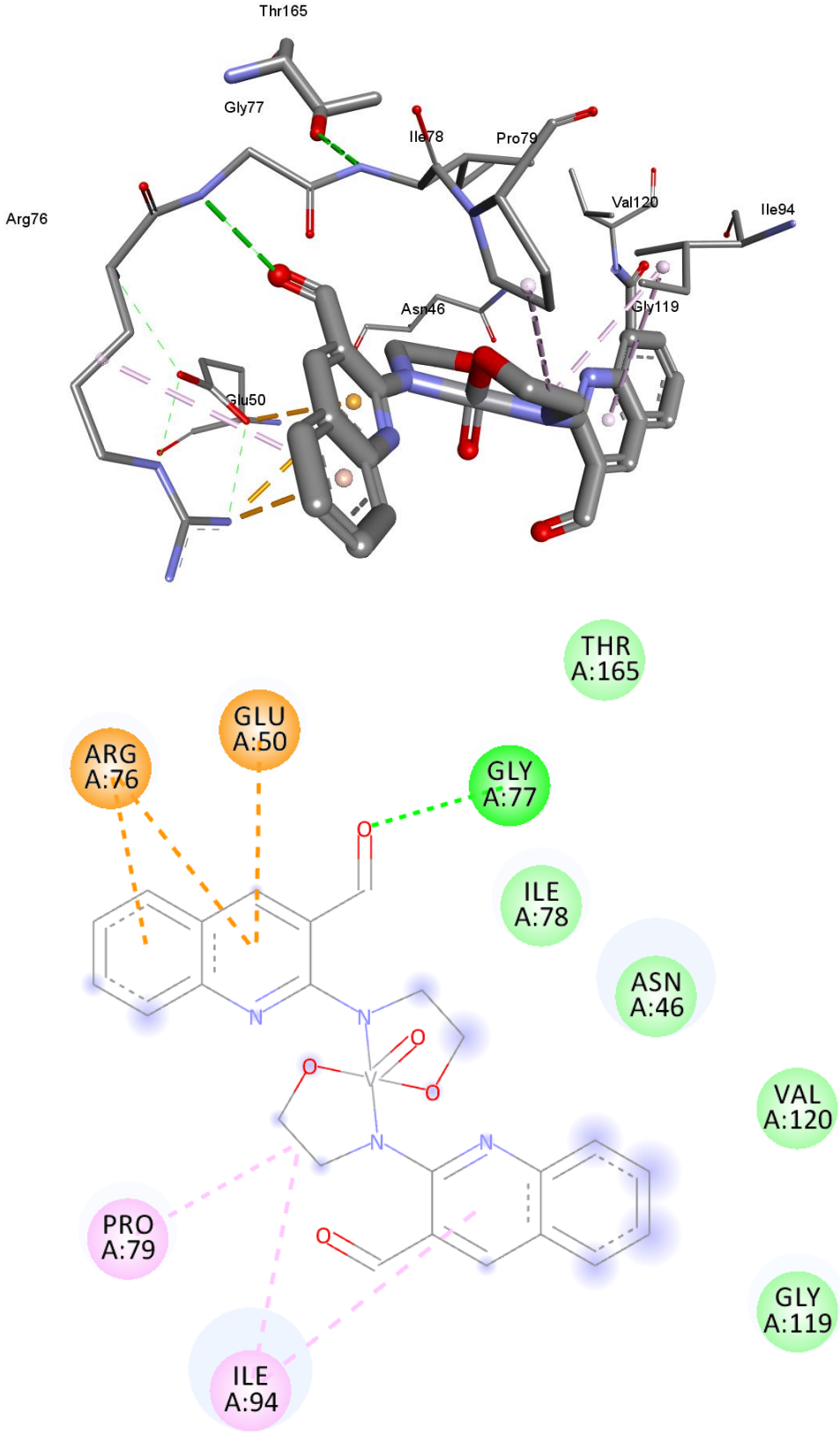

Figure 57. The interactions of the **10** against *E. Coli* DNA gyrase B (PDB ID: 6F86).

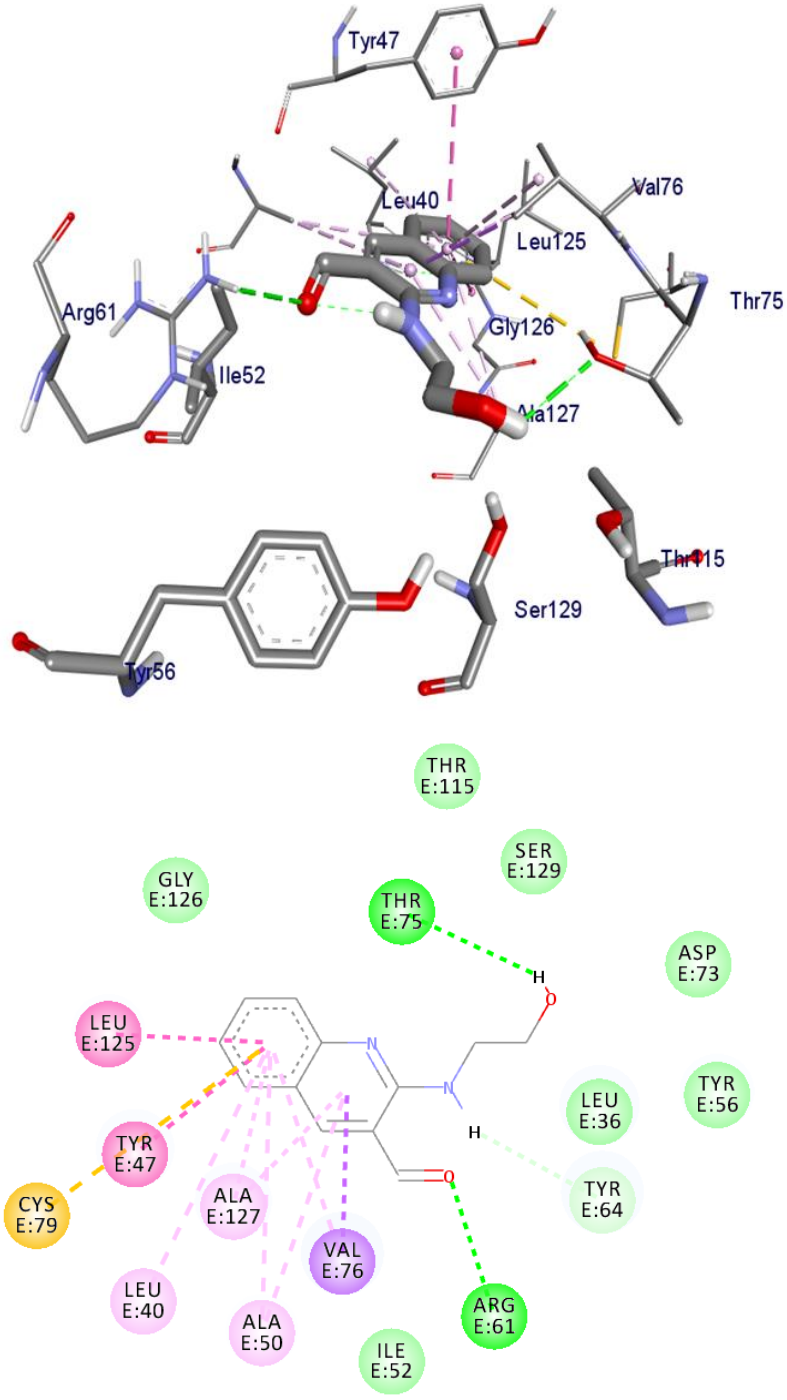

Figure 58. The interactions of the **L2** against *P. aeruginosa* LasR.DNA (PDB: 2UV0).

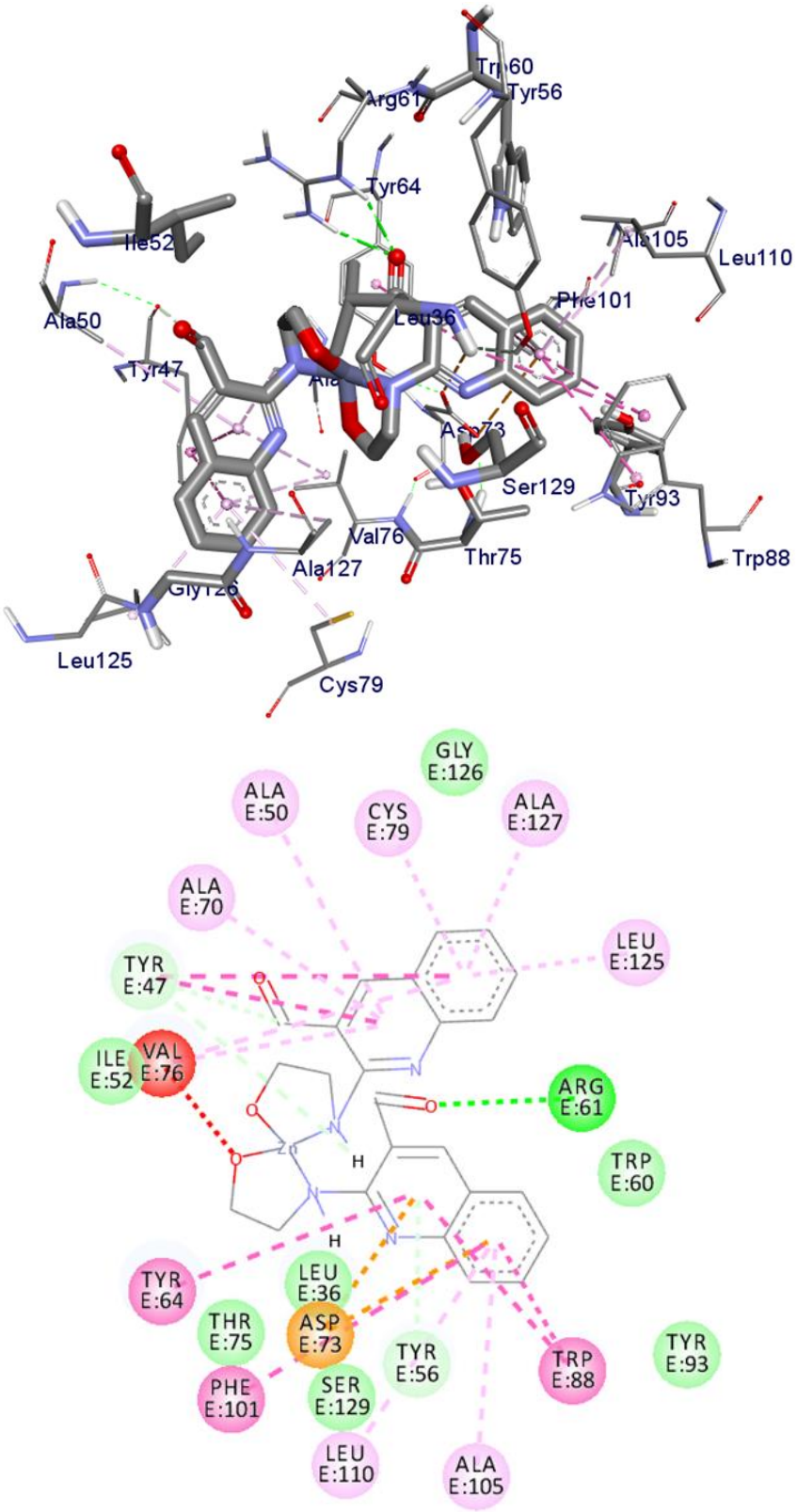

Figure 59. The interactions of the **6** against *P. aeruginosa* LasR.DNA (PDB: 2UV0).

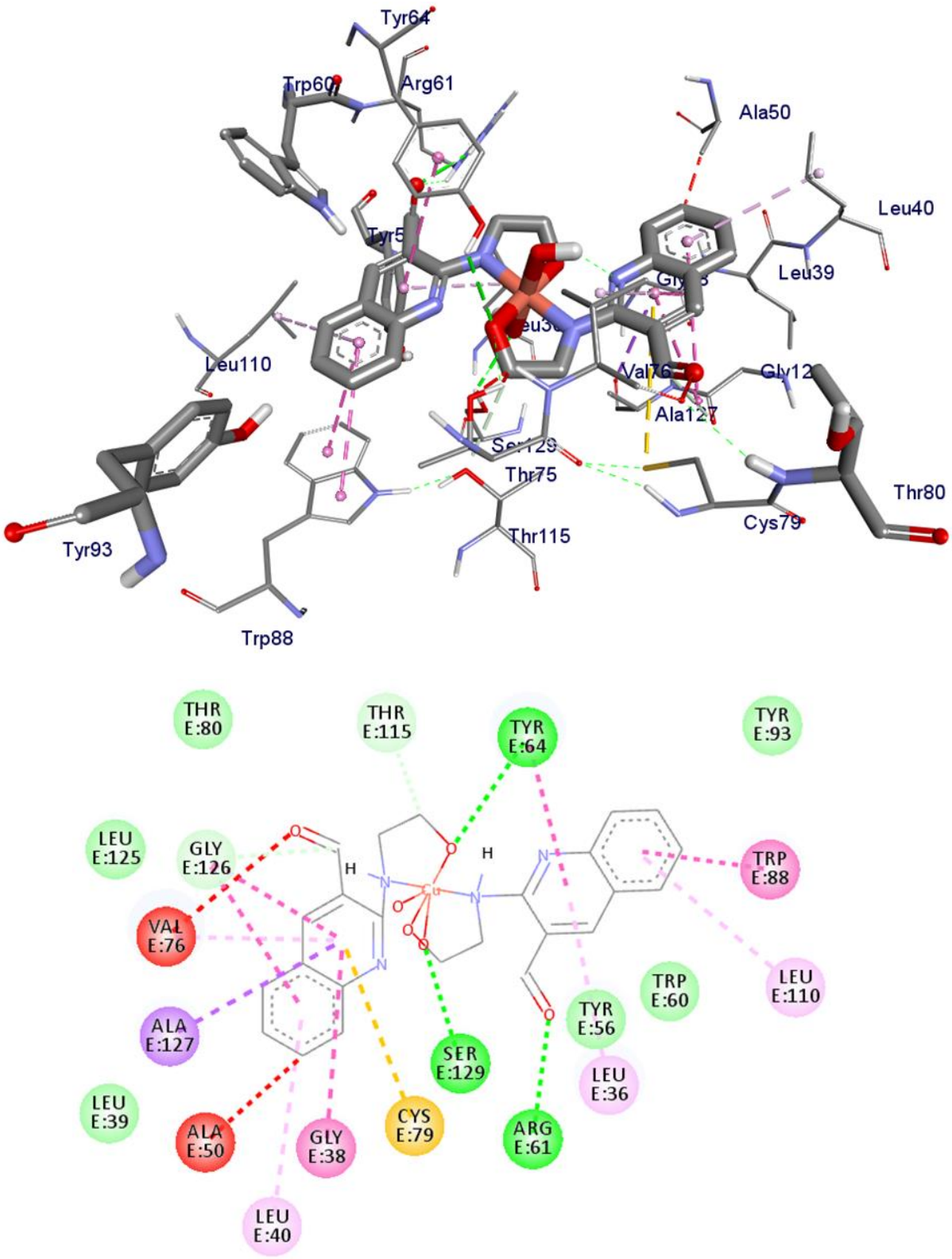

Figure 60. The interactions of the **7** against *P. aeruginosa* LasR.DNA (PDB: 2UV0).

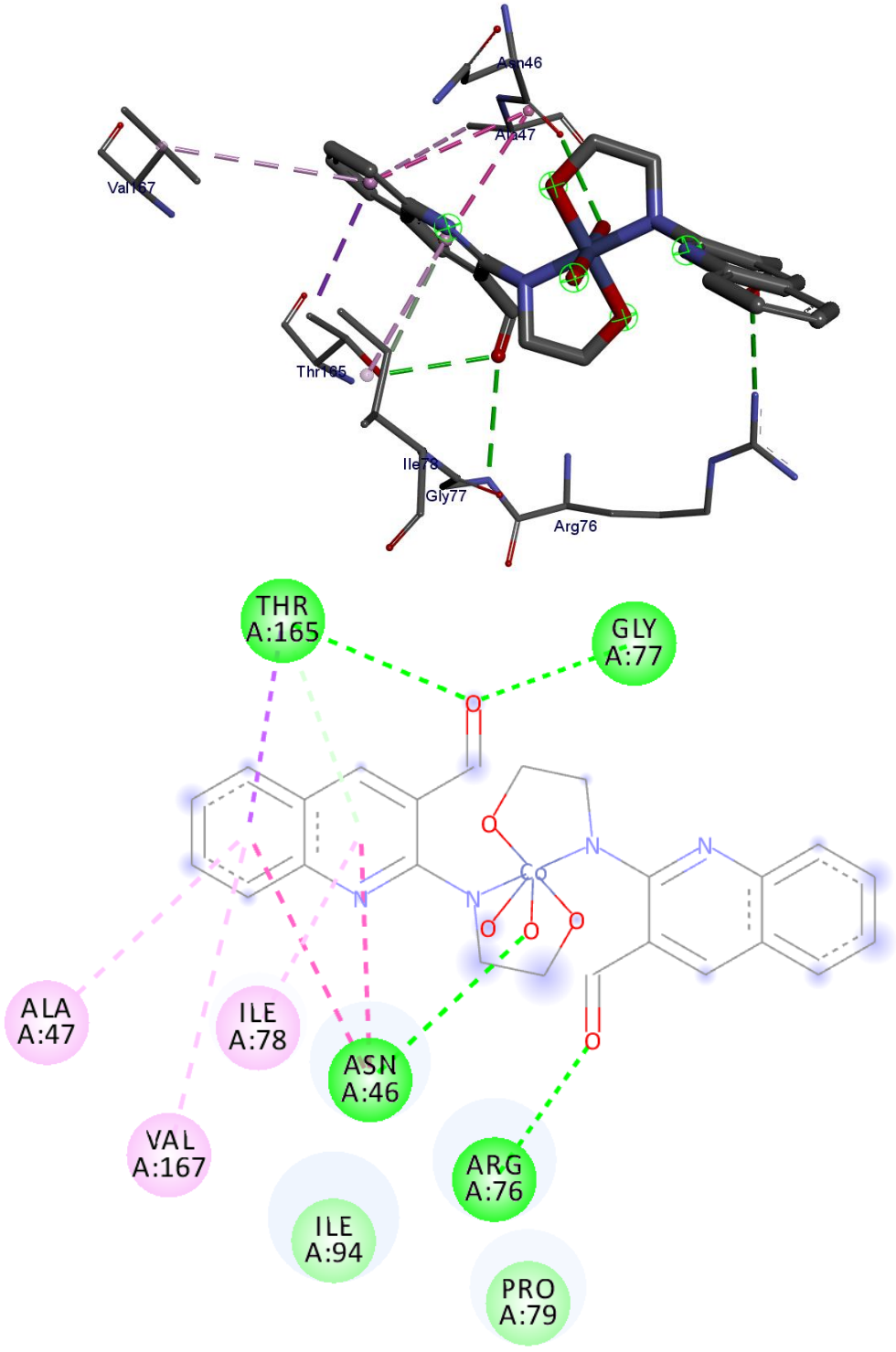

Figure 61. The interactions of the **8** against *P. aeruginosa* LasR.DNA (PDB: 2UV0).

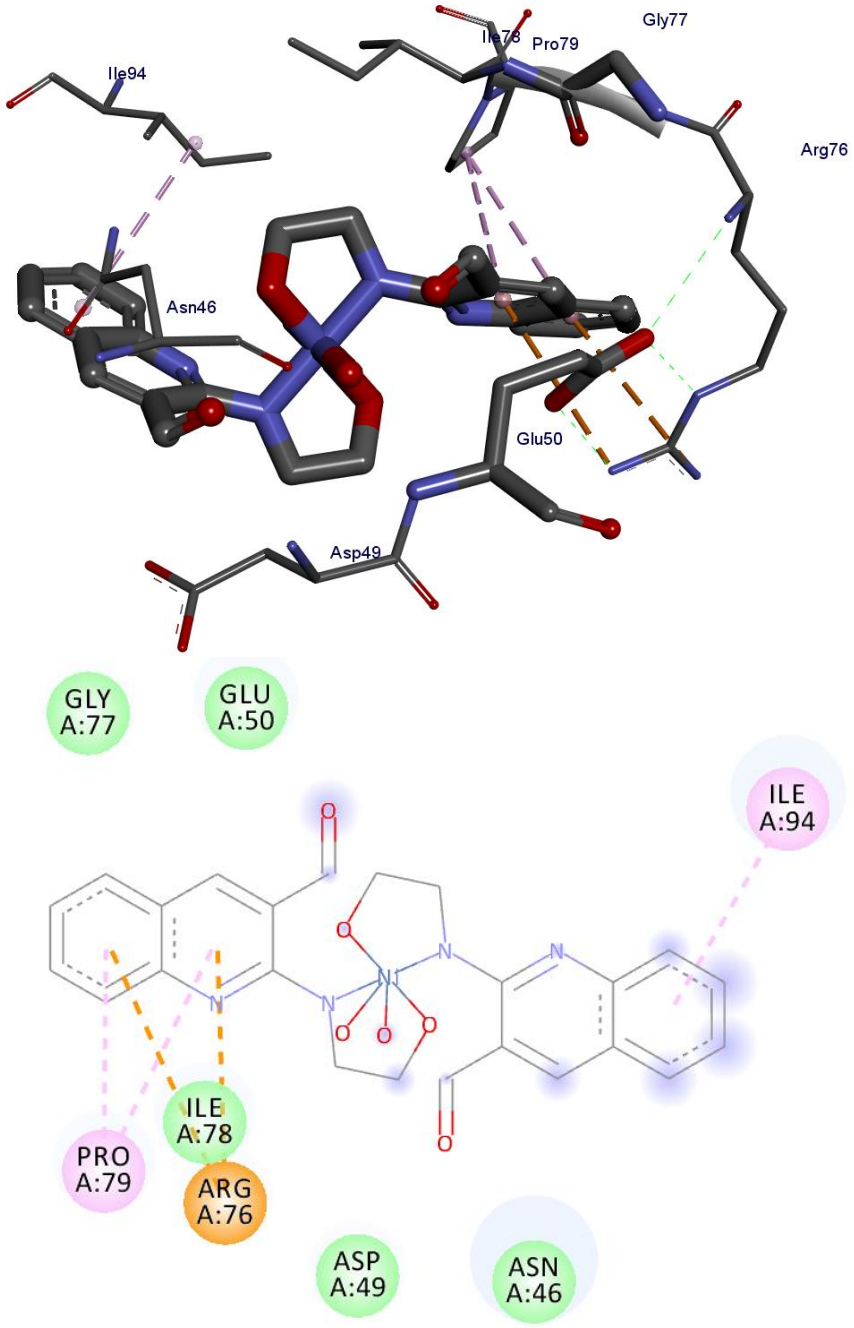

Figure 62. The interactions of the **9** against *P. aeruginosa* LasR.DNA (PDB: 2UV0).

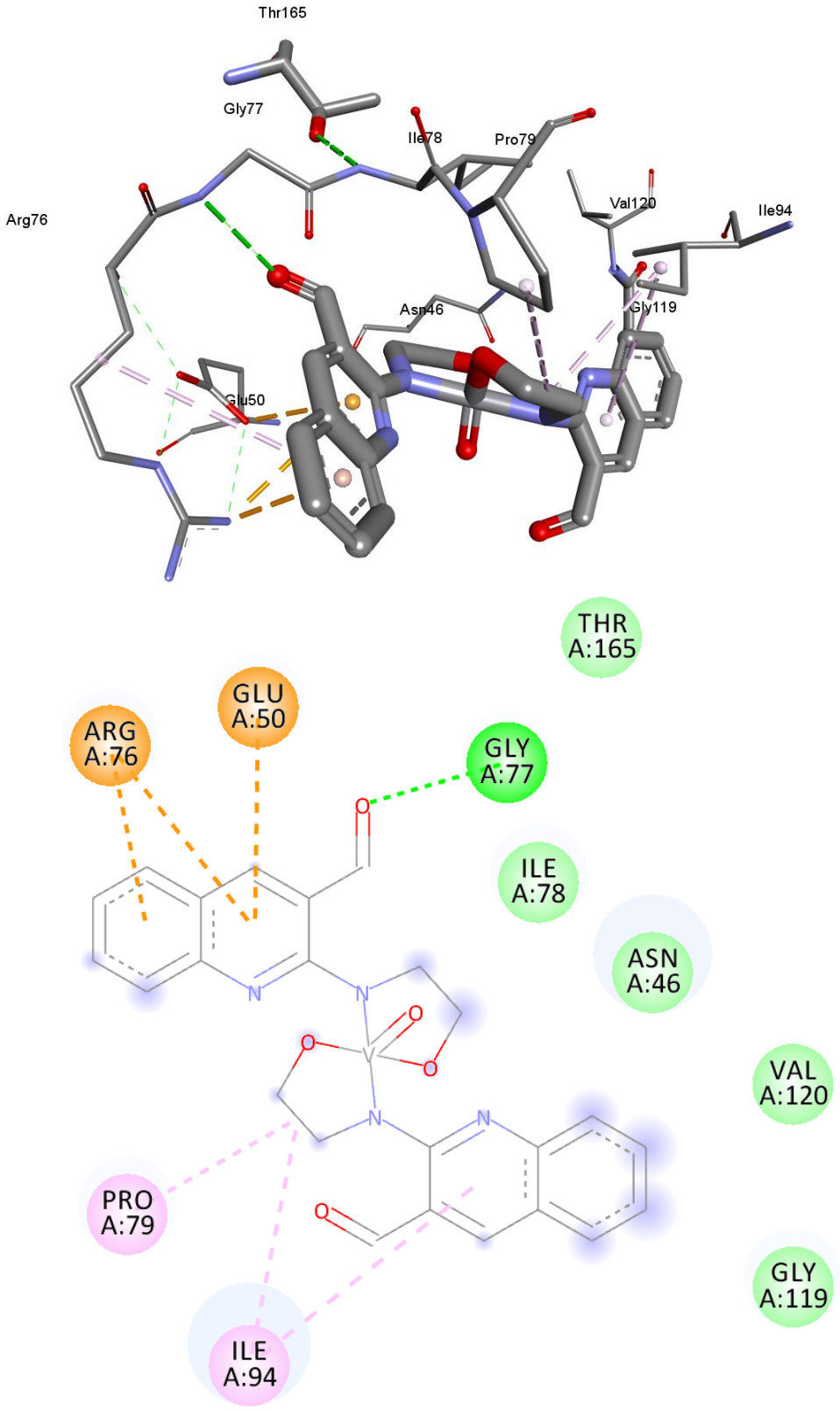

Figure 63. The interactions of **10** against *P. aeruginosa* LasR.DNA (PDB: 2UV0).

5. CONCLUSIONS

Quinoline derivatives have been a successful scaffold to develop bioactive molecules. In the present work, novel Zn(II), Cu(II), Co(II), Ni(II) and V(IV) complexes were successfully synthesized from a tridentate ONN [(*E*)-2-(((2-((2-hydroxyethyl)amino)quinolin-3-yl)methylene)amino)ethan-1-ol, (**H_3L**) and bidentate ON 2-((2-hydroxyethyl)amino)quinoline-3-carbaldehyde (**H_2L**) atoms donor ligands. The compounds were characterized by physicochemical and spectroscopic methods. The analysis was supported by DFT and TD-DFT calculations. The DFT calculated IR frequencies and TD-B3LYP calculated absorption spectra are in good agreement with the corresponding experimental results, which further confirmed the overall analysis. From both experimental (EDX, MS and TGA) and DFT analysis, the ligand (**L1**) acts as an ONN donor tridentate chelating agent while **L2** act as bidentate ligand. The analyses also indicated that the complex **1** has a distorted tetrahedral geometrical structure, on the other hand, the complex **2** showed distorted square pyramidal geometry similarly, complex **3** showed octahedral, while that of complex **4** has square planar geometry, complex **5,** showed octahedral structure, complex **6** showed tetrahedral and complex **7, 8** and **9** showed octahedral structure while complex 10 showed bipyramidal structure which were confirmed from the visualization of the DFT optimized geometries. The formation constants of the complexes were determined spectroscopically. Accordingly, the stability of the metal complexes of **L1** are ($K_{Zn(II)} = 2.3 \times 10^6$, $K_{Cu(II)} = 2.9 \times 10^6$, $K_{Co(II)} = 1.10 \times 10^8$, $K_{Ni(II)} = 3.8 \times 10^5$ and $K_{V(IV)} = 7.6 \times 10^5$) and **L2** complexes ($K_{Zn(II)} = 2.47 \times 10^8$, $K_{Cu(II)} = 4.29 \times 10^8$, $K_{Co(II)} = 2.05 \times 10^6$, $K_{Ni(II)} = 2.36 \times 10^7$ and $K_{V(IV)} = 6.29 \times 10^5$). All metal complexes are stable at the specified temperatures, and the thermodynamic parameters indicated that the reactions are spontaneous with exothermic nature of metal-ligand interactions. *In vitro* antibacterial activity analysis of both the ligands and their complexes were studied with disc diffusion and agar dilution methods, in which the complexes showed better activity than the free ligands. The analysis of the antibacterial data revealed that all the first five (**1 – 5**) transition metal complexes exhibited activity ranging from low to high mean inhibition zones, with MIZ of 7.32 ± 0.90 mm to 20.65 ± 0.18 mm respectively. All the **1 – 4** complexes exhibited good activities with *P. aeruginosa* (18.85 ± 0.34, 20.65 ± 0.18, 18.62 ± 0.19 and 15.64 ± 0.22 mm diameter, respectively) compared to ciprofloxacin with MIZ of 22.98 ± 0.08 mm diameter. Complex **2** showed higher percent activity index (*AI* = 62, 90%), than all Zn(II) (*AI* = 54, 82%), Co (*AI* = 54, 81%) and Ni(II) (*AI* = 41, 68%) complexes of ligand (**L1**) against both *E. coli* and *P. aeruginosa*, respectively.

Similarly, the complexes (**6 – 10**) of ligand (**L2**) showed that all the four (**6 – 9**) metal complexes exhibited antibacterial activities ranging from medium to high MIZ, with 11.79 ± 1.07 mm and 20.9 ± 2.00 mm. All the (**6 – 9**) complexes exhibited good activities with *P. aeruginosa* (20.75 ± 2.05, 20.9 ± 2.00, 20.75 ± 2.07 and 18.90 ± 2.06 mm diameter respectively) compared to ciprofloxacin with MIZ of 20.94 ± 2.01mm diameter, but complex **7** showed higher percent activity index against the three bacterial strain (*P. aeruginosa*, *S. aureus* and *S. pyogenes* respectively, than all complexes of ligand (**L2**). The complexes were also evaluated for their antioxidant properties using DPPH assay in which all metal complexes showed higher antioxidant activities than the free ligand. Among these, **1, 2, 6, 7** and **8** complexes exhibited higher values of antioxidant activities (IC_{50} = 10.46, 8.62, 8.2, 4.7, and 9.2 µg/mL, respectively, whereas that of the positive control is 4.28 µg/mL). From the *in silico (*drug likeness and molecular docking) analysis all complexes (**1 – 5**) fulfil Lipinski's rule of five and the binding modes of all compounds (**1 – 10**) against the two bacterial are in good agreement with the experimental biological activities. Overall, the newly synthesized Zn(II), Cu(II), Co(II), and Ni(II) complexes have biological activities, where the Cu(II) complex showed much better activity than other complexes. The results of binding mode of these compounds against *E. coli* DNA gyrase B were in good agreement with the *in vitro* biological activity results. The high antibacterial activity of copper complexes against Gram-negative bacteria compared to ciprofloxacin makes the complexes potential alternative drug for treating diseases caused by Gram-negative bacteria after passing cytotoxicity testing. It is obvious that the compounds that can scavenge DPPH radicals might exhibit anticancer, antiaging, anti-inflammatory activities. As our complexes have pronounced DPPH radical scavenging activities due to their nitrogen and oxygen atom donating ability, they may have the anticancer and related activities and the door is open for any interested researchers.

6. REFERENCES

[1] Hamdani, H. EL; Amane, M. EL. Preparation, Spectral, Antimicrobial Properties and Anticancer Studies of New Metal Complexes [M(Caffeine) 4] (PF 6) 2; M = Fe(II), Co(II), Mn(II), Cd(II), Zn(II), Cu(II), Ni(II). *J. Mol. Struct.*, **2019**, *1184*, 262–270.

[2] Nagesh, G. Y.; Mahendra Raj, K.; Mruthyunjayaswamy, B. H. M. Synthesis, Characterization, Thermal Study and Biological Evaluation of Cu(II), Co(II), Ni(II) and Zn(II) Complexes of Schiff Base Ligand Containing Thiazole Moiety. *J. Mol. Struct.*, **2015**, *1079*, 423–432. https://doi.org/10.1016/j.molstruc.2014.09.013.

[3] Ali, I. A. I.; El-Sakka, S. S. A.; Soliman, M. H. A.; Mohamed, O. E. A. In Silico, In Vitro and Docking Applications for Some Novel Complexes Derived from New Quinoline Derivatives. *J. Mol. Struct.*, **2019**, *1196*, 8–32.

[4] Malik, M. A.; Raza, K.; Mohammed, A.; Wani, M. Y.; Al-bogami, A. S.; Hashmi, A. A. Unravelling the Anticancer Potential of a Square Planar Copper Complex : Toward Non-Platinum Chemotherapy †. *RSC Adv.*, **2021**, *11*, 39349–39361.

[5] Azam, A.; Raza, M. A.; Sumrra, S. H. Therapeutic Application of Zinc and Vanadium Complexes against Diabetes Mellitus a Coronary Disease: A Review. *Open Chem.*, **2018**, *16* (1), 1153–1165. https://doi.org/10.1515/chem-2018-0118.

[6] Koleša-Dobravc, T.; Maejima, K.; Yoshikawa, Y.; Meden, A.; Yasui, H.; Perdih, F. Bis(Picolinato) Complexes of Vanadium and Zinc as Potential Antidiabetic Agents: Synthesis, Structural Elucidation and: In Vitro Insulin-Mimetic Activity Study. *New J. Chem.*, **2018**, *42* (5), 3619–3632. https://doi.org/10.1039/c7nj04189f.

[7] Murugavel, S.; Jacob Prasanna Stephen, C. S.; Subashini, R.; AnanthaKrishnan, D. Synthesis, Structural Elucidation, Antioxidant, CT-DNA Binding and Molecular Docking Studies of Novel Chloroquinoline Derivatives: Promising Antioxidant and Anti-Diabetic Agents. *J. Photochem. Photobiol. B Biol.*, **2017**, *173*, 216–230.

[8] Ramírez–Prada, J.; Robledo, S. M.; Vélez, I. D.; Crespo, M. del P.; Quiroga, J.; Abonia, R.; Montoya, A.; Svetaz, L.; Zacchino, S.; Insuasty, B. Synthesis of Novel Quinoline–Based 4,5–Dihydro–1H–Pyrazoles as Potential Anticancer, Antifungal, Antibacterial and Antiprotozoal Agents. *Eur. J. Med. Chem.*, **2017**, *131*, 237–254.

[9] Pinz, M. P.; Reis, A. S.; de Oliveira, R. L.; Voss, G. T.; Vogt, A. G.; Sacramento, M. do; Roehrs, J. A.; Alves, D.; Luchese, C.; Wilhelm, E. A. 7-Chloro-4-Phenylsulfonyl Quinoline, a New Antinociceptive and Anti-Inflammatory Molecule: Structural Improvement of a Quinoline Derivate with Pharmacological Activity. *Regul. Toxicol.*

Pharmacol., **2017**, *90*, 72–77. https://doi.org/10.1016/j.yrtph.2017.08.014.

[10] Yaakov, D. Ben; Shadkchan, Y.; Albert, N.; Kontoyiannis, D. P.; Osherov, N. The Quinoline Bromoquinol Exhibits Broad-Spectrum Antifungal Activity and Induces Oxidative Stress and Apoptosis in Aspergillus Fumigatus. *J. Antimicrob. Chemother.*, **2017**, *72* (8), 2263–2272. https://doi.org/10.1093/jac/dkx117.

[11] Digafie, Z.; Melaku, Y.; Belay, Z.; Eswaramoorthy, R. Synthesis , Molecular Docking Analysis , and Evaluation of Antibacterial and Antioxidant Properties of Stilbenes and Pinacol of Quinolines. *Adv. Pharmacol. Pharm. Sci.*, **2021**, *2021*, 1–17.

[12] Zeng, Z.; Cai, J.; Li, F.; Weng, Y.; Huang, Q.; Yang, H.; Huang, Q.; Wei, Y. Synthesis, Crystal Structures, DNA Interactions, and Antitumor Activity of Two New Dinuclear Copper(Ii) Complexes with Thiazole Ligand . *RSC Adv.*, **2021**, *11* (63), 40040–40050. https://doi.org/10.1039/d1ra05798g.

[13] Fetoh, A.; El-Gammal, O. A.; Abu El-Reash, G. M. Antioxidant and Antitumor Activities of Cr(III), Mn(II), Fe(III), Cd(II), Zn(II) and Hg(II) Complexes Containing a Carbohydrazone Ligand Ending by 4-Pyridyl Ring. *J. Mol. Struct.*, **2018**, *1173*, 100–110. https://doi.org/10.1016/j.molstruc.2018.06.087.

[14] Sumalatha, V.; Daravath, S.; Rambabu, A.; Ramesh, G.; Shivaraj. Antioxidant, Antimicrobial, DNA Binding and Cleavage Studies of Novel Co(II), Ni(II) and Cu(II) Complexes of N, O Donor Schiff Bases: Synthesis and Spectral Characterization. *J. Mol. Struct.*, **2021**, *1229*, 1–14. https://doi.org/10.1016/j.molstruc.2020.129606.

[15] Abu-Dief, A. M.; El-Metwaly, N. M.; Alzahrani, S. O.; Alkhatib, F.; Abualnaja, M. M.; El-Dabea, T.; El-Remaily, M. A. E. A. A. A. Synthesis and Characterization of Fe(III), Pd(II) and Cu(II)-Thiazole Complexes; DFT, Pharmacophore Modeling, in-Vitro Assay and DNA Binding Studies. *J. Mol. Liq.*, **2021**, *326*, 1–15.

[16] Al-Hazmi, G. A. A.; Abou-Melha, K. S.; Althagafi, I.; El-Metwaly, N. M.; Shaaban, F.; Abdul Galil, M. S.; El-Bindary, A. A. Synthesis and Structural Characterization of Oxovanadium(IV) Complexes of Dimedone Derivatives. *Appl. Organomet. Chem.*, **2020**, *34* (8), 1–16. https://doi.org/10.1002/aoc.5672.

[17] Damena, T.; Zeleke, D.; Desalegn, T.; B. Demissie, T.; Eswaramoorthy, R. Synthesis, Characterization, and Biological Activities of Novel Vanadium(IV) and Cobalt(II) Complexes. *ACS Omega*, **2022**, *7* (5), 4389–4404.

[18] Al-Hazmi, G. A. A.; Abou-Melha, K. S.; El-Metwaly, N. M.; Althagafi, I.; Shaaban, F.; Zaky, R. Green Synthesis Approach for Fe (III), Cu (II), Zn (II) and Ni (II)-Schiff Base Complexes, Spectral, Conformational, MOE-Docking and Biological Studies.

Appl. Organomet. Chem., **2020**, *34* (3), 1–15. https://doi.org/10.1002/aoc.5403.

[19] Azam, M.; Mohammad Wabaidur, S.; Alam, M.; Trzesowska-Kruszynska, A.; Kruszynski, R.; Al-Resayes, S. I.; Fahhad Alqahtani, F.; Rizwan Khan, M.; Rajendra. Design, Structural Investigations and Antimicrobial Activity of Pyrazole Nucleating Copper and Zinc Complexes. *Polyhedron*, **2021**, *195*, 1–10.

[20] Kaya, Y.; Erçağ, A.; Uğuz, Ö.; Koca, A.; Zorlu, Y.; Hacıoğlu, M.; Seher Birteksöz Tan, A. New Asymmetric Bisthiocarbohydrazones and Their Mixed Ligand Nickel(II) Complexes: Synthesis, Characterization, Crystal Structure, Electrochemical-Spectroelectrochemical Property, Antimicrobial and Antioxidant Activity. *Polyhedron*, **2021**, *207* (May), 1–10. https://doi.org/10.1016/j.poly.2021.115372.

[21] Kargar, H.; Ardakani, A. A.; Tahir, M. N.; Ashfaq, M.; Munawar, K. S. Synthesis, Spectral Characterization, Crystal Structure and Antibacterial Activity of Nickel(II), Copper(II) and Zinc(II) Complexes Containing ONNO Donor Schiff Base Ligands. *J. Mol. Struct.*, **2021**, *1233*, 1–12. https://doi.org/10.1016/j.molstruc.2021.130112.

[22] El-Gammal, O. A.; Mohamed, F. S.; Rezk, G. N.; El-Bindary, A. A. Synthesis, Characterization, Catalytic, DNA Binding and Antibacterial Activities of Co(II), Ni(II) and Cu(II) Complexes with New Schiff Base Ligand. *J. Mol. Liq.*, **2021**, *326*, 1–17.

[23] Ghazal, K.; Shoaib, S. Synthesis , Characterization , X-Ray Diffraction Study , in-Vitro Cytotoxicity , Antibacterial and Antifungal Activities of Nickel (II) and Copper (II) Complexes with Acyl Thiourea Ligand. *J. Mol. Struct.*, **2019**, *1177*, 124–130.

[24] Cao, Q.; Zhou, D. J.; Pan, Z. Y.; Yang, G. G.; Zhang, H.; Ji, L. N.; Mao, Z. W. CAIXplatins: Highly Potent Platinum(IV) Prodrugs Selective Against Carbonic Anhydrase IX for the Treatment of Hypoxic Tumors. *Angew. Chemie - Int. Ed.*, **2020**, *59* (42), 18556–18562. https://doi.org/10.1002/anie.202005362.

[25] Ruiz, M. C.; Perelmulter, K.; Levín, P.; Romo, A. I. B.; Lemus, L.; -Fogolín, M. B.; León, I. E.; Di Virgilio, A. L. Antiproliferative Activity of Two Copper (II) Complexes on Colorectal Cancer Cell Models: Impact on ROS Production, Apoptosis Induction and NF-KB Inhibition. *Eur. J. Pharm. Sci.*, **2022**, *169* (September 2021), 1–9. https://doi.org/10.1016/j.ejps.2021.106092.

[26] El-Metwaly, N.; Althagafi, I.; Katouah, H. A.; Al-Fahemi, J. H.; Bawazeer, T. M.; Khedr, A. M. Synthesis of Novel VO (II)-Thaizole Complexes; Spectral, Conformational Characterization, MOE-Docking and Genotoxicity. *Appl. Organomet. Chem.*, **2019**, *33* (9), 1–17. https://doi.org/10.1002/aoc.5095.

[27] Abou-Melha, K. S.; Al-Hazmi, G. A.; Althagafi, I.; Alharbi, A.; Shaaban, F.; El-

Metwaly, N. M.; El-Bindary, A. A.; El-Bindary, M. A. Synthesis, Characterization, DFT Calculation, DNA Binding and Antimicrobial Activities of Metal Complexes of Dimedone Arylhydrazone. *J. Mol. Liq.*, **2021**, *334*, 1–10.

[28] Abumelha, H. M.; Alkhatib, F.; Alzahrani, S.; Abualnaja, M.; Alsaigh, S.; Alfaifi, M. Y.; Althagafi, I.; El-Metwaly, N. Synthesis and Characterization for Pharmaceutical Models from Co(II), Ni(II) and Cu(II)-Thiophene Complexes; Apoptosis, Various Theoretical Studies and Pharmacophore Modeling. *J. Mol. Liq.*, **2021**, *328*, 1–12.

[29] Atasever Arslan, B.; Kaya, B.; Şahin, O.; Baday, S.; Saylan, C. C.; Ülküseven, B. The Iron(III) and Nickel(II) Complexes with Tetradentate Thiosemicarbazones. Synthesis, Experimental, Theoretical Characterization, and Antiviral Effect against SARS-CoV-2. *J. Mol. Struct.*, **2021**, *1246*, 1–7. https://doi.org/10.1016/j.molstruc.2021.131166.

[30] Aly, A. A.; Ramadan, M.; Abuo-Rahma, G. E. D. A.; Elshaier, Y. A. M. M.; Elbastawesy, M. A. I.; Brown, A. B.; Bräse, S. Quinolones as Prospective Drugs: Their Syntheses and Biological Applications. *Adv. Heterocycl. Chem.*, **2020**, 1–50.

[31] Chen, Z. F.; Qin, Q. P.; Qin, J. L.; Zhou, J.; Li, Y. L.; Li, N.; Liu, Y. C.; Liang, H. Water-Soluble Ruthenium(II) Complexes with Chiral 4-(2,3-Dihydroxypropyl)-Formamide Oxoaporphine (FOA): In Vitro and in Vivo Anticancer Activity by Stabilization of G-Quadruplex DNA, Inhibition of Telomerase Activity, and Induction of Tumor Cell Apoptosis. *J. Med. Chem.*, **2015**, *58* (11), 4771–4789.

[32] Murugavel, S.; Jacob Prasanna Stephen, C. S.; Subashini, R.; AnanthaKrishnan, D. Synthesis, Structural Elucidation, Antioxidant, CT-DNA Binding and Molecular Docking Studies of Novel Chloroquinoline Derivatives: Promising Antioxidant and Anti-Diabetic Agents. *J. Photochem. Photobiol. B Biol.*, **2017**, *173* (March), 216–230.

[33] Cretton, S.; Breant, L.; Pourrez, L.; Ambuehl, C.; Marcourt, L.; Ebrahimi, S. N.; Hamburger, M.; Perozzo, R.; Karimou, S.; Kaiser, M.; et al. Antitrypanosomal Quinoline Alkaloids from the Roots of Waltheria Indica. *J. Nat. Prod.*, **2014**, *77* (10), 2304–2311. https://doi.org/10.1021/np5006554.

[34] Zeleke, D.; Eswaramoorthy, R.; Belay, Z.; Melaku, Y. Synthesis and Antibacterial, Antioxidant, and Molecular Docking Analysis of Some Novel Quinoline Derivatives. *J. Chem.*, **2020**, *2020*, 1–16. https://doi.org/10.1155/2020/1324096.

[35] Nainwal, L. M.; Tasneem, S.; Akhtar, W.; Verma, G.; Khan, M. F.; Parvez, S.; Shaquiquzzaman, M.; Akhter, M.; Alam, M. M. Green Recipes to Quinoline: A Review. *Eur. J. Med. Chem.*, **2019**, *164*, 121–170.

[36] Boyd, D. R.; Sharma, N. D.; Loke, P. L.; Malone, J. F.; McRoberts, W. C.; Hamilton,

J. T. G. Synthesis, Structure and Stereochemistry of Quinoline Alkaloids from Choisya Ternata. *Org. Biomol. Chem.*, **2007**, *5* (18), 2983–2991.

[37] Sun, N.; Du, R. L.; Zheng, Y. Y.; Huang, B. H.; Guo, Q.; Zhang, R. F.; Wong, K. Y.; Lu, Y. J. Antibacterial Activity of N-Methylbenzofuro[3,2-b]Quinoline and N-Methylbenzoindolo[3,2-b]-Quinoline Derivatives and Study of Their Mode of Action. *Eur. J. Med. Chem.*, **2017**, *135*, 1–11. https://doi.org/10.1016/j.ejmech.2017.04.018.

[38] Zablotskaya, A.; Segal, I.; Geronikaki, A.; Shestakova, I.; Nikolajeva, V.; Makarenkova, G. N-Heterocyclic Choline Analogues Based on 1,2,3,4-Tetrahydro(Iso)Quinoline Scaffold with Anticancer and Anti-Infective Dual Action. *Pharmacol. Reports*, **2017**, *69* (3), 575–581.

[39] Fouda, A. M. Halogenated 2-Amino-4H-Pyrano[3,2-h]Quinoline-3-Carbonitriles as Antitumor Agents and Structure–Activity Relationships of the 4-, 6-, and 9-Positions. *Med. Chem. Res.*, **2017**, *26* (2), 302–313. https://doi.org/10.1007/s00044-016-1747-z.

[40] García, E.; Coa, J. C.; Otero, E.; Carda, M.; Vélez, I. D.; Robledo, S. M.; Cardona, W. I. Synthesis and Antiprotozoal Activity of Furanchalcone–Quinoline, Furanchalcone–Chromone and Furanchalcone–Imidazole Hybrids. *Med. Chem. Res.*, **2018**, *27* (2), 497–511. https://doi.org/10.1007/s00044-017-2076-6.

[41] Senthil Raja, D.; Bhuvanesh, N. S. P.; Natarajan, K. Synthesis, Crystal Structure and Pharmacological Evaluation of Two New Cu(II) Complexes of 2-Oxo-1,2-Dihydroquinoline-3-Carbaldehyde (Benzoyl) Hydrazone: A Comparative Investigation. *Eur. J. Med. Chem.*, **2012**, *47* (1), 73–85.

[42] Bukhari, S. B.; Memon, S.; Tahir, M. M.; Bhanger, M. I. Synthesis , Characterization and Investigation of Antioxidant Activity of Cobalt – Quercetin Complex. *J. Mol. Struct.*, **2008**, *892* (1–3), 39–46. https://doi.org/10.1016/j.molstruc.2008.04.050.

[43] Zou, B. Q.; Lu, X.; Qin, Q. P.; Bai, Y. X.; Zhang, Y.; Wang, M.; Liu, Y. C.; Chen, Z. F.; Liang, H. Three Novel Transition Metal Complexes of 6-Methyl-2-Oxo-Quinoline-3-Carbaldehyde Thiosemicarbazone: Synthesis, Crystal Structure, Cytotoxicity, and Mechanism of Action. *RSC Adv.*, **2017**, *7* (29), 17923–17933.

[44] Vardatsikos, G.; Pandey, N. R.; Srivastava, A. K. Insulino-Mimetic and Anti-Diabetic Effects of Zinc. *J. Inorg. Biochem.*, **2013**, *120*, 8–17. https://doi.org/10.1016/j.jinorgbio.2012.11.006.

[45] Yoshikawa, Y.; Yasui, H. Zinc Complexes Developed as Metallopharmaceutics for Treating Diabetes Mellitus Based on the Bio-Medicinal Inorganic Chemistry. *Curr. Top. Med. Chem.*, **2012**, *12* (3), 210–218.

[46] Coulston, L.; Dandona, P. Insulin-like Effect of Zinc on Adipocytes. *Diabetes*, **1980**, *29* (8), 665–667. https://doi.org/10.2337/diab.29.8.665.

[47] Patel, R. N.; Pratap, Y.; Singh, Y. New Oxidovanadium(V) Complexes with NNO Donor Schiff Bases: Synthesis, Crystal Structures and Electrochemical Studies. *Polyhedron*, **2017**, *133*, 102–109. https://doi.org/10.1016/j.poly.2017.05.028.

[48] Amiri Rudbari, H.; Iravani, M. R.; Moazam, V.; Askari, B.; Khorshidifard, M.; Habibi, N.; Bruno, G. Synthesis, Characterization, X-Ray Crystal Structures and Antibacterial Activities of Schiff Base Ligands Derived from Allylamine and Their Vanadium(IV), Cobalt(III), Nickel(II), Copper(II), Zinc(II) and Palladium(II) Complexes. *J. Mol. Struct.*, **2016**, *1125* (2016), 113–120. https://doi.org/10.1016/j.molstruc.2016.06.055.

[49] Halevas, E.; Mavroidi, B.; Pelecanou, M.; Hatzidimitriou, A. G. Structurally Characterized Zinc Complexes of Flavonoids Chrysin and Quercetin with Antioxidant Potential. *Inorg. Chim. Acta*, **2021**, *523* (March), 1–11.

[50] Azam, M.; Al-Resayes, S. I.; Trzesowska-Kruszynska, A.; Kruszynski, R.; Shakeel, F.; Soliman, S. M.; Alam, M.; Khan, M. R.; Wabaidur, S. M. Zn(II) Complex Derived from Bidentate Schiff Base Ligand: Synthesis, Characterization, DFT Studies and Evaluation of Anti-Inflammatory Activity. *J. Mol. Struct.*, **2020**, *1201*, 1–8.

[51] Tarushi, A.; Totta, X.; Papadopoulos, A.; Kljun, J.; Turel, I.; Kessissoglou, D. P.; Psomas, G. Antioxidant Activity and Interaction with DNA and Albumins of Zinc-Tolfenamato Complexes. Crystal Structure of [Zn(Tolfenamato) 2(2,2′-Dipyridylketoneoxime)2]. *Eur. J. Med. Chem.*, **2014**, *74*, 187–198.

[52] Tarushi, A.; Raptopoulou, C. P.; Psycharis, V.; Terzis, A.; Psomas, G.; Kessissoglou, D. P. Zinc(II) Complexes of the Second-Generation Quinolone Antibacterial Drug Enrofloxacin: Structure and DNA or Albumin Interaction. *Bioorganic Med. Chem.*, **2010**, *18* (7), 2678–2685. https://doi.org/10.1016/j.bmc.2010.02.021.

[53] Ruan, B. F.; Zhu, Y. Z.; Liu, W. D.; Song, B. A.; Tian, Y. P. Synthesis, Characterization, Cytotoxicity and Antibacterial Activity of an Anthracenyl-Linked Bis(Pyrazolyl)Methane Ligand and Its Zinc(II) Complexes. *Eur. J. Med. Chem.*, **2014**, *72*, 46–51. https://doi.org/10.1016/j.ejmech.2013.10.064.

[54] Aslkhademi, S.; Noshiranzadeh, N.; Sadjadi, M. S.; Mehrani, K.; Farhadyar, N. Synthesis, Crystal Structure and Investigation of the Catalytic and Spectroscopic Properties of a Zn(II) Complex with Coumarin-Hydrazone Ligand. *Polyhedron*, **2019**, *160*, 115–122. https://doi.org/10.1016/j.poly.2018.12.023.

[55] Azam, M.; Al-Resayes, S. I.; Trzesowska-Kruszynska, A.; Kruszynski, R.; Shakeel, F.;

Soliman, S. M.; Alam, M.; Khan, M. R.; Wabaidur, S. M. Zn(II) Complex Derived from Bidentate Schiff Base Ligand: Synthesis, Characterization, DFT Studies and Evaluation of Anti-Inflammatory Activity. *J. Mol. Struct.*, **2020**, *1201* (2020), 1–8.

[56] Sadeek, S. A.; El-Attar, M. S.; Abd El-Hamid, S. M. Preparation and Characterization of New Tetradentate Schiff Base Metal Complexes and Biological Activity Evaluation. *J. Mol. Struct.*, **2013**, *1051* (3), 30–40. https://doi.org/10.1016/j.molstruc.2013.07.053.

[57] Kuchárová, V.; Kuchár, J.; Lüköová, A.; Jendželovský, R.; Majerník, M.; Fedoročko, P.; Vilková, M.; Radojević, I. D.; Čomić, L. R.; Potočňák, I. Low-Dimensional Compounds Containing Bioactive Ligands. Part XII: Synthesis, Structures, Spectra, in Vitro Antimicrobial and Cytotoxic Activities of Zinc(II) Complexes with Halogen Derivatives of Quinolin-8-Ol. *Polyhedron*, **2019**, *170*, 447–457.

[58] Patel, R. N.; Singh, Y. P. Synthesis , Structural Characterization , DFT Studies and in-Vitro Antidiabetic Activity of New Mixed Ligand Oxovanadium (IV) Complex with Tridentate Schiff Base. *J. Mol. Struct.*, **2018**, *1153*, 162–169.

[59] Sanna, D.; Palomba, J.; Lubinu, G. Role of Ligands in the Uptake and Reduction of V(V) Complexes in Red Blood Cells. *J. Med. Chem.*, **2019**, *62*, 654−664. https://doi.org/10.1021/acs.jmedchem.8b01330.

[60] Yamaguchi, T.; Watanabe, S.; Matsumura, Y.; Tokuoka, Y.; Yokoyama, A. Oxovanadium Complexes with Quinoline and Pyridinone Ligands: Syntheses of the Complexes and Effect of Alkyl Chains on Their Apoptosis-Inducing Activity in Leukemia Cells. *Bioorganic Med. Chem.*, **2012**, *20* (9), 3058–3064.

[61] Mir, J. M.; Rajak, D. K.; Maurya, R. C. Oxovanadium (IV) Complex of 8-Hydroxy Quinoline and Theoretical and Antibacterial Evaluation. *J. King Saud Univ. - Sci.*, **2018**, *31*, 1034–1041.

[62] Patel, N.; Prajapati, A. K. Model Investigations for Vanadium-Protein Interactions: Synthesis, Characterization and Antidiabetic Properties. *Inorganica Chim. Acta*, **2019**, *493* (April), 20–28. https://doi.org/10.1016/j.ica.2019.04.050.

[63] Sheikhshoaie, I.; Ebrahimipour, S. Y.; Lotfi, N.; Mague, J. T.; Khaleghi, M. Synthesis, Spectral Characterization, X-Ray Crystal Structure and Antimicrobial Activities of Two Cis Dioxido-Vanadium(V) Complexes Incorporating Unsymmetrical Dimalonitrile-Based (NNO) Schiff Base Ligands. *Inorganica Chim. Acta*, **2016**, *442*, 151–157. https://doi.org/10.1016/j.ica.2015.11.026.

[64] Sehimi, H.; Essghaier, B.; Barea, E.; Sadfi-Zouaoui, N.; Zid, M. F. Synthesis, Structural Study, Magnetic Susceptibility and Antimicrobial Activity of the First (μ-

Oxo)-Bis(Oxalato)-Vanadium(IV) 1D Coordination Polymer. *J. Mol. Struct.*, **2019**, *1175*, 865–873. https://doi.org/10.1016/j.molstruc.2018.08.053.

[65] Senthil Raja, D.; Ramachandran, E.; Bhuvanesh, N. S. P.; Natarajan, K. Synthesis, Structure and in Vitro Pharmacological Evaluation of a Novel 2-Oxo-1,2-Dihydroquinoline-3-Carbaldehyde (2′-Methylbenzoyl) Hydrazone Bridged Copper(II) Coordination Polymer. *Eur. J. Med. Chem.*, **2013**, *64*, 148–159.

[66] Joseph, J.; Nagashri, K.; Rani, G. A. B. Synthesis, Characterization and Antimicrobial Activities of Copper Complexes Derived from 4-Aminoantipyrine Derivatives. *J. Saudi Chem. Soc.*, **2013**, *17* (3), 285–294. https://doi.org/10.1016/j.jscs.2011.04.007.

[67] Kordestani, N.; Amiri Rudbari, H.; Fernandes, A. R.; Raposo, L. R.; Luz, A.; Baptista, P. V.; Bruno, G.; Scopelliti, R.; Fateminia, Z.; Micale, N.; et al. Copper(Ii) Complexes with Tridentate Halogen-Substituted Schiff Base Ligands: Synthesis, Crystal Structures and Investigating the Effect of Halogenation, Leaving Groups and Ligand Flexibility on Antiproliferative Activities. *Dalt. Trans.*, **2021**, *50* (11), 3990–4007.

[68] Singh, V. P.; Gupta, P. Synthesis, Physico-Chemical Characterization and Antimicrobial Activity of Cobalt(II), Nickel(II), Copper(II), Zinc(II) and Cadmium(II) Complexes with Some Acyldihydrazones. *J. Enzyme Inhib. Med. Chem.*, **2008**, *23* (6), 797–805. https://doi.org/10.1080/14756360701733136.

[69] Li, Y.; Li, Y.; Liu, X.; Yang, Y.; Lin, D.; Gao, Q. The Synthesis, Characterization, DNA/Protein Interaction, Molecular Docking and Catecholase Activity of Two Co(II) Complexes Constructed from the Aroylhydrazone Ligand. *J. Mol. Struct.*, **2020**, *1202*, 1–15. https://doi.org/10.1016/j.molstruc.2019.127229.

[70] Guo, J.; Liu, H.; Bi, J.; Zhang, C.; Zhang, H.; Bai, C.; Hu, Y.; Zhang, X. Pyridine-Oxazoline and Quinoline-Oxazoline Ligated Cobalt Complexes: Synthesis, Characterization, and 1,3-Butadiene Polymerization Behaviors. *Inorganica Chim. Acta*, **2015**, *435*, 305–312. https://doi.org/10.1016/j.ica.2015.07.013.

[71] Bombicz, P.; Forizs, E.; Madarász, J.; Deák, A.; Kálmán, A. Inclusion Compounds Containing a Drug: Structure and Thermal Stability of the First Clathrates of Nitrazepam and Isothiocyanato Ethanol Complexes of Co(II) and Ni(II). *Inorganica Chim. Acta*, **2001**, *315* (2), 229–235. https://doi.org/10.1016/S0020-1693(01)00375-9.

[72] Betanzos-Lara, S.; Gómez-Ruiz, C.; Barrón-Sosa, L. R.; Gracia-Mora, I.; Flores-Álamo, M.; Barba-Behrens, N. Cytotoxic Copper(II), Cobalt(II), Zinc(II), and Nickel(II) Coordination Compounds of Clotrimazole. *J. Inorg. Biochem.*, **2012**, *114*, 82–93. https://doi.org/10.1016/j.jinorgbio.2012.05.001.

[73] Skyrianou, K. C.; Efthimiadou, E. K.; Psycharis, V.; Terzis, A.; Kessissoglou, D. P.; Psomas, G. Nickel-Quinolones Interaction. Part 1 - Nickel(II) Complexes with the Antibacterial Drug Sparfloxacin: Structure and Biological Properties. *J. Inorg. Biochem.*, **2009**, *103* (12), 1617–1625. https://doi.org/10.1016/j.jinorgbio.2009.08.011.

[74] Alomar, K.; Landreau, A.; Allain, M.; Bouet, G.; Larcher, G. Synthesis, Structure and Antifungal Activity of Thiophene-2,3- Dicarboxaldehyde Bis(Thiosemicarbazone) and Nickel(II), Copper(II) and Cadmium(II) Complexes: Unsymmetrical Coordination Mode of Nickel Complex. *J. Inorg. Biochem.*, **2013**, *126*, 76–83.

[75] Ramírez-Macías, I.; Maldonado, C. R.; Marín, C.; Olmo, F.; Gutiérrez-Sánchez, R.; Rosales, M. J.; Quirós, M.; Salas, J. M.; Sánchez-Moreno, M. In Vitro Anti-Leishmania Evaluation of Nickel Complexes with a Triazolopyrimidine Derivative against Leishmania Infantum and Leishmania Braziliensis. *J. Inorg. Biochem.*, **2012**, *112*, 1–9. https://doi.org/10.1016/j.jinorgbio.2012.02.025.

[76] Perontsis, S.; Tialiou, A.; Hatzidimitriou, A. G.; Papadopoulos, A. N.; Psomas, G. Nickel(II)-Indomethacin Mixed-Ligand Complexes: Synthesis, Characterization, Antioxidant Activity and Interaction with DNA and Albumins. *Polyhedron*, **2017**, *138*, 258–269. https://doi.org/10.1016/j.poly.2017.09.008.

[77] Sathyadevi, P.; Krishnamoorthy, P.; Jayanthi, E.; Butorac, R. R.; Cowley, A. H.; Dharmaraj, N. Studies on the Effect of Metal Ions of Hydrazone Complexes on Interaction with Nucleic Acids, Bovine Serum Albumin and Antioxidant Properties. *Inorganica Chim. Acta*, **2012**, *384*, 83–96. https://doi.org/10.1016/j.ica.2011.11.033.

[78] Belkhir-Talbi, D.; Makhloufi-Chebli, M.; Terrachet-Bouaziz, S.; Hikem-Oukacha, D.; Ghemmit, N.; Ismaili, L.; M.S Silva, A.; Hamdi, M. Synthesis, Characterization, Theoretical Studies, ADMET and Drug-Likeness Analysis: Electrochemical and Biological Activities of Metal Complexes of 3-(2-Hydroxybenzoyl)-2H-Chromen-2-One. *J. Mol. Struct.*, **2019**, *1179*, 495–505.

[79] Belkhir-Talbi, D.; Ghemmit-Doulache, N.; Terrachet-Bouaziz, S.; Makhloufi-Chebli, M.; Rabahi, A.; Ismaili, L.; Silva, A. M. S. Transition-Metal Complexes of N,N′-Di(4-Bromophenyl)-4-Hydroxycoumarin-3-Carboximidamide: Synthesis, Characterization, Biological Activities, ADMET and Drug-Likeness Analysis. *Inorg. Chem. Commun.*, **2021**, *127* (March), 1–12. https://doi.org/10.1016/j.inoche.2021.108509.

[80] Vivekanand, B.; Mahendra Raj, K.; Mruthyunjayaswamy, B. H. M. Synthesis, Characterization, Antimicrobial, DNA-Cleavage and Antioxidant Activities of 3-((5-Chloro-2-Phenyl-1H-Indol-3-Ylimino)Methyl)Quinoline-2(1H)-Thione and Its Metal

Complexes. *J. Mol. Struct.*, **2015**, *1079*, 214–224.

[81] Ismael, M.; Abdel-Mawgoud, A. M. M.; Rabia, M. K.; Abdou, A. Design and Synthesis of Three Fe(III) Mixed-Ligand Complexes: Exploration of Their Biological and Phenoxazinone Synthase-like Activities. *Inorg. Chim. Acta*, **2020**, *505* (December 2019), 1–11. https://doi.org/10.1016/j.ica.2020.119443.

[82] El-Sonbati, A. Z.; Diab, M. A.; Abbas, S. Y.; Mohamed, G. G.; Morgan, S. M. Preparation, Characterization and Biological Activity Screening on Some Metal Complexes Based of Schiff Base Ligand. *Egypt. J. Chem.*, **2021**, *64* (8), 4125–4136.

[83] Vicente, D.; Basterretxea, M.; de la Caba, I.; Sancho, R.; López-Olaizola, M.; Cilla, G. Low Antimicrobial Resistance Rates of Mycobacterium Tuberculosis Complex between 2000 and 2015 in Gipuzkoa, Northern Spain. *Enferm. Infecc. Microbiol. Clin.*, **2019**, *37* (9), 574–579. https://doi.org/10.1016/j.eimc.2019.01.016.

[84] Alanis, A. J. Resistance to Antibiotics: Are We in the Post-Antibiotic Era? *Arch. Med. Res.*, **2005**, *36* (6), 697–705. https://doi.org/10.1016/j.arcmed.2005.06.009.

[85] Ng, N. S.; Leverett, P.; Hibbs, D. E.; Yang, Q.; Bulanadi, J. C.; Jie Wu, M.; Aldrich-Wright, J. R. The Antimicrobial Properties of Some Copper(Ii) and Platinum(Ii) 1,10-Phenanthroline Complexes. *Dalt. Trans.*, **2013**, *42* (9), 3196–3209.

[86] Łoboda, D.; Rowińska-Zyrek, M. Candida Albicans Zincophore and Zinc Transporter Interactions with Zn(II) and Ni(II). *Dalt. Trans.*, **2018**, *47* (8), 2646–2654.

[87] Anacona, J. R.; Noriega, N.; Camus, J. Synthesis, Characterization and Antibacterial Activity of a Tridentate Schiff Base Derived from Cephalothin and Sulfadiazine, and Its Transition Metal Complexes. *Spectrochim. Acta - Part A Mol. Biomol. Spectrosc.*, **2015**, *137*, 16–22. https://doi.org/10.1016/j.saa.2014.07.091.

[88] Creaven, B. S.; Czeglédi, E.; Devereux, M.; Enyedy, É. A.; Foltyn-Arfa Kia, A.; Karcz, D.; Kellett, A.; McClean, S.; Nagy, N. V.; Noble, A.; et al. Biological Activity and Coordination Modes of Copper(II) Complexes of Schiff Base-Derived Coumarin Ligands. *Dalt. Trans.*, **2010**, *39* (45), 10854–10865.

[89] Manjunatha, M.; Naik, V. H.; Kulkarni, A. D. Activities , and Spectroscopic Studies of Co (II), Ni (II), and Cu (II) Complexes of Biologically Potential Coumarin Schiff Bases. *J. Coord. Chem.*, **2011**, *64* (24), 4264–4275.

[90] Gulcan, M.; Özdemir, S.; Dündar, A.; Ispir, E.; Kurtoğlu, M. Mononuclear Complexes Based on Pyrimidine Ring Azo Schiff-Base Ligand: Synthesis, Characterization, Antioxidant, Antibacterial, and Thermal Investigations. *Zeitschrift fur Anorg. und Allg. Chemie*, **2014**, *640* (8–9), 1754–1762. https://doi.org/10.1002/zaac.201400078.

[91] Yang, Y.; Weaver, M. N.; Merz, K. M. Assessment of the "6-31+Gt; + LANL2DZ" Mixed Basis Set Coupled with Density Functional Theory Methods and the Effective Core Potential: Prediction of Heats of Formation and Ionization Potentials for First-Row-Transition-Metal Complexes. *J. Phys. Chem. A*, **2009**, *113* (36), 9843–9851.

[92] Johnstone, T. C.; Suntharalingam, K.; Lippard, S. J. The Next Generation of Platinum Drugs: Targeted Pt(II) Agents, Nanoparticle Delivery, and Pt(IV) Prodrugs. *Chem. Rev.*, **2016**, *116* (5), 3436–3486. https://doi.org/10.1021/acs.chemrev.5b00597.

[93] Biot, C.; Nosten, F.; Fraisse, L.; Ter-Minassian, D.; Khalife, J.; Dive, D. The Antimalarial Ferroquine: From Bench to Clinic. *Parasite*, **2011**, *18* (3), 207–214.

[94] Monro, S.; Colón, K. L.; Yin, H.; Roque, J.; Konda, P.; Gujar, S.; Thummel, R. P.; Lilge, L.; Cameron, C. G.; McFarland, S. A. Transition Metal Complexes and Photodynamic Therapy from a Tumor-Centered Approach: Challenges, Opportunities, and Highlights from the Development of TLD1433. *Chem. Rev.*, **2019**, *119* (2), 797–828. https://doi.org/10.1021/acs.chemrev.8b00211.

[95] Zeng, L.; Gupta, P.; Chen, Y.; Wang, E.; Ji, L.; Chao, H.; Chen, Z. S. The Development of Anticancer Ruthenium(II) Complexes: From Single Molecule Compounds to Nanomaterials. *Chem. Soc. Rev.*, **2017**, *46* (19), 5771–5804.

[96] Gasser, G. Metal Complexes and Medicine: A Successful Combination. *Chimia (Aarau).*, **2015**, *69* (7–8), 442–446. https://doi.org/10.2533/chimia.2015.442.

[97] Malik, M. A.; Dar, O. A.; Gull, P.; Wani, M. Y.; Hashmi, A. A. Heterocyclic Schiff Base Transition Metal Complexes in Antimicrobial and Anticancer Chemotherapy. *Medchemcomm*, **2018**, *9* (3), 409–436. https://doi.org/10.1039/c7md00526a.

[98] Lovering, F.; Bikker, J.; Humblet, C. Escape from Flatland: Increasing Saturation as an Approach to Improving Clinical Success. *J. Med. Chem.*, **2009**, *52* (21), 6752–6756.

[99] Lovering, F. Escape from Flatland 2: Complexity and Promiscuity. *Medchemcomm*, **2013**, *4* (3), 515–519. https://doi.org/10.1039/c2md20347b.

[100] Marella, A.; Tanwar, O. P.; Saha, R.; Ali, M. R.; Srivastava, S.; Akhter, M.; Shaquiquzzaman, M. Quinoline : A Versatile Heterocyclic. *Saudi Pharm. J.*, **2013**, *21* (1), 1–12. https://doi.org/10.1016/j.jsps.2012.03.002.

[101] Yadav, P.; Shah, K. Quinolines, a Perpetual, Multipurpose Scaffold in Medicinal Chemistry. *Bioorg. Chem.*, **2021**, *109* (2020), 1–42.

[102] Digafie, Z.; Melaku, Y.; Belay, Z.; Eswaramoorthy, R. Synthesis, Antibacterial, Antioxidant, and Molecular Modeling Studies of Novel [2,3′-Biquinoline]-4-Carboxylic Acid and Quinoline-3-Carbaldehyde Analogs. *J. Chem.*, **2021**, *2021*, 1–17.

[103] Cao, W.; Qi, J.; Qian, K.; Tian, L.; Cheng, Z.; Wang, Y. Structure−activity Relationships of 2-quinolinecarboxaldehyde Thiosemicarbazone Gallium(III) Complexes with Potent and Selective Anticancer Activity. *J. Inorg. Biochem.*, **2019**, *191* (August 2018), 174–182. https://doi.org/10.1016/j.jinorgbio.2018.11.017.

[104] Abdel-Wahab, B. F.; Mohamed, H. A. Recent Progress in the Synthesis of Pyrimidothiazines. *Phosphorus, Sulfur Silicon Relat. Elem.*, **2017**, *192* (7), 787–793.

[105] Amer, A. M.; El-Eraky, W. I.; Mahgoub, S. Synthesis, Characterization and Antimicrobial Activity of Some Novel Quinoline Derivatives Bearing Pyrazole and Pyridine Moieties. *Egypt. J. Chem.*, **2018**, *61*, 1–8.

[106] Akkachairin, B.; Rodphon, W.; Reamtong, O.; Mungthin, M. Synthesis of Neocryptolepines and Carbocycle-Fused Quinolines and Evaluation of Their Anticancer and Antiplasmodial Activities. *Bioorganic Chem. J.*, **2020**, *98* (2020), 1–6.

[107] Kaur, K.; Jain, M.; Reddy, R. P.; Jain, R. Quinolines and Structurally Related Heterocycles as Antimalarials. *Eur. J. Med. Chem.*, **2010**, *45* (8), 3245–3264.

[108] Afzal, O.; Kumar, S.; Haider, M. R.; Ali, M. R.; Kumar, R.; Jaggi, M.; Bawa, S. A Review on Anticancer Potential of Bioactive Heterocycle Quinoline. *Eur. J. Med. Chem.*, **2015**, *97* (1), 871–910. https://doi.org/10.1016/j.ejmech.2014.07.044.

[109] Lamhasni, T.; Barbache, S.; Lyazidi, S. A.; Haddad, M.; Hnach, M.; Desmaële, D. Photo-Physics Study of a Styrylquinoline as Inhibitor of Pim-1 Kinase : *Chem. Phys. Lett.*, **2018**, *695* (2018), 59–62. https://doi.org/10.1016/j.cplett.2018.02.004.

[110] Su, W.; Weng, Y.; Jiang, L.; Yang, Y.; Zhao, L.; Chen, Z.; Li, Z.; Li, J. Recent Progress in the Use of Vilsmeier-Type Reagents. *Org. Prep. Proced. Int.*, **2010**, *42* (6), 503–555. https://doi.org/10.1080/00304948.2010.513911.

[111] Kimura, Y.; Matsuura, D. Novel Synthetic Method for the Vilsmeier-Haack Reagent and Green Routes to Acid Chlorides, Alkyl Formates, and Alkyl Chlorides. *Int. J. Org. Chem.*, **2013**, *03* (03), 1–7. https://doi.org/10.4236/ijoc.2013.33a001.

[112] Kimura, Y.; Warashina, T. Convenient Preparation of Dichloromethyl Alkyl Ethers. *Tetrahedron Lett.*, **2017**, *58* (49), 4598–4599.

[113] Kimura, Y.; Matsuura, D.; Hanawa, T.; Kobayashi, Y. New Preparation Method for Vilsmeier Reagent and Related Imidoyl Chlorides. *Tetrahedron Lett.*, **2012**, *53* (9), 1116–1118. https://doi.org/10.1016/j.tetlet.2011.12.087.

[114] Meth-Cohn, O.; Narine, B.; Tarnowski, B. A Versatile New Synthesis of Quinolines and Related Fused Pyridines. Part 5. The Synthesis of 2-Chloroquinoline-3-Carbaldehydes. *J. Chem. Soc. Perkin Trans. 1*, **1981**, 1520–1530.

[115] Farghaly, A. M.; Habib, N. S.; Khalil, M. A.; El-Sayed, O. A.; Bistawroos, A. E. Synthesis of Novel 2-Substituted Quinoline Derivatives: Antimicrobial, Inotropic, and Chronotropic Activities. *Arch. Pharm. (Weinheim).*, **1990**, *323* (4), 247–251.

[116] Herencia, F.; Ferrándiz, M. L.; Ubeda, A.; Domínguez, J.; Charris, J. E.; Lobo, G. M.; Alcaraz, M. J. Synthesis and Anti-Inflammatory Activity of Chalcone Derivatives. *Bioorg. Med. Chem. Lett.*, **1998**, *8* (10), 1169–1174. https://doi.org/10.1016/S0960-894X(98)00179-6.

[117] Sekar, M.; Prasad, K. J. R. Synthesis of Some Novel 2-Oxo-pyrano(2,3-b)- and 2-Oxo-pyrido(2,3-b)Quinoline Derivatives as Potential Antimalarial, Diuretic, Clastogenic and Antimicrobial Agents. *J. Chem. Technol. Biotechnol.*, **1998**, *72* (1), 50–54.

[118] Abdel-Wahab, B. F.; Khidre, R. E. 2-Chloroquinoline-3-Carbaldehyde Ii: Synthesis, Reactions, and Applications. *J. Chem.*, **2013**, *2013* (Scheme 1), 1–13.

[119] Hamama, W. S.; Ibrahim, M. E.; Gooda, A. A.; Zoorob, H. H. Recent Advances in the Chemistry of 2-Chloroquinoline-3-Carbaldehyde and Related Analogs. *RSC Adv.*, **2018**, *8* (16), 8484–8515. https://doi.org/10.1039/c7ra11537g.

[120] Mandewale, M. C.; Thorat, B.; Nivid, Y.; Jadhav, R.; Nagarsekar, A.; Yamgar, R. Synthesis, Structural Studies and Antituberculosis Evaluation of New Hydrazone Derivatives of Quinoline and Their Zn(II) Complexes. *J. Saudi Chem. Soc.*, **2018**, *22* (2), 218–228. https://doi.org/10.1016/j.jscs.2016.04.003.

[121] Ren, Y.; Ruan, Y.; Cheng, B.; Li, L.; Liu, J.; Fang, Y.; Chen, J. Design, Synthesis and Biological Evaluation of Novel Acridine and Quinoline Derivatives as Tubulin Polymerization Inhibitors with Anticancer Activities. *Bioorganic Med. Chem.*, **2021**, *46* (August), 1–13. https://doi.org/10.1016/j.bmc.2021.116376.

[122] Wang, M.; Zhang, G.; Zhao, J.; Cheng, N.; Wang, Y.; Fu, Y.; Zheng, Y.; Wang, J.; Zhu, M.; Cen, S.; et al. Synthesis and Antiviral Activity of a Series of Novel Quinoline Derivatives as Anti-RSV or Anti-IAV Agents. *Eur. J. Med. Chem.*, **2021**, *214*, 1–13.

123] Mandewale, M. C.; Kokate, S.; Thorat, B.; Sawant, S.; Yamgar, R. Zinc Complexes of Hydrazone Derivatives Bearing 3,4-Dihydroquinolin-2(1H)-One Nucleus as New Anti-Tubercular Agents. *Arab. J. Chem.*, **2019**, *12* (8), 4479–4489.

[124] Mandewale, M. C.; Patil, U. C.; Shedge, S. V.; Dappadwad, U. R.; Yamgar, R. S. A Review on Quinoline Hydrazone Derivatives as a New Class of Potent Antitubercular and Anticancer Agents. *Beni-Suef Univ. J. Basic Appl. Sci.*, **2017**, *6* (4), 354–361.

[125] Oliveri, V.; Lanza, V.; Milardi, D.; Viale, M.; Maric, I.; Sgarlata, C.; Vecchio, G. Amino- and Chloro-8-Hydroxyquinolines and Their Copper Complexes as Proteasome

Inhibitors and Antiproliferative Agents. *Metallomics*, **2017**, *9* (10), 1439–1446..

[126] Tardito, S.; Barilli, A.; Bassanetti, I.; Tegoni, M.; Bussolati, O.; Franchi-Gazzola, R.; Mucchino, C.; Marchiò, L. Copper-Dependent Cytotoxicity of 8-Hydroxyquinoline Derivatives Correlates with Their Hydrophobicity and Does Not Require Caspase Activation. *J. Med. Chem.*, **2012**, *55* (23), 10448–10459.

[127] Mirzaahmadi, A.; Hosseini-Yazdi, S. A.; Safarzadeh, E.; Baradaran, B.; Samolova, E.; Dusek, M. New Series of Water-Soluble Thiosemicarbazones and Their Copper(II) Complexes as Potentially Promising Anticancer Compounds. *J. Mol. Liq.*, **2019**, *293* (2019), 1–11. https://doi.org/10.1016/j.molliq.2019.111412.

[128] Kenny, R. G.; Marmion, C. J. Toward Multi-Targeted Platinum and Ruthenium Drugs - A New Paradigm in Cancer Drug Treatment Regimens? *Chem. Rev.*, **2019**, *119* (2), 1058–1137. https://doi.org/10.1021/acs.chemrev.8b00271.

[129] Mansour, A. M. Pd(Ii) and Pt(Ii) Complexes of Tridentate Ligands with Selective Toxicity against Cryptococcus Neoformans and Candida Albicans . *RSC Adv.*, **2021**, *11* (63), 39748–39757. https://doi.org/10.1039/d1ra06559a.

[130] Frei, A.; Ramu, S.; Lowe, G. J.; Dinh, H.; Semenec, L.; Elliott, A. G.; Zuegg, J.; Deckers, A.; Jung, N.; Bräse, S.; et al. Platinum Cyclooctadiene Complexes with Activity against Gram-Positive Bacteria. *ChemMedChem*, **2021**, *16* (20), 3165–3171.

[131] Andrejević, T. P.; Warżajtis, B.; Glišić, B.; Vojnovic, S.; Mojicevic, M.; Stevanović, N. L.; Nikodinovic-Runic, J.; Rychlewska, U.; Djuran, M. I. Zinc(II) Complexes with Aromatic Nitrogen-Containing Heterocycles as Antifungal Agents: Synergistic Activity with Clinically Used Drug Nystatin. *J. Inorg. Biochem.*, **2020**, *208* (2020), 1–11. https://doi.org/10.1016/j.jinorgbio.2020.111089.

[132] Beyramabadi, S. A.; Saadat-Far, M.; Faraji-Shovey, A.; Javan-Khoshkholgh, M.; Morsali, A. Synthesis, Experimental and Computational Characterizations of a New Quinoline Derived Schiff Base and Its Mn(II), Ni(II) and Cu(II) Complexes. *J. Mol. Struct.*, **2020**, *1208*, 1–10. https://doi.org/10.1016/j.molstruc.2020.127898.

[133] Lawrance, G. A. *Introduction to Coordination Chemistry*; 2009.

[134] Abu-Dief, A. M.; Mohamed, I. M. A. A Review on Versatile Applications of Transition Metal Complexes Incorporating Schiff Bases. *Beni-Suef Univ. J. Basic Appl. Sci.*, **2015**, *4* (2), 119–133. https://doi.org/10.1016/j.bjbas.2015.05.004.

[135] Vijayan, P.; Viswanathamurthi, P.; Velmurugan, K.; Nandhakumar, R.; Balakumaran, M. D.; Kalaichelvan, P. T.; Malecki, J. G. Nickel(Ii) and Copper(Ii) Complexes Constructed with N2S2 Hybrid Benzamidine-Thiosemicarbazone Ligand: Synthesis,

X-Ray Crystal Structure, DFT, Kinetico-Catalytic and in Vitro Biological Applications. *RSC Adv.*, **2015**, *5* (125), 103321–103342.

[136] Das, K.; Datta, A.; Liu, P. H.; Huang, J. H.; Hsu, C. L.; Chang, W. T.; MacHura, B.; Sinha, C. Structural Characterization of Cobalt(II) Complexes of an N,O Donor Schiff Base and Their Activity on Carcinoma Cells. *Polyhedron*, **2014**, *71* (3), 85–90.

[137] Yang, J.; Shi, R.; Zhou, P.; Qiu, Q.; Li, H. Asymmetric Schiff Bases Derived from Diaminomaleonitrile and Their Metal Complexes. *J. Mol. Struct.*, **2016**, *1106*, 242–258. https://doi.org/10.1016/j.molstruc.2015.10.092.

[138] Knittl, E. T.; Abou-Hussein, A. A.; Linert, W. Syntheses, Characterization, and Biological Activity of Novel Mono- and Binuclear Transition Metal Complexes with a Hydrazone Schiff Base Derived from a Coumarin Derivative and Oxalyldihydrazine. *Monatshefte fur Chemie*, **2018**, *149* (2), 431–443. https://doi.org/10.1007/s00706-017-2075-9.

[139] Panja, A. Syntheses and Structural Characterizations of Cobalt(II) Complexes with N4-Donor Schiff Base Ligands: Influence of Methyl Substitution on Structural Parameters and on Phenoxazinone Synthase Activity. *Polyhedron*, **2014**, *80*, 81–89.

[140] Erxleben, A. Transition Metal Salen Complexes in Bioinorganic and Medicinal Chemistry. *Inorganica Chim. Acta*, **2018**, *472*, 40–57.

[141] Hasanzadeh, M.; Salehi, M.; Kubicki, M.; Shahcheragh, S. M.; Dutkiewicz, G.; Pyziak, M.; Khaleghian, A. Synthesis, Crystal Structures, Spectroscopic Studies and Antibacterial Properties of a Series of Mononuclear Cobalt(III) Schiff Base Complexes. *Transit. Met. Chem.*, **2014**, *39* (6), 623–632.

[142] Chino, M.; Leone, L.; Zambrano, G.; Pirro, F.; D'Alonzo, D.; Firpo, V.; Aref, D.; Lista, L.; Maglio, O.; Nastri, F.; et al. Oxidation Catalysis by Iron and Manganese Porphyrins within Enzyme-like Cages. *Biopolymers*, **2018**, *109* (10), 1–19.

[143] Valgimigli, L.; Baschieri, A.; Amorati, R. Antioxidant Activity of Nanomaterials. *J. Mater. Chem. B*, **2018**, *6* (14), 2036–2051. https://doi.org/10.1039/c8tb00107c.

[144] Maurya, M. R.; Chaudhary, N.; Avecilla, F.; Correia, I. Mimicking Peroxidase Activity by a Polymer-Supported Oxidovanadium(IV) Schiff Base Complex Derived from Salicylaldehyde and 1,3-Diamino-2-Hydroxypropane. *J. Inorg. Biochem.*, **2015**, *147*, 181–192. https://doi.org/10.1016/j.jinorgbio.2015.01.012.

[145] Panda, M. K.; Shaikh, M. M.; Butcher, R. J.; Ghosh, P. Functional Mimics of Catechol Oxidase by Mononuclear Copper Complexes of Sterically Demanding [NNO] Ligands. *Inorganica Chim. Acta*, **2011**, *372* (1), 145–151.

[146] El-Sonbati, A. Z.; Diab, M. A.; Morgan, S. M.; Abou-Dobara, M. I.; El-Ghettany, A. A. Synthesis, Characterization, Theoretical and Molecular Docking Studies of Mixed-Ligand Complexes of Cu(II), Ni(II), Co(II), Mn(II), Cr(III), UO2(II) and Cd(II). *J. Mol. Struct.*, **2020**, *1200* (2020), 1–17. https://doi.org/10.1016/j.molstruc.2019.127065.

[147] Thompson, K. .; Chiles, J.; Yuen, V. . Comparison of Anti-Hyperglycemic Effect amongst Vanadium, Molybdenum and Other Metal Maltol Complexes. *J. Inorg. Biochem.*, **2004**, *98* (5), 683–690. https://doi.org/10.1016/j.jinorgbio.2004.01.006.

[148] Treviño, S.; Diaz, A. Vanadium and Insulin: Partners in Metabolic Regulation. *J. Inorg. Biochem.*, **2020**, *208* (2020), 1–19.

[149] Wilmot, E.; Idris, I. Early Onset Type 2 Diabetes: Risk Factors, Clinical Impact and Management. *Ther. Adv. Chronic Dis.*, **2014**, *5* (6), 234–244.

[150] Winterbourn, C. C. Reconciling the Chemistry and Biology of Reactive Oxygen Species. *Nat. Chem. Biol.*, **2008**, *4* (5), 278–286. https://doi.org/10.1038/nchembio.85.

[151] Wise, J. Type 1 Diabetes Is Still Linked to Lower Life Expectancy. *BMJ*, **2016**, *353* (2016), 1. https://doi.org/10.1136/bmj.i1988.

[152] Xia T, Wang J, W. C. Novel Complex-Coprecipitation Route to Form High Quality Triethanolamine-Coated Fe3O4 Nanocrystals: Their High Saturation Magnetizations and Excellent Water Treatment Properties. *CrystEngComm*, **2012**, *14(18)*, 5741–5744.

[153] Xie, M. jin; Yang, X. Da; Liu, W. ping; Yan, S. ping; Meng, Z. hui. Insulin-Enhancing Activity of a Dinuclear Vanadium Complex: 5-Chloro-Salicylaldhyde Ethylenediamine Oxovanadium(V) and Its Permeability and Cytotoxicity. *J. Inorg. Biochem.*, **2010**, *104* (8), 851–857. https://doi.org/10.1016/j.jinorgbio.2010.03.018.

[154] Yoshikawa, Y.; Ueda, E.; Miyake, H.; Sakurai, H.; Kojima, Y. Insulinomimetic Bis(Maltolato)Zinc(II) Complex: Blood Glucose Normalizing Effect in KK-Ay Mice with Type 2 Diabetes Mellitus. *Biochem. Biophys. Res. Commun.*, **2001**, *281* (5), 1190–1193. https://doi.org/10.1006/bbrc.2001.4456.

[155] Kharadi, G. J.; Patel, K. D. In-Vitro Antimicrobial, Thermal and Spectral Studies Ofmixed Ligand Cu(II) Heterochelates of Clioquinol and Coumarin Derivatives. *Appl. Organomet. Chem.*, **2010**, *24* (4), 332–337. https://doi.org/10.1002/aoc.1617.

[156] Otaif, H. Y.; Adams, S. J.; Horton, P. N.; Coles, S. J.; Beames, J. M.; Pope, S. J. A. Bis-Cyclometalated Iridium(Iii) Complexes with Terpyridine Analogues: Syntheses, Structures, Spectroscopy and Computational Studies . *RSC Adv.*, **2021**, *11* (63), 39718–39727. https://doi.org/10.1039/d1ra07213g.

[157] Vranec, P.; Potočňák, I.; Sabolová, D.; Farkasová, V.; Ipóthová, Z.; Pisarčíková, J.;

Paulíková, H. Low-Dimensional Compounds Containing Bioactive Ligands. V: Synthesis and Characterization of Novel Anticancer Pd(II) Ionic Compounds with Quinolin-8-Ol Halogen Derivatives. *J. Inorg. Biochem.*, **2014**, *131*, 37–46.

[158] Potočňák, I.; Ali Drweesh, S.; Farkasová, V.; Lüköová, A.; Sabolová, D.; Radojević, I. D.; Arsenijevic, A.; Djordjevic, D.; Volarevic, V. Low-Dimensional Compounds Containing Bioactive Ligands. Part IX: Synthesis, Structures, Spectra, in Vitro Antimicrobial and Anti-Tumor Activities and DNA Binding of Pd(II) Complexes with 7-Bromo-Quinolin-8-Ol. *Polyhedron*, **2017**, *135* (Ii), 195–205.

[159] Farkasová, V.; Drweesh, S. A.; Lüköová, A.; Sabolová, D.; Radojević, I. D.; Čomić, L. R.; Vasić, S. M.; Paulíková, H.; Fečko, S.; Balašková, T.; et al. Low-Dimensional Compounds Containing Bioactive Ligands. Part VIII: DNA Interaction, Antimicrobial and Antitumor Activities of Ionic 5,7-Dihalo-8-Quinolinolato Palladium(II) Complexes with K+ and Cs+ Cations. *J. Inorg. Biochem.*, **2017**, *167* (Ii), 80–88.

[160] Song, Y.; Xu, H.; Chen, W.; Zhan, P.; Liu, X. 8-Hydroxyquinoline: A Privileged Structure with a Broad-Ranging Pharmacological Potential. *Medchemcomm*, **2015**, *6* (1), 61–74. https://doi.org/10.1039/c4md00284a.

[161] Qin, Q. P.; Wang, Z. F.; Huang, X. L.; Tan, M. X.; Zou, B. Q.; Liang, H. Strong in Vitro and Vivo Cytotoxicity of Novel Organoplatinum(II) Complexes with Quinoline-Coumarin Derivatives. *Eur. J. Med. Chem.*, **2019**, *184* (2019), 1–9.

[162] Kuchárová, V.; Kuchár, J.; Zaric, M.; Canovic, P.; Arsenijevic, N.; Volarevic, V.; Misirkic, M.; Trajkovic, V.; Radojević, I. D.; Čomić, L. R.; et al. Low-Dimensional Compounds Containing Bioactive Ligands. Part XI: Synthesis, Structures, Spectra, in Vitro Anti-Tumor and Antimicrobial Activities of 3d Metal Complexes with 8-Hydroxyquinoline-5-Sulfonic Acid. *Inorganica Chim. Acta*, **2019**, *497* (2019), 1–12.

[163] Tremlett, W. D. J.; Tong, K. K. H.; Steel, T. R.; Movassaghi, S.; Hanif, M.; Jamieson, S. M. F.; Söhnel, T.; Hartinger, C. G. Hydroxyquinoline-Derived Anticancer Organometallics: Introduction of Amphiphilic PTA as an Ancillary Ligand Increases Their Aqueous Solubility. *J. Inorg. Biochem.*, **2019**, *199* (2019), 1–7.

[164] Lüköová, A.; Baran, P.; Volarevic, V.; Ilic, A.; Vilková, M.; Litecká, M.; Harmošová, M.; Potočňák, I. Low-Dimensional Compounds Containing Bioactive Ligands. Part XVI: Halogenated Derivatives of 8-Quinolinol N-Oxides and Their Copper(II) Complexes. *J. Mol. Struct.*, **2021**, *1246* (2021), 1–12.

[165] dos Santos Chagas, C.; Fonseca, F. L. A.; Bagatin, I. A. Quinoline-Derivative Coordination Compounds as Potential Applications to Antibacterial and Antineoplasic

Drugs. *Mater. Sci. Eng. C*, **2019**, *98* (2019), 1043–1052.

[166] Ramachandran, E.; Gandin, V.; Bertani, R.; Sgarbossa, P.; Natarajan, K.; Bhuvanesh, N. S. P.; Venzo, A.; Zoleo, A.; Glisenti, A.; Dolmella, A.; et al. Synthesis, Characterization and Cytotoxic Activity of Novel Copper(II) Complexes with Aroylhydrazone Derivatives of 2-Oxo-1,2-Dihydrobenzo[h]Quinoline-3-Carbaldehyde. *J. Inorg. Biochem.*, **2018**, *182* (September 2017), 18–28.

[167] Rogolino, D.; Cavazzoni, A.; Gatti, A.; Tegoni, M.; Pelosi, G.; Verdolino, V.; Fumarola, C.; Cretella, D.; Petronini, P. G.; Carcelli, M. Anti-Proliferative Effects of Copper(II) Complexes with Hydroxyquinoline-Thiosemicarbazone Ligands. *Eur. J. Med. Chem.*, **2017**, *128* (Ii), 140–153. https://doi.org/10.1016/j.ejmech.2017.01.031.

[168] Maret, W. Zinc Biochemistry: From a Single Zinc Enzyme to a Key Element of Life. *Adv. Nutr.*, **2013**, *4* (1), 82–91. https://doi.org/10.3945/an.112.003038.

[169] Larson, C. P.; Saha, U. R.; Nazrul, H. Impact Monitoring of the National Scale up of Zinc Treatment for Childhood Diarrhea in Bangladesh: Repeat Ecologic Surveys. *PLoS Med.*, **2009**, *6* (11), 1–10. https://doi.org/10.1371/journal.pmed.1000175.

[170] Creaven, B. S.; Devereux, M.; Georgieva, I.; Karcz, D.; McCann, M.; Trendafilova, N.; Walsh, M. Molecular Structure and Spectroscopic Studies on Novel Complexes of Coumarin-3-Carboxylic Acid with Ni(II), Co(II), Zn(II) and Mn(II) Ions Based on Density Functional Theory. *Spectrochim. Acta - Part A Mol. Biomol. Spectrosc.*, **2011**, *84* (1), 275–285. https://doi.org/10.1016/j.saa.2011.09.041.

[171] Mandewale, M. C.; Thorat, B.; Nivid, Y.; Jadhav, R.; Nagarsekar, A.; Yamgar, R. Synthesis, Structural Studies and Antituberculosis Evaluation of New Hydrazone Derivatives of Quinoline and Their Zn(II) Complexes. *J. Saudi Chem. Soc.*, **2018**, *22* (2), 218–228. https://doi.org/10.1016/j.jscs.2016.04.003.

[172] Kumar, A.; Das, Y.; Pattnaik, S.; Routaray, A.; Nath, N. Novel Polystyrene - Anchored Zinc Complex : Efficient Catalyst for Phenol Oxidation. *Chinese J. Catal.*, **2014**, *35* (10), 1701–1708. https://doi.org/10.1016/S1872-2067(14)60113-3.

[173] Biswas, S.; Khatun, R.; Sengupta, M.; Manirul, S. Polystyrene Supported Zinc Complex as an e Ffi Cient Catalyst for Cyclic Carbonate Formation via CO 2 Fi Xation under Atmospheric Pressure and Organic Carbamates Production. *Mol. Catal.*, **2018**, *452* (April), 129–137. https://doi.org/10.1016/j.mcat.2018.04.009.

[174] Gao, A.; Yao, W.; Xiao, Y.; Zhang, M.; Zhu, G.; Zhang, N.; Wang, S. Dinuclear Zinc Complexes with Chiral Tetra-Azane Ligands : Synthesis , Structures and Catalytic Properties for Ring-Opening Polymerization of Cyclic Esters. *Polyhedron*, **2015**, *85*,

537–542. https://doi.org/10.1016/j.poly.2014.08.067.

[175] Chai, L.; Hu, Q.; Zhang, K.; Zhou, L.; Huang, J. Synthesis , Structural Characterization , Spectroscopic , and DFT Studies of Two Penta-Coordinated Zinc (II) Complexes Containing Quinazoline and 1 , 10- Phenanthroline as Mixed Ligands. *J. Lumin. J.*, **2018**, *203* (June), 234–246.

[176] Indira, S.; Vinoth, G.; Bharathi, M.; Shanmuga Bharathi, K. Synthesis, Spectral, Electrochemical, in-Vitro Antimicrobial and Antioxidant Activities of Bisphenolic Mannich Base and 8-Hydroxyquinoline Based Mixed Ligands and Their Transition Metal Complexes. *J. Mol. Struct.*, **2019**, *1198*, 1–8.

[177] Szemik-Hojniak, A.; Deperasińska, I.; Nizhnik, Y.; Jerzykiewicz, L. Luminescent Properties of Chameleon-like Metal-Organic Framework between Zinc(II) Dichloride and Two Quinoline-N-Oxide Molecules. *Spectrochim. Acta - Part A Mol. Biomol. Spectrosc.*, **2020**, *239*, 1–8. https://doi.org/10.1016/j.saa.2020.118464.

[178] Chagas, S.; Fonseca, F. L. A.; Bagatin, I. A. Quinoline-Derivative Coordination Compounds as Potential Applications to Antibacterial and Antineoplasic Drugs. *Mater. Sci. Eng. C*, **2019**, *98* (2019), 1043–1052.

[179] Whitfield, D. R.; Vallortigara, J.; Alghamdi, A.; Hortobágyi, T.; Ballard, C.; Thomas, A. J.; O'Brien, J. T.; Aarsland, D.; Francis, P. T. Depression and Synaptic Zinc Regulation in Alzheimer Disease, Dementia with Lewy Bodies, and Parkinson Disease Dementia. *Am. J. Geriatr. Psychiatry*, **2015**, *23* (2), 141–148.

[180] Forouzandeh, F.; Keypour, H.; Zebarjadian, M. H.; Mahmoudabadi, M.; Hosseinzadeh, L.; Karamian, R.; Ahmadi Khoei, M.; Gable, R. W. Synthesis, Characterization and X-Ray Crystal Structure of Potentially N6O2 Coordinating Macroacyclic Schiff Base Ligands and Their Mn(II), Zn(II) and Cd(II) Complexes; Cytotoxic, Antibacterial Properties and Competitive 7Li NMR Studies. *Polyhedron*, **2019**, *160*, 238–246. https://doi.org/10.1016/j.poly.2018.12.052.

[181] Majumdar, D.; Biswas, J. K.; Mondal, M.; Surendra Babu, M. S.; Metre, R. K.; Das, S.; Bankura, K.; Mishra, D. Coordination of N,O-Donor Appended Schiff Base Ligand (H2L1) towards Zinc(II) in Presence of Pseudohalides: Syntheses, Crystal Structures, Photoluminescence, Antimicrobial Activities and Hirshfeld Surfaces. *J. Mol. Struct.*, **2018**, *1155* (Ii), 745–757. https://doi.org/10.1016/j.molstruc.2017.11.052.

[182] Azam, M.; Wabaidur, S. M.; Alam, M. J.; Trzesowska-Kruszynska, A.; Kruszynski, R.; Alam, M.; Al-Resayes, S. I.; Dwivedi, S.; Khan, M. R.; Islam, M. S.; et al. Synthesis, Structural Investigations and Pharmacological Properties of a New Zinc

Complex with a N4-Donor Schiff Base Incorporating 2-Pyridyl Ring. *Inorganica Chim. Acta*, **2019**, *487*, 97–106. https://doi.org/10.1016/j.ica.2018.12.009.

[183] Su, W. Y.; Pan, R. K.; Song, J. L.; Li, G. B.; Liu, S. G. Synthesis, Crystal Structures and Cytotoxic Activity of Two Zinc(II) Complexes Derived from Benzimidazole Derivatives. *Polyhedron*, **2019**, *161*, 268–275.

[184] Ambala, A.; Lincoln, C. A. Synthesis, Characterization, Antimicrobial Activity and DNA Cleavage Study of (E)-2-(((2-(P-Tolyloxy)Quinolin-3-Yl)Methylene)Amino)Benzenethiol Schiff Base Metal Complexes. *Chem. Data Collect.*, **2020**, *27*, 1–6. https://doi.org/10.1016/j.cdc.2020.100372.

[185] Chai, L. Q.; Zhang, J. Y.; Chen, L. C.; Li, Y. X.; Tang, L. J. Synthesis, Crystal Structure, Spectroscopic Properties and DFT Calculations of a New Schiff Base-Type Zinc(II) Complex. *Res. Chem. Intermed.*, **2016**, *42* (4), 3473–3488.

[186] Chai, L. Q.; Tang, L. J.; Chen, L. C.; Huang, J. J. Structural, Spectral, Electrochemical and DFT Studies of Two Mononuclear Manganese(II) and Zinc(II) Complexes. *Polyhedron*, **2017**, *122* (Ii), 228–240. https://doi.org/10.1016/j.poly.2016.11.032.

[187] Zianna, A.; Geromichalos, G.; Psoma, E.; Kalogiannis, S.; Hatzidimitriou, A. G.; Psomas, G. Structure and in Vitro and in Silico Biological Activity of Zinc(II) Complexes with 3,5–Dichloro–Salicylaldehyde. *J. Inorg. Biochem.*, **2022**, *229* (2022), 1–15. https://doi.org/10.1016/j.jinorgbio.2022.111727.

[188] Iraji, A.; Firuzi, O.; Khoshneviszadeh, M.; Nadri, H.; Edraki, N.; Miri, R. Synthesis and Structure-Activity Relationship Study of Multi-Target Triazine Derivatives as Innovative Candidates for Treatment of Alzheimer's Disease. *Bioorg. Chem.*, **2018**, *77*, 223–235. https://doi.org/10.1016/j.bioorg.2018.01.017.

[189] Jozefíková, F.; Perontsis, S.; Koňáriková, K.; Švorc, Ľ.; Mazúr, M.; Psomas, G.; Moncol, J. In Vitro Biological Activity of Copper(II) Complexes with NSAIDs and Nicotinamide: Characterization, DNA- and BSA-Interaction Study and Anticancer Activity. *J. Inorg. Biochem.*, **2022**, *228* (2021), 1–14.

[190] Ramachandran, E.; Gandin, V.; Bertani, R.; Sgarbossa, P.; Natarajan, K.; Bhuvanesh, N. S. P.; Venzo, A.; Zoleo, A.; Glisenti, A.; Dolmella, A.; et al. Synthesis, Characterization and Cytotoxic Activity of Novel Copper(II) Complexes with Aroylhydrazone Derivatives of 2-Oxo-1,2-Dihydrobenzo[h]Quinoline-3-Carbaldehyde. *J. Inorg. Biochem.*, **2018**, *182* (January), 18–28.

[191] Hussain, A.; AlAjmi, M. F.; Rehman, M. T.; Amir, S.; Husain, F. M.; Alsalme, A.; Siddiqui, M. A.; AlKhedhairy, A. A.; Khan, R. A. Copper(II) Complexes as Potential

Anticancer and Nonsteroidal Anti-Inflammatory Agents: In Vitro and in Vivo Studies. *Sci. Rep.*, **2019**, *9* (1), 1–17. https://doi.org/10.1038/s41598-019-41063-x.

[192] Barmpa, A.; Hatzidimitriou, A. G.; Psomas, G. Copper(II) Complexes with Meclofenamate Ligands: Structure, Interaction with DNA and Albumins, Antioxidant and Anticholinergic Activity. *J. Inorg. Biochem.*, **2021**, *217* (2021), 1–12.

[193] Kouris, E.; Kalogiannis, S.; Perdih, F.; Turel, I.; Psomas, G. Cobalt(II) Complexes of Sparfloxacin: Characterization, Structure, Antimicrobial Activity and Interaction with DNA and Albumins. *J. Inorg. Biochem.*, **2016**, *163*, 18–27.

[194] Mirica, L. M.; Ottenwaelder, X.; Stack, T. D. P. Structure and Spectroscopy of Copper − Dioxygen Complexes. *ACS*, **2004**, No. I, 1013–1045.

[195] Abd El-Halim, H. F.; Mohamed, G. G.; Khalil, E. A. M. Synthesis, Spectral, Thermal and Biological Studies of Mixed Ligand Complexes with Newly Prepared Schiff Base and 1,10-Phenanthroline Ligands. *J. Mol. Struct.*, **2017**, *1146*, 153–163.

[196] Tuna, M.; Yildiz, S. Z.; Arabaci, G.; Denli, Z.; Delibaş, N. Ç.; Hökelek, T. Functional Substituted Cu(II) Schiff Base Complexes, Syntheses, X-Ray and Theoretical Characterizations, and Investigations of Their Polyphenol Oxidase- and Peroxidase-like Activities. *J. Mol. Struct.*, **2021**, *1232* (2021), 1–10.

[197] Nanjundan, N.; Narayanasamy, R.; Geib, S.; Velmurugan, K.; Nandhakumar, R.; Balakumaran, M. D.; Kalaichelvan, P. T. Distorted Tetrahedral Bis-(N,S) Bidentate Schiff Base Complexes of Ni(II), Cu(II) and Zn(II): Synthesis, Characterization and Biological Studies. *Polyhedron*, **2016**, *110*, 203–220.

[198] Senthil, D.; Bhuvanesh, N. S. P.; Natarajan, K. Synthesis , Crystal Structure and Pharmacological Evaluation of Two New Cu (II) Complexes of 2-Oxo-1 , 2-Dihydroquinoline-3-Carbaldehyde (Benzoyl) Hydrazone : A Comparative Investigation. *Eur. J. Med. Chem.*, **2012**, *47*, 73–85.

[199] Shawish, H. B.; Wong, W. Y.; Wong, Y. L.; Loh, S. W.; Looi, C. Y.; Hassandarvish, P.; Phan, A. Y. L.; Wong, W. F.; Wang, H.; Paterson, I. C.; et al. Nickel(II) Complex of Polyhydroxybenzaldehyde N4-Thiosemicarbazone Exhibits Anti-Inflammatory Activity by Inhibiting NF-KB Transactivation. *PLoS One*, **2014**, *9* (6), 1–13.

[200] Totta, X.; Papadopoulou, A. A.; Hatzidimitriou, A. G.; Papadopoulos, A.; Psomas, G. Synthesis, Structure and Biological Activity of Nickel(II) Complexes with Mefenamato and Nitrogen-Donor Ligands. *J. Inorg. Biochem.*, **2015**, *145*, 79–93.

[201] Hsu, C. W.; Kuo, C. F.; Chuang, S. M.; Hou, M. H. Elucidation of the DNA-Interacting Properties and Anticancer Activity of a Ni(II)-Coordinated Mithramycin

Dimer Complex. *BioMetals*, **2013**, *26* (1), 1–12. https://doi.org/10.1007/s10534-012-9589-8.

[202] Masaryk, L.; Tesarova, B.; Choquesillo-lazarte, D.; Milosavljevic, V. Structural and Biological Characterization of Anticancer Nickel (II) Bis (Benzimidazole) Complex. *J. Inorg. Biochem.*, **2021**, *217* (2021), 1–10.

[203] Perontsis, S.; Tialiou, A.; Hatzidimitriou, A. G.; Papadopoulos, A. N.; Psomas, G. Nickel-Diflunisal Complexes: Synthesis, Characterization, in Vitro Antioxidant Activity and Interaction with DNA and Albumins. *Polyhedron*, **2017**, *138*, 258–269.

[204] Masaryk, L.; Tesarova, B.; Choquesillo-Lazarte, D.; Milosavljevic, V.; Heger, Z.; Kopel, P. Structural and Biological Characterization of Anticancer Nickel(II) Bis(Benzimidazole) Complex. *J. Inorg. Biochem.*, **2021**, *217* (February), 1–10.

[205] Deng, J. G.; Su, G.; Chen, P.; Du, Y.; Gou, Y.; Liu, Y. Evaluation of DNA Binding and DNA Cleavage of Nickel(II) Complexes with Tridentate α-N-Heterocyclic Thiosemicarbazones Ligands. *Inorganica Chim. Acta*, **2018**, *471* (Ii), 194–202.

[206] Liu, H.; Wang, F.; Jia, X.; Liu, L.; Bi, J.; Zhang, C. Synthesis, Characterization, and 1,3-Butadiene Polymerization Studies of Co(II), Ni(II), and Fe(II) Complexes Bearing 2-(N-Arylcarboximidoylchloride)Quinoline Ligand. *J. Mol. Catal. A Chem.*, **2014**, *391*, 25–35.

[207] Hall, M. D.; Failes, T. W.; Yamamoto, N.; Hambley, T. W. Bioreductive Activation and Drug Chaperoning in Cobalt Pharmaceuticals. *Dalt. Trans.*, **2007**, No. 36, 3983–3990. https://doi.org/10.1039/b707121c.

[208] Soliman, M. H.; Mohamed, G. G. Cr (III), Mn (II), Fe (III), Co (II), Ni (II), Cu (II) and Zn (II) New Complexes of 5-Aminosalicylic Acid : Spectroscopic , Thermal Characterization and Biological Activity. *Spectrochim. Acta Part A Mol. Biomol. Spectrosc.*, **2013**, *107*, 8–15.

[209] Kefala, L.; Hatzidimitriou, A. G.; Kessissoglou, D. P.; Perdih, F. Cobalt (II) Complexes with Non-Steroidal Anti-in Fl Ammatory Drugs and α -Diimines. *J. Inorg. Biochem.*, **2016**, *160*, 125–139.

[210] Munteanu, C. R.; Suntharalingam, K. Advances in Cobalt Complexes as Anticancer Agents. *Dalt. Trans.*, **2015**, *44* (31), 13796–13808.

[211] Mohamad, A. D. M.; Abualreish, M. J. A.; Abu-Dief, A. M. Antimicrobial and Anticancer Activities of Cobalt (III)-Hydrazone Complexes: Solubilities and Chemical Potentials of Transfer in Different Organic Co-Solvent-Water Mixtures. *J. Mol. Liq.*, **2019**, *290* (2019), 1–10. https://doi.org/10.1016/j.molliq.2019.111162.

[212] Li, Y.; Yang, Z.; Zhou, M.; Li, Y. Synthesis and Crystal Structure of New Monometallic Ni(II) and Co(II) Complexes with an Asymmetrical Aroylhydrazone: Effects of the Complexes on DNA/Protein Binding Property, Molecular Docking, and: In Vitro Anticancer Activity. *RSC Adv.*, **2017**, *7* (78), 49404–49422.

[213] Sultan, S.; Ashiq, U.; Jamal, R. A.; Mahroof-Tahir, M.; Shaikh, Z.; Shamshad, B.; Lateef, M.; Iqbal, L. Vanadium(V) Complexes with Hydrazides and Their Spectroscopic and Biological Properties. *BioMetals*, **2017**, *30* (6), 873–891.

[214] Farzanfar, J.; Ghasemi, K.; Rezvani, A. R.; Delarami, H. S.; Ebrahimi, A.; Hosseinpoor, H.; Eskandari, A.; Rudbari, H. A.; Bruno, G. Synthesis, Characterization, X-Ray Crystal Structure, DFT Calculation and Antibacterial Activities of New Vanadium(IV, V) Complexes Containing Chelidamic Acid and Novel Thiourea Derivatives. *J. Inorg. Biochem.*, **2015**, *147*, 54–64.

[215] Nunes, P.; Correia, I.; Cavaco, I.; Marques, F.; Pinheiro, T.; Avecilla, F.; Pessoa, J. C. Therapeutic Potential of Vanadium Complexes with 1,10-Phenanthroline Ligands, Quo Vadis? Fate of Complexes in Cell Media and Cancer Cells. *J. Inorg. Biochem.*, **2021**, *217* (August 2020), 1–16. https://doi.org/10.1016/j.jinorgbio.2020.111350.

[216] Ahmed, T. T.; Alajrawy, O. I. Oxovanadinum (IV) Complexes with Bidentate Ligands Synthesis, Characterization, and Comparison between Experimental and Theoretical. *Mater. Today Proc.*, **2021**, *5* (2021), 1–14.

[217] Pessoa, J. C.; Etcheverry, S.; Gambino, D. Vanadium Compounds in Medicine. *Coord. Chem. Rev.*, **2015**, *301–302*, 24–48. https://doi.org/10.1016/j.ccr.2014.12.002.

[218] Galloni, P.; Conte, V.; Floris, B. A Journey into the Electrochemistry of Vanadium Compounds. *Coord. Chem. Rev.*, **2015**, *301–302*, 240–299.

[219] Patel, N.; Prajapati, A. K.; Jadeja, R. N.; Patel, R. N.; Patel, S. K.; Gupta, V. K.; Tripathi, I. P.; Dwivedi, N. Model Investigations for Vanadium-Protein Interactions: Synthesis, Characterization and Antidiabetic Properties. *Inorganica Chim. Acta*, **2019**, *493* (April), 20–28. https://doi.org/10.1016/j.ica.2019.04.050.

[220] Biswal, D.; Pramanik, N. R.; Chakrabarti, S.; Drew, M. G. B.; Acharya, K.; Chandra, S. Syntheses, Crystal Structures, DFT Calculations, Protein Interaction and Anticancer Activities of Water Soluble Dipicolinic Acid-Imidazole Based Oxidovanadium(Iv) Complexes. *Dalt. Trans.*, **2017**, *46* (47), 16682–16702.

[221] Sumrra, S. H.; Chohan, Z. H. Metal Based New Triazoles: Their Synthesis, Characterization and Antibacterial/Antifungal Activities. *Spectrochim. Acta - Part A Mol. Biomol. Spectrosc.*, **2012**, *98*, 53–61. https://doi.org/10.1016/j.saa.2012.08.026.

[222] Rosu, T.; Pahontu, E.; Reka-Stefana, M.; Ilies, D. C.; Georgescu, R.; Shova, S.; Gulea, A. Synthesis, Structural and Spectral Studies of Cu(II) and V(IV) Complexes of a Novel Schiff Base Derived from Pyridoxal. Antimicrobial Activity. *Polyhedron*, **2012**, *31* (1), 352–360. https://doi.org/10.1016/j.poly.2011.09.044.

[223] Chohan, Z. H.; Sumrra, S. H.; Youssoufi, M. H.; Hadda, T. B. Metal Based Biologically Active Compounds: Design, Synthesis, and Antibacterial/Antifungal/Cytotoxic Properties of Triazole-Derived Schiff Bases and Their Oxovanadium(IV) Complexes. *Eur. J. Med. Chem.*, **2010**, *45* (7), 2739–2747.

[224] Adriazola, I. O.; Amaral, A. E. Do; Amorim, J. C.; Correia, B. L.; Petkowicz, C. L. O.; Mercê, A. L. R.; Noleto, G. R. Macrophage Activation and Leishmanicidal Activity by Galactomannan and Its Oxovanadium (IV/V) Complex in Vitro. *J. Inorg. Biochem.*, **2014**, *132* (1), 45–51. https://doi.org/10.1016/j.jinorgbio.2013.09.017.

[225] Crans, D. C.; Tarlton, M. L.; McLauchlan, C. C. Trigonal Bipyramidal or Square Pyramidal Coordination Geometry? Investigating the Most Potent Geometry for Vanadium Phosphatase Inhibitors. *Eur. J. Inorg. Chem.*, **2014**, *2014* (27), 4450–4468.

[226] Gambino, D. Potentiality of Vanadium Compounds as Anti-Parasitic Agents. *Coord. Chem. Rev.*, **2011**, *255* (19–20), 2193–2203. https://doi.org/10.1016/j.ccr.2010.12.028.

[227] Elsayed, S. A.; Noufal, A. M.; El-Hendawy, A. M. Synthesis, Structural Characterization and Antioxidant Activity of Some Vanadium(IV), Mo(VI)/(IV) and Ru(II) Complexes of Pyridoxal Schiff Base Derivatives. *J. Mol. Struct.*, **2017**, *1144* (2017), 120–128. https://doi.org/10.1016/j.molstruc.2017.05.020.

[228] Shaker, M.; Adam, S.; Elsawy, H. Biological Potential of Oxo-Vanadium Salicylediene Amino-Acid Complexes as Cytotoxic , Antimicrobial , Antioxidant and DNA Interaction. *J. Photochem. Photobiol. , B Biol.*, **2018**, *184* (January), 34–43.

[229] C, L. V. The Antibiotic Resistance Crisis - Causes and Threats. *P T J.*, **2015**, *40* (4), 277–283.

[230] Allahverdiyev, A. M.; Abamor, E. S.; Bagirova, M.; Rafailovich, M. Antimicrobial Effects of TiO 2 and Ag 2 O Nanoparticles against Drug-Resistant Bacteria And. *Futur. Med.*, **2011**, 933–940.

[231] Zablotskaya, A.; Segal, I.; Geronikaki, A.; Shestakova, I.; Nikolajeva, V.; Makarenkova, G. N-Heterocyclic Choline Analogues Based on 1,2,3,4-Tetrahydro(Iso)Quinoline Scaffold with Anticancer and Anti-Infective Dual Action. *Pharmacol. Reports*, **2017**, *69* (3), 575–581.

[232] Thangaraj, M.; Gengan, R. M.; Ranjan, B.; Muthusamy, R. Synthesis, Molecular

Docking, Antimicrobial, Antioxidant and Toxicity Assessment of Quinoline Peptides. *J. Photochem. Photobiol. B Biol.*, **2018**, *178* (November 2017), 287–295.

[233] Wright, G. D. Antibiotics: A New Hope. *Chem. Biol.*, **2012**, *19* (1), 3–10.

[234] Zhang, S. X.; Zhou, Y. M.; Xu, W.; Tian, L. G.; Chen, J. X.; Chen, S. H.; Dang, Z. S.; Gu, W. P.; Yin, J. W.; Serrano, E.; et al. Impact of Co-Infections with Enteric Pathogens on Children Suffering from Acute Diarrhea in Southwest China. *Infect. Dis. Poverty*, **2016**, *5* (1), 1–13. https://doi.org/10.1186/s40249-016-0157-2.

[235] Abdel-Rahman, L. H.; El-Khatib, R. M.; Nassr, L. A. E.; Abu-Dief, A. M.; Lashin, F. E. D. Design, Characterization, Teratogenicity Testing, Antibacterial, Antifungal and DNA Interaction of Few High Spin Fe(II) Schiff Base Amino Acid Complexes. *Spectrochim. Acta - Part A Mol. Biomol. Spectrosc.*, **2013**, *111*, 266–276.

[236] Abu-Dief, A. M.; Nassr, L. A. E. Tailoring, Physicochemical Characterization, Antibacterial and DNA Binding Mode Studies of Cu(II) Schiff Bases Amino Acid Bioactive Agents Incorporating 5-Bromo-2-Hydroxybenzaldehyde. *J. Iran. Chem. Soc.*, **2015**, *12* (6), 943–955. https://doi.org/10.1007/s13738-014-0557-9.

[237] Chebout, O.; Trifa, C.; Bouacida, S.; Boudraa, M.; Imane, H.; Merzougui, M.; Mazouz, W.; Ouari, K.; Boudaren, C.; Merazig, H. Two New Copper (II) Complexes with Sulfanilamide as Ligand: Synthesis, Structural, Thermal Analysis, Electrochemical Studies and Antibacterial Activity. *J. Mol. Struct.*, **2022**, *1248*, 1–16.

[238] Ramesh, G.; Daravath, S.; Swathi, M.; Sumalatha, V.; Shiva Shanker, D.; Shivaraj, S. Investigation on Co(II), Ni(II), Cu(II) and Zn(II) Complexes Derived from Quadridentate Salen-Type Schiff Base: Structural Characterization, DNA Interactions, Antioxidant Proficiency and Biological Evaluation. *Chem. Data Collect.*, **2020**, *28*, 1–17. https://doi.org/10.1016/j.cdc.2020.100434.

[239] Halliwell, B. Oxidative Stress, Nutrition and Health. Experimental Strategies for Optimization of Nutritional Antioxidant Intake in Humans. *Free Radic. Res.*, **1996**, *25* (1), 57–74. https://doi.org/10.3109/10715769609145656.

[240] Nimse, S. B.; Pal, D. Free Radicals, Natural Antioxidants, and Their Reaction Mechanisms. *RSC Adv.*, **2015**, *5* (35), 27986–28006.

[241] Kumar, J.; Kumar, N.; Sati, N.; Hota, P. K. Antioxidant Properties of Ethenyl Indole: DPPH Assay and TDDFT Studies. *New J. Chem.*, **2020**, *44* (21), 8960–8970.

[242] El Jemli, M.; Kamal, R.; Marmouzi, I.; Zerrouki, A.; Cherrah, Y.; Alaoui, K. Radical-Scavenging Activity and Ferric Reducing Ability of Juniperus Thurifera (L.), J. Oxycedrus (L.), J. Phoenicea (L.) and Tetraclinis Articulata (L.). *Adv. Pharmacol. Sci.*,

2016, *2016*, 1–6. https://doi.org/10.1155/2016/6392656.

[243] Kedare, S. B.; Singh, R. P. Genesis and Development of DPPH Method of Antioxidant Assay. *J. Food Sci. Technol.*, **2011**, *48* (4), 412–422. https://doi.org/10.1007/s13197-011-0251-1.

[244] Psomas, G. Copper(II) and Zinc(II) Coordination Compounds of Non-Steroidal Anti-Inflammatory Drugs: Structural Features and Antioxidant Activity. *Coord. Chem. Rev.*, **2020**, *412*, 1–13. https://doi.org/10.1016/j.ccr.2020.213259.

[245] Contreras-Guzmán, E. S.; Strong, F. C. Determination of Tocopherols (Vitamin E) by Reduction of Cupric Ion. *J. AOAC Int.*, **1982**, *65* (5), 1215–1221.

[246] Sánchez-Moreno, C. Methods Used to Evaluate the Free Radical Scavenging Activity in Foods and Biological Systems. *Food Sci. Technol. Int.*, **2002**, *8* (3), 121–137. https://doi.org/10.1106/108201302026770.

[247] Liang, N.; Kitts, D. Antioxidant Property of Coffee Components: Assessment of Methods That Define Mechanisms of Action. *Molecules*, **2014**, *19* (11), 19180–19208.

[248] Damena, T.; Alem, M. B.; Zeleke, D.; Desalegn, T.; Eswaramoorthy, R.; Demissie, T. B. Novel Zinc (II) and Copper (II) Complexes of 2 - ((2- Hydroxyethyl) Amino) Quinoline-3-Carbaldehyde for Antibacterial and Antioxidant Activities : A Combined Experimental , DFT , and Docking Studies. *ACS Omega*, **2022**, *7* (2022), 26336–2635.

[249] Molyneux, P. The Use of the Stable Free Radical Diphenylpicryl- Hydrazyl (DPPH) for Estimating Antioxidant Activity. *J. Sci. Technol.*, **2004**, *26* (2), 211–219.

[250] Tai, A.; Ohno, A.; Ito, H. Isolation and Characterization of the 2,2′-Azinobis(3-Ethylbenzothiazoline-6-Sulfonic Acid) (ABTS) Radical Cation-Scavenging Reaction Products of Arbutin. *J. Agric. Food Chem.*, **2016**, *64* (38), 7285–7290.

[251] Konan, K. V.; Le Tien, C.; Mateescu, M. A. Electrolysis-Induced Fast Activation of the ABTS Reagent for an Antioxidant Capacity Assay. *Anal. Methods*, **2016**, *8* (28), 5638–5644. https://doi.org/10.1039/c6ay01088a.

[252] Ilyasov, I. R.; Beloborodov, V. L.; Selivanova, I. A.; Terekhov, R. P. ABTS/PP Decolorization Assay of Antioxidant Capacity Reaction Pathways. *Int. J. Mol. Sci.*, **2020**, *21* (3), 1–27. https://doi.org/10.3390/ijms21031131.

[253] Benzie, I. F. F.; Strain, J. J. Ferric Reducing/Antioxidant Power Assay: Direct Measure of Total Antioxidant Activity of Biological Fluids and Modified Version for Simultaneous Measurement of Total Antioxidant Power and Ascorbic Acid Concentration. *Methods Enzymol.*, **1999**, *299* (1995), 15–27.

[254] Benzie, I. F. F.; Devaki, M. The Ferric Reducing/Antioxidant Power (FRAP) Assay for

Non-Enzymatic Antioxidant Capacity: Concepts, Procedures, Limitations and Applications. *Meas. Antioxid. Act. Capacit. Recent Trends Appl.*, **2017**, 77–106.

[255] Ben Ahmed, Z.; Yousfi, M.; Viaene, J.; Dejaegher, B.; Demeyer, K.; Mangelings, D.; Heyden, Y. Vander. Determination of Optimal Extraction Conditions for Phenolic Compounds from: Pistacia Atlantica Leaves Using the Response Surface Methodology. *Anal. Methods*, **2016**, *8* (31), 6107–6114.

[256] Spiegel, M.; Kapusta, K.; Kołodziejczyk, W.; Saloni, J.; Zbikowska, B.; Hill, G. A.; Sroka, Z. Antioxidant Activity of Selected Phenolic Acids–Ferric Reducing Antioxidant Power Assay and QSAR Analysis of the Structural Features. *Molecules*, **2020**, *25* (13), 1–15. https://doi.org/10.3390/molecules25133088.

[257] Ruch, R. J.; Cheng, S. jun; Klaunig, J. E. Prevention of Cytotoxicity and Inhibition of Intercellular Communication by Antioxidant Catechins Isolated from Chinese Green Tea. *Carcinogenesis*, **1989**, *10* (6), 1003–1008.

[258] Keser, S.; Celik, S.; Turkoglu, S.; Yilmaz, Ö.; Turkoglu, I. Hydrogen Peroxide Radical Scavenging and Total Antioxidant Activity of Hawthorn. *Chem. J.*, **2012**, *02* (01), 1–4.

[259] Tian, S.; Wang, J.; Li, Y.; Li, D.; Xu, L.; Hou, T. The Application of in Silico Drug-Likeness Predictions in Pharmaceutical Research. *Adv. Drug Deliv. Rev.*, **2015**, *86* (November), 2–10. https://doi.org/10.1016/j.addr.2015.01.009.

[260] Walters, W. P.; Murcko, A.; Murcko, M. A. Recognizing Molecules with Drug-like Properties. *Curr. Opin. Chem. Biol.*, **1999**, *3* (4), 384–387.

[261] Jia, C. Y.; Li, J. Y.; Hao, G. F.; Yang, G. F. A Drug-Likeness Toolbox Facilitates ADMET Study in Drug Discovery. *Drug Discov. Today*, **2020**, *25* (1), 248–258.

[262] Jia, C. Y.; Li, J. Y.; Hao, G. F.; Yang, G. F. A Drug-Likeness Toolbox Facilitates ADMET Study in Drug Discovery. *Drug Discov. Today*, **2020**, *25* (1), 248–258.

[263] Agoni, C.; Olotu, F. A.; Ramharack, P.; Soliman, M. E. Druggability and Drug-Likeness Concepts in Drug Design: Are Biomodelling and Predictive Tools Having Their Say? *J. Mol. Model.*, **2020**, *26* (6), 1–11. https://doi.org/10.1007/s00894-020-04385-6.

[264] Lipinski, C. A. Rule of Five in 2015 and beyond: Target and Ligand Structural Limitations, Ligand Chemistry Structure and Drug Discovery Project Decisions. *Adv. Drug Deliv. Rev.*, **2016**, *101*, 34–41. https://doi.org/10.1016/j.addr.2016.04.029.

[265] Chen, X.; Li, H.; Tian, L.; Li, Q.; Luo, J.; Zhang, Y. Analysis of the Physicochemical Properties of Acaricides Based on Lipinski's Rule of Five. *J. Comput. Biol.*, **2020**, *27* (9), 1397–1406. https://doi.org/10.1089/cmb.2019.0323.

[266] Huang, H.; Chu, C. L.; Chen, L.; Shui, D. Evaluation of Potential Inhibitors of Squalene Synthase Based on Virtual Screening and in Vitro Studies. *Comput. Biol. Chem.*, **2019**, *80* (April), 390–397.

[267] Lipinski, C. A.; Lombardo, F.; Dominy, B. W.; Feeney, P. J. Experimental and Computational Approaches to Estimate Solubility and Permeability in Drug Discovery and Development Settings. *Adv. Drug Deliv. Rev.*, **2012**, *64* (SUPPL.), 4–17.

[268] Khan, S. U.; Ahemad, N.; Chuah, L.-H.; Naidu, R.; Htar, T. T. Illustrated Step by Step Protocol to Perform Molecular Docking: Human Estrogen Receptor Complex with 4-Hydroxytamoxifen. *Prog. Drug Discov. Biomed. Sci.*, **2020**, *3* (1), 1–21.

[269] Salmaso, V.; Moro, S. Bridging Molecular Docking to Molecular Dynamics in Exploring Ligand-Protein Recognition Process: An Overview. *Front. Pharmacol.*, **2018**, *9* (AUG), 1–16. https://doi.org/10.3389/fphar.2018.00923.

[270] Rohs, R.; Bloch, I.; Sklenar, H.; Shakked, Z.; Delbru, M. Molecular Flexibility in Ab Initio Drug Docking to DNA : Binding-Site and Binding-Mode Transitions in All-Atom Monte Carlo Simulations. **2005**, *33* (22), 7048–7057.

[271] Dar, A. M.; Mir, S. Molecular Docking: Approaches, Types, Applications and Basic Challenges. *J. Anal. Bioanal. Tech.*, **2017**, *08* (02), 8–10. https://doi.org/10.4172/2155-9872.1000356.

[272] Agarwal, S.; Chadha, D.; Mehrotra, R. Molecular Modeling and Spectroscopic Studies of Semustine Binding with DNA and Its Comparison with Lomustine-DNA Adduct Formation. *J. Biomol. Struct. Dyn.*, **2015**, *33* (8), 1653–1668.

[273] Naz, S.; Uddin, N.; Ullah, K.; Haider, A.; Gul, A.; Faisal, S.; Nadhman, A.; Bibi, M.; Yousuf, S.; Ali, S. Homo- and Heteroleptic Zinc(II) Carboxylates: Synthesis, Structural Characterization, and Assessment of Their Biological Significance in in Vitro Models. *Inorg. Chim. Acta*, **2020**, *511* (June), 1–12.

[274] El-Sonbati, A. Z.; Diab, M. A.; Mohamed, G. G.; Saad, M. A. Polymer Complexes. LXXVII. Synthesis, Characterization, Spectroscopic Studies and Immune Response in Cattle of Quinoline Polymer Complexes. *Appl. Organomet. Chem.*, **2019**, *33* (8), 1–13.

[275] Ramachandran, E.; Gandin, V.; Bertani, R.; Sgarbossa, P.; Natarajan, K.; Bhuvanesh, N. S. P.; Venzo, A.; Zoleo, A.; Glisenti, A.; Dolmella, A.; et al. Synthesis, Characterization and Cytotoxic Activity of Novel Copper(II) Complexes with Aroylhydrazone Derivatives of 2-Oxo-1,2-Dihydrobenzo[h]Quinoline-3-Carbaldehyde. *J. Inorg. Biochem.*, **2018**, *182* (September 2017), 18–28.

[276] Ramachandran, E.; Senthil Raja, D.; Bhuvanesh, N. S. P.; Natarajan, K. Synthesis,

Characterization and in Vitro Pharmacological Evaluation of New Water Soluble Ni(II) Complexes of 4N-Substituted Thiosemicarbazones of 2-Oxo-1,2-Dihydroquinoline-3-Carbaldehyde. *Eur. J. Med. Chem.*, **2013**, *64* (3), 179–189.

[277] Refat, M. S. Synthesis, Characterization, Thermal and Antimicrobial Studies of Diabetic Drug Models: Complexes of Vanadyl(II) Sulfate with Ascorbic Acid (Vitamin C), Riboflavin (Vitamin B2) and Nicotinamide (Vitamin B3). *J. Mol. Struct.*, **2010**, *969* (1–3), 163–171. https://doi.org/10.1016/j.molstruc.2010.01.064.

[278] Sutradhar, M.; Roy Barman, T.; Ghosh, S.; Drew, M. G. B. Synthesis and Characterization of Mixed-Ligand Complexes Using a Precursor Mononuclear Oxidovanadium(V) Complex Derived from a Tridentate Salicylhydrazone Oxime Ligand. *J. Mol. Struct.*, **2013**, *1037*, 276–282.

[279] Ibrahim, M. M.; Mersal, G. A. M.; Ramadan, A. M. M. Synthesis, Characterization and Antioxidant/Cytotoxic Activity of Oxovanadium(IV) Complexes of Methyliminodiacetic Acid and Ethylenediaminetetracetic Acid. *J. Mol. Struct.*, **2017**, *1137*, 742–755. https://doi.org/10.1016/j.molstruc.2017.02.080.

[280] Shalaby, A. A.; Mohamed, A. A. Determination of Stoichiometry and Stability Constants of Iron Complexes of Phenanthroline , Tris (2 - Pyridyl)- s - Triazine , and Salicylate Using a Digital Camera. *Chem. Pap.*, **2020**, *74* (0123456789), 1–8.

[281] Ahmad, S.; Hamid, F.; Hamid, M.; Wattoo, S.; Sarwar, S.; Nawaz, A. Spectrophotometric Study of Stability Constants of Cimetidine – Ni (II) Complex at Different Temperatures. *Arab. J. Chem.*, **2012**, *5* (3), 309–314.

[282] Damena, T.; Tesema, T. E.; Alvi, N. I.; Siraj, K. Effect of Pyridoxine on the Transport of Iron Across Microfilter Supported Bilayer Lipid Membrane. *J. Surf. Interfac. Mater.*, **2014**, *1* (2), 130–135. https://doi.org/10.1166/jsim.2013.1016.

[283] Daina, A.; Michielin, O.; Zoete, V. SwissADME: A Free Web Tool to Evaluate Pharmacokinetics, Drug-Likeness and Medicinal Chemistry Friendliness of Small Molecules. *Sci. Rep.*, **2017**, *7* (October 2016), 1–13. https://doi.org/10.1038/srep42717.

[284] M. J. Frisch, G. W. Trucks, H. B. Schlegel, G. E. S.; M. A. Robb, J. R. Cheeseman, G. Scalmani, V. B.; G. A. Petersson, H. Nakatsuji, X. Li, M. Caricato, A. V. M.; J. Bloino, B. G. Janesko, R. Gomperts, B. Mennucci, H. P. H.; J. V. Ortiz, A. F. Izmaylov, J. L. Sonnenberg, D. W.-Y.; F. Ding, F. Lipparini, F. Egidi, J. Goings, B. Peng, A. P.; T. Henderson, D. Ranasinghe, V. G. Zakrzewski, J. Gao, N. R.; G. Zheng, W. Liang, M. Hada, M. Ehara, K. Toyota, R. F.; J. Hasegawa, M. Ishida, T. Nakajima, Y. Honda, O. Kitao, H. N.; T. Vreven, K. Throssell, J. A. Montgomery, Jr., J. E. P.; et

al. Gaussian 16, Revision C. 01. *Gaussian, Inc., Wallingford CT*. 2016.

[285] Becke, A. D. Thermochemistry. III. The Role of Exact Exchange. *J. Chem. Phys.*, **1993**, *98*, 5648–5652.

[286] Lee, C.; Yang, W.; Parr, R. G. Development of the Colle-Salvetti Correlation-Energy Formula into a Functional of the Electron Density. *Phys. Rev. B*, **1988**, *37* (2), 785–789. https://doi.org/10.1103/PhysRevB.37.785.

[287] Stephens, P. J.; Devlin, F. J.; Chabalowski, C. F.; Frisch, M. J. Ab Initio Calculation of Vibrational Absorption and Circular Dichroism Spectra Using Density Functional Force Fields. *J. Phys. Chem.*, **1994**, *98* (45), 11623–11627.

[288] Krishnan, R.; Binkley, J. S.; Seeger, R.; Pople, J. A. Self-Consistent Molecular Orbital Methods. XX. A Basis Set for Correlated Wave Functions. *J. Chem. Phys.*, **1980**, *72* (1), 650–654. https://doi.org/10.1063/1.438955.

[289] Grimme, S. Calculation of the Electronic Spectra of Large Molecules. *Rev. Comput. Chem.*, **2004**, *20*, 153−218.

[290] Tomasi, J.; Mennucci, B.; Cammi, R. Quantum Mechanical Continuum Solvation Models. *Chem. Rev.*, **2005**, *105* (8), 2999–3093. https://doi.org/10.1021/cr9904009.

[291] Allouche, A. Software News and Updates Gabedit — A Graphical User Interface for Computational Chemistry Softwares. *J. Comput. Chem.*, **2012**, *32*, 174–182.

[292] Mendez, M.; Green, L.; Corvalan, J.; Jia, X.; Maynard-Currie, C.; Jakobovits, A. © 199 7 Nature Publishing Group Http://Www.Nature.Com/Naturegenetics. *Nat. Genet.*, **1997**, *15*, 57–61.

[293] Wendorff, T. J.; Schmidt, B. H.; Heslop, P.; Austin, C. A.; Berger, J. M. The Structure of DNA-Bound Human Topoisomerase II Alpha: Conformational Mechanisms for Coordinating Inter-Subunit Interactions with DNA Cleavage. *J. Mol. Biol.*, **2012**, *424* (3–4), 109–124. https://doi.org/10.1016/j.jmb.2012.07.014.

[294] Bottomley, M. J.; Muraglia, E.; Bazzo, R.; Carfì, A. Molecular Insights into Quorum Sensing in the Human Pathogen Pseudomonas Aeruginosa from the Structure of the Virulence Regulator LasR Bound to Its Autoinducer. *J. Biol. Chem.*, **2007**, *282* (18), 13592–13600. https://doi.org/10.1074/jbc.M700556200.

[295] Bitew, M.; Desalegn, T.; Demissie, T. B.; Belayneh, A.; Endale, M.; Eswaramoorthy, R. Pharmacokinetics and Drug-Likeness of Antidiabetic Flavonoids: Molecular Docking and DFT Study. *PLoS One*, **2021**, *16* (12), 1–22.

[296] Wiegand, I.; Hilpert, K.; Hancock, R. E. W. Agar and Broth Dilution Methods to Determine the Minimal Inhibitory Concentration (MIC) of Antimicrobial Substances.

Nat. Protoc., **2008**, *3* (2), 163–175. https://doi.org/10.1038/nprot.2007.521.

[297] Chen, S. C.; Liu, J. W.; Wu, X. Z.; Cao, W.; Wang, F.; Huang, J. M.; Han, Y.; Zhu, X. Y.; Zhu, B. Y.; Gan, Q.; et al. Comparison of Microdilution Method with Agar Dilution Method for Antibiotic Susceptibility Test of Neisseria Gonorrhoeae. *Infect. Drug Resist.*, **2020**, *13*, 1775–1780. https://doi.org/10.2147/IDR.S253811.

[298] Atta-ur-Rahman; Choudhary, M. I.; Thomson, W. J.; Pharmaceuticals, A.; Diego, S.; USA. *Bioassay Techniques for Drug Development*; 2001.

[299] Tamene, D.; Endale, M. Antibacterial Activity of Coumarins and Carbazole Alkaloid from Roots of Clausena Anisata . *Adv. Pharmacol. Sci.*, **2019**, *2019*, 1–8.

[300] Mogana, R.; Adhikari, A.; Tzar, M. N.; Ramliza, R.; Wiart, C. Antibacterial Activities of the Extracts, Fractions and Isolated Compounds from Canarium Patentinervium Miq. Against Bacterial Clinical Isolates. *BMC Complement. Med. Ther.*, **2020**, *20* (1), 1–11. https://doi.org/10.1186/s12906-020-2837-5.

[301] Ekennia, A. C.; Onwudiwe, D. C.; Olasunkanmi, L. O.; Osowole, A. A.; Ebenso, E. E. Synthesis, DFT Calculation, and Antimicrobial Studies of Novel Zn(II), Co(II), Cu(II), and Mn(II) Heteroleptic Complexes Containing Benzoylacetone and Dithiocarbamate. *Bioinorg. Chem. Appl.*, **2015**, *2015*, 1–12. https://doi.org/10.1155/2015/789063.

[302] Sallam, S. A.; Orabi, A. S.; Abbas, A. M. DNA Interaction with Octahedral and Square Planar Ni(II) Complexes of Aspartic-Acid Schiff-Bases. *J. Mol. Struct.*, **2011**, *1006* (1–3), 272–281. https://doi.org/10.1016/j.molstruc.2011.09.020.

[303] Sathyadevi, P.; Krishnamoorthy, P.; Bhuvanesh, N. S. P.; Kalaiselvi, P.; Vijaya Padma, V.; Dharmaraj, N. Organometallic Ruthenium(II) Complexes: Synthesis, Structure and Influence of Substitution at Azomethine Carbon towards DNA/BSA Binding, Radical Scavenging and Cytotoxicity. *Eur. J. Med. Chem.*, **2012**, *55*, 420–431. https://doi.org/10.1016/j.ejmech.2012.08.001.

[304] Neethu, K. S.; Sivaselvam, S.; Theetharappan, M.; Ranjitha, J.; Bhuvanesh, N. S. P.; Ponpandian, N.; Neelakantan, M. A.; Kaveri, M. V. In Vitro Evaluations of Biomolecular Interactions, Antioxidant and Anticancer Activities of Nickel(II) and Copper(II) Complexes with 1:2 Coordination of Anthracenyl Hydrazone Ligands. *Inorg. Chim. Acta*, **2021**, *524* (November 2020), 1–15.

[305] Elsayed, S. A.; Badr, H. E.; di Biase, A.; El-Hendawy, A. M. Synthesis, Characterization of Ruthenium(II), Nickel(II), Palladium(II), and Platinum(II) Triphenylphosphine-Based Complexes Bearing an ONS-Donor Chelating Agent: Interaction with Biomolecules, Antioxidant, in Vitro Cytotoxic, Apoptotic Activity and

Cell. *J. Inorg. Biochem.*, **2021**, *223* (April), 1–19.

[306] Ayyannan, G.; Mohanraj, M.; Gopiraman, M.; Uthayamalar, R.; Raja, G.; Bhuvanesh, N.; Nandhakumar, R.; Jayabalakrishnan, C. New Palladium(II) Complexes with ONO Chelated Hydrazone Ligand: Synthesis, Characterization, DNA/BSA Interaction, Antioxidant and Cytotoxicity. *Inorganica Chim. Acta*, **2020**, *512* (2020).

[307] Sathisha, M. P.; Revankar, V. K.; Pai, K. S. R. Synthesis, Structure, Electrochemistry, and Spectral Characterization of Bis-Isatin Thiocarbohydrazone Metal Complexes and Their Antitumor Activity against Ehrlich Ascites Carcinoma in Swiss Albino Mice. *Met. Based. Drugs*, **2008**, *2008*, 1–11. https://doi.org/10.1155/2008/362105.

[308] Abane-Merzouk, L.; Adkhis, A.; Terrachet-Bouaziz, S.; Makhloufi-Chebli, M. Synthesis, DFT/TD-DFT Theoretical Studies, Experimental Characterization, Electrochemical and Antioxidant Activity of Fe(III) Complexes of Bis (Dimethylglyoximato) Guanine. *J. Mol. Struct.*, **2019**, *1186*, 413–422.

[309] Zhu, S.-S.; Dong, X.; Zhou, Z.-H. Mixed Ligand Oxidovanadium(IV) Complexes: Synthesis, Spectral, Structural Characterization and Catalytic Degradations of Methyl Orange. *Inorganica Chim. Acta*, **2019**, *486* (October 2018), 395–400.

[310] Dalal, M. Charge Transfer Spectra. In *A Textbook of Inorganic Chemistry*; Dalal Institute; Vol. I, pp 214–341.

[311] Kargar, H.; Behjatmanesh-Ardakani, R.; Torabi, V.; Kashani, M.; Chavoshpour-Natanzi, Z.; Kazemi, Z.; Mirkhani, V.; Sahraei, A.; Tahir, M. N.; Ashfaq, M.; et al. Synthesis, Characterization, Crystal Structures, DFT, TD-DFT, Molecular Docking and DNA Binding Studies of Novel Copper(II) and Zinc(II) Complexes Bearing Halogenated Bidentate N,O-Donor Schiff Base Ligands. *Polyhedron*, **2021**, *195* (2021), 1–13. https://doi.org/10.1016/j.poly.2020.114988.

[312] Saikumari, N. Synthesis and Characterization of Amino Acid Schiff Base and Its Copper (II) Complex and Its Antimicrobial Studies. *Mater. Today Proc.*, **2021**, *47* (xxxx), 1777–1781. https://doi.org/10.1016/j.matpr.2021.02.607.

[313] Chai, L.; Tang, L.; Chen, L.; Huang, J. Structural , Spectral , Electrochemical and DFT Studies of Two Mononuclear Manganese (II) and Zinc (II) Complexes. *Polyhedron*, **2017**, *122*, 228–240.

[314] María S. Islas a, Juan J. Martínez Medina b, Oscar E. Piro c, Gustavo A. Echeverría c, Evelina G. Ferrer a, P. A. M. W. Comparisons of the Spectroscopic and Microbiological Activities among Coumarin-3-Carboxylate, o-Phenanthroline and Zinc(II) Complexes. *Spectrochim. Acta Part A Mol. Biomol. Spectrosc.*, **2018**, *198*,

212–221.

[315] Sezi, S.; Varghese, R.; Vilaivan, T.; Wagenknecht, H.-A. Conformational Control of Dual Emission by Pyrrolidinyl PNA-DNA Hybrids. *ChemistryOpen*, **2012**, *1* (4), 173–176. https://doi.org/10.1002/open.201200016.

[316] Ferrer, E. G.; Williams, P. A. M. Comparisons of the Spectroscopic and Microbiological Activities among Coumarin-3-Carboxylate, o-Phenanthroline and Zinc(II) Complexes María. *Spectrochim. Acta Part A Mol. Biomol. Spectrosc.*, **2018**, *198*, 212–221.

[317] Hazra, M.; Dolai, T.; Pandey, A.; Dey, S. K.; Patra, A. Synthesis and Characterisation of Copper(II) Complexes with Tridentate NNO Functionalized Ligand: Density Function Theory Study, DNA Binding Mechanism, Optical Properties, and Biological Application. *Bioinorg. Chem. Appl.*, **2014**, *2014*, 1–13.

[318] Tyagi, P.; Chandra, S.; Saraswat, B. S.; Yadav, D. Design, Spectral Characterization, Thermal, DFT Studies and Anticancer Cell Line Activities of Co(II), Ni(II) and Cu(II) Complexes of Schiff Bases Derived from 4-Amino-5-(Pyridin-4-Yl)-4H-1,2,4-Triazole-3-Thiol. *Spectrochim. Acta Part a Mol. Biomol. Spectrosc.*, **2015**, *145*, 127–137. https://doi.org/http://dx.doi.org/10.1016/j.saa.2015.03.034.

[319] El-Sonbati, A. Z.; Diab, M. A.; Eldesoky, A. M.; Morgan, S. M.; Salem, O. L. Polymer Complexes. LXXVI. Synthesis, Characterization, CT-DNA Binding, Molecular Docking and Thermal Studies of Sulfoxine Polymer Complexes. *Appl. Organomet. Chem.*, **2019**, *33* (5), 1–22. https://doi.org/10.1002/aoc.4839.

[320] Chiriac, H.; Moga, A. E.; Gherasim, C. Synthesis and Characterization of Co and Ni Magnetic Nanoparticles. *J. Optoelectron. Adv. Mater.*, **2008**, *10* (3), 654–658.

[321] Aiyelabola, T.; Akinkunmi, E. Synthesis Characterization and Biological Activities of Coordination Compounds of 4-Hydroxy-3-Nitro-2 H-Chromen-2-One and Its Aminoethanoic Acid and Pyrrolidine-2-Carboxylic Acid Mixed Ligand Complexes. *Bioinorg. Chem. Appl.*, **2017**, *2017* (January), 1–9.

[322] Orabi, A. S.; Abbas, A. M.; Sallam, S. A. Spectral, Magnetic, Thermal, and DNA Interaction of Ni(II) Complexes of Glutamic Acid Schiff Bases. *Synth. React. Inorganic, Met. Nano-Metal Chem.*, **2013**, *43* (1), 63–75.

[323] Wang, J.; Cui, C.; Gao, G.; Zhou, X.; Wu, J.; Yang, H.; Li, Q.; Wu, G. A New Method to Prepare Vanadium Oxide Nano-Urchins as a Cathode for Lithium Ion Batteries. *RSC Adv.*, **2015**, *5* (59), 47522–47528. https://doi.org/10.1039/c5ra02508g.

[324] Devi, R. K. B.; Devi, S. P.; Singh, R. K. H. Synthesis, Characterization and DNA

Interaction Study of a New Oxovanadium (IV) Complex Containing Acetylacetone and Dicyandiamide as Ligands. *Spectrosc. Lett.*, **2012**, *45* (2), 93–103.

[325] Srivastva, A. N.; Singh, N. P.; Shriwastaw, C. K. In Vitro Antibacterial and Antifungal Activities of Binuclear Transition Metal Complexes of ONNO Schiff Base and 5-Methyl-2,6-Pyrimidine-Dione and Their Spectroscopic Validation. *Arab. J. Chem.*, **2016**, *9* (1), 48–61. https://doi.org/10.1016/j.arabjc.2014.10.004.

[326] Sridharan, K. *Spectral Methods in Transition Metal Complexes*; 2016.

[327] Morgan, S. M.; El-Sonbati, A. Z.; Eissa, H. R. Geometrical Structures, Thermal Properties and Spectroscopic Studies of Schiff Base Complexes: Correlation between Ionic Radius of Metal Complexes and DNA Binding. *J. Mol. Liq.*, **2017**, *240*, 752–776. https://doi.org/10.1016/j.molliq.2017.05.114.

[328] El-Metwaly, N.; Althagafi, I.; Khedr, A. M.; Al-Fahemi, J. H.; Katouah, H. A.; Hossan, A. S.; Al-Dawood, A. Y.; Al-Hazmi, G. A. Synthesis and Characterization for Novel Cu(II)-Thiazole Complexes-Dyes and Their Usage in Dyeing Cotton to Be Special Bandage for Cancerous Wounds. *J. Mol. Struct.*, **2019**, *1194*, 86–103.

[329] Refat, M. S.; El-Sayed, M. Y.; Adam, A. M. A. Cu(II), Co(II) and Ni(II) Complexes of New Schiff Base Ligand: Synthesis, Thermal and Spectroscopic Characterizations. *J. Mol. Struct.*, **2013**, *1038*, 62–72. https://doi.org/10.1016/j.molstruc.2013.01.059.

[330] Bursey, M. M. *Mass Spectrometry of Inorganic and Organometallic Compounds*; 1974; Vol. 57. https://doi.org/10.1093/jaoac/57.2.421.

[331] Chandra, S.; Kumar, U. Spectral and Magnetic Studies on Manganese(II), Cobalt(II) and Nickel(II) Complexes with Schiff Bases. *Spectrochim. Acta - Part A Mol. Biomol. Spectrosc.*, **2005**, *61* (1–2), 219–224. https://doi.org/10.1016/j.saa.2004.03.036.

[332] Mahmoud, W. H.; Mohamed, G. G.; Elsawy, H. A.; Radwan, M. A. Metal Complexes of Novel Schiff Base Derived from the Condensation of 2-Quinoline Carboxaldehyde and Ambroxol Drug with Some Transition Metal Ions. *Appl. Organomet. Chem.*, **2018**, *32* (7), 1–14. https://doi.org/10.1002/aoc.4392.

[333] Badwaik, V. B.; Deshmukh, R. D.; Aswar, A. S. Transition Metal Complexes of a Schiff Base: Synthesis, Characterization, and Antibacterial Studies. *J. Coord. Chem.*, **2009**, *62* (12), 2037–2047. https://doi.org/10.1080/00958970902741244.

[334] Zordok, W. A.; Sadeek, S. A. Synthesis, Spectroscopic Characterization, Biological Studies and DFT Calculations on Some Transition Metal Complexes of NO Donor Ligand. *J. Mol. Struct.*, **2018**, *1158*, 205–220. https://doi.org/10.1016/j.molstruc.2018.01.030.

[335] Niu, M. J.; Li, Z.; Chang, G. L.; Kong, X. J.; Hong, M.; Zhang, Q. Crystal Structure, Cytotoxicity and Interaction with DNA of Zinc (II) Complexes with o-Vanillin Schiff Base Ligands. *PLoS One*, **2015**, *10* (6), 1–14.

[336] Halevas, E.; Mavroidi, B.; Pelecanou, M.; Hatzidimitriou, A. G. Structurally Characterized Zinc Complexes of Flavonoids Chrysin and Quercetin with Antioxidant Potential. *Inorganica Chim. Acta*, **2021**, *523* (January), 1–11.

[337] Krasnovskaya, O.; Naumov, A.; Guk, D.; Gorelkin, P.; Erofeev, A.; Beloglazkina, E.; Majouga, A. Copper Coordination Compounds as Biologically Active Agents. *Int. J. Mol. Sci.*, **2020**, *21* (11). https://doi.org/10.3390/ijms21113965.

[338] Panhwar, Q. K.; Memon, S.; Bhanger, M. I. Synthesis, Characterization, Spectroscopic and Antioxidation Studies of Cu(II)-Morin Complex. *J. Mol. Struct.*, **2010**, *967* (1–3), 47–53. https://doi.org/10.1016/j.molstruc.2009.12.037.

[339] Konarikova, K.; Andrezalova, L.; Rapta, P. Effect of the Schiff Base Complex Diaqua-(N-Salicylidene-l-Glutamato) Copper(II) Monohydrate on Human Tumor Cells. *Eur. J. Pharmacol.*, **2013**, *721* (1–3), 178–184. https://doi.org/10.1016/j.ejphar.2013.09.038.

[340] Sharfalddin, A. A.; Emwas, A. H.; Jaremko, M.; Hussien, M. A. Practical and Computational Studies of Bivalence Metal Complexes of Sulfaclozine and Biological Studies. *Front. Chem.*, **2021**, *9* (June), 1–16.

[341] Bhuiya, S.; Chowdhury, S.; Haque, L.; Das, S. Spectroscopic, Photophysical and Theoretical Insight into the Chelation Properties of Fisetin with Copper (II) in Aqueous Buffered Solutions for Calf Thymus DNA Binding. *Int. J. Biol. Macromol.*, **2018**, *120* (Ii), 1156–1169. https://doi.org/10.1016/j.ijbiomac.2018.08.162.

[342] Li, X.; Zhang, Y.; Xu, Y. Modified Asynchronous Orthogonal Sample Design Scheme @ Job's Method to Determine the Stoichiometric Ratio in the Molecular Association System. *J. Mol. Struct.*, **2020**, *1206*, 1–7.

[343] Kale, K. B.; Shinde, M. A. S. A.; Patil, R. H.; Ottoor, D. P. Exploring the Interaction of Valsartan and Valsartan-Zn(Ll) Complex with DNA by Spectroscopic and in Silico Methods. *Spectrochim. Acta - Part A Mol. Biomol. Spectrosc.*, **2022**, *264*, 1–13.

[344] Balajee, R.; Srinivasadesikan, V.; Sakthivadivel, M.; Gunasekaran, P. In Silico Screening, Alanine Mutation, and DFT Approaches for Identification of NS2B/NS3 Protease Inhibitors. *Biochem. Res. Int.*, **2016**, *2016*, 1–13.

[345] Khojasteh, S. C.; Wong, H.; Hop, C. E. C. A. *Drug Metabolism and Pharmacokinetics Quick Guide*; 2011. https://doi.org/10.1007/978-1-4419-5629-3.

[346] Al Zoubi, W.; Al-Hamdani, A. A. S.; Kaseem, M. Synthesis and Antioxidant Activities

of Schiff Bases and Their Complexes: A Review. *Appl. Organomet. Chem.*, **2016**, *30* (10), 810–817. https://doi.org/10.1002/aoc.3506.

[347] Hamdani, S. S.; Khan, B. A.; Ahmed, M. N.; Hameed, S.; Akhter, K.; Ayub, K.; Mahmood, T. Synthesis, Crystal Structures, Computational Studies and α-Amylase Inhibition of Three Novel 1,3,4-Oxadiazole Derivatives. *J. Mol. Struct.*, **2020**, *1200*, 1–9. https://doi.org/10.1016/j.molstruc.2019.127085.

[348] Pearson, R. G. Hard and Soft Acids and Bases , HSAB , Part I Fundamental Principles. *J. Chemi. Educ.*, **1968**, *45* (9), 581–587.

[349] Akbar Ali, M.; Mirza, A. H.; Bujang, F. H.; Hamid, M. H. S. A.; Bernhardt, P. V. Synthesis, Characterization and X-Ray Crystallographic Structural Study of Copper(II) and Nickel(II) Complexes of the 2-Quinoline Carboxaldehyde Schiff Base of S-Methyldithiocarbazate (Hqaldsme). *Polyhedron*, **2006**, *25* (17), 3245–3252.

[350] Andrade, G. R.; Kunsminskas, J.; Pizzuti, L.; Dos Anjos, A.; Inglez, S. D.; Tirloni, B.; Suegama, P. H. Synthesis and X-Ray Structural Characterization of Square-Pyramidal Copper(II) Complex with Aminoguanidine Derivative. *Inorg. Chem. Commun.*, **2015**, *61*, 210–213. https://doi.org/10.1016/j.inoche.2015.09.022.

[351] Habibi, M.; Beyramabadi, S. A.; Allameh, S.; Khashi, M.; Morsali, A.; Pordel, M.; Khorsandi-Chenarboo, M. Synthesis, Experimental and Theoretical Characterizations of a New Schiff Base Derived from 2-Pyridincarboxaldehyde and Its Ni (II) Complex. *J. Mol. Struct.*, **2017**, *1143*, 424–430. https://doi.org/10.1016/j.molstruc.2017.04.114.

[352] Collin, F.; Karkare, S.; Maxwell, A. Exploiting Bacterial DNA Gyrase as a Drug Target: Current State and Perspectives. *Appl. Microbiol. Biotechnol.*, **2011**, *92* (3), 479–497. https://doi.org/10.1007/s00253-011-3557-z.

[353] Kostylev, M.; Kim, D. Y.; Smalley, N. E.; Salukhe, I.; Peter Greenberg, E.; Dandekar, A. A. Evolution of the Pseudomonas Aeruginosa Quorum-Sensing Hierarchy. *Proc. Natl. Acad. Sci. U. S. A.*, **2019**, *116* (14), 7027–7032.

[354] Suneby, E. G.; Herndon, L. R.; Schneider, T. L. Pseudomonas Aeruginosa LasR·DNA Binding Is Directly Inhibited by Quorum Sensing Antagonists. *ACS Infect. Dis.*, **2017**, *3* (3), 183–189. https://doi.org/10.1021/acsinfecdis.6b00163.

[355] Hussein, R. K.; Elkhair, H. M. Molecular Docking Identification for the Efficacy of Some Zinc Complexes with Chloroquine and Hydroxychloroquine against Main Protease of COVID-19. *J. Mol. Struct.*, **2021**, *1231*, 1–9.

APPENDIXES

Appendix 1. One-way analysis of variance of **L1** and its **1 – 5** complexes

Table Analyzed	E. Coli				
One-way analysis of variance					
P value	< 0.0001				
P value summary	***				
Are means signif. different? (P < 0.05)	Yes				
Number of groups	7				
F	476.6				
R squared	0.9951				
ANOVA Table	SS	df	MS		
Treatment (between columns)	476.1	6	79.34		
Residual (within columns)	2.331	14	0.1665		
Total	478.4	20			
Bonferroni's Multiple Comparison Test	Mean Diff.	t	Significant? P < 0.05?	Summary	95% CI of diff
1 vs 2	-2.070	6.213	Yes	***	-3.302 to -0.8376
1 vs 3	-0.1600	0.4802	No	ns	-1.392 to 1.072
1 vs 4	2.620	7.864	Yes	***	1.388 to 3.852
1 vs 5	3.300	9.905	Yes	***	2.068 to 4.532
1 vs Ligand	4.400	13.21	Yes	***	3.168 to 5.632
1 vs Ciprofloxacin	-10.88	32.66	Yes	***	-12.11 to -9.648
2 vs 3	1.910	5.733	Yes	**	0.6776 to 3.142
2 vs 4	4.690	14.08	Yes	***	3.458 to 5.922
2 vs 5	5.370	16.12	Yes	***	4.138 to 6.602
2 vs Ligand	6.470	19.42	Yes	***	5.238 to 7.702
2 vs Ciprofloxacin	-8.810	26.44	Yes	***	-10.04 to -7.578
3 vs 4	2.780	8.344	Yes	***	1.548 to 4.012
3 vs 5	3.460	10.39	Yes	***	2.228 to 4.692
3 vs Ligand	4.560	13.69	Yes	***	3.328 to 5.792
3 vs Ciprofloxacin	-10.72	32.18	Yes	***	-11.95 to -9.488
4 vs 5	0.6800	2.041	No	ns	-0.5524 to 1.912
4 vs Ligand	1.780	5.343	Yes	**	0.5476 to 3.012
4 vs Ciprofloxacin	-13.50	40.52	Yes	***	-14.73 to -12.27
5 vs Ligand	1.100	3.302	No	ns	-0.1324 to 2.332
5 vs Ciprofloxacin	-14.18	42.56	Yes	***	-15.41 to -12.95
Ligand vs Ciprofloxacin	-15.28	45.86	Yes	***	-16.51 to -14.05

Table Analyzed	P. Aeruginosa				
One-way analysis of variance					
P value	< 0.0001				
P value summary	***				
Are means signif. different? (P < 0.05)	Yes				
Number of groups	7				
F	3040				
R squared	0.9992				
ANOVA Table	SS	df	MS		
Treatment (between columns)	1034	6	172.3		
Residual (within columns)	0.7936	14	0.05669		
Total	1035	20			
Tukey's Multiple Comparison Test	Mean Diff.	q	Significant? P < 0.05?	Summary	95% CI of diff
1 vs 2	-1.820	13.24	Yes	***	-2.484 to -1.156
1 vs 3	-1.180	8.584	Yes	***	-1.844 to -0.5162
1 vs 4	1.620	11.79	Yes	***	0.9562 to 2.284
1 vs 5	16.69	121.4	Yes	***	16.03 to 17.35
1 vs Ligand	10.69	77.77	Yes	***	10.03 to 11.35
1 vs Ciprofloxacin	-3.830	27.86	Yes	***	-4.494 to -3.166
2 vs 3	0.6400	4.656	No	ns	-0.02379 to 1.304
2 vs 4	3.440	25.03	Yes	***	2.776 to 4.104
2 vs 5	18.51	134.7	Yes	***	17.85 to 19.17
2 vs Ligand	12.51	91.01	Yes	***	11.85 to 13.17
2 vs Ciprofloxacin	-2.010	14.62	Yes	***	-2.674 to -1.346
3 vs 4	2.800	20.37	Yes	***	2.136 to 3.464
3 vs 5	17.87	130.0	Yes	***	17.21 to 18.53
3 vs Ligand	11.87	86.35	Yes	***	11.21 to 12.53
3 vs Ciprofloxacin	-2.650	19.28	Yes	***	-3.314 to -1.986
4 vs 5	15.07	109.6	Yes	***	14.41 to 15.73
4 vs Ligand	9.070	65.98	Yes	***	8.406 to 9.734

4 vs Ciprofloxacin	-5.450	39.65	Yes	***	-6.114 to -4.786
5 vs Ligand	-6.000	43.65	Yes	***	-6.664 to -5.336
5 vs Ciprofloxacin	-20.52	149.3	Yes	***	-21.18 to -19.86
Ligand vs Ciprofloxacin	-14.52	105.6	Yes	***	-15.18 to -13.86

Table Analyzed	S. Aureus				
One-way analysis of variance					
P value	< 0.0001				
P value summary	***				
Are means signif. different? (P < 0.05)	Yes				
Number of groups	7				
F	767.5				
R squared	0.9970				
ANOVA Table	SS	df	MS		
Treatment (between columns)	723.6	6	120.6		
Residual (within columns)	2.200	14	0.1571		
Total	725.8	20			
Tukey's Multiple Comparison Test	Mean Diff.	q	Significant? P < 0.05?	Summary	95% CI of diff
1 vs 2	-5.800	25.34	Yes	***	-6.905 to -4.695
1 vs 3	-0.8100	3.539	No	ns	-1.915 to 0.2952
1 vs 4	-1.200	5.243	Yes	*	-2.305 to -0.09479
1 vs 5	4.300	18.79	Yes	***	3.195 to 5.405
1 vs Ligand	11.30	49.37	Yes	***	10.19 to 12.41
1 vs Ciprofloxacin	-7.700	33.64	Yes	***	-8.805 to -6.595
2 vs 3	4.990	21.80	Yes	***	3.885 to 6.095
2 vs 4	4.600	20.10	Yes	***	3.495 to 5.705
2 vs 5	10.10	44.13	Yes	***	8.995 to 11.21
2 vs Ligand	17.10	74.72	Yes	***	15.99 to 18.21
2 vs Ciprofloxacin	-1.900	8.302	Yes	***	-3.005 to -0.7948
3 vs 4	-0.3900	1.704	No	ns	-1.495 to 0.7152
3 vs 5	5.110	22.33	Yes	***	4.005 to 6.215
3 vs Ligand	12.11	52.91	Yes	***	11.00 to 13.22
3 vs Ciprofloxacin	-6.890	30.10	Yes	***	-7.995 to -5.785
4 vs 5	5.500	24.03	Yes	***	4.395 to 6.605
4 vs Ligand	12.50	54.62	Yes	***	11.39 to 13.61
4 vs Ciprofloxacin	-6.500	28.40	Yes	***	-7.605 to -5.395
5 vs Ligand	7.000	30.59	Yes	***	5.895 to 8.105
5 vs Ciprofloxacin	-12.00	52.43	Yes	***	-13.11 to -10.89
Ligand vs Ciprofloxacin	-19.00	83.02	Yes	***	-20.11 to -17.89

Table Analyzed	S. Pyogenes				
One-way analysis of variance					
P value	< 0.0001				
P value summary	***				
Are means signif. different? (P < 0.05)	Yes				
Number of groups	7				
F	673.1				
R squared	0.9965				
ANOVA Table	SS	df	MS		
Treatment (between columns)	689.7	6	115.0		
Residual (within columns)	2.391	14	0.1708		
Total	692.1	20			
Tukey's Multiple Comparison Test	Mean Diff.	q	Significant? P < 0.05?	Summary	95% CI of diff
1 vs 2	1.720	7.209	Yes	**	0.5678 to 2.872
1 vs 3	10.22	42.83	Yes	***	9.068 to 11.37
1 vs 4	10.22	42.83	Yes	***	9.068 to 11.37
1 vs 5	10.22	42.83	Yes	***	9.068 to 11.37
1 vs Ligand	4.020	16.85	Yes	***	2.868 to 5.172
1 vs Ciprofloxacin	-5.680	23.81	Yes	***	-6.832 to -4.528
2 vs 3	8.500	35.62	Yes	***	7.348 to 9.652
2 vs 4	8.500	35.62	Yes	***	7.348 to 9.652
2 vs 5	8.500	35.62	Yes	***	7.348 to 9.652
2 vs Ligand	2.300	9.640	Yes	***	1.148 to 3.452
2 vs Ciprofloxacin	-7.400	31.01	Yes	***	-8.552 to -6.248
3 vs 4	0.0000	0.0000	No	ns	-1.152 to 1.152
3 vs 5	0.0000	0.0000	No	ns	-1.152 to 1.152
3 vs Ligand	-6.200	25.99	Yes	***	-7.352 to -5.048
3 vs Ciprofloxacin	-15.90	66.64	Yes	***	-17.05 to -14.75

4 vs 5	0.0000	0.0000	No	ns	-1.152 to 1.152
4 vs Ligand	-6.200	25.99	Yes	***	-7.352 to -5.048
4 vs Ciprofloxacin	-15.90	66.64	Yes	***	-17.05 to -14.75
5 vs Ligand	-6.200	25.99	Yes	***	-7.352 to -5.048
5 vs Ciprofloxacin	-15.90	66.64	Yes	***	-17.05 to -14.75
Ligand vs Ciprofloxacin	-9.700	40.65	Yes	***	-10.85 to -8.548

Appendix 2. One-way analysis of variance of **L2** and its complexes **6 – 7**

Table Analyzed	***E. coli***				
Data sets analyzed	A-G				
ANOVA summary					
F	34.41				
P value	<0.0001				
P value summary	****				
Significant diff. among means (P < 0.05)?	Yes				
R squared	0.9672				
Brown-Forsythe test					
F (DFn, DFd)	3.178e+029 (6, 7)				
P value	<0.0001				
P value summary	****				
Are SDs significantly different (P < 0.05)?	Yes				
Bartlett's test					
Bartlett's statistic (corrected)					
P value					
P value summary					
Are SDs significantly different (P < 0.05)?					
ANOVA table	SS	DF	MS	F (DFn, DFd)	P value
Treatment (between columns)	171.5	6	28.59	F (6, 7) = 34.41	P<0.0001
Residual (within columns)	5.815	7	0.8307		
Total	177.3	13			
Data summary					
Number of treatments (columns)	7				
Number of values (total)	14				

Number of families	1							
Number of comparisons per family	6							
Alpha	0.05							
Dunnett's multiple comparisons test	Mean Diff.	95.00% CI of diff.	Below threshold?	Summary	Adjusted P Value	G-?		
Ciprofloxacin vs. Complex 6	5.500	2.464 to 8.536	Yes	**	0.0023	A	Complex 1	
Ciprofloxacin vs. Complex7	6.995	3.959 to 10.03	Yes	***	0.0005	B	Complex 2	
Ciprofloxacin vs. Complex 8	5.500	2.464 to 8.536	Yes	**	0.0023	C	Complex 3	
Ciprofloxacin vs. Complex 9	8.995	5.959 to 12.03	Yes	***	0.0001	D	Complex 4	
Ciprofloxacin vs. Complex 10	11.36	8.319 to 14.39	Yes	****	<0.0001	E	Complex 5	
Ciprofloxacin vs. Ligand	10.06	7.024 to 13.10	Yes	****	<0.0001	F	Ligand	
Test details	Mean 1	Mean 2	Mean Diff.	SE of diff.	n1	n2	q	DF
Ciprofloxacin vs. Complex 6	21.17	15.67	5.500	0.9115	2	2	6.034	7
Ciprofloxacin vs. Complex 7	21.17	14.17	6.995	0.9115	2	2	7.675	7
Ciprofloxacin vs. Complex 8	21.17	15.67	5.500	0.9115	2	2	6.034	7
Ciprofloxacin vs. Complex 9	21.17	12.17	8.995	0.9115	2	2	9.869	7
Ciprofloxacin vs. Complex 10	21.17	9.810	11.36	0.9115	2	2	12.46	7

Ciprofloxacin vs. Ligand	21.17	11.11	10.06	0.9115	2	2	11.04	7

Table Analyzed	P. aerug
Data sets analyzed	A-G
ANOVA summary	
F	40.14
P value	<0.0001
P value summary	****
Significant diff. among means (P < 0.05)?	Yes
R squared	0.9718
Brown-Forsythe test	
F (DFn, DFd)	5.683e+028 (6, 7)
P value	<0.0001
P value summary	****
Are SDs significantly different (P < 0.05)?	Yes
Bartlett's test	
Bartlett's statistic (corrected)	
P value	
P value summary	
Are SDs significantly different (P < 0.05)?	

ANOVA table	SS	DF	MS	F (DFn, DFd)	P value
Treatment (between columns)	264.2	6	44.03	F (6, 7) = 40.14	P<0.0001
Residual (within columns)	7.678	7	1.097		
Total	271.9	13			

Data summary	
Number of treatments (columns)	7
Number of values (total)	14

Number of families	1							
Number of comparisons per family	6							
Alpha	0.05							
Dunnett's multiple comparisons test	Mean Diff.	95.00% CI of diff.	Below threshold?	Summary	Adjusted P Value	G-?		
Ciprofloxacin vs. Complex 6	0.7550	-2.734 to 4.244	No	ns	0.9399	A	Complex 1	
Ciprofloxacin vs. Complex 7	0.2350	-3.254 to 3.724	No	ns	0.9997	B	Complex 2	
Ciprofloxacin vs. Complex 8	0.7550	-2.734 to 4.244	No	ns	0.9399	C	Complex 3	
Ciprofloxacin vs. Complex 9	2.235	-1.254 to 5.724	No	ns	0.2430	D	Complex 4	
Ciprofloxacin vs. Complex 10	8.965	5.476 to 12.45	Yes	***	0.0003	E	Complex 5	
Ciprofloxacin vs. Ligand	11.42	7.926 to 14.90	Yes	****	<0.0001	F	Ligand	

Test details	Mean 1	Mean 2	Mean Diff.	SE of diff.	n1	n2	q	DF
Ciprofloxacin vs. Complex 6	20.47	19.71	0.7550	1.047	2	2	0.7209	7
Ciprofloxacin vs. Complex 7	20.47	20.23	0.2350	1.047	2	2	0.2244	7
Ciprofloxacin vs. Complex 8	20.47	19.71	0.7550	1.047	2	2	0.7209	7
Ciprofloxacin vs. Complex 9	20.47	18.23	2.235	1.047	2	2	2.134	7
Ciprofloxacin vs. Complex 10	20.47	11.50	8.965	1.047	2	2	8.560	7
Ciprofloxacin vs. Ligand	20.47	9.050	11.42	1.047	2	2	10.90	7

Table Analyzed	S. aureus				
Data sets analyzed	A-G				
ANOVA summary					
F	75.58				
P value	<0.0001				
P value summary	****				
Significant diff. among means (P < 0.05)?	Yes				
R squared	0.9848				
Brown-Forsythe test					
F (DFn, DFd)	4.666e+028 (6, 7)				
P value	<0.0001				
P value summary	****				
Are SDs significantly different (P < 0.05)?	Yes				
Bartlett's test					
Bartlett's statistic (corrected)					
P value					
P value summary					
Are SDs significantly different (P < 0.05)?					
ANOVA table	SS	DF	MS	F (DFn, DFd)	P value
Treatment (between columns)	263.7	6	43.96	F (6, 7) = 75.58	P<0.0001
Residual (within columns)	4.071	7	0.5816		
Total	267.8	13			
Data summary					
Number of treatments (columns)	7				
Number of values (total)	14				

Number of families	1							
Number of comparisons per family	6							
Alpha	0.05							
Dunnett's multiple comparisons test	Mean Diff.	95.00% CI of diff.	Below threshold?	Summary	Adjusted P Value	G-?		
Ciprofloxacin vs. Complex 6	7.035	4.494 to 9.576	Yes	***	0.0002	A	Complex 1	
Ciprofloxacin vs. Complex 7	2.065	-0.4756 to 4.606	No	ns	0.1140	B	Complex 2	
Ciprofloxacin vs. Complex 8	7.035	4.494 to 9.576	Yes	***	0.0002	C	Complex 3	
Ciprofloxacin vs. Complex 9	5.510	2.969 to 8.051	Yes	***	0.0008	D	Complex 4	
Ciprofloxacin vs. Complex 10	13.77	11.22 to 16.31	Yes	****	<0.0001	E	Complex 5	
Ciprofloxacin vs. Ligand	10.46	7.914 to 13.00	Yes	****	<0.0001	F	Ligand	
Test details	Mean 1	Mean 2	Mean Diff.	SE of diff.	n1	n2	q	DF
Ciprofloxacin vs. Complex 6	21.27	14.23	7.035	0.7626	2	2	9.225	7
Ciprofloxacin vs. Complex 7	21.27	19.20	2.065	0.7626	2	2	2.708	7
Ciprofloxacin vs. Complex 8	21.27	14.23	7.035	0.7626	2	2	9.225	7
Ciprofloxacin vs. Complex 9	21.27	15.76	5.510	0.7626	2	2	7.225	7
Ciprofloxacin vs. Complex 10	21.27	7.500	13.77	0.7626	2	2	18.05	7
Ciprofloxacin vs. Ligand	21.27	10.81	10.46	0.7626	2	2	13.71	7

Table Analyzed	S. pyogene				
Data sets analyzed	A-G				
ANOVA summary					
F	194.3				
P value	<0.0001				
P value summary	****				
Significant diff. among means (P < 0.05)?	Yes				
R squared	0.9940				

Brown-Forsythe test					
F (DFn, DFd)	2.066e+029 (6, 7)				
P value	<0.0001				
P value summary	****				
Are SDs significantly different (P < 0.05)?	Yes				
Bartlett's test					
Bartlett's statistic (corrected)					
P value					
P value summary					
Are SDs significantly different (P < 0.05)?					
ANOVA table	SS	DF	MS	F (DFn, DFd)	P value
Treatment (between columns)	630.2	6	105.0	F (6, 7) = 194.3	P<0.0001
Residual (within columns)	3.784	7	0.5406		
Total	634.0	13			
Data summary					
Number of treatments (columns)	7				
Number of values (total)	14				

Number of families	1							
Number of comparisons per family	6							
Alpha	0.05							
Dunnett's multiple comparisons test	Mean Diff.	95.00% CI of diff.	Below threshold?	Summary	Adjusted P Value	G-?		
Ciprofloxacin vs. Complex 6	8.065	5.616 to 10.51	Yes	****	<0.0001	A	Complex 1	
Ciprofloxacin vs. Complex 7	0.9950	-1.454 to 3.444	No	ns	0.6061	B	Complex 2	
Ciprofloxacin vs. Complex 8	1.040	-1.409 to 3.489	No	ns	0.5699	C	Complex 3	
Ciprofloxacin vs. Complex9	3.960	1.511 to 6.409	Yes	**	0.0044	D	Complex 4	
Ciprofloxacin vs. Complex 10	10.66	8.211 to 13.11	Yes	****	<0.0001	E	Complex 5	
Ciprofloxacin vs. Ligand	20.16	17.71 to 22.61	Yes	****	<0.0001	F	Ligand	
Test details	Mean 1	Mean 2	Mean Diff.	SE of diff.	n1	n2	q	DF
Ciprofloxacin vs. Complex 6	20.16	12.10	8.065	0.7353	2	2	10.97	7
Ciprofloxacin vs. Complex 7	20.16	19.17	0.9950	0.7353	2	2	1.353	7
Ciprofloxacin vs. Complex 8	20.16	19.12	1.040	0.7353	2	2	1.414	7
Ciprofloxacin vs. Complex 9	20.16	16.20	3.960	0.7353	2	2	5.386	7
Ciprofloxacin vs. Complex 10	20.16	9.500	10.66	0.7353	2	2	14.50	7
Ciprofloxacin vs. Ligand	20.16	0.000	20.16	0.7353	2	2	27.42	7

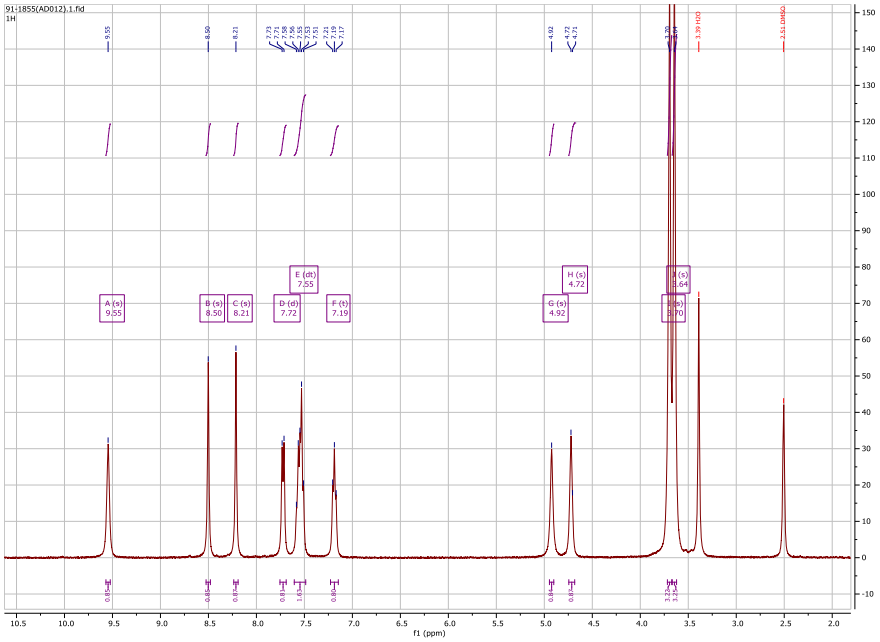

Appendix 3. ^{1}HNMR, spectrum of the ligand (**L1**)

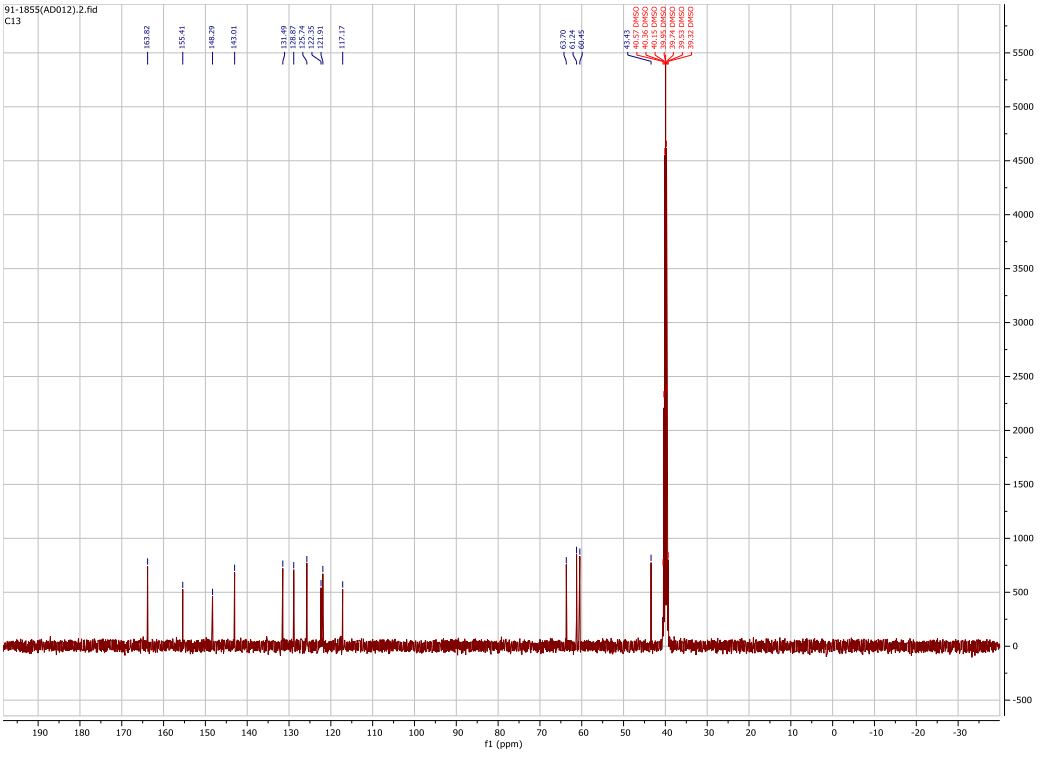

Appendix 4. ^{13}CNMR spectrum of the ligand (**L1**)

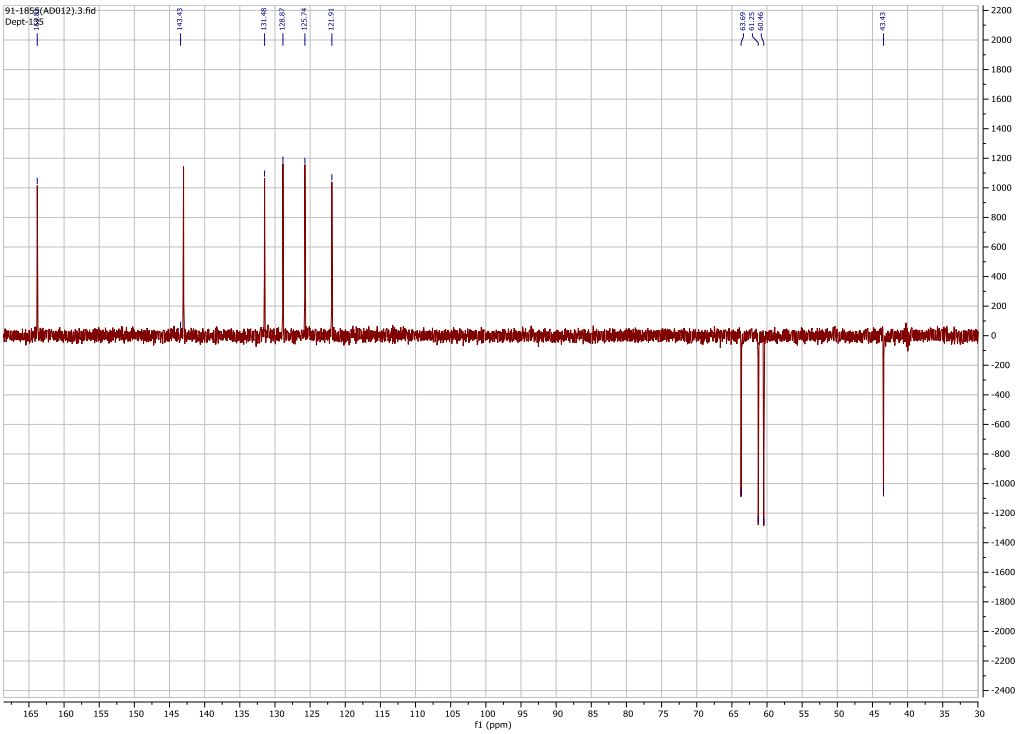

Appendix 5. 3DEPT-135 spectrum of the (ligand (**L1**)

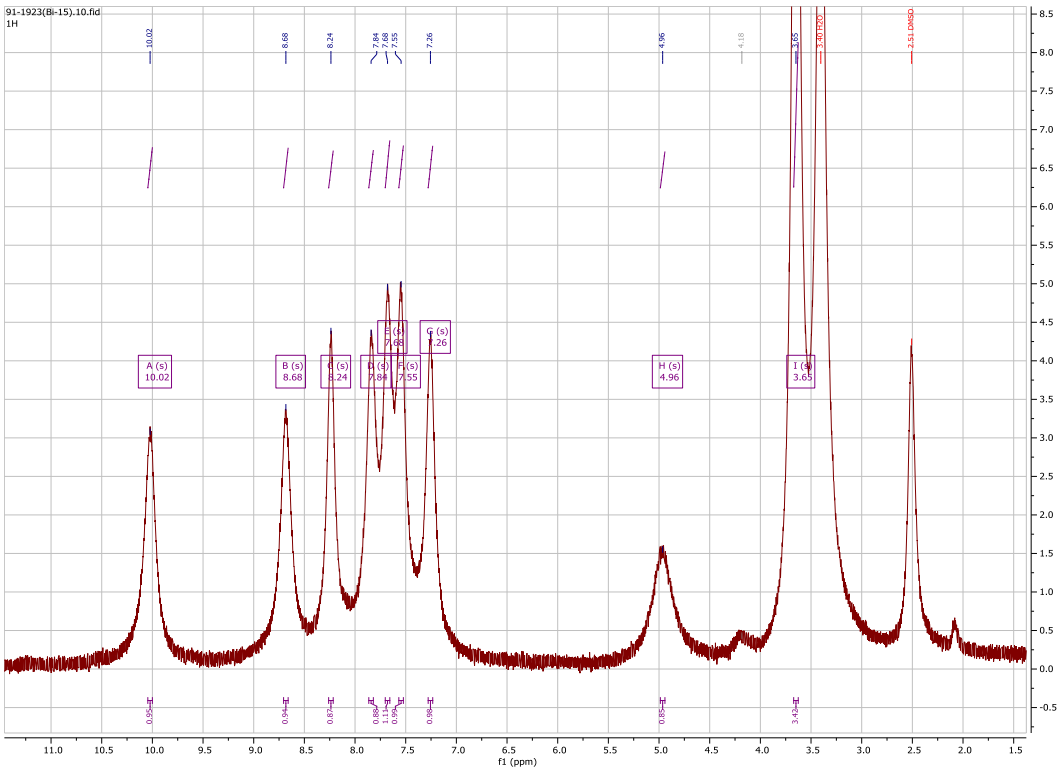

Appendix 6 ^{1}HNMR, spectrum of ligand (**L2**)

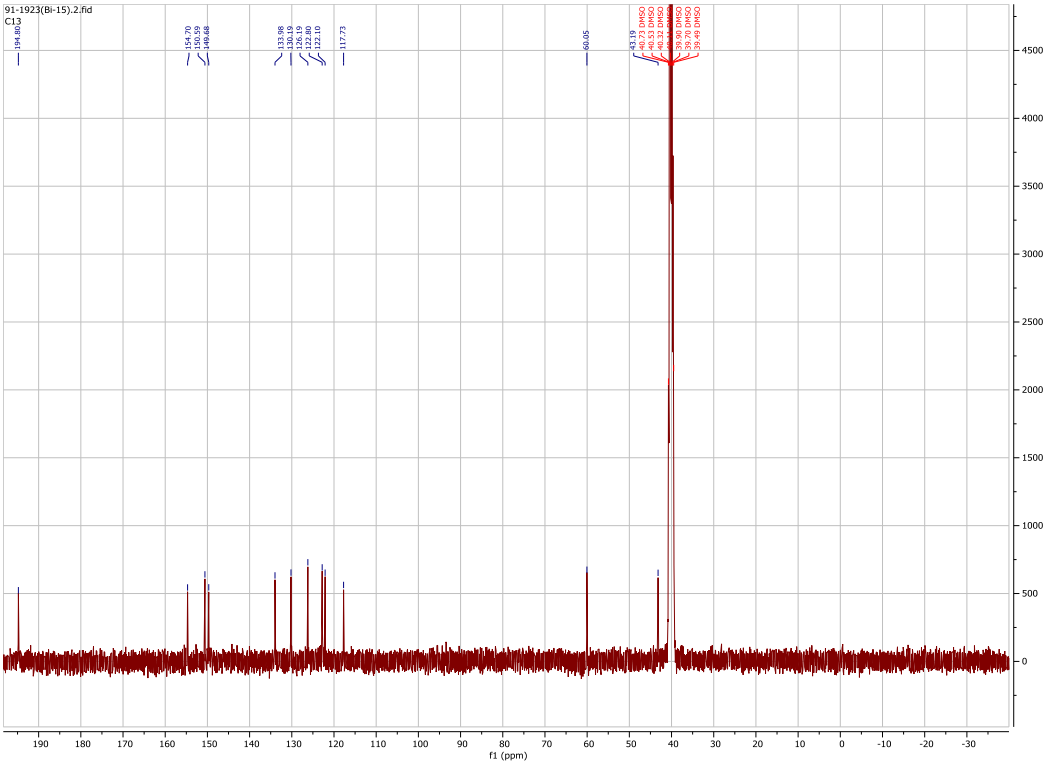

Appendix 7. ^{13}CNMR spectrum of ligand (**L2**)

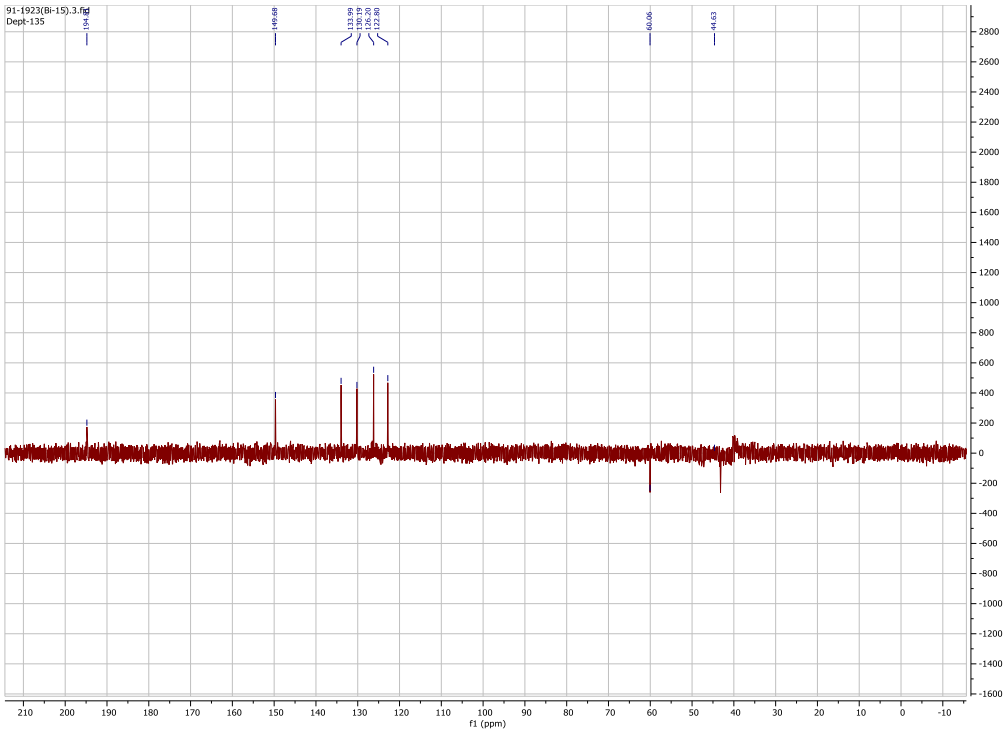

Appendix 8. DEPT-135 spectrum of ligand (**L2**)

Appendix 9. Wavelength, band assignment of ligands and their metal complexes

Compounds	Absorption (nm)	Transition
L1	223, 258, 300, 383	(π→π*), n→π*)
1	231, 258, 300, 380	(π→π*),(n→π*)
2	235, 267, 317, 406	(π→π*),(n→π*), LMCT
3	234, 258, 293, 427	(π→π*),(n→π*), LMCT
4	229, 259, 302, 401	(π→π*),(n→π*), LMCT
5	231, 260, 304, 409	(π→π*),(n→π*), LMCT
L2	231, 261, 305, 408	(π→π*), (n→π*)
6	231, 259, 303, 393	(π→π*), (n→π*)
7	255, 351	(n→π*), LMCT
8	231, 260, 304, 407	(π→π*), (n→π*), LMCT
9	229, 259, 302, 397	(π→π*), (n→π*) LMCT
10	231, 261, 305, 407	(π→π*), (n→π*), LMCT

Appendix 10. The absorption and emission of synthesised compounds

Compounds	Absorption λ_{max} (Intensity)	Emission λ_{max}(Intensity)
L1	383 (0.16)	526 (22.77)
1	380 (0.35)	608 (96.40)
2	401 (0.45)	511 (35.04)
3	409 (0.09)	521 (90.09)
4	427 (0.23)	420 (45.85)
5	406 (0.32)	471 (45.22)
L2	408 (0.10)	486 (102.05)
6	393 (0.09)	460 (483.91)
7	351 (0.25)	471 (835.57)
8	407 (0.03)	463 (126.93)
(9)	397 (0.03)	457 (47.55)
10	409 (0.20)	469 (324.89)

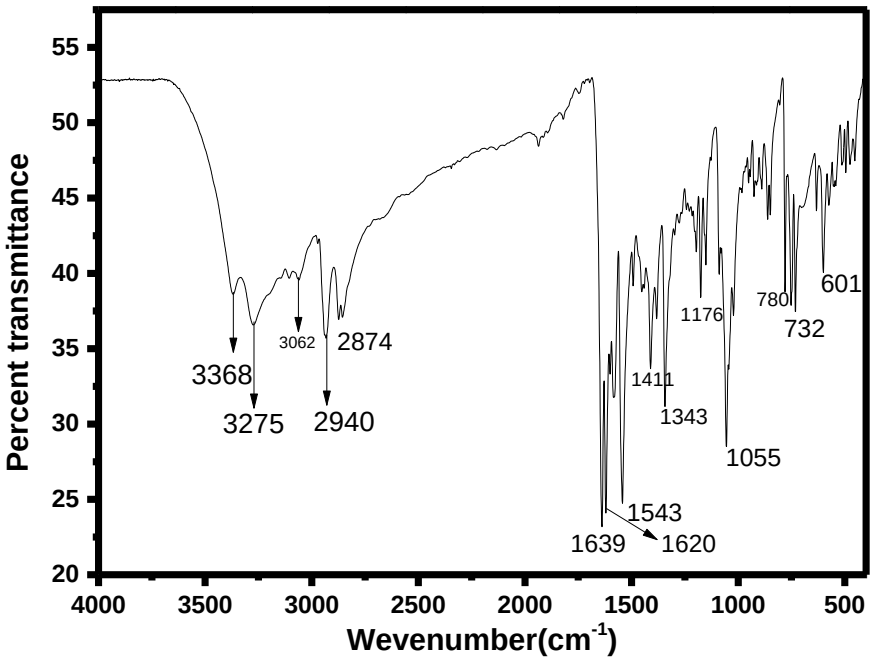

Appendix 11. FT-IR spectra of free ligand (**L1**)

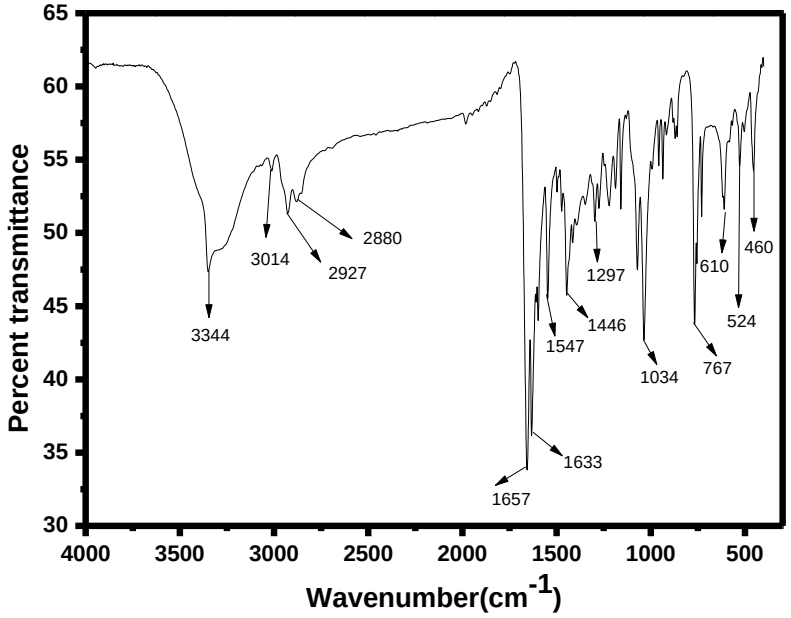

Appendix 12. FT-IR spectrum of complex **1**

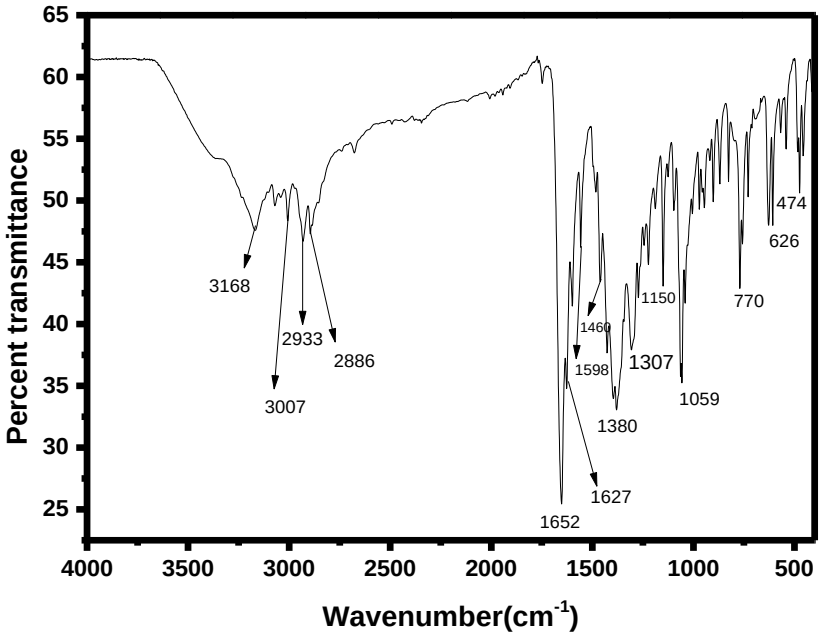

Appendix 13. FT-IR spectrum of complex **2**

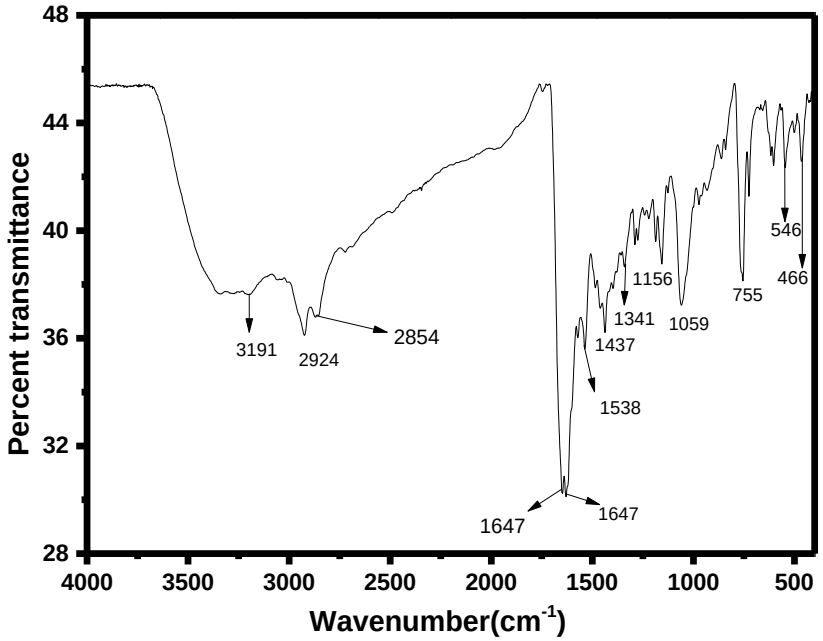

Appendix 14. FT-IR s spectrum of complex **3**

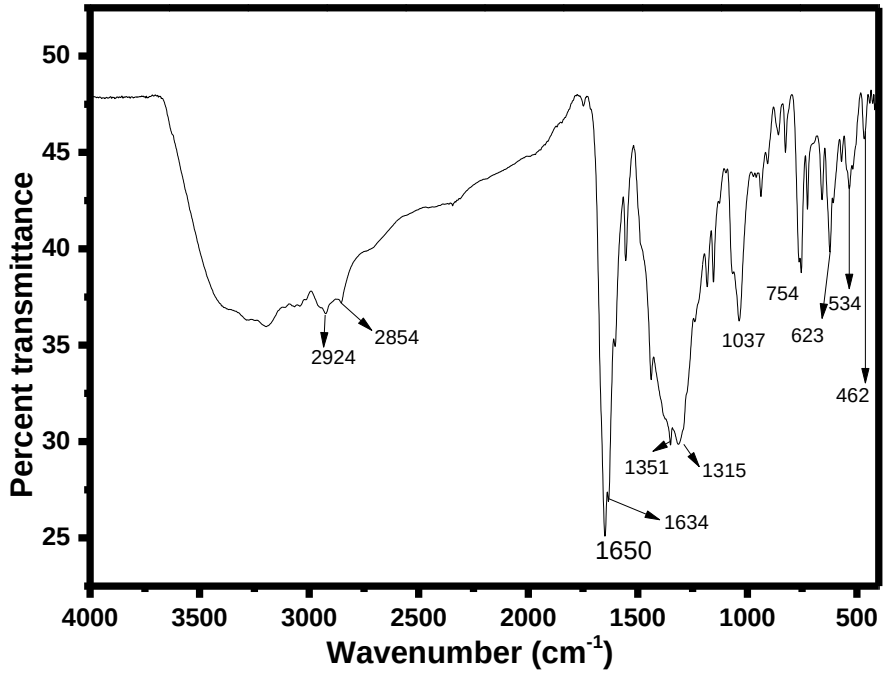

Appendix 15. FT-IR spectrum of complex **4**

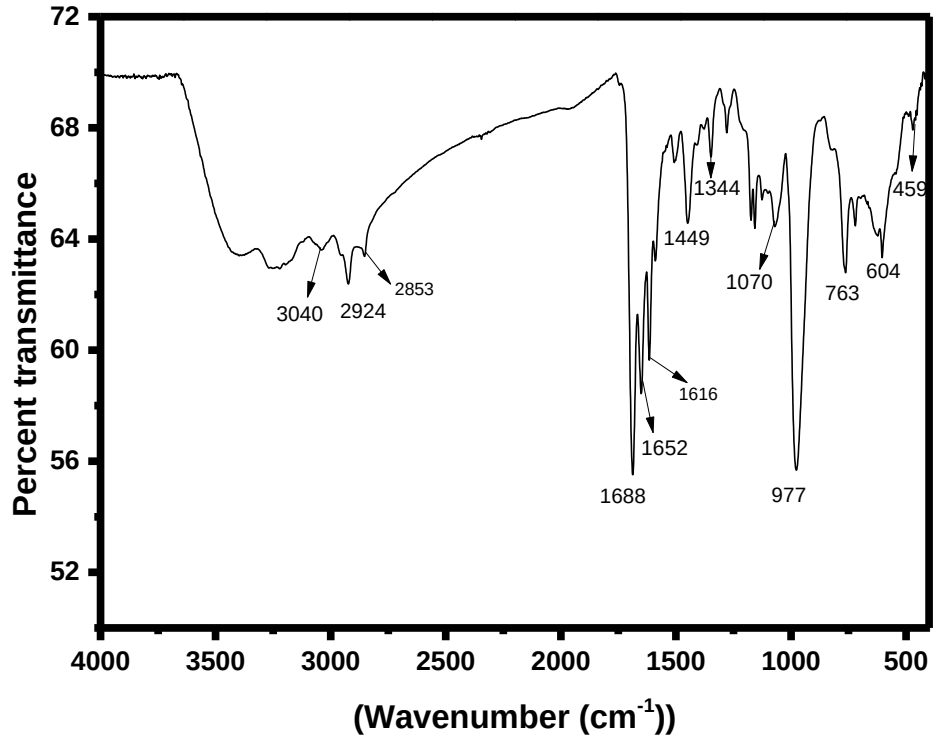

Appendix 16. FT-IR spectrum of complex **5**

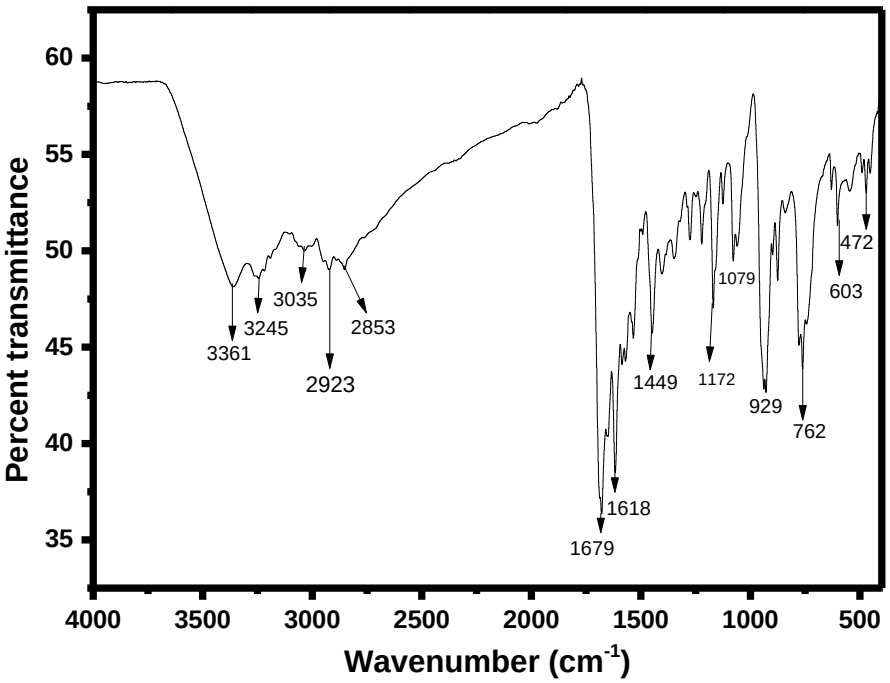

Appendix 17. FT-IR spectrum of: ligand **L2**

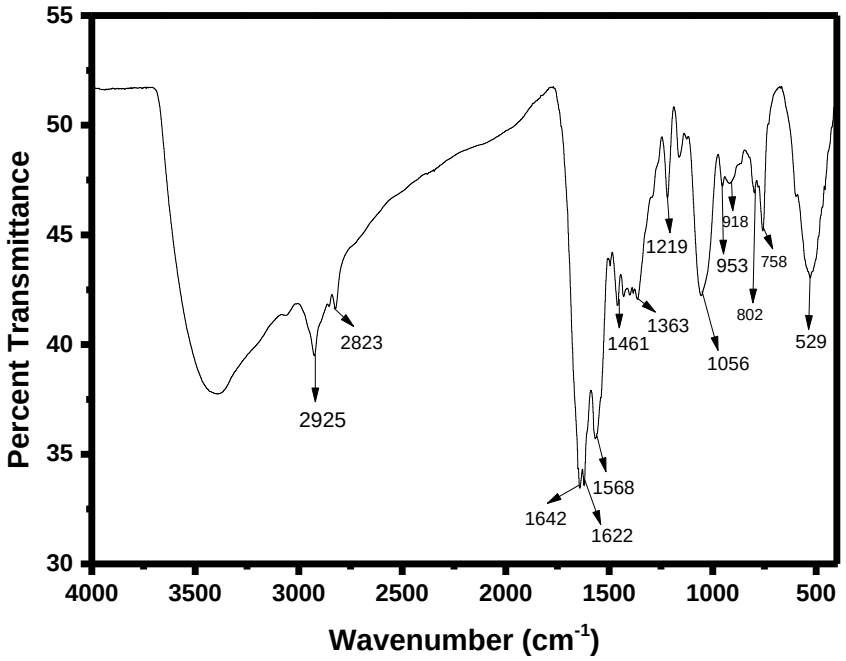

Appendix 18. FT-IR spectrum of complex **6**

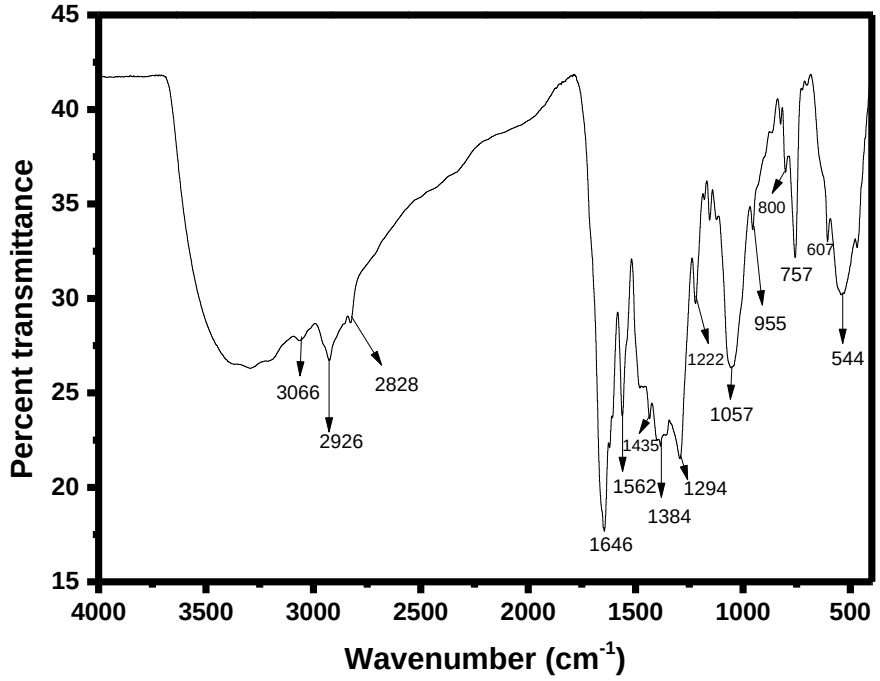

Appendix 19. FT-IR spectrum of complex **7**

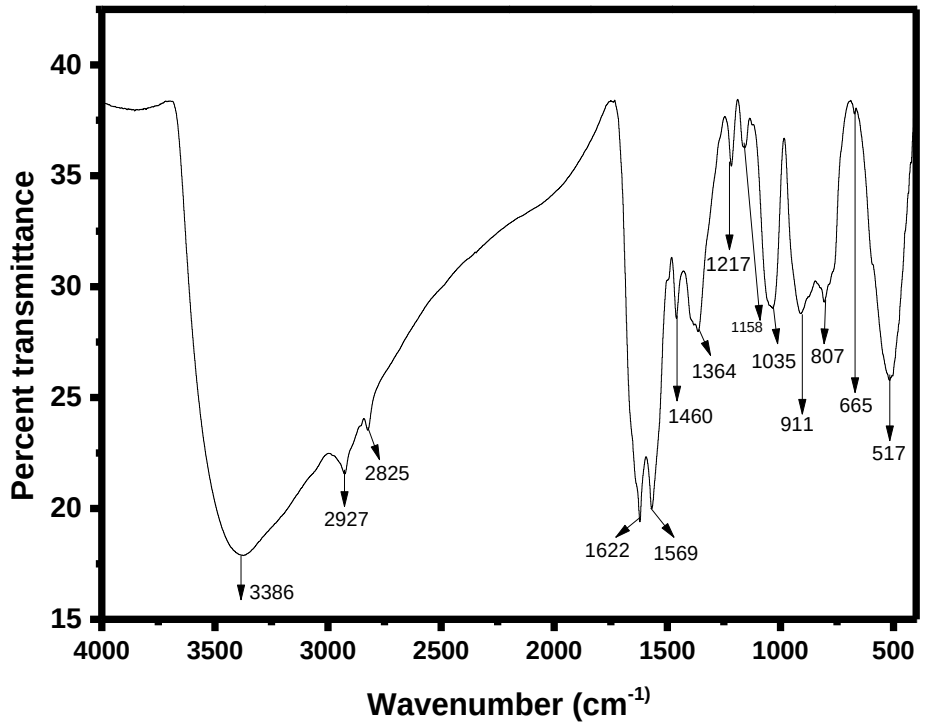

Appendix 20. FT-IR spectrum of complex **8**

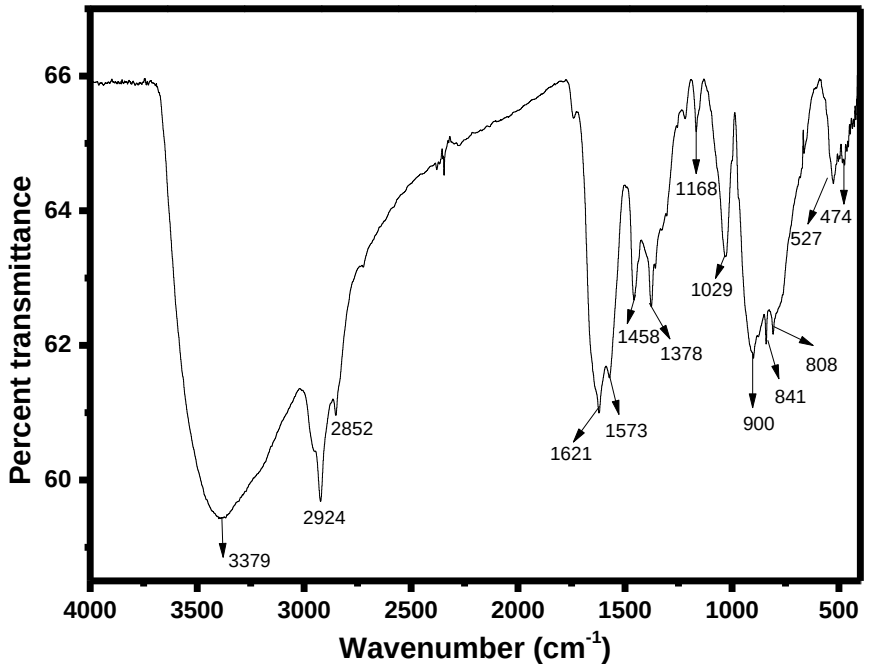

Appendix 21. FT-IR spectrum of complex **9**

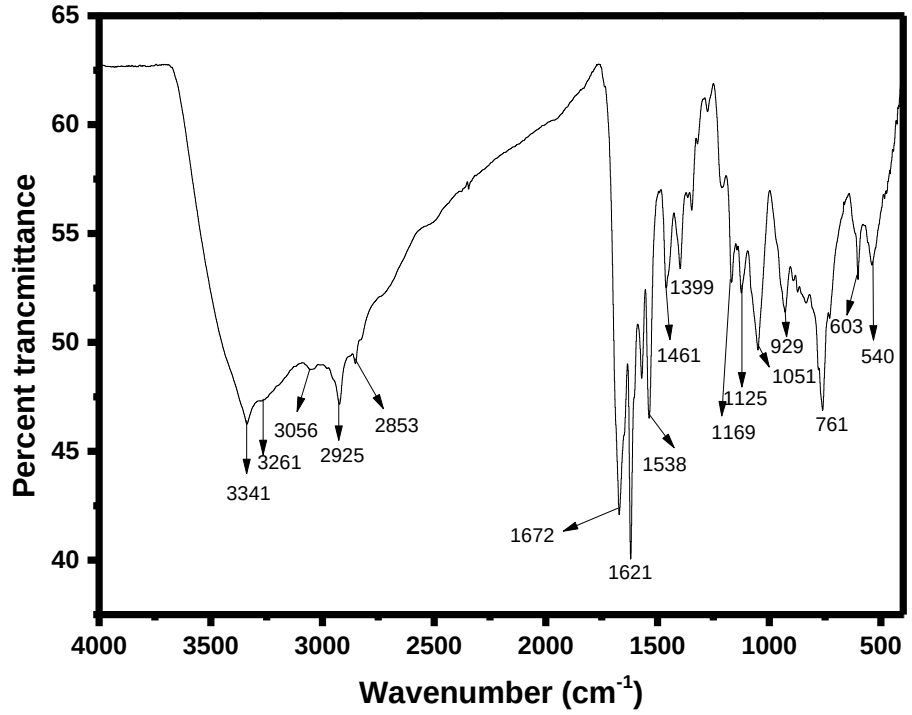

Appendix 22. FT-IR spectrum of complex **10**

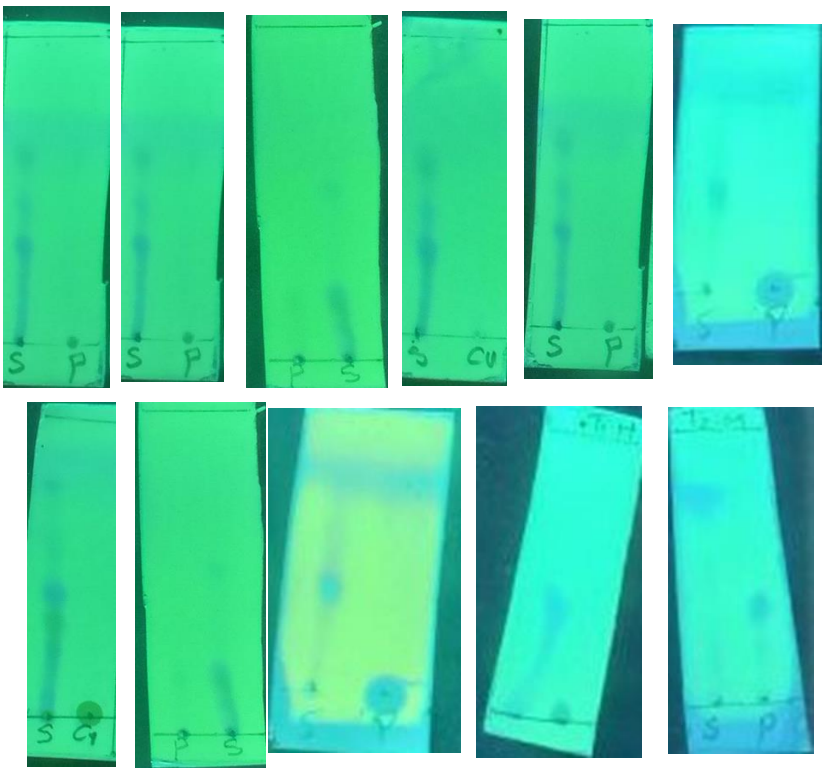

Appendix 23. Sample thin layer chromatography

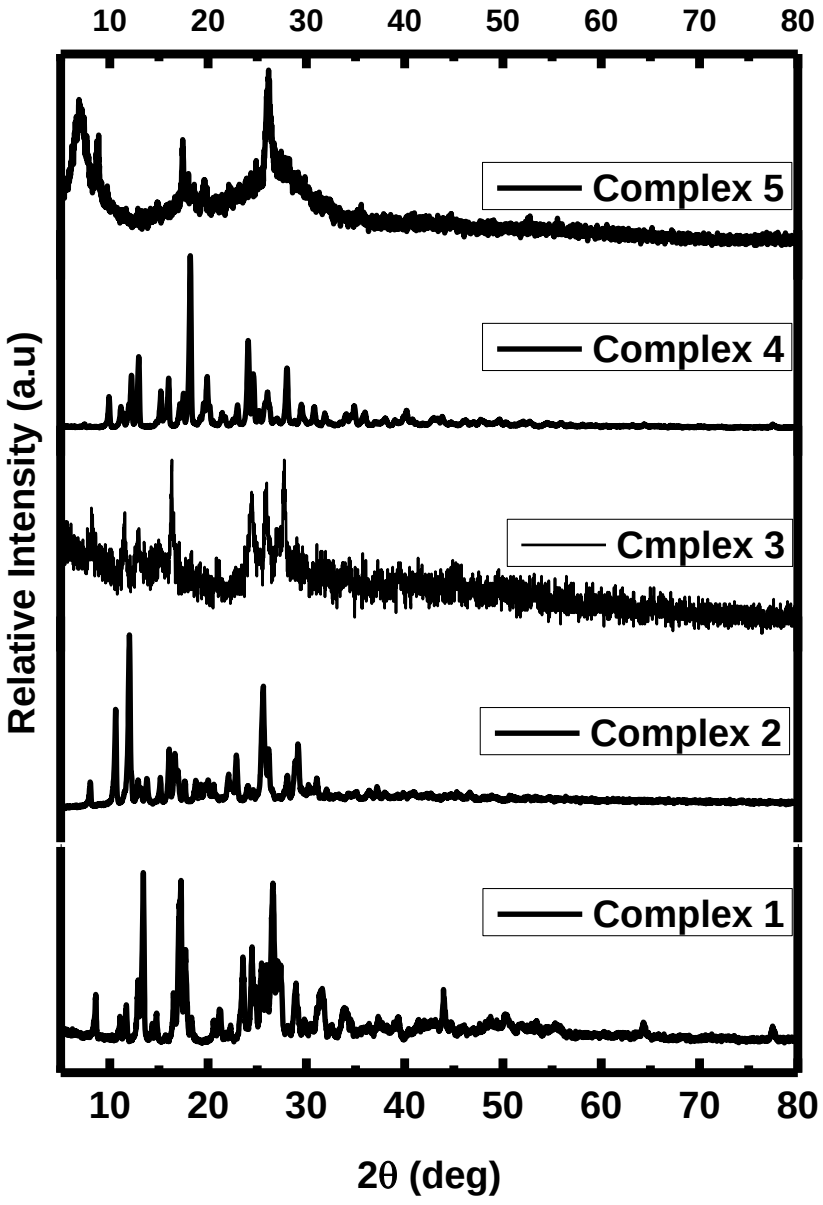

Appendix 24. Powder XRD spectra of complexes **1 – 5**

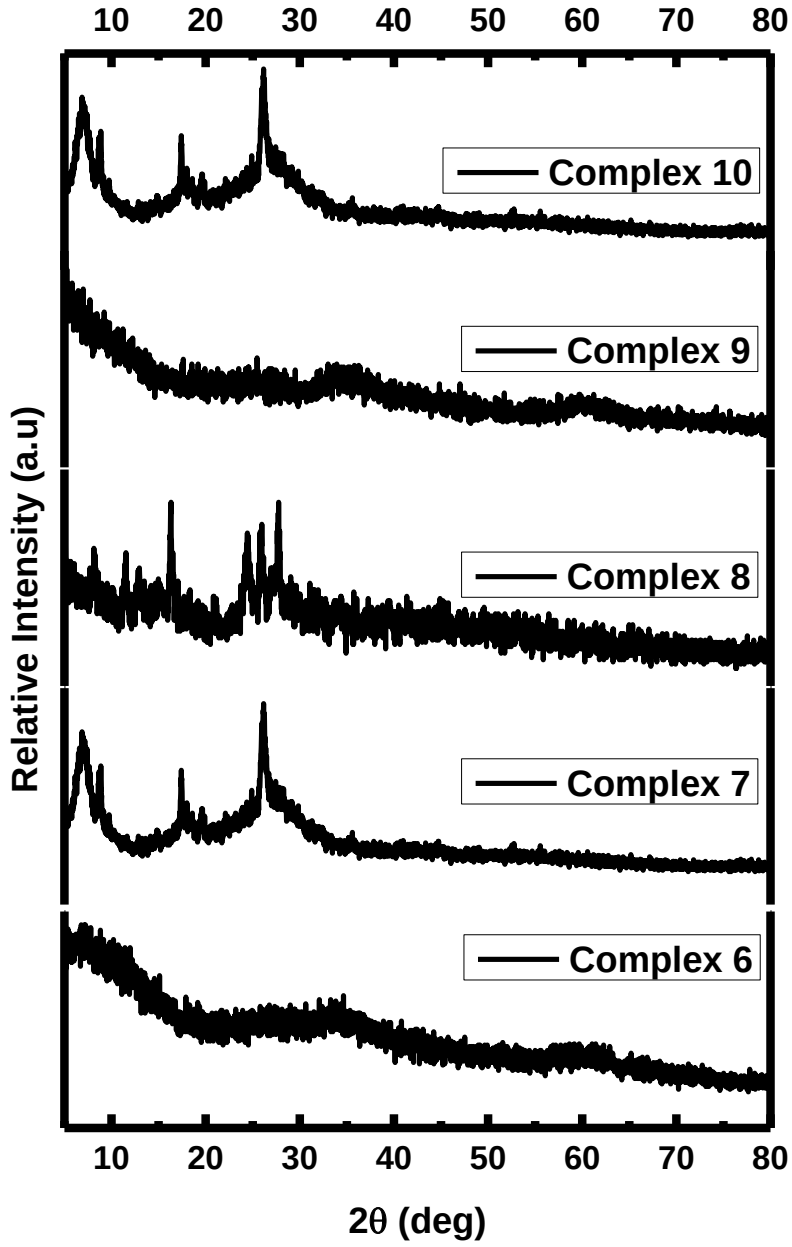

Appendix 25. Powder XRD spectra of complexes **6 – 10**

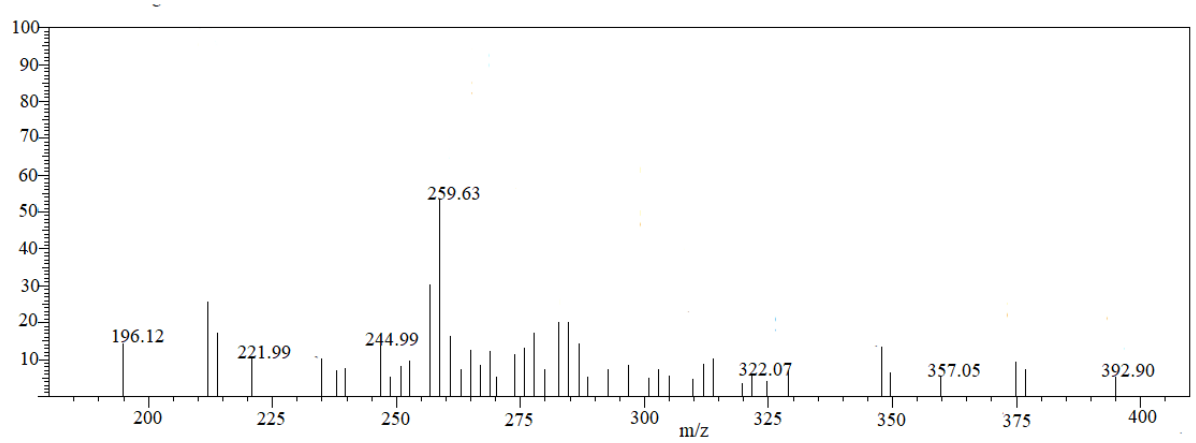

Appendix 26. Mass spectrum of complex **1**.

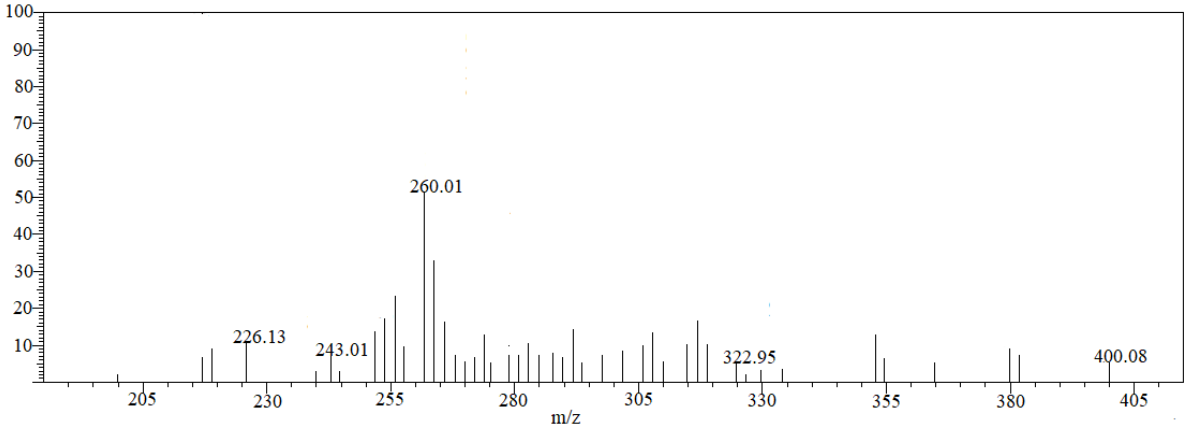

Appendix 27. Mass spectrum of complex **2**.

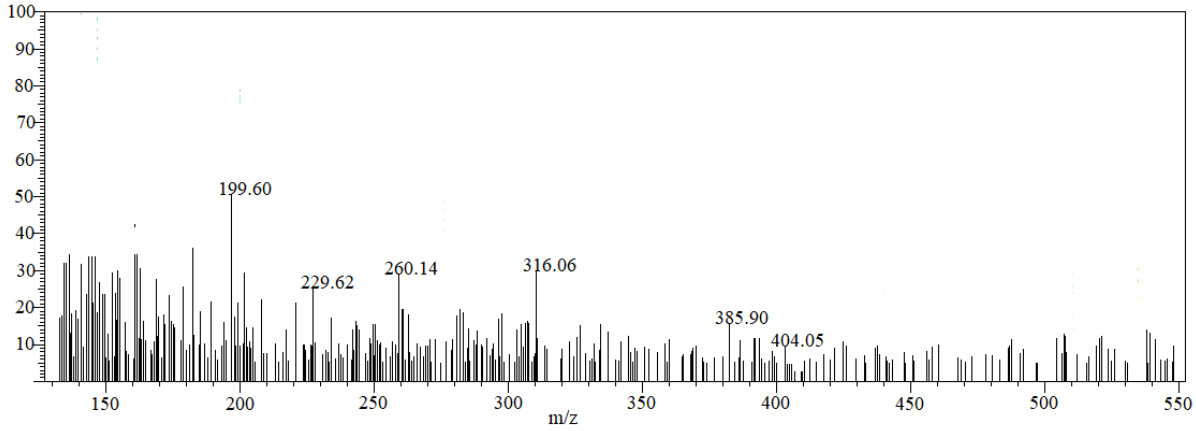

Appendix 28. Mass spectrum of complex **3**.

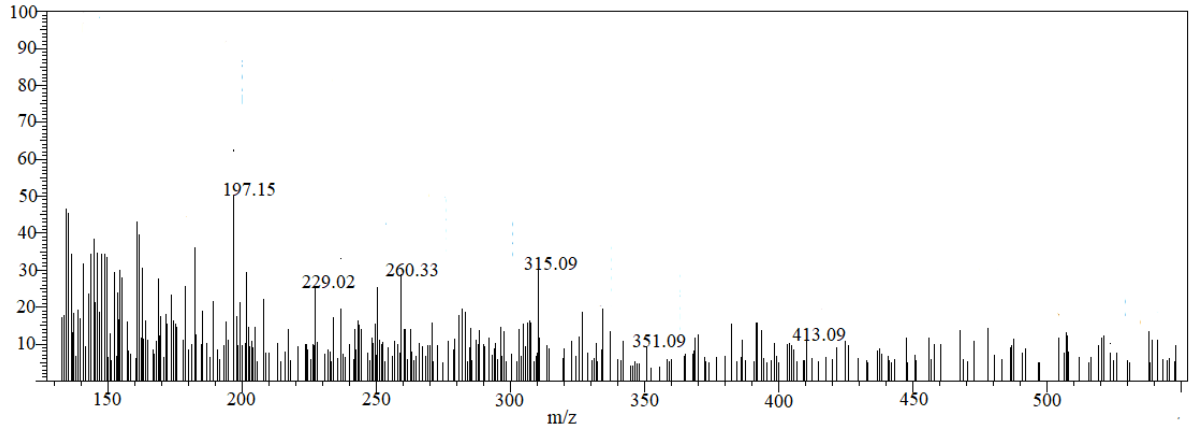

Appendix 29. Mass spectrum of complex **4**.

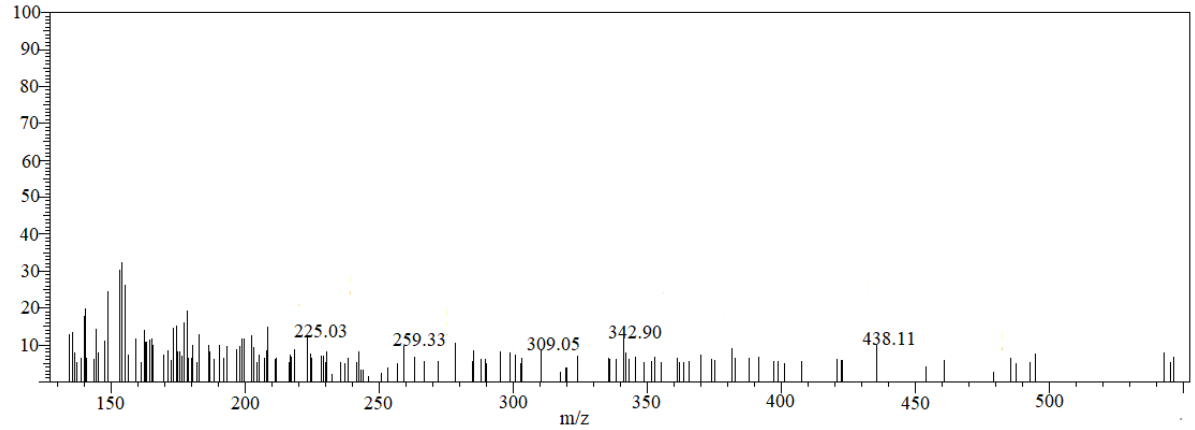

Appendix 30. Mass spectrum of complex 5**.**

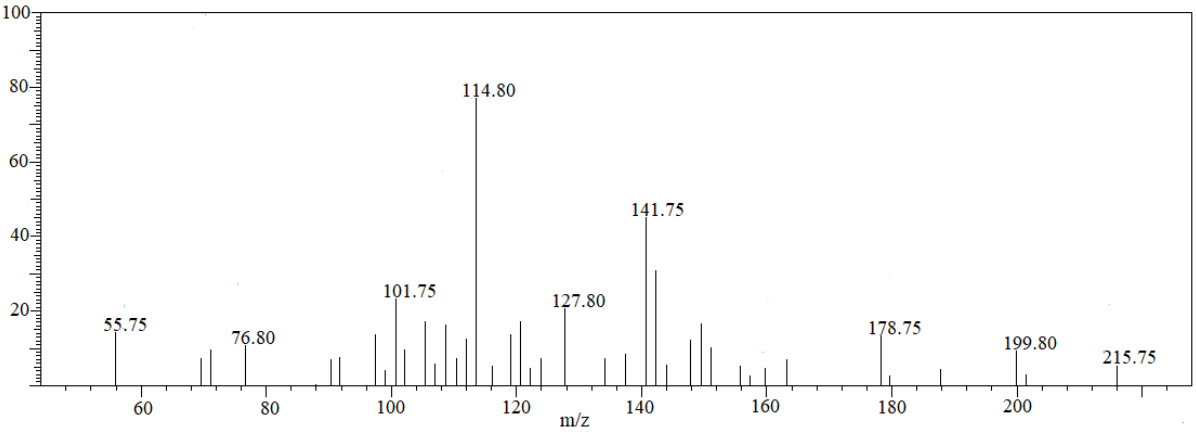

Appendix 31. Mass spectrum of ligand **L2**.

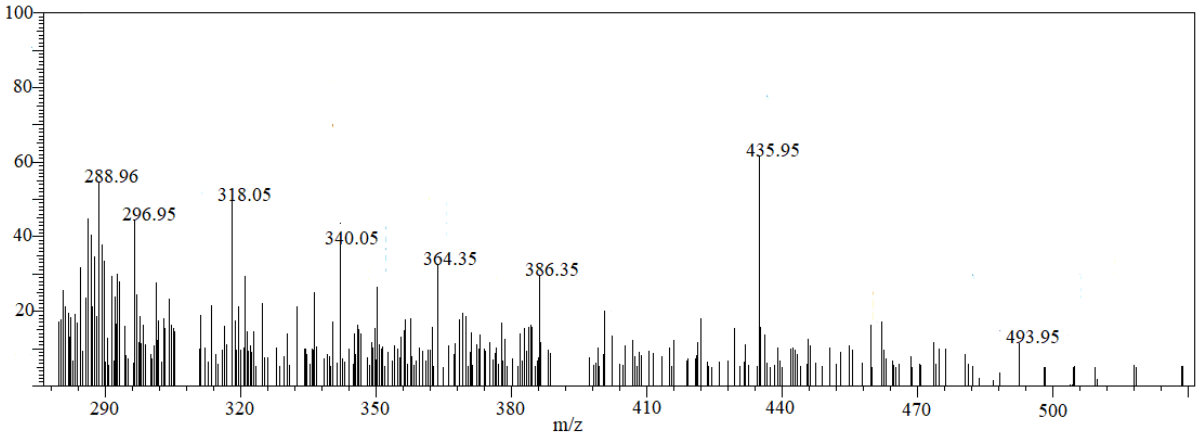

Appendix 32. Mass spectrum of complex **6**.

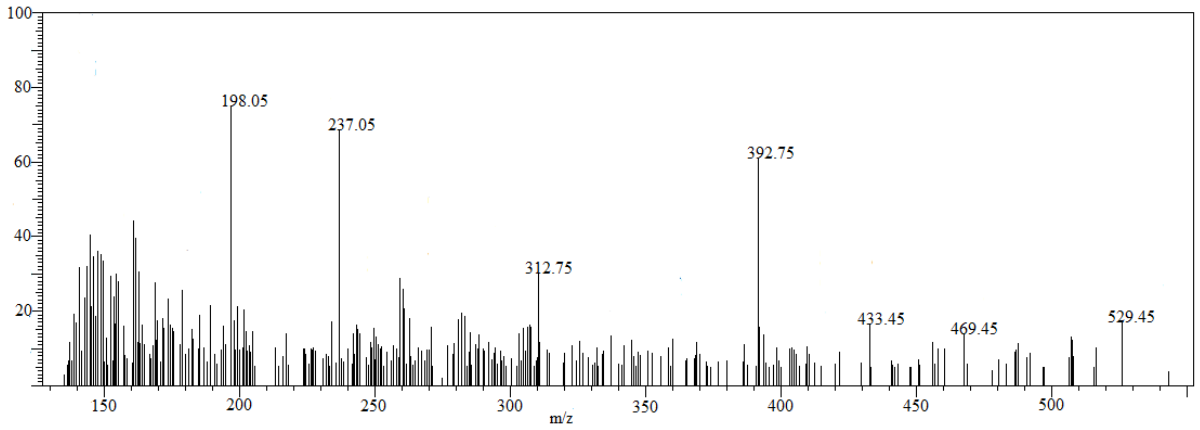

Appendix 33. Mass spectrum of complex **7**.

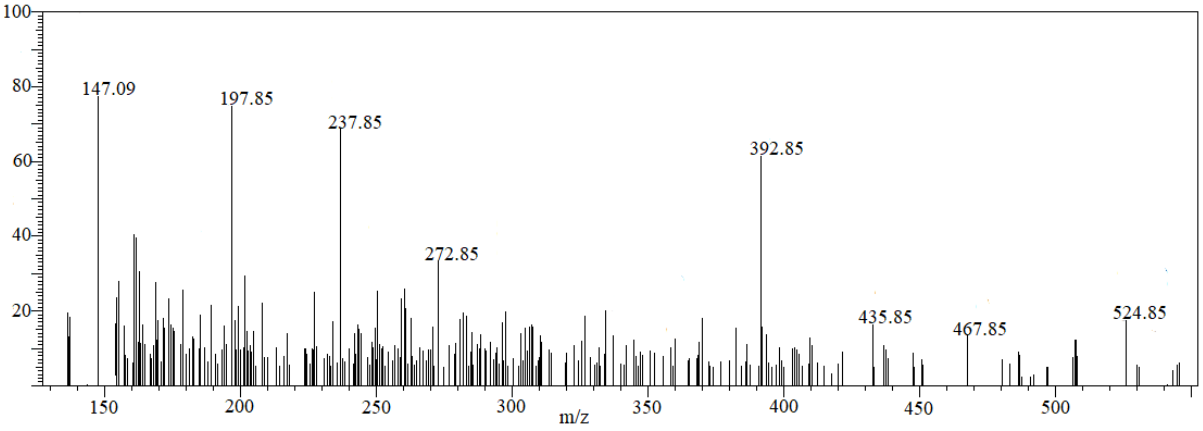

Appendix 34. Mass spectrum of complex **8**.

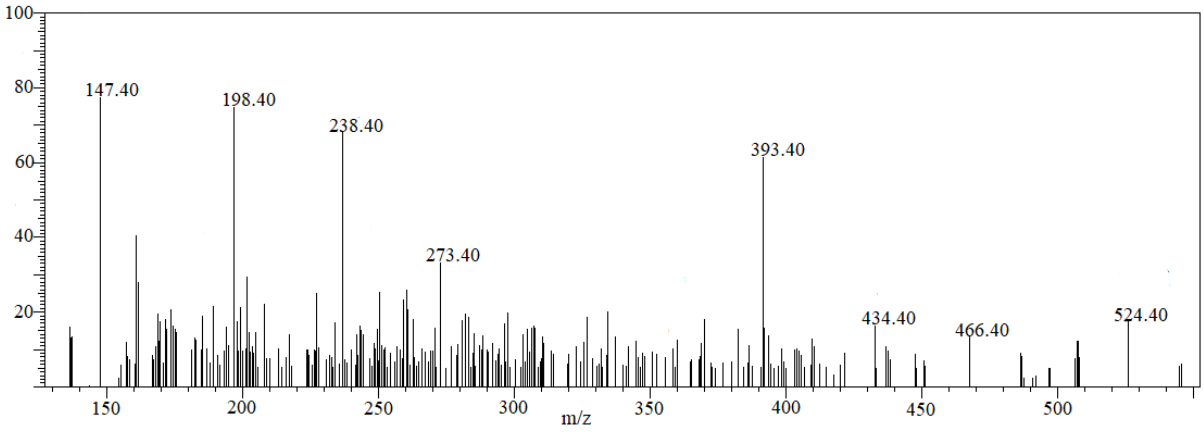

Appendix 35. Mass spectrum of complex **9**.

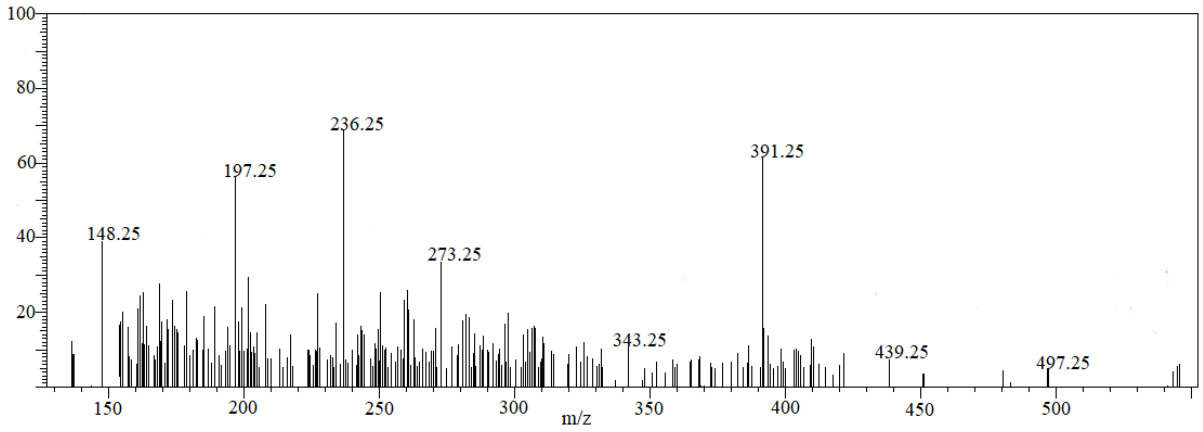

Appendix 36. Mass spectrum of complex **10**.

Appendix 37. Mean inhibition zone of of complexes (**1** – **5**) in mm (mean ± SD**).**

Bacterial strains	**Conc. (µg/mL)**	**Compounds**						
		1	**2**	**3**	**4**	**5**	**L1**	**Ciprofloxacin**
E.coli	150	10.62 ± 0.36	12.69 ± 0.23	10.78 ± 0.24	8.00 ± 0.13	7.32 ± 0.90	6.22 ± 0.14	21.50 ± 0.28
	300	12.00 ± 0.66	13.57 ± 0.29	11.91 ± 0.10	9.00 ± 0.64	9.52 ± 0.49	6.5 ± 0.36	22.00 ± 0.50
P. aeruginosa	150	16.69 ± 0.18	18.51 ± 0.37	17.87 ± 0.07	15.07 ± 0.01	0.00	6.00 ± 0.25	20.52 ± 0.40
	300	18.85 ± 0.34	20.65 ± 0.18	18.62 ± 0.19	15.64 ± 0.22	0.00	6.24 ± 0.39	22.98 ± 0.08
S. aureus	150	11.30 ± 0.17	17.10 ± 0.10	12.11 ± 0.15	12.50 ± 0.31	7.00 ± 0.31	0.00	19.00 ± 0.92
	300	13.22 ± 0.74	17.99 ± 0.03	14.63 ± 0.20	13.24 ± 0.21	8.00 ± 0.52	0.00	20.80 ± 0.37
S. pyogenes	150	10.22 ± 0.89	8.50 ± 0.28	0.00	0.00	0.00	6.20 ± 0.15	15.90 ± 0.55
	300	12.22 ± 0.66	10.64 ± 0.70	0.00	0.00	0.00	7.00 ± 0.11	17.00 ± 0.94

Appendix 38. Mean inhibition zone of complexes (6 – 10) in mm (mean ± SD)

.Bacterial strains	Conc. (µg/mL)	Compounds						
		6	7	8	9	10	H_2L	Ciprofloxacin
E.coli	100	14.62 ± 2.00	13.79 ± 0.65	14.62 ± 1.06	11.79 ± 1.07	9.50 ± 1.00	10.66 ± 1.75	20.79 ± 2.00
	200	16.71 ± 1.50	14.55 ±1.75	16.71 ± 1.45	12.55 ± 1.03	10.12 ± 0. 90	11.55 ± 0.68	21.54 ± 1.78
P. aeruginosa	100	18.67 ± 0.50	19.56 ± 0.84	18.67 ± 0.70	17.56 ± 0.64	11.00 ± 0.31	8.50 ± 0.52	19.99 ± 0.95
	200	20.75 ± 2.05	20.90 ± 2.00	20.75 ± 2.07	18.90 ± 2.06	12.00 ± 0.81	9.60 ± 2.00	20.94 ± 2.01
S. aureus	100	13.76 ± 0.75	18.71 ± 0.82	13.76 ± 0.64	14.82 ± 0.72	7.00 ± 0.59	10.66 ± 0. 39	20.81 ± 0.84
	200	14.70 ± 0.86	19.69 ± 0.71	14.70 ± 0.55	16.69 ± 0.63	8.00 ± 0.52	10.96 ± 0.96	21.72 ± 0.64
S. pyogenes	100	11.57 ± 0.79	18.58 ± 1.04	18.55 ± 1.02	15.65 ± 1.09	9.00 ± 0.47	0.00	19.53 ± 0.91
	200	12.62 ± 0.50	19.75 ± 0.93	19.69 ± 0.69	16.75 ± 0.53	10.00 ± 0.19	0.00	20.79 ± 0.73

Appendix 39. Percentage radical scavenging activity of complexes (**1** – **5**) (mean ± SD)

Conc. (µg/mL)	**L1**	**1**	**2**	**3**	**4**	**5**	**Ascorbic acid**
115	55.50 ± 0.32	94.19 ± 0.45	93.96 ± 0.25	91.68 ± 0.40	60.44 ± 0.34	56.46 ± 0.26	97.71 ± 0.39
100	55.39 ± 0.13	93.65 ± 0.22	93.24 ± 0.41	90.74 ± 0.56	60.09 ± 0.26	55.69 ± 0.45	97.23 ± 0.37
85	54.61 ± 0.16	91.68 ± 0.19	82.70 ± 0.17	85.12 ± 0.18	58.75 ± 0.45	54.81 ± 0.25	96.25 ± 0.05
70	53.80 ± 0.32	82.9 ± 0.09	74.56 ± 0.25	70.91± 0.27	58.21 ± 0.25	52.55 ± 0.35	91.80 ± 0.34
55	52.74 ± 0.13	80.67 ± 0.39	63.80 ± 0.13	65.31± 0.26	55.67 ± 0.20	50.16 ± 0.20	87.85 ± 0.13
40	51.66 ± 0.27	75.63 ± 0.30	55.51 ± 0.36	61.55± 0.20	48.49 ± 0.33	49.70 ± 0.33	75.55 ± 0.49
25	48.23 ± 0.18	51.72 ± 0.15	54.62 ± 0.30	50.45 ± 0.33	48.18 ± 0.33	49.30 ± 0.19	60.89 ± 0.92
10	47.07± 0.23	44.04 ± 0.81	53.97 ± 0.11	48.09 ± 0.78	47.85 ± 0.19	48.52 ± 0.05	47.35 ± 0.23
5	46.99 ± 0.40	43.67 ± 0.29	53.86 ± 0.20	47.58 ± 0.25	47.8 ± 0.05	48.19 ± 0.41	41.67 ± 0.65
IC_{50} (µg/mL)	35.36	10.46	8.62	16.01	27.56	34.79	4.49

Appendix 40. Percentage radical scavenging activity of complexes (**6** – **10**) (mean ± SD)

Conc. (µg/mL)	**L2**	**6**	**7**	**8**	**9**	**10**	**Ascorbic acid**
200	60.50 ± 0.50	85.88 ± 0.22	88.75 ± 0.59	83.90 ± 0.77	62.90 ± 0.31	66.73 ± 0.41	89.33 ± 0.45
100	59.90 ± 1.50	85.45 ± 0.35	88.64 ± 0.46	83.63 ± 0.81	62.51 ± 0.55	65.81 ± 0.93	88.91 ± 0.81
50	58.61 ± 0.31	76.63 ± 0.11	77.94 ± 0.88	68.52 ± 0.35	58.75 ± 0.74	58.49 ± 0.66	78.84 ± 0.36
25	56.72 ± 0.21	60.79 ± 0.60	61.16 ± 0.19	65.91 ± 0.21	58.21 ± 0.85	55.33 ± 0.79	60.25 ± 0.73
12.5	53.14 ± 0.40	58.07 ± 0.80	59.62 ± 0.62	60.90 ± 0. 61	55.67 ± 0.33	54.16 ± 0.80	58.62 ± 0.66
6.25	45.96 ± 0.25	39.90 ± 0.38	40.82 ± 0.44	39.71 ± 0. 59	35.26 ± 0.49	39.05 ± 0.25	40.72 ± 0. 53
3.125	35.75 ± 0.14	38.02 ± 0.41	38.31 ± 0.39	36.45 ± 0.60	34.81 ± 0.73	38.58 ± 0.51	39.41 ± 0.98
1.56	35.27 ± 0.52	37.04 ± 0.33	37.97 ± 0.53	36.09 ± 0.90	34.26 ± 0.11	38.41 ± 0.88	38.84 ± 0.11
IC_{50} (µg/mL)	42.50	8.20	4.72	9.15	33.08	34.69	4.28

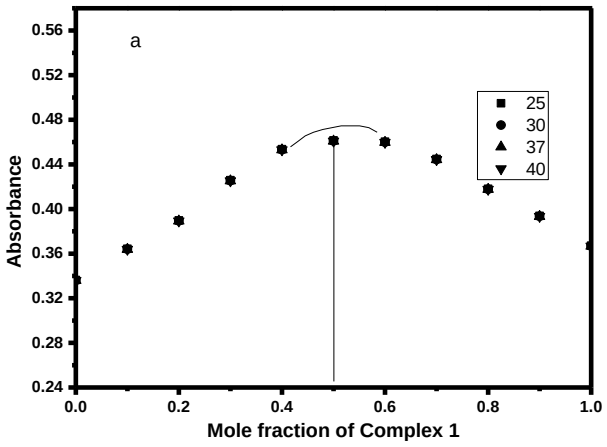

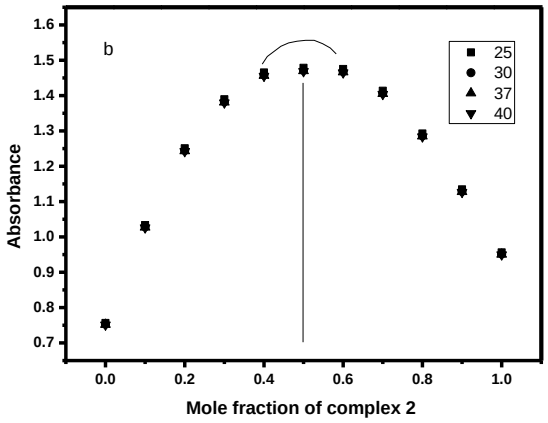

Appendix 41. Job's curves at 25, 30, 37 and 40 ^{o}C for complexes (**1a** and **2b)**.

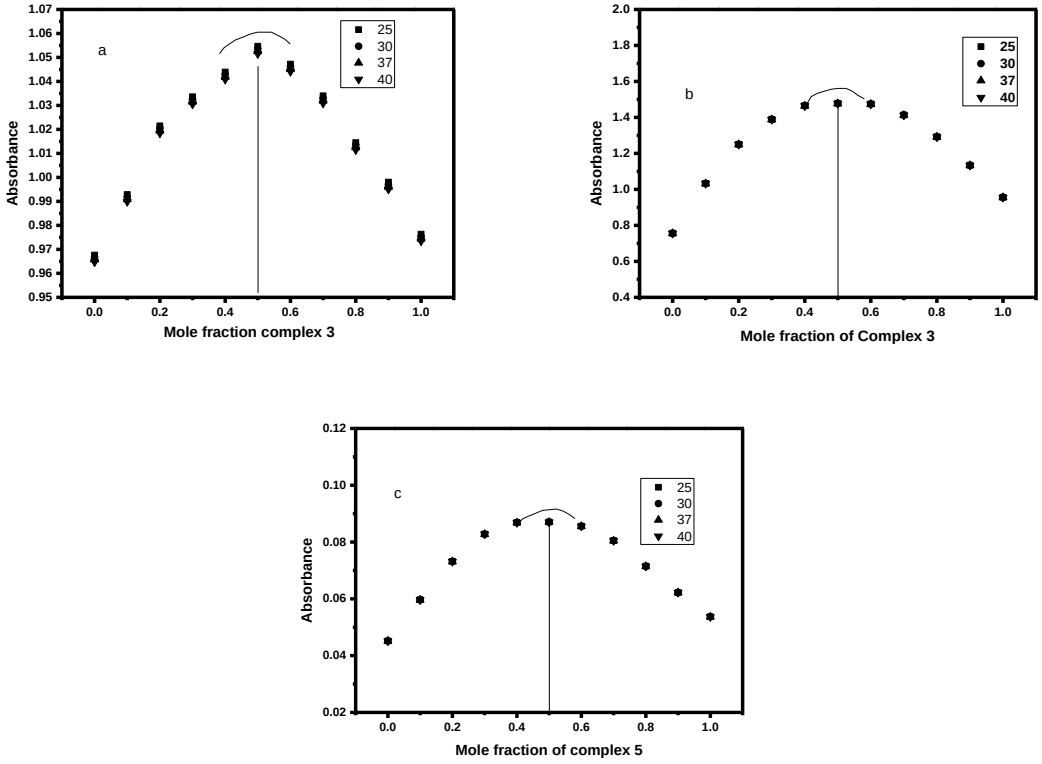

Appendix 42. Job's curves at 25, 30, 37 and 40 ^{o}C for complexes (**3a, 4b** and **5c)**.

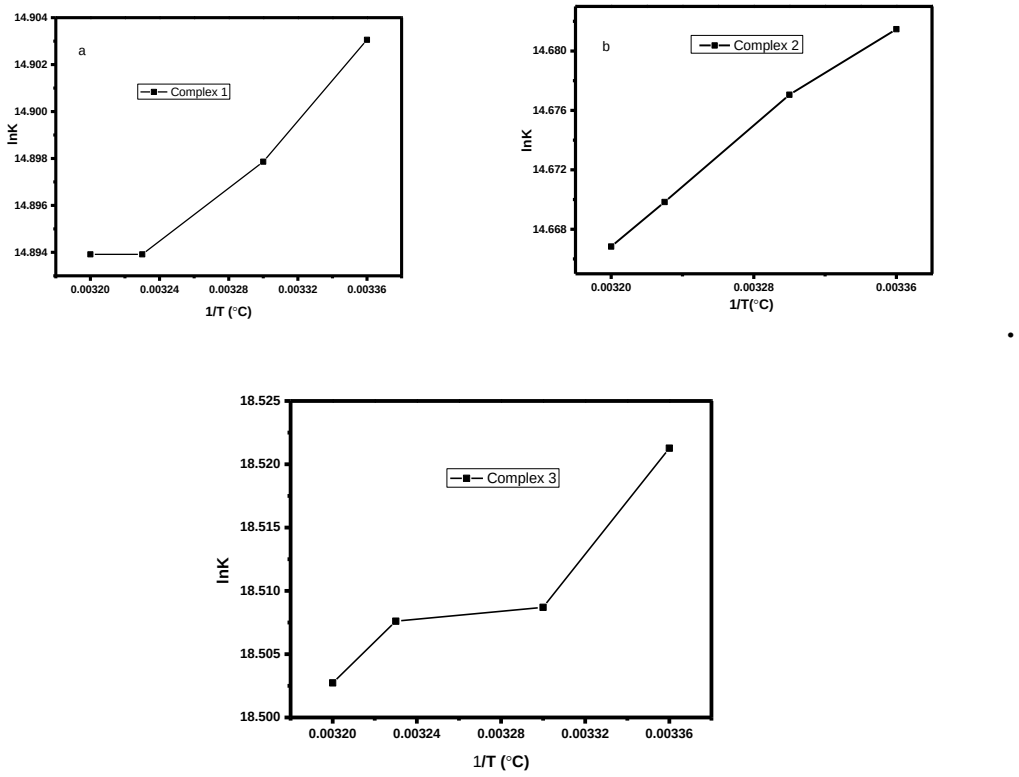

Appendix 43. Plot of lnK versus 1/T of complexes (**1a, 2b** and **3c**)

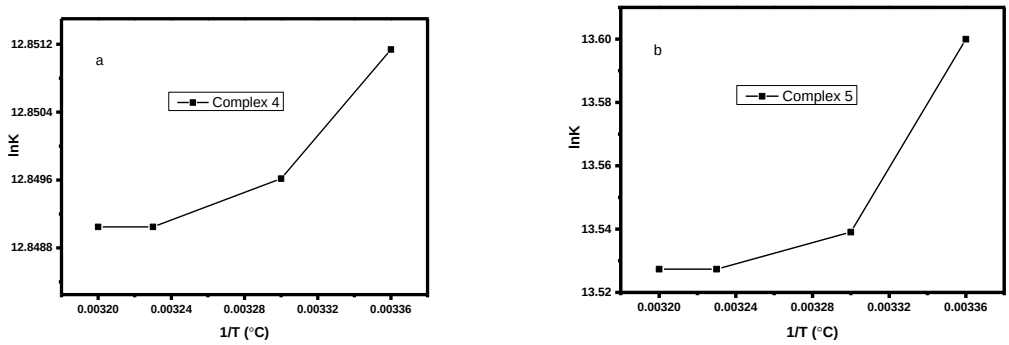

Appendix 44. Plot of lnK versus 1/T of complexes (**4a** and **5b**)

Appendix 45. ADME and Drug likeness descriptors of complexes (**1 – 5**)

Comp	**SwissADME descriptors**									
	Mw g/mol	#H-BAs	#H-BDs	MR	TPSA	GI absorption	BBB permeant	log Kp (cm/s)	Lipinski violations	LogP
L1	259.3	4	3	76.44	77.74	High	No	-7.38	no	2.22
1	359.13	4	2	94.25	66.74	High	Yes	-7.1	no	0.78
2	400.85	8	3	92.79	142.02	Low	No	-7.53	no	-0.74
3	388.71	5	3	94.25	78.18	High	No	-7.15	no	0.78
4	378.99	7	2	94.73	121.79	High	No	-7.5	no	-1.05
5	440.32	5	2	83.23	95.25	High	No	-8.29	no	-0.47
Cipro	331.34	5	2		74.57	High	No	-9.09	no	2.24

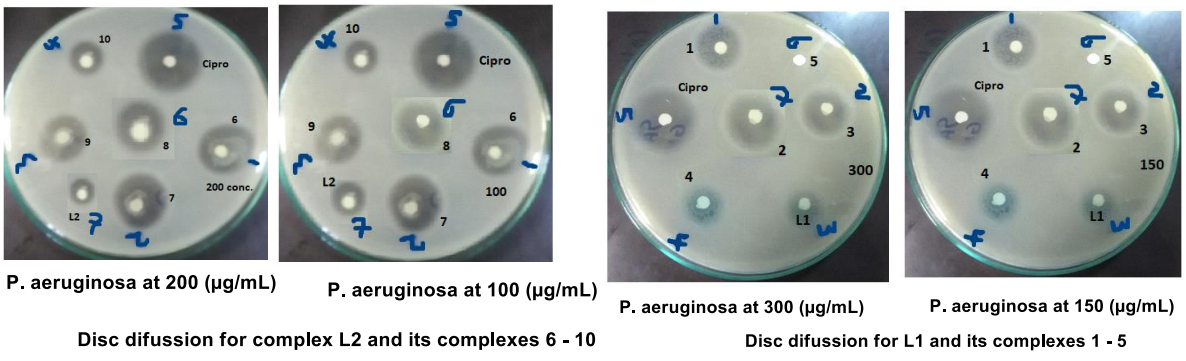

P. aeruginosa at 200 (µg/mL)

P. aeruginosa at 100 (µg/mL)

Disc difussion for complex L2 and its complexes 6 - 10

P. aeruginosa at 300 (µg/mL)

P. aeruginosa at 150 (µg/mL)

Disc difussion for L1 and its complexes 1 - 5

Appendix 46. Sample disc diffusion for ligands and their complexes

LIST OF PUBLICATIONS

1. **Tadewos Damena,** Digafie Zeleke, Tegene Desalegn**,** Taye B. Demissie**,** and Rajalakshmanan Eswaramoorthy, *ACS Omega* (**2022**), 7, 5, 4389–4404.

   (Publisher: American Chemical Society, **Impact factor = 4.132)**

   Title: *Synthesis, Characterization, and Biological Activities of Novel Vanadium(IV) and Cobalt(II) Complexes*

2. **Tadewos Damena**, Mamaru Bitew, Digafie Zeleke, Tegene Desalegn , Rajalakshmanan Eswaramoorthy and Taye B. Demissie, *ACS Omega* (**2022**), (Publisher: American Chemical Society, **Impact factor = 4.132)**

   Title: Novel Zinc(II) and Copper(II) Complexes of 2-((2-Hydroxyethyl)Amino)Quinoline-3-Carbaldehyde for Antibacterial and Antioxidant Activities: A Combined Experimental, DFT and Docking Studies